Halogen Bonding Metallo-Tripodal Receptors for the Recognition and Sensing of Phosphate Anionic Species

Hena Bagha

St Hugh's College, University of Oxford



A thesis submitted for the degree of Doctor of Philosophy

Inorganic Chemistry Laboratory

University of Oxford

Trinity Term 2019

Halogen Bonding Metallo-Tripodal Receptors for the Recognition and Sensing of Phosphate Anionic Species

Hena Bagha, St Hugh's College, University of Oxford

Abstract of thesis submitted for the degree of D.Phil., Trinity Term 2019

This thesis describes the preparation and study of C_{3v} symmetric, tris(iodotriazole) containing metallo-tripodal host molecules exploiting halogen bonding for the selective molecular recognition and sensing of phosphate anionic guest species.

Chapter One introduces the field of supramolecular chemistry, highlighting the areas of relevance to this thesis *viz*. anion coordination and recognition, halogen bonding (XB), and the importance and design of artificial receptors for the selective recognition of phosphate and its derivatives.

Chapter Two describes the synthesis of a family of Zn(II)- and Cu(II)-based XB redox-active, optical and water-soluble tripodal sensory hosts derived from the novel 'general XB metallo-tripodal motif' and details their inorganic monophosphate and simple phosphate-ester anion discriminatory capabilities. In conjunction, tris(prototriazole) containing hydrogen bonding (HB) metallo-tripodal host analogues are also prepared and the influences of XB and HB on the fundamental anion recognition and sensing properties of the receptors discussed.

Chapter Three expands on the work of Chapter Two and details the incorporation of the 'general XB metallo-tripodal motif' into more exotic, chiral XB Zn(II)-tripodal host frameworks for XB-mediated enantioselective chiral anion binding and sensing applications. In particular, the enantiodiscriminatory behaviour of these hosts towards of a series of biologically-relevant carboxylate oxo-anions and BINOL phosphate-ester chiral anion guest species is investigated.

Chapter Four describes synthetic attempts to further exploit the 'general XB metallo-tripodal motif' towards the construction of a more complex, higher-order dimetallic XB cryptate host envisioned for the recognition of inorganic polyphosphate anionic species. Specifically cryptate formation is investigated harnessing a di-amine based [2+3] Schiff base strategy.

Chapter Five provides a summary of the main conclusions of this thesis.

Chapter Six details the experimental procedures employed in this work, including synthetic protocols and characterisation data for novel compounds.

Additional information pertaining to crystallographic data, electrochemical measurements and also the relevant theory of electrochemical anion sensing are provided in the Appendices.

Acknowledgements

I would not be writing the acknowledgements section for my thesis were it not for many individuals who have all made this DPhil such an incredible graduate experience. Firstly, a hearty thank you to Professor Paul Beer for welcoming me so warmly into his group and providing endless streams of guidance and support during my time in (and away from!) Oxford. Your tireless efforts in particular at proofreading this thesis are greatly appreciated. A special thanks also goes to my industrial supervisor Dr Mark Sambrook, as well as my industrial sponsor, Dstl, for the funding used to conduct this research.

The past few years that I have spent in the Beer group have been fantastic, enabling me to not only develop my skills as a chemist but also grow both in mind and spirit. This is entirely to the credit of the great group members, past and present, whom I have had the privilege of working alongside and am lucky enough to call my friends. For helping me settle so well into the S7 lab when I first arrived as well as their synthetic advice and expertise, I am very grateful to Drs Asha Brown, Matthew Langton, Jason Lim and Stuart Cornes, the original 'Pod Squad' for helping me embark on this tripod making adventure. Jason, you have my continual gratitude for always managing to step aside from the countless projects of yours and taking the time to answer all of my never ending questions – you are an asset to Science. A big thank you also goes to the DPhils in my cohort, (the now Dr!) Valentine Bunchuay (Ka) and the one and only Sam Sutton for their brilliant companionship and ample provisions of entertainment, respectively! Other familiar faces who have ensured there was never a dull day to be had in the office and are owed just as many thanks are Harry Klein, George Li, Grace Turner, Luiza Bondila, Jane Liew, Andrew Docker, Robert Hein and of course, Drs Jessica Pancholi, Lydia Gilday and Tim Barendt. An immense amount of gratitude I express to Robert again, for your invaluable assistance with all things relating to electrochemistry and proofreading of Chapter Two – may we all be as fearless in our approach to chemistry as you!

Additionally much of the work presented here would not have been possible without the brilliant technical support I have received from the CRL staff, for which I must thank: Dr Christopher Durr (Charlotte Williams group) for solving the crystal structures, Dr Will Myers (CAESR) for performing all of the EPR measurements (and so diligently explaining them) and Dr Nick Rees for running such a great NMR service also.

Away from the CRL, I have been incredibly fortunate to have the support of some amazing friends who thankfully expressed no desire to discuss the marvels of halogen bonding and instead provided much needed distraction away from work. Especially to the friendships I first formed in Notts, thank you for carrying me through this journey. A special note of thanks here goes to my dearest friend Morgan Fulcher who from the very beginning has kept me sane, made me laugh, and universed when I needed it most.

Finally to my strongest anchors, my parents and siblings to whom this thesis is dedicated, I am eternally grateful. Without your unwavering support, encouragement and love, I would not be where I am today. For this I cannot say thank you enough - but I'll keep on trying.

Hena Bagha, 9th October 2019

Abbreviations

δ	chemical shift
λ	wavelength
μ	micro
ξ	magnitude of choral selectivity ($\xi = K_S / K_R$)
+ve	positive
Δ	change in (a physical quantity)
Å	Angstrom
$A_{\parallel}$	hyperfine coupling constant parallel to a unique symmetry axis
A^-	anion
a.u.	arbitrary units
ADP	adenosine diphosphate
AMP	adenosine monophosphate
aq.	aqueous
ATP	adenosine triphosphate
bistren	bis-tris(2-aminoethyl)amine
BINOL	1,1'-Bi-2-naphthol
Boc	tert-butyloxycarbonyl (protecting group)
br.	broad
Bu	butyl
calc.	calculated
cat.	catalytic
ca.	*circa*
cf.	*confer*
°C	degrees Celsius
CD	cyclodextrin
ClO_4^-	perchlorate anion
conc.	concentrated
COSY	homonuclear correlation spectroscopy
CuAAC	copper(I)-catalysed azide-alkyne cycloaddition
CV	cyclic voltammetry
CW	continuous wave

d	doublet
dd	doublet of doublets
D	diffusion coefficient
DBU	1,8-diazabicycloundec-7-ene
DFT	density functional theory
DIPEA	*N*,*N*-diisopropylethylamine
DMAP	4-dimethylaminopyridine
DMF	*N*,*N*-dimethylformamide
DMSO	dimethyl sulfoxide
DNA	deoxyribonucleic acid
DOSY	diffusion ordered spectroscopy
DPV	differential pulse voltammetry
e.g.	*exempli gratia*
en	ethylenediamine
$E_{1/2}$	half-wave potential
EDTA	ethylenediaminetetraacetate
em	emission
EPR	electron paramagnetic resonance
eq.	equivalents
ESI	electrospray ionisation (mass spectrometry)
ex	excitation
F	Faraday constant (96485.309 C mol^{-1})
Fc	ferrocene
Fc^+	ferrocenium
g	gram
$g\parallel$	g factor parallel to a unique symmetry axis
$g\perp$	g factor perpendicular to a unique symmetry axis
G	Gibbs free energy
h	hour
H	enthalpy
HB	hydrogen bonding
HEPES	4-(2-hydroxyethyl)-1-piperizineethanesulfonic acid
HRMS	high resolution mass spectrometry

Hz	Hertz
i.e.	*id est*
IDA	indicator display assay
J	coupling constant
J	joule
k	kilo
K	Kelvin
K_a	association constant
L	litre
m	metre, milli (prefix), multiplet
m	meta
M	molar (moles per litre)
m/z	mass to charge ratio
MD	molecular dynamics
Me	methyl
MS	mass spectrometry
n	nano
NMR	nuclear magnetic resonance
OAc^-	acetate anion
OTf^-	triflate anion
p	para
pH	$-log_{10}[H^+]$
pK_a	$-log_{10}K_a$
pmβCD	permethylated-β-cyclodextrin
ppm	parts per million
PMP^-	pinacolyl methyl phosphonate anion
PPi	pyrophosphate
PPPi	inorganic triphosphate

quart.	quartet
quint.	quintet
rt	room temperature
r_H	hydrodynamic radius
R	universal gas constant (8.3145 J mol^{-1} K^{-1})
R_f	retention factor
RNA	ribonucleic acid
S	entropy
s	second, singlet
sat.	saturated
SWV	square wave voltammetry
t	triplet
T	temperature
TBA	tetrabutylammonium
TBTA	tris[(1-benzyl-1,2,3-triazol-4-yl)methyl]amine
^{t}Bu	*tert*-butyl
T	Tesla
TEG	tri(ethylene glycol)
TFA	trifluoroacetic acid
THF	tetrahydrofuran
TPMA	tris(2-pyridylmethyl)amine
TREN	tris(2-aminoethyl)amine
TRIS	tris(hydroxymethyl)aminomethane
Ts	tosyl
TTF	tetrathiafulvalene
UV	ultra-violet
v/v	volume/ volume percent
vdW	van der Waals

Vis.	visible
V	volt
XB	halogen bonding

Table of contents

1 Introduction 1

1.1 Fundamentals of anion supramolecular chemistry 2

1.1.1 Introduction to supramolecular chemistry 2

1.1.2 The case for anion recognition 5

1.1.3 The challenges of anion coordination 6

1.1.4 Biological anion receptors 9

1.1.5 The design of synthetic anion receptors 11

1.2 Synthetic receptors for anion recognition and sensing 20

1.2.1 Overview of modern synthetic anion receptors 20

1.2.2 Cationic receptors 20

1.2.3 Neutral hydrogen bonding receptors 25

1.2.4 Lewis acid and transition-metal based receptors 31

1.2.5 Halogen bonding (XB) receptors 32

1.2.6 Anion sensing 36

1.3 Artificial receptors for the recognition of phosphate and its derivatives 41

1.3.1 The importance and challenges of phosphate recognition 41

1.3.2 Receptors for inorganic phosphates 44

1.3.3 Receptors for organophosphate derivatives 54

1.4 Project Aims 62

1.5 References 63

2 Halogen bonding metallo-tripodal receptors for the recognition and sensing of inorganic monophosphate and simple phosphate-ester anionic species 73

2.1 Introduction 74

2.1.1 XB receptors for the selective recognition of inorganic monophosphate 74

2.1.2 A rational approach to phosphate host design: C_{3v} metallo-tripodal receptors 77

2.1.3 Chapter aims 77

2.2 The '*general* XB metallo-tripodal Motif' 79

2.3 A tris(octyl-chain)-appended XB Zn(II) tripod 80

2.3.1 Synthesis and characterisation of **2.16I**·2ClO_4 and **2.16H**·2ClO_4 80

2.3.2 ^{1}H NMR anion binding studies with **2.16I**·2ClO_4 and **2.16H**·2ClO_4 89

2.4 A tris(ferrocene)-appended XB Zn(II) tripod 93

2.4.1 XB-mediated redox anion sensing 93

2.4.2 Synthesis and characterisation of **2.20I**·2ClO_4 and **2.20H**·2ClO_4 95
2.4.3 Crystal structures of **2.20I**·2ClO_4 and **2.20H**·2ClO_4 98
2.4.4 ^{1}H NMR binding studies with **2.20I**·2ClO_4 and **2.20H**·2ClO_4 101
2.4.5 Electrochemical anion sensing studies with **2.20I**·2ClO_4 and **2.20H**·2ClO_4 104
2.5 A water soluble, tris(triethylene glycol)-appended XB Zn(II) tripod 107
2.5.1 XB-mediated anion recognition in water 107
2.5.2 Synthesis and characterisation of **2.25I**·2ClO_4 108
2.5.3 Isothermal calorimetry and ^{1}H NMR binding studies with **2.25I**·2ClO_4 in water 110
2.5.4 Investigation of the duplicate ^{1}H NMR resonances of **2.25I**·2ClO_4 in D_2O 113
2.6 A tris(triethylene glycol)-appended XB Cu(II) tripod analogue 117
2.6.1 Synthesis and characterisation of **2.26I**·2OTf and **2.26H**·2OTf 117
2.6.2 UV-Vis anion binding studies with **2.26I**·2OTf and **2.26H**·2OTf 120
2.6.3 Electrochemical anion sensing studies with **2.26I**·2OTf and **2.26H**·2OTf 125
2.7 An alternative tris(permethylated-*β*-cyclodextrin)-appended XB Cu(II) tripod 129
2.7.1 Synthesis and characterisation of **2.36I**·2OTf 129
2.7.2 UV-Vis anion binding studies with **2.36I**·2OTf 134
2.8 Conclusions 136
2.9 Future work 138
2.10 References 139

3 Chiral halogen bonding metallo-tripodal receptors for enantioselective anion recognition and sensing 141
3.1 Introduction 142
3.1.1 Theory of chiral recognition 142
3.1.2 Artificial chiral receptors for enantioselective chiral anion recognition 143
3.1.3 XB-mediated chiral anion recognition 145
3.1.4 Chapter aims 147
3.2 A tris(*N*Boc-(*S*)-tryptophan)-appended XB Zn(II) chiral tripod 148
3.2.1 General design 148
3.2.2 Synthesis and characterisation of **3.3I**·2ClO_4 and **3.3H**·2ClO_4 148
3.2.3 ^{1}H-NMR chiral anion binding studies with **3.3I**·2ClO_4 152
3.3 A tris(*N*Boc-(*S*)-tryptophan)-appended XB Zn(II) chiral tripod 153
3.3.1 Synthesis and investigation of the chiral anion binding properties of **3.6I**·2ClO_4 153
3.4 Optical chiral anion sensing studies with **3.3I**·2ClO_4 and **3.3H**·2ClO_4 155
3.5 Conclusions 162
3.6 Future work 163

3.7 References 164

4 A dimetallic halogen bonding cryptate for the recognition of inorganic polyphosphate anionic species 165

4.1 Introduction 166

4.1.1 Cryptands for anion recognition 166

4.1.2 Ditopic cryptands for anion recognition 169

4.1.3 Chapter aims 172

4.2 Towards a dimetallic Zn(II) XB cryptate host 173

4.2.1 General design 173

4.2.2 Synthetic attempts towards **4.9I**·4ClO_4 173

4.3 Conclusions and future work 181

4.4 References 182

5 Conclusions 183

6 Experimental 187

6.1 General considerations 188

6.1.1 Solvents and reagents 188

6.1.2 Instrumentation 189

6.1.3 ^{1}H-NMR titration protocols 189

6.1.4 Electrochemical titration protocols 191

6.1.5 Isothermal Calorimetry (ITC) titration protocols 193

6.1.6 UV-Vis titration protocols 194

6.1.7 Fluorescence titration protocols 195

6.1.8 2D DOSY experiments 196

6.2 Synthetic Procedures 197

6.2.1 Synthesis of key and novel compounds from Chapter Two 197

6.2.2 Synthesis of novel compounds from Chapter Three 229

6.2.3 Synthesis of novel compounds from Chapter Four 237

6.3 References 245

Appendices 246

Appendix A: Crystallographic data 247

Appendix B: Electrochemical reversibility studies 249

Appendix C: Theory of electrochemical anion sensing 256

References 257

Chapter One

Introduction

1 Introduction

1.1 Fundamentals of anion supramolecular chemistry

1.1.1 Introduction to supramolecular chemistry

'Mankind is divisible into two great classes: hosts and guests.' - Max Beerbohm (b. 1872), Hosts and Guests.

Aptly described by Lehn as 'chemistry beyond the molecule',[1] the field of Supramolecular chemistry revolves around the chemistry of the intermolecular bond, 'covering the structures and functions of the entities formed by the association of two or more chemical species'.[1] Drawing heavy inspiration from Nature, where hierarchical biological assemblies dominate and regulate fundamental biochemical processes through non-covalent interactions, it similarly aims at developing elaborate molecular architectures and functional systems from discrete components interacting through intermolecular forces. To carve out this 'complexity from simplicity', Desiraju first introduced the concept of the supramolecular synthon: 'If molecules are built by connecting atoms with covalent bonds, *supermolecules* are built by connecting molecules with non-covalent intermolecular interactions'.[2] Whilst its origins are firmly rooted in (1) 'host-guest' chemistry – the selective recognition and binding of one chemical entity to another, work in modern supramolecular chemistry also encompasses the processes of (2) 'self-assembly and organisation' – the spontaneous association of molecules into more complex entities.[3] The marrying of the two has resulted in an enormous diversity of chemical systems and over the last quarter of a century, fuelled numerous developments at the interfaces with biology and physics (including molecular nanotechnology[4,5], biomaterials[6,7] and systems chemistry[8]), firmly cementing supramolecular science and technology as a wide multidisciplinary and interdisciplinary domain.

The term 'Supramolecular chemistry' and the principles of molecular recognition were built upon the concept proposed by Emil Fischer towards the end of the 19th century, likening biological enzyme-substrate behaviour to a 'lock and key'.[9] Koshland later expanded on this analogy with the 'induced-fit' model, where a substrate can induce a conformational change in the enzyme host, with

a concomitant enhancement in guest recognition and selectivity.[10] As such, host-guest chemistry is based upon complementarity between the species involved; selective binding is achieved by a complementary shape, size and chemical functionality between the host (lock) and guest (key).[11] The latter witnessed its formal beginnings with the appearance of Charles Pedersen's seminal paper in 1967 which detailed the ability of crown ethers to complex alkali metal ions (Figure 1.1A)[12] and consequently heralded the development of an array of host systems capable of selective guest binding – most notably Lehn's three-dimensional cryptands (Figure 1.1B)[13] and Cram's rigid spherands (Figure 1.1C)[14,15] which exhibited enhanced Group I metal cation recognition properties. Ultimately, the trio were lauded '*for their development and use of molecules with structure-specific interactions of high selectivity',* jointly earning the 1987 Nobel Prize in Chemistry. Shortly after Pedersen's crown-ethers, Park and Simmons prepared the first series of abiotic anion receptors in the form of protonated katapinands (Figure 1.1D)[16] shown to encapsulate halide anions in aqueous trifluoroacetic acid (TFA) solution and hence are considered the point of genesis for anion supramolecular chemistry. Despite this and in contrast to the more popular field of cation recognition which received much attention in subsequent years, the forum of anion recognition remained relatively dormant until the early 1980's. Nonetheless, the influx of synthetic anion receptors over the last two decades has in particular established anion supramolecular chemistry as a highly fertile ground for research, with current efforts directed on the use of anions to template molecular assemblies, for membrane transport and in chemical applications such as catalysis, ion extraction and as stimuli for responsive materials.[17]

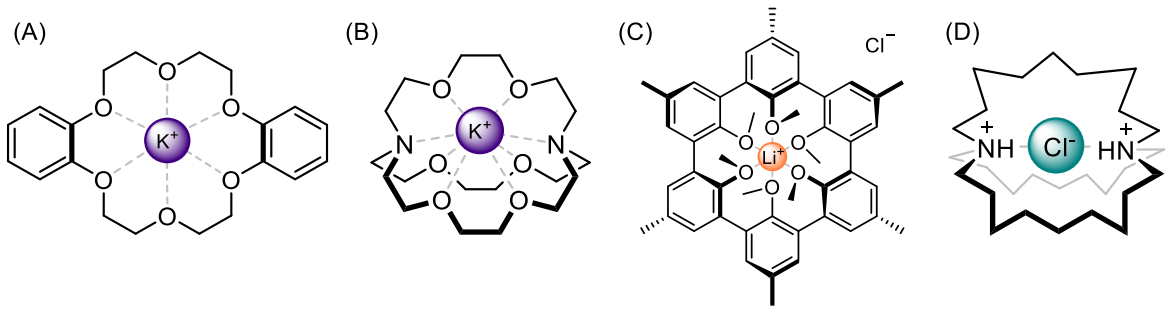


Figure 1.1: *(A) Pedersen's dibenzo-18-crown-6;[12] (B) Lehn's [2,2,2]cryptand;[13] (C) Cram's spherand;[14], (D) Park and Simmons' 'katapinate' chloride anion receptor.[16]*

Lehn further termed supramolecular chemistry as an 'information science' in which the instruction set for the creation of a large complex assembly is contained within its constituent components.[18] Whilst early work focused largely on molecular recognition, contemporary efforts utilise this powerful synthetic methodology in the construction of higher order, complex architectures from the autonomous arrangement of relatively simple, specifically-designed synthons – as exemplified by Leigh's tetrameric 8_{19} knot (Figure 1.2A)[19] and Stoddart's Borromean rings (Figure 1.2B).[20] Additionally, since these 'self-assembly and organisation' processes implement information, they offer extreme promise towards forging a 'bottom-up' approach to the emerging field of nanotechnology, over half a century after Feynman pointed out that 'there's plenty of room at the bottom'[21] without offering any blueprint to the chemist.[18,22,23] Nature, meanwhile, provides the most spectacular examples of discrete molecular assemblies encoded for substrate recognition. Supermolecules such as the octahedral iron storage vessel ferritin are assembled from numerous smaller subunits that contain precise information for their correct integration into the larger framework (Figure 1.2C).[24,25] This elegant demonstration of the interplay between molecular recognition and self-assembly has increasingly driven supramolecular chemists towards the study and manipulation of intrinsic 'molecular information' and led to tremendous advances in the specialist sub-fields of biomaterials,[6,7,26] DNA nanotechnology[27-28] as well as in the fabrication of molecular devices and switches.[29,30] Whilst this shift in emphasis is nothing more than a healthy expansion of the field from its roots in host–guest chemistry, it has enabled 'the chemistry of the entities' to encompass and inform a much broader range of concepts and activities.

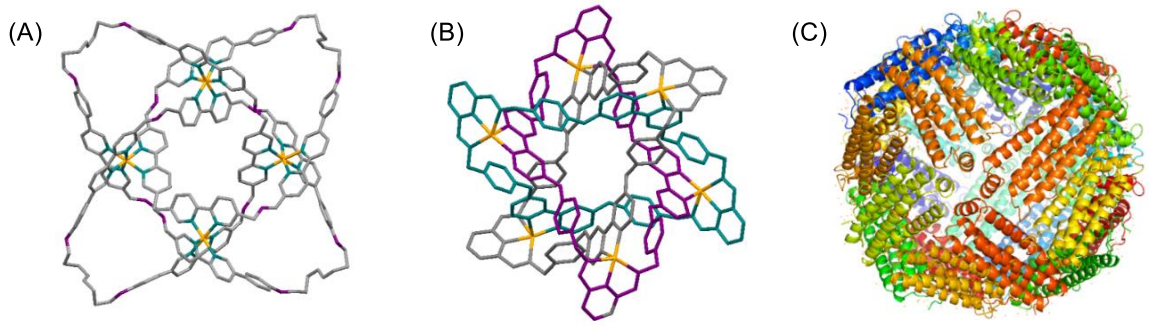


Figure 1.2: *Crystal structures of (A) Leigh's tetrameric 8_{19} knot;[19] (B) Stoddart's Borromean rings;[20] (C) Bullfrog M ferritin (Protein Data Bank (PDB) ID: 3RBC).[31]*

Most relevant to this thesis, this introductory chapter focuses on the fundamental aspects of *anion binding* in supramolecular chemistry with emphasis on the use of halogen bonding as part of the fledgling class of sigma (σ)-hole interactions for molecular recognition purposes. There is particular discussion on the importance and design of artificial receptors for the selective recognition of phosphate and its derivatives – these guest species being the anions of interest in the following work.

1.1.2 The case for anion recognition

The pivotal role of anions in various biological, chemical and environmental processes is well recognised. Chemically, anions function as nucleophiles, bases and catalysts – whose efficacy can be tuned by modifying their coordination properties. In a biological context, the macromolecules of life, DNA and ribonucleic acid (RNA) which govern the transmission and translation of genetic information within living organisms, exist as phosphate-ester containing polyanions.[32] Similarly, the molecular energy currency, adenosine triphosphate (ATP), responsible for intercellular energy transfer and purinergic signalling is also phosphate derived. Indeed, the significance of this particular anion cannot be overstated and being most pertinent to this thesis, the importance of phosphate and its derivatives is described in greater detail in Section 1.3. Meanwhile, other oxoanions such as glutamate and aspartate serve as neurotransmitters whilst lactate, pyruvate and oxaloacetate are crucial metabolic intermediates; it is unsurprising therefore, that the majority of all biological substrates and enzymatic co-factors are negatively charged under physiological conditions.[33] Many inorganic ions also play crucial roles *in vivo*: amongst the halides, iodide is essential for hormone biosynthesis in the thyroid gland[34] whilst chloride, present extensively in extracellular fluid, performs a critical role in respiratory, osmotic and homeostatic processes.[35-36] Imbalances of the latter in the bloodstream can lead to hyperchloremia[37] whilst the hereditary misregulation of chloride in cellular transmembrane transport manifests itself in deleterious diseases such as cystic fibrosis[38] and familial nephropathies such as Bartter's syndrome.[39]

Environmentally, nitrates in fertilisers are beneficial to agriculture but also constitute major biolimiting, pollution hazards; their excessive use in arable farming has led to algal blooms and the eutrophication of natural water-courses, resulting in depleted water-oxygen levels which are unable to support aquatic life.[40] The anthropogenic production of radioactive pertechnetate ($^{99}TcO_4^-$) as a by-product of the nuclear fuels industry and perchlorate, arising from the manufacture of explosives and rocket propellant, has also led to elevated concentrations of these anionic pollutants in the biosphere.[41] Furthermore, epidemiologically important natural pollutants such as arsenate and cyanide pose significant health risks due to their inherent toxicity.[35] Whilst cyanide is infinitesimally present in its inactive form in a multitude of fruits and legumes, its extensive use in metallurgy and controversial farming processes such as cyanide fishing, has resulted in environmental contamination. Consequently, acute exposure to cyanide and its chronic ingestion are associated with increased morbidity and mortality, respectively.[42]

In light of these examples, it is evident that the case for the design and synthesis of artificial anion receptors, sensors and sequestering agents is a compelling one, and their application in environmental and medical contexts remains highly relevant.

1.1.3 The challenges of anion coordination

Whilst cation-binding receptors are legion, anion receptor chemistry remains comparatively underdeveloped. This discrepancy may be attributed, in part, to the intrinsic properties of anions which pose formidable challenges in the design of host systems for their selective recognition, as outlined below:

Size: Anions are larger than their isoelectronic cationic analogues and consequently exhibit a lower charge-to-radius ratio (Table 1.1). Their lower charge density leads to diminished Coulombic attractive interactions often requiring supplementary interactions for effective complexation. Nonetheless, anions possess a higher degree of polarizability which permits dispersive forces to contribute more substantially towards stabilising the host-guest complex.

***Geometry*:** In contrast to metal cations which are exclusively spherical in shape, anions adopt a diverse range of geometries (Figure 1.3). Although such heterogeneity can be exploited to achieve selectivity *via* host-guest complementarity, it also demands careful design of a receptor's binding site.

***pH dependence*:** Many anions exhibit multiple protonation equilibria in aqueous solution (the quintessential example being phosphate (see Section 1.3) and are susceptible to protonation under acidic conditions. The subsequent loss of negative charge impairs the use of electrostatic interactions for anion binding. Furthermore, certain classes of receptors, such as those containing polyammonium (pK_a 9.3) and guanidinium (pK_a 13.7) moieties cease to exist in their protic form at an elevated pH, thus losing the complementary positive charge and hydrogen bond donor capabilities prerequisite for anion binding. Accordingly, recognition is confined to a narrow range in which the receptor can function within the 'pH window' of their target guest (Figure 1.4). Moreover, highly basic anions such as fluoride and cyanide can abstract acidic protons from receptor molecules to become protonated themselves

***Solvation*:** Finally**,** anions display large free energies of solvation relative to cations of comparable charge and size (Table 1.1), due to their ability to form hydrogen bonds with the solvent. Any putative anion receptor therefore, must overcome the desolvation energy barrier and effectively compete with the solvent environment. The *Hofmeister series*[44] which ranks anions according to their hydrophobicity (Figure 1.5) is often invoked when considering anion binding in polar, protic solvents such as water. Larger, charge-diffuse anions tend to be more lipophilic, hence hydrophobic effects (*vide infra*) may be employed to bias their selectivity in aqueous media; whereas, in order to achieve selectivity for the more charge-dense, hydrophilic anions, the host must overcome the penalty of relatively high free energies of anion-guest solvation. Contrastingly, in aprotic organic solvents with low dielectric constants such as chloroform, ion-pairing between the anion and its counter-cation becomes an important association which needs to be overcome for host-guest recognition to occur.

Table 1.1: *Effective ionic radii and free energies of hydration of selected isoelectronic cations and anions.*[3,43]

Cation	Ionic radius /Å	ΔG_{hyd} /KJ mol^{-1}	**Anion**	Ionic radius /Å	ΔG_{hyd} /KJ mol^{-1}
Na^+	1.16	-365	F^-	1.19	-465
K^+	1.52	-295	Cl^-	1.67	-340
Rb^+	1.66	-	Br^-	1.82	-315
Cs^+	1.81	-250	I^-	2.06	-275

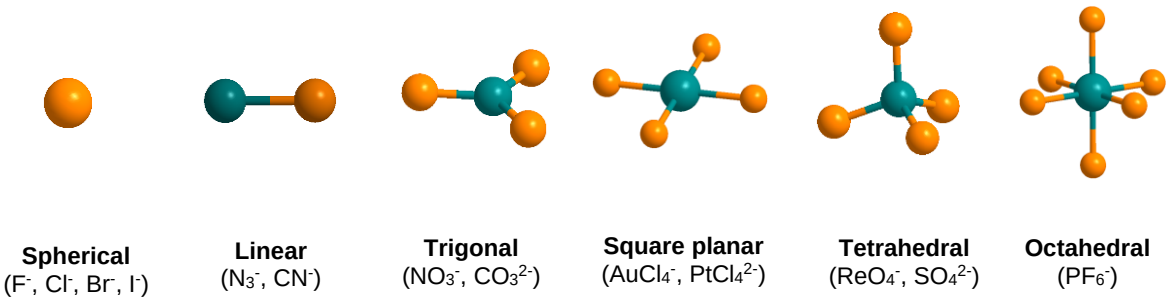


Figure 1.3: *Examples of different geometries adopted by anions.*

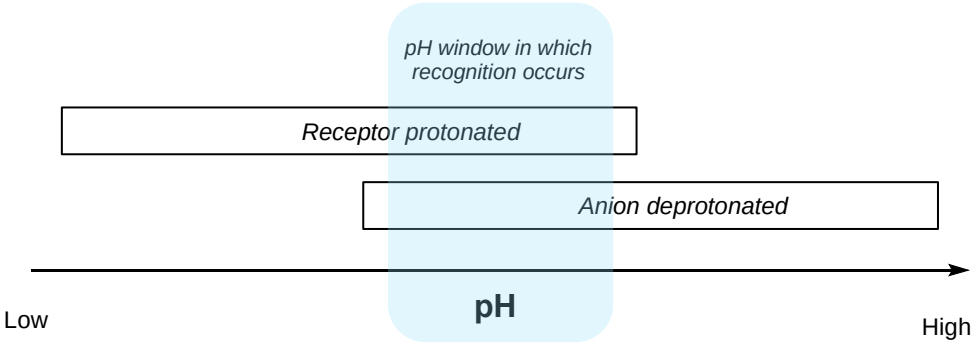


Figure 1.4: *Schematic view of the pH window in which anion recognition by a pH-dependent receptor may occur.*

.

Hydrophilic **Hydrophobic**

$$HPO_4^{2-} < SO_4^{2-} \approx F^- < H_2PO_4^- < OAc^- < Cl^- < Br^- < I^- < ClO_4^- < SCN^-$$

Strongly hydrated *Weakly hydrated*

Figure 1.5: *The Hofmeister Series.*

1.1.4 Biological anion receptors

Despite the intrinsic challenges of anion recognition, a variety of biotic receptors have evolved capable of binding and transporting anions with exquisite selectivity in aqueous environments. In particular, elucidation of the X-ray crystal structures of their constituent protein-anion complexes has allowed for the direct visualization of these phenomena, in terms of the mode of binding and interactions involved. Notably, combinations of non-covalent interactions (primarily hydrogen bonding and electrostatics) are employed, in well-defined complementary arrangements to facilitate highly selective and strong anion association. For example, the 2.4 Å-resolution X-ray structure of haloalkane dehalogenase from *Xanthobacter autotrophicus* GJ10 reported by Dijkstra[45] reveals a chloride anion bound to the active site of the enzyme (Figure 1.6), providing important evidence to resolve the mechanism that converts 1- haloalkanes into the corresponding primary alcohols and a halide ion *via* hydrolytic cleavage of the carbon-halogen bond.[45,35]

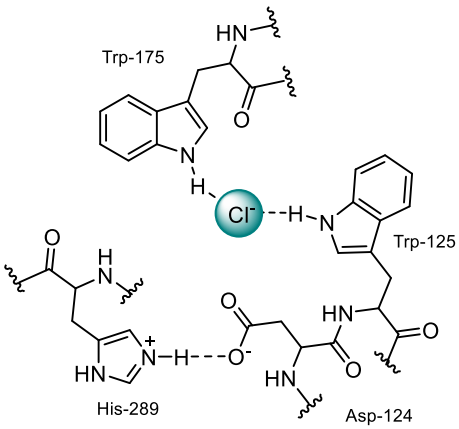


Figure 1.6: *Enzymatic active site of haloalkane dehalogenase with chloride bound by Trp-125 and Trp-175.*[45,35]

More archetypal examples of course, are Nature's phosphate-binding protein (PBP) and sulfate-binding protein (SBP). Considered apotheoses of host-guest complementarity, together they demonstrate the superb ability of biological systems to discriminate tetrahedrally shaped oxoanions *via* the precise arrangement of hydrogen bond donors and acceptors. Comprising a binding cavity structurally distinct to that of the SBP, the PBP selectively binds hydrogen phosphate with a remarkably high affinity (K_a = 3.2 x 10^6 M^{-1}) and is incapable of recognising other inorganic oxoanions, binding sulfate at least five orders of magnitude less tightly.[46] Reported by Leucke and Quiocho,[46] the 1.7 Å resolution X-ray structure of the PBP (Figure 1.7A) reveals the hydrogen phosphate nestled in a deep cleft (~8 Å below the protein surface) and held tightly *via* a constellation of twelve hydrogen bonds by the surrounding peptide residues: nine originate from neutral donors and two from the positively charged guanidinium salt bridge of Arg-135, whilst the twelfth is donated from the anion to the

carboxylate of Asp-56. The latter is key to the selectivity of the binding site, being the only discriminatory residue to repel the dianionic sulfate through unfavourable electrostatic interactions, whereas for hydrogen phosphate it acts as a hydrogen bond acceptor.

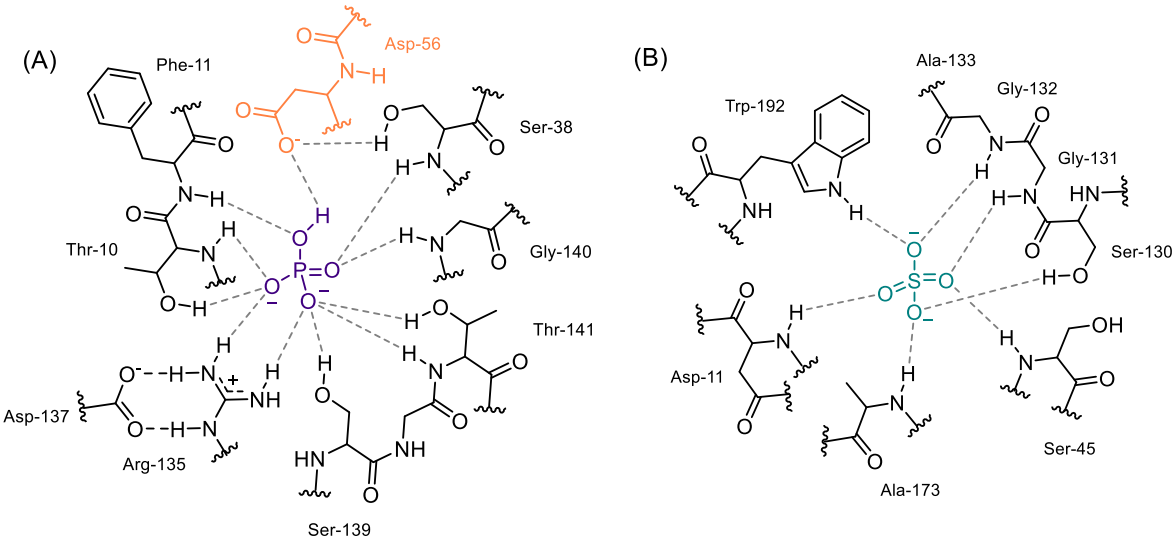


Figure 1.7: *Two dimensional projection of the binding cavities of truncated biological protein structures (A) phosphate binding protein (PBP);[46] (B) sulfate binding protein (SBP).[47]*

By contrast, the SBP is able to accommodate only fully deprotonated anions and almost exclusively binds sulfate with high affinity (K_a = 8.3 x 10^6 M^{-1}).[47] The 2Å resolution crystal structure of SBP in *Salmonella typhimirium* (Figure 1.7B) shows the de-solvated sulfate within the binding cleft, except immobilised by a network of seven hydrogen bonds and with anion binding mediated exclusively by neutral peptide residues. The major difference compared to the PBP recognition site is the absence of the carboxylate side chain which prevents unfavourable electrostatic interactions from hampering the selectivity of the receptor.

1.1.5 The design of synthetic anion receptors

'*Few scientists acquainted with the chemistry of biological systems at the molecular level can avoid being inspired…and knowing the marvels of [enzyme] specificity, must dream of designing and synthesizing simpler organic compounds that imitate working features of those naturally occurring compounds.'* – Donald J. Cram, (The Design of Molecular Hosts, Guests and Their Complexes) 1988.

1.1.5.1 General considerations

Following the striking natural anion receptors previously discussed, supramolecular architects aim to incorporate similar structural features and interaction principles into the design of less enigmatic, artificial host systems. Most prominent are their structurally-rigid and well-defined three-dimensional cavities which, ornate with judiciously-placed functional groups capable of encapsulating and interacting with the guest in a geometrically-optimal manner, serve as valuable blueprints for this pursuit. The essentials of these features have been refined by chemists into the following concepts, upon which the entirety of supramolecular chemistry is also construed:

***Complementarity*:** The concepts of the 'lock and key' and 'induced-fit' mechanisms briefly mentioned earlier are more generally encompassed by the principle of *complementarity* which states that '[in order] to complex, hosts must have binding sites which cooperatively contact and attract binding sites of guests without generating strong non-bonded repulsions'.[48] Consequently, the design of potential hosts for guests involves the geometric and stereoelectronic match of the anion, with the *size* and s*hape* of the binding cavity of its cognate host. The strength of association between the two species can be maximised with the careful selection and inclusion of non-covalent interactions, which further aids selectivity of the target guest over mismatched guests of incorrect size/shape.

***Preorganisation and the chelate/macrocyclic effects*:** based upon his observation that an enhancement in binding strength occurs when the host exists in a favourable conformation prior to guest association, Cram first introduced the concept of preorganisation in the 1980's stating that

'*the more highly hosts and guests are organised for binding and low solvation prior to their complexation, the more stable will be their complexes'*.[48] Preorganisation manifests itself in the chelate effect which refers to the enhanced thermodynamic stability of complexes containing multidentate coordination sites compared with monodentate ligands.[49,50] An elaboration of the latter, the macrocyclic effect refers to the further incorporation of these ligand donors within a cyclic framework.[51,52] The resulting increased stability of the enclosed complex compared to its acyclic counterpart is attributed to the relatively lower solvation of macrocycles, resulting in a reduced desolvation enthalpic penalty, and more favourable entropy owing to fewer degrees of freedom lost upon host-guest association. Additionally, by being more structurally well-defined and rigid, macrocycles offer better shape and size complementarity to the guest than acyclic hosts, giving rise to stronger binding enthalpies.

1.1.5.2 The supramolecular toolkit: non-covalent interactions

Other than the structural concepts of preorganisation and complementarity, the efficacy of host-guest association is largely governed by the operating intermolecular forces. Non-covalent interactions which are generally reversible and subject to thermodynamic control are commonly employed by biological receptors to aid their molecular recognition and self-assembly processes, and hence also constitute the 'toolkit' for supramolecular chemists. With the exception of electrostatic attraction between two opposite charges, non-covalent interactions tend to be much weaker than conventional covalent bonds, encompassing bond enthalpies spanning 4-200 kJ mol^{-1} as compared to 300-500 kJ mol^{-1} for covalent carbon-carbon single bonds.[53] However, when used in concert, the strength of their association can afford strong and selective binding affinities, elegantly demonstrated by the aforementioned phosphate and sulfate binding proteins (Section 1.1.4). Whilst hydrogen bonding is the most prevalent, electrostatics, coordinate bonds with Lewis acidic metal centres and Solvophobic interactions are also found. However, less frequent in nature for anion recognition are anion-pi and halogen bonding interactions. These are surveyed in greater detail below.

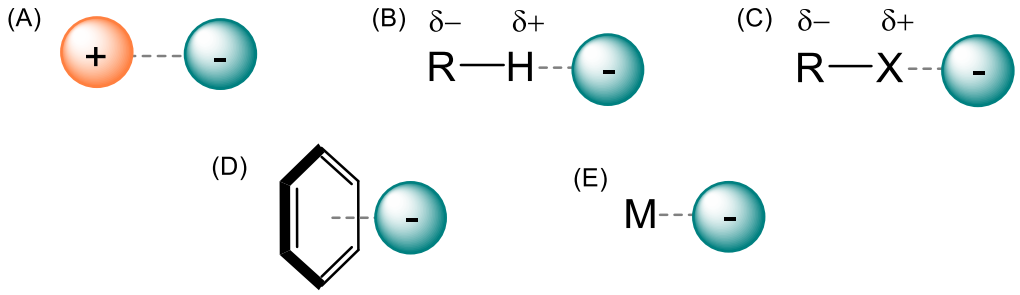


Figure 1.8: *Intermolecular interactions for anion recognition: (A) electrostatic ion-ion; (B) hydrogen bonding; (C) halogen bonding; (D) anion-π interactions; (E) coordinate bonds. (R = electronegative atom or electron withdrawing group, X= Br, I, M = Lewis acidic metal cation or main-group element).*

Coulombic forces: Attractive forces between opposing permanent charges constitute the basis for most non-covalent bonds in supramolecular complexes, the strongest of which are electrostatic interactions. Classified as either ion-ion, ion-dipole or dipole-dipole, their strength is dependent on the magnitude of charge and separation between the interacting species. Despite their bond strengths approaching those of covalent bonds and facilitating anion coordination in highly competitive, polar, protic solvent media, the isotropic nature of ion-ion interactions (Figure 1.8A) results in non-directionality and unselective binding. Contrastingly, ion-dipole interactions (which include hydrogen and halogen bonding) and dipole-dipole interactions, whilst individually weaker than the former, display pronounced directionality as the strength of interaction is maximised according to the relative orientation of the dipole.[54] Accordingly, they are widely employed in receptors designed to exhibit selectivity for an anionic guest by means of its discrete geometry.

Hydrogen bonding (HB): Given its ubiquity in Nature's fundamental biological processes, for example DNA base pairing and subsequent stabilisation of the DNA helical structure (Figure 1.9), hydrogen bonding (HB) is considered to be the 'master key' of molecular recognition.[55] Arising from the interaction of a hydrogen atom covalently attached to a more electronegative atom (*e.g.* C, N, O, F) with a neighbouring dipole or anion (Figure 1.8B), the hydrogen bond is considered primarily electrostatic in nature, with polarisation, dispersion and charge-transfer playing small but significant contributions.[56] Whilst its strengths can vary dramatically depending on the interacting system (from 1 kJ mol^{-1} in $CH_4 \cdots$F-CH_3[57] to 162 kJ mol^{-1} in HF_2^-)[58], the linearity of HB also directly

affects the strength of interaction. Strong hydrogen bonds tend to exhibit a higher degree of linearity than weak ones, with the latter displaying a large range of possible A-H···:B bond angles. Consequently, their strength and directionality, coupled with the plethora of readily-accessible donor motifs of hydrogen bonds makes them the most important and widely exploited instruments for artificial molecular recognition especially with anions.

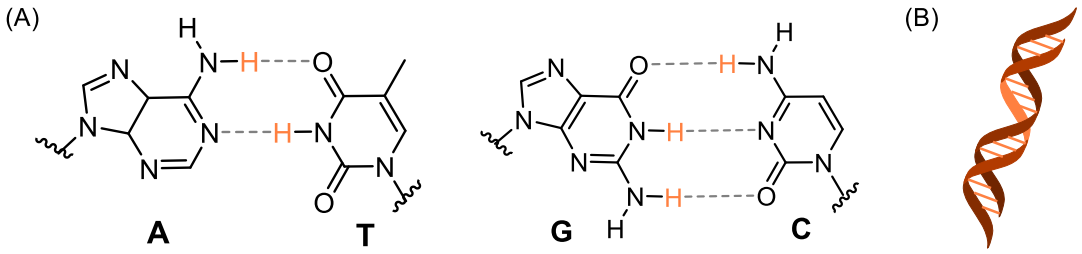


Figure 1.9: *(A) Traditional Watson-Crick pairing of DNA bases via hydrogen bonding; (B) pairing of DNA bases via hydrogen bonds.*

Halogen bonding (XB): Closely related to the analogous hydrogen bond, except with a halogen *in lieu* of the hydrogen atom (Figure 1.8C), halogen bonding exists, perhaps, as the most fully-fledged subset of the family of σ-hole (groups 14-17) interactions.[59,60] Defined by IUPAC to occur when '*there is evidence of a net attractive interaction between an electrophilic region associated with a halogen atom in a molecular entity and a nucleophilic region in another, or same, molecular entity*',[61] halogen bonding (XB) was identified by Guthrie in the latter part of the 19th century,[62] and subsequently demonstrated crystallographically in the 1950's by Hassel.[63–66] However it was not until 1983, following the reports of Dumas *et al.*, that the term 'halogen bond' was fully incorporated into the chemist's vernacular.[67]

Although counterintuitive for an electronegative halogen atom (X) to possess an electrophilic region, its electron density can become anisotropically distributed when covalently bound to an electron-withdrawing R-group, developing an equatorial belt of negative electrostatic potential and a region of partial positive charge diametrically opposite to the R-X bond, termed the 'σ-hole' (Figure 1.10).[68] The latter is capable of interacting with electron-rich Lewis bases (B, both neutral and anionic) in a highly linear manner, with electrostatics, charge-transfer and dispersion

components all thought to play significant roles in the association.[69] As is the general case for σ-hole donors, heavier, more polarisable atoms in the order F < Cl < Br < I, serve as better XB donors, with typical interaction energies spanning 5-180 kJ mol^{-1} – broadly similar to those of hydrogen bonds.[70] The strength of binding can be further maximised by increasing the electron-withdrawing nature of the R-group and/or varying the *sp*-hybridisation in the order C(sp^3)-X < C(sp^2)-X < C(*sp*)-X. This, coupled with the extremely directional nature of halogen bonds, advantageously affords an impressive degree of tunability and selectivity to the resultant R-X···B interaction.[71]

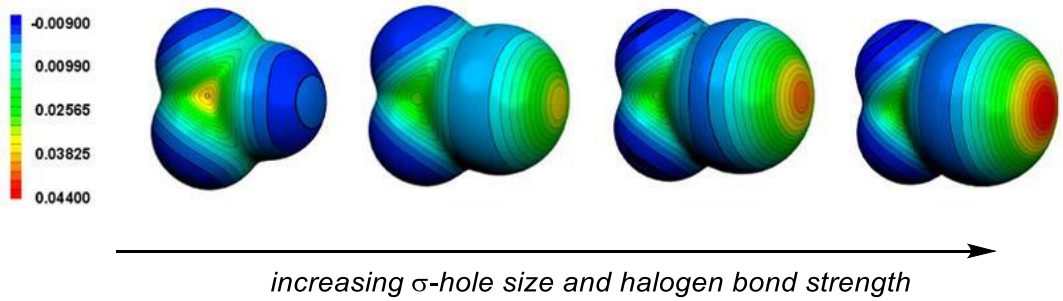


Figure 1.10: *Molecular electrostatic potential, in hartrees, at the 0.001 e/bohr^3 isodensity surface of CF_3X (from left to right, X = F, Cl, Br, I) showing the σ-hole as the region of positive potential (red).*[68]

Whilst the diktat of stringent linearity has enabled XB to be studied extensively for solid state crystal engineering purposes (Figure 1.11A)[72,73] and led to numerous applications in solid-state functional materials,[74,75] the potential of solution-phase XB has only lately been explored with seminal reports of application in catalysis,[76–78] self-assembly,[79–81] gelation[82,83] and medicinal chemistry[84] surfacing in the last decade. For example, Li recently reported a conjugated triazole foldamer capable of binding a tridentate, neutral organoiodine species in $CDCl_3$ *via* multiple N···I XB interactions (Figure 1.11B).[85] Additionally, although XB has not generally been part of the biologist's lexicon, studies highlighting its stabilising effects within protein-ligand complexes has engendered the use of polyhalogenated compounds in rational drug design.[86,87] Halogenation of the integrin-α4β1 inhibitor shown in Figure 1.11C led to optimised receptorial fitting and hence an enhancement in the drug binding affinity *via* a XB interaction to a backbone carbonyl oxygen atom within the binding cleft of the protein.[88] In the realm of anion recognition, Resnati and Metrangolo's

seminal report of a neutral XB heteroditopic receptor for NaI (Figure 1.11D) in 2005 launched a flurry of research into the area;[89] dramatic advances in the exploitation of XB in anion receptors have since been made which are discussed in Section 1.2.5.

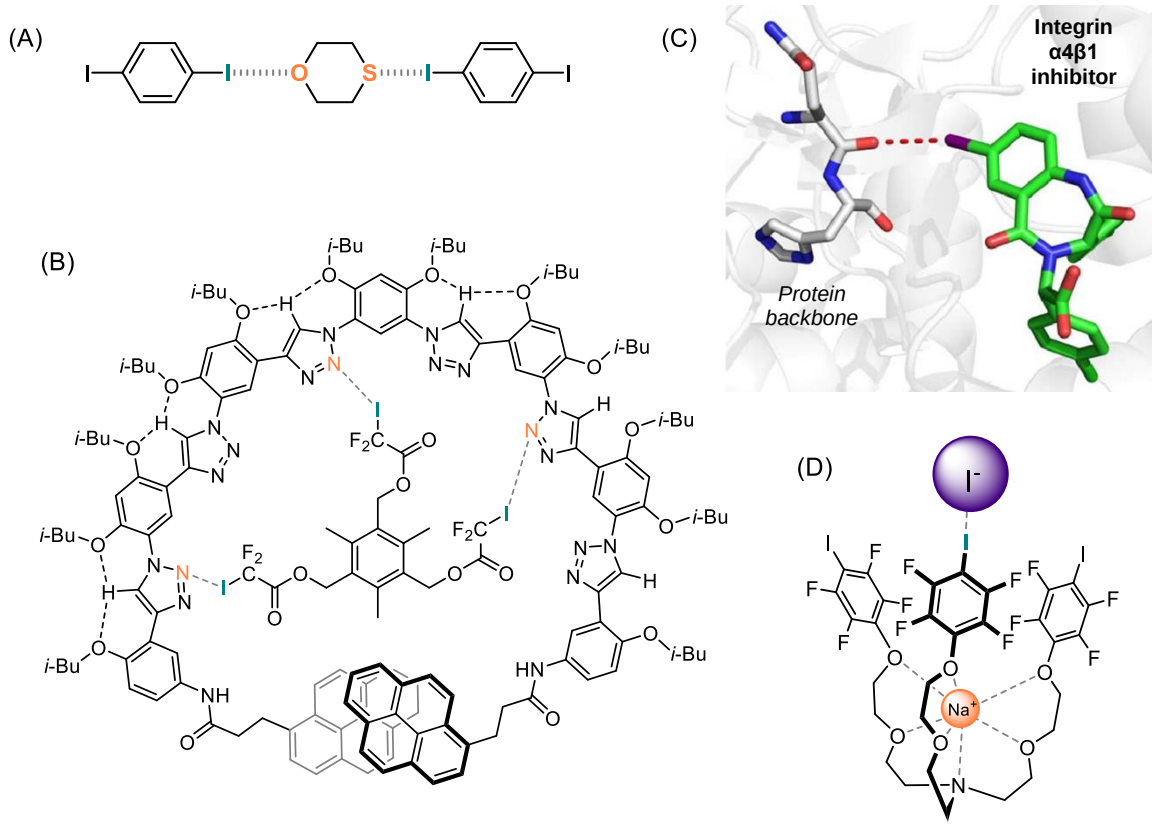


Figure 1.11: *(A) XB in the solid state;[72] (B) Li's XB-directed foldamer;[85] (C) the integrin –α4β41 inhibitor which forms a XB (red dashed line) to a protein backbone carbonyl oxygen atom;[88] (D) Resnati's heteroditopic receptor for NaI.[89]*

Anion-π interaction: Defined as the attractive interaction between an anion and electron-deficient aromatic surface (Figure 1.8D), the term 'anion-π' can be nominally misleading as the π electrons do not directly interact with the anion. Rather, it is the electrostatic interaction between the anion and *either* the anion-induced polarisation of the delocalised aromatic electron density or the inherent aromatic dipole which are responsible. Coined by Deyà in 2002,[90] anion-π interactions represent a relatively nascent and underexploited class of interactions for anion recognition which have been more widely studied in the solid and gas phases than in solution. X-ray crystallographic studies have revealed the multiple hapticities of the interaction,[91,92] where the anion can reside in various loci above the centroid of an aromatic ring system (Figure 1.12A). Indeed, the interaction energies

display little variation when the position of the anion is changed within the *xy*-plane but decrease significantly with increasing distance from the ring along the *z*-plane.[93,94] More recently, they have found functional relevance in biomimetic anion transport and catalysis. For example Mareda and Matile have reported anion-π interactions between halides and a series of naphthalenediimide derivatives and demonstrated the ability of such compounds to transport anions across bilayer membranes (Figure 1.12B).[95] However, owing to their relative weakness in solution (with energies of 20-70 kJ mol^{-1}), anion-π interactions are often employed to supplement additional (usually stronger) non-covalent interactions and hence are utilised in aprotic, weakly competitive solvents. This strategy is evident in Johnson's acyclic receptor (Figure 1.12C) where chloride binding to the sulphonamide motif was enhanced by an anion-π interaction with the electron-deficient perfluorinated aromatic ring in $CDCl_3$.[96]

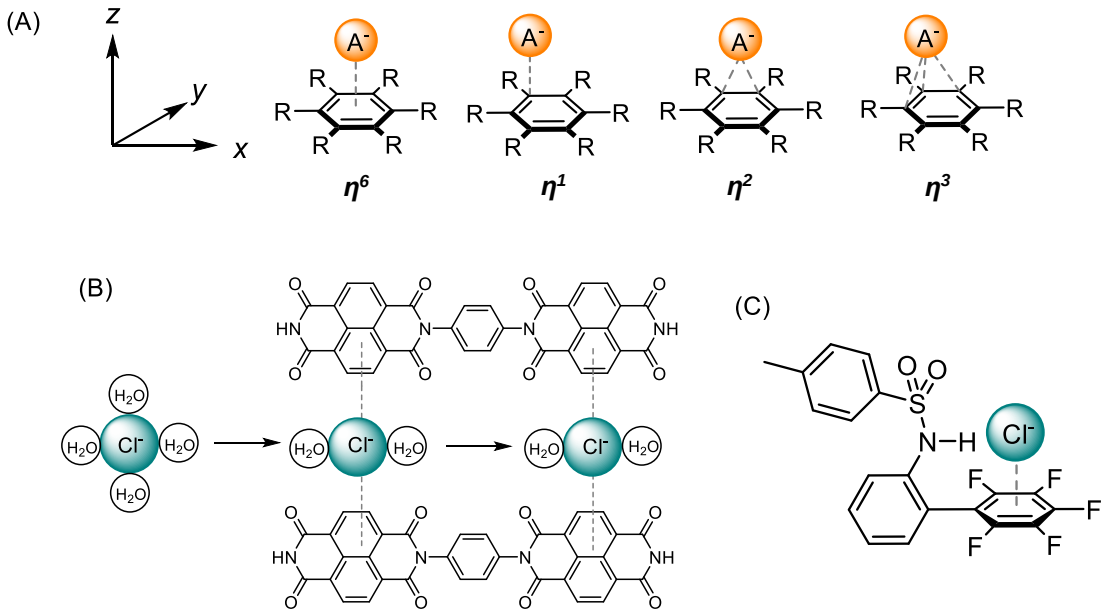


Figure 1.12: *(A) Hapticity of anion-π interactions; (B) Matile's anion-π slides for transmembrane transport;[95] (C) Johnson's acyclic receptor.[96]*

Coordinate bonds: Whilst Lewis acid-base interactions (encompassing metal-ligand coordination) lie beyond the realm of non-covalent interactions due to the significant degree of orbital overlap involved, supramolecular systems often profit from their use. The lability and reversibility of coordinate bonds are reminiscent of the characteristics of non-covalent interactions and hence they

enjoy frequent application in the formation of strong host-guest complexes, self-assembled systems and in the construction of higher order supramolecular architectures, particularly where the specific coordination geometries of metal ions are concerned.[97,98] Lewis-acidic motifs such as main group elements (boron, silicon, tin and antimony), transition metal cations (Zn^{2+}, Ni^{2+} and Cu^{2+}) as well as lanthanide cations are commonly employed to form coordinate bonds to the anion guest. For instance, Gabbaï's recently reported neutral bidentate antimony(V)-containing receptor selectively binds fluoride over other anions in water *via* coordinate bonds between both Sb centres (Figure 1.13); which is most impressive given the anion's extreme hydration enthalpy.[99]

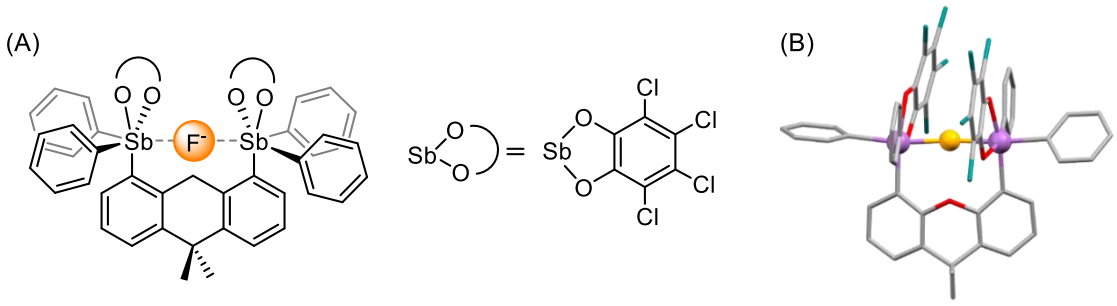


Figure 1.13: *(A) Gabbai's bidentate antimony (V) receptor for F^- and (B) the corresponding solid state adduct.* [99]

Solvophobic interactions: The preferential aggregation of apolar molecules driven by their weak interaction with vicinal polar solvent molecules is termed the 'solvophobic effect' and when in an aqueous environment, referred to as the 'hydrophobic effect'. Whilst the latter phenomenon is still poorly understood, hydrophobic effects are known to play pivotal roles in many biochemical processes, for example, the tertiary structure of proteins in aqueous solution depends critically upon interactions between apolar moieties. The 'classical' hydrophobic effect is entropically driven due to the release of highly-ordered water molecules from the hydration shells of the host and guest during their association,[100,101] whereas the 'non-classical' hydrophobic effect brings forth a dominant enthalpic term arising from the liberation of high-energy water molecules from the receptor (upon guest association), forming stronger and more cohesive hydrogen bonding networks with the bulk water solution than when encapsulated.[102,103] Although under-developed, exploitation of the hydrophobic effect for anion recognition in aqueous solution has lately witnessed many

successes, with host molecules characteristically employing deep hydrophobic cavities capable of shielding often charge-diffuse, poorly-hydrated anions from the ambient solvent. Nau reported the strong binding of a dodecaborate cluster ($B_{12}Br_{12}^{2-}$) within the cavity of a large-ring cyclodextrin (LRCD) δ-CD in pure water (K_a = 2600 M^{-1}) (Figure 1.14A)[104] while Gibb's 'octa-acid cavitand' displayed significant affinity for the usually non-coordinating PF_6^- anion (K_a = 790 M^{-1}) in phosphate buffer at pH 11.3 – a seemingly counterintuitive feat, given the host's polyanionic character (Figure 1.14B).[105] Notably, the marked enthalpic gains and entropic losses in both systems indicated significant structure recovery in bulk water (arising from the reformation of hydrogen bonds in the bulk solution upon anion complexation) and hence are excellent demonstrations of the 'non-classical' hydrophobic effect in play.

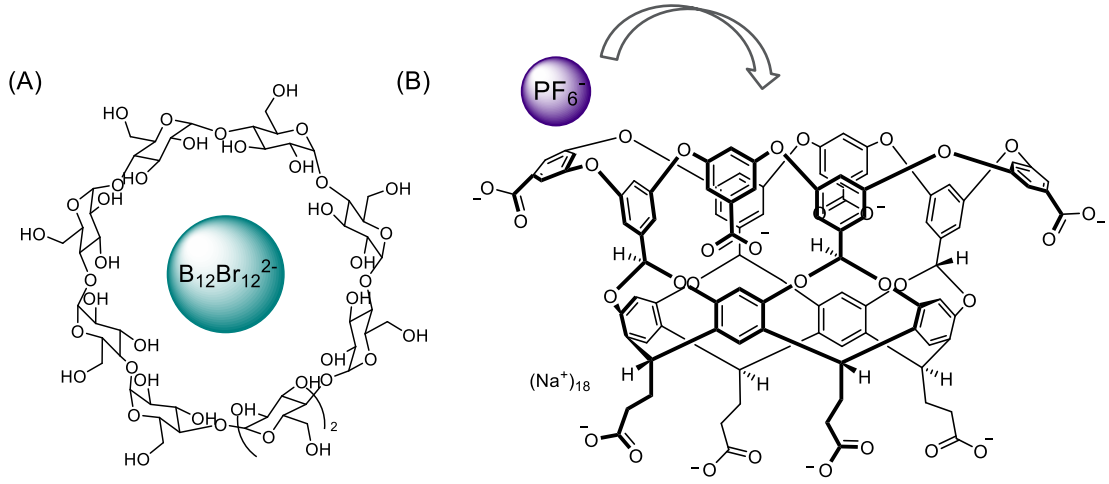


Figure 1.14: *(A) Nau's δ-CD capable of $B_{12}Br_{12}^{2-}$ cluster encapsulation;[104] (B) Gibb's octa-acid cavitand.[105]*

1.2 Synthetic receptors for anion recognition and sensing

1.2.1 Overview of modern synthetic anion receptors

Following the aforementioned design principles alongside the library of non-covalent interactions at the disposal of the synthetic chemist (Section 1.1.5.2), a multitude of artificial anion hosts varying in structural complexities have been prepared over the years which can be trifurcated as cationic, neutral and Lewis acidic. Whilst cationic receptors, in form of a series of *katapinate* hosts utilising solely electrostatics and hydrogen bonding birthed anion receptor chemistry (see Section 1.1, Figure 1.1D), contemporary receptors embrace the full spectrum of supramolecular forces available. Recently, there has been a marked rise in the proportion of systems incorporating non-classical non-covalent forces such as σ-hole interactions[60] and in particular XB (the focal interaction in this thesis), to exploit their unique properties which complement those of classical hydrogen bonding analogues. Thus, in addition to surveying prominent hydrogen bonding and Lewis-acidic anion-coordinating motifs, the forthcoming section importantly sheds light on the advancements in XB anion receptor design. Due to the increase in shift towards receptors capable of functioning under 'real-world' conditions, the development of hosts capable of performing in pure water or competitive aqueous organic solvent media is also highlighted. Finally, the development of receptors that produce a macroscopic, detectable response upon anion binding, known as anion *sensors* are further discussed.

1.2.2 Cationic receptors

Historically, anion recognition has primarily been the domain of positively charged hosts, which by their intrinsic nature, are advantageously able to function in highly competitive polar, protic solvent media. The principle disadvantage of such receptors however, is their reliance upon omni-directional electrostatic interactions which may impair anion selectivity; hence they are often supplemented with more discriminative hydrogen bonding interactions. Accordingly, a variety of cationic motifs including ammonium, guanidinium, imidazolium and triazolium functionalities have been incorporated into host frameworks as detailed below.

- **Protonated amine, quaternary ammonium- and guanidinium-based receptors**

Following Park and Simmons' original work in which a series of polyammonium cages were demonstrated to encapsulate halide ions in aqueous TFA solution *via* electrostatics and hydrogen bonding (Section 1.1, Figure 1.1D),[16] the literature has since been coloured with reports of many other highly-charged polyammonium based receptors. Lehn and co-workers notably developed a range of macrocyclic and macrobicyclic polyammonium hosts capable of anion recognition in highly competitive aqueous solvent mixtures. The receptor depicted in Figure 1.15A selectively bound azide with high affinity (log K_a = 4.6 in H_2O, pH 5) due to geometric complementarity between the linear guest and the host's ellipsoidal binding cavity,[106,107] whereas the protonated octaazacryptand in Figure 1.15B better accommodated fluoride in acidic media (log K_a = 10.6 in H_2O) by virtue of its smaller size.[108,109] Recently, Bencini and co-workers reported a bis-triazacyclononane based polyammonium receptor capable of the impressive enantiomeric recognition and sensing of the tartrate anion in aqueous buffer (Figure 1.15C),[110] exhibiting over a three-fold selectivity for (*S*,*S*)-tartrate (log*K* = 6.1 in 0.1M TRIS buffer at pH 7) over its (*R*,*R*)-enantiomer by means of the modulated emission from the host's integrated (*S*)- 1,1'-bi-2-naphthol (BINOL) fluorophore. In view of the largely pH dependent function and efficacies of these protonated hosts, Schmidtchen pioneered a series of macrotricyclic quaternary ammonium receptors capable of halide and oxoanion encapsulation in pure water (Figure 1.15D).[111,112] Whilst quaternisation of the amine apices negates the influence of the hydrogen bond donors and results in a purely electrostatic interaction that inevitably leads to a diminished anion binding affinity, importantly the overall charge of the host remains independent of pH, with the advantageous result that anion binding is not confined to highly acidic media.

One concern with charged receptors in general, is that they inexorably possess a counter-anion which may contest the target guest for the binding site. Thus, to minimise any effects of competitive association, relatively non-coordinating anions such as hexafluorophosphate, perchlorate or nitrate are often utilised. Adopting a holistic approach, Schmidtchen further prepared electroneutral zwitterionic quaternary ammonium cages (Figure 1.15D) with negatively-charged borate and

carboxylate moieties appended on the periphery.[113,114] The resultant hosts displayed marked enhancements in halide binding in water, when compared to the cationic equivalents which possessed competing counter-anions.

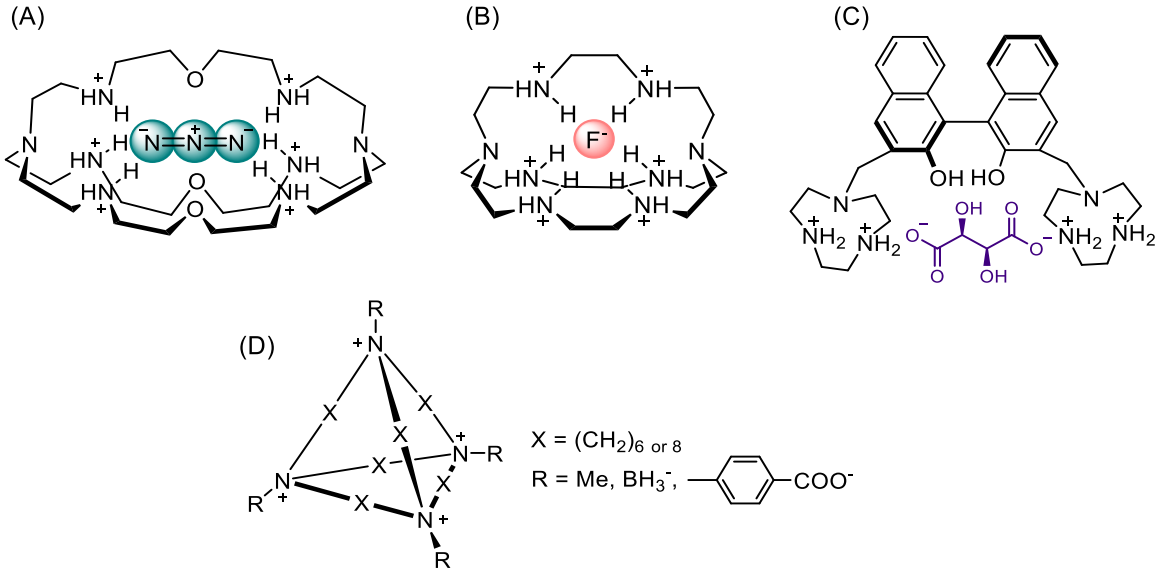


Figure 1.15: *Polyammonium-based anion receptors. Lehn's hexaprotonated macrobicyclic polyammonium hosts (A) azide-selective ellipsoidal receptor;[106,107] (B) fluoride-selective octaazacryptand;[108,109] (C) Bencini's (S)-BINOL based polyammonium receptor;[110] (D) Schmidtchen's tetrahedral polyammonium cages and zwitterionic analogues.[111–114]*

Previously evidenced in the arginine residue of the PBP (see Section 1.1.4) and prevalent in enzymes such as carboxypeptidase-A,[115] the naturally occurring guanidinium anion-binding motif has been widely incorporated into a variety of synthetic host systems. In light of its highly basic nature (pK_a ~ 13.6) which permits it to remain functional over a large pH window,[116] and characteristic planar Y-shaped geometry offering two parallel N-H hydrogen bond donor sites, the guanidinium moiety is well-equipped for strong interaction with oxoanions. Consequently, it has been extensively studied in the context of phosphate recognition (*vida infra*).[117–119] Whilst Lehn's early macrocyclic examples initially demonstrated poor anion binding (Figure 1.16A)[120], partially attributed to the inherent flexibility of guanidinium, enhancement in anion recognition was achieved *via* constraining the motif into cyclic structures of greater rigidity (Figure 1.16B)[121] or through augmenting the interaction with supplementary hydrogen bond donor functionalities. Exemplary of the latter, Schmuck described a tridentate guanidiniocarbonyl-pyrrole 'molecular flytrap' (Figure

1.16C) capable of binding citrate with high affinity ($K_a > 10^5$ M^{-1}) and other tricarboxylates in pure water.[122]

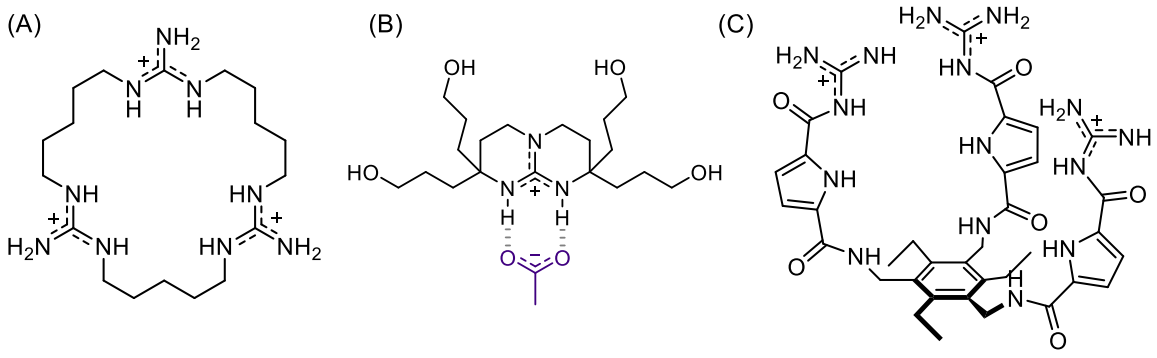


Figure 1.16: *Guanidinium-based anion receptors. (A) Lehn's tris-guanidinium macrocycle;[120] (B) Schmidtchen's pre-organised bi-cyclic guanidinium;[121] (C) Schmuck's tridentate guanidinio-carbonylpyrrole citrate receptor.[122]*

- **Imidazolium-based receptors**

Originally demonstrated to form hydrogen bonds with halides in solution in the field of ionic liquids, the imidazolium moiety combines electrostatic and C-H···A^- interactions to promote anion recognition. Since Sato[123] and Alcalde's[124] seminal reports in 1999, which detailed the ability of imidazolium-based receptors to bind anions with great affinity, it has since been fervently incorporated into the structural frameworks of various host systems. Notably, Sato's preorganised tris-imidazolium appended tripodal receptor (Figure 1.17A) strongly bound halide anions in CD_3CN *via* convergent charge-assisted hydrogen bonds, whilst Alcade's family of 'imidazoliophane' macrocycles (Figure 1.17B) recognised a variety of anions in the order $H_2PO_4^-$ > F^- > OAc^- > CN^- > Cl^- in d_6-DMSO. Sessler and co-workers recently described a tetracationic macrocyclic receptor termed the 'Texas-sized' molecular box (Figure 1.17C), which was comprised of two pyridine bis-imidazolium subunits and demonstrated to bind mono- and di-terephthalate (K_a = 2.1 x 10^3 M^{-1} and 3.3 x 10^3 M^{-1} respectively) in d_6-DMSO through formation of a 1:1 stoichiometric complex.[125] Related systems such as Kim's benzimidazolium-based cyclophane (Figure 1.17D) was further reported to selectively bind the biologically relevant guanosine-5′-15 triphosphate and iodide anions, in aqueous solution at physiological pH.[126]

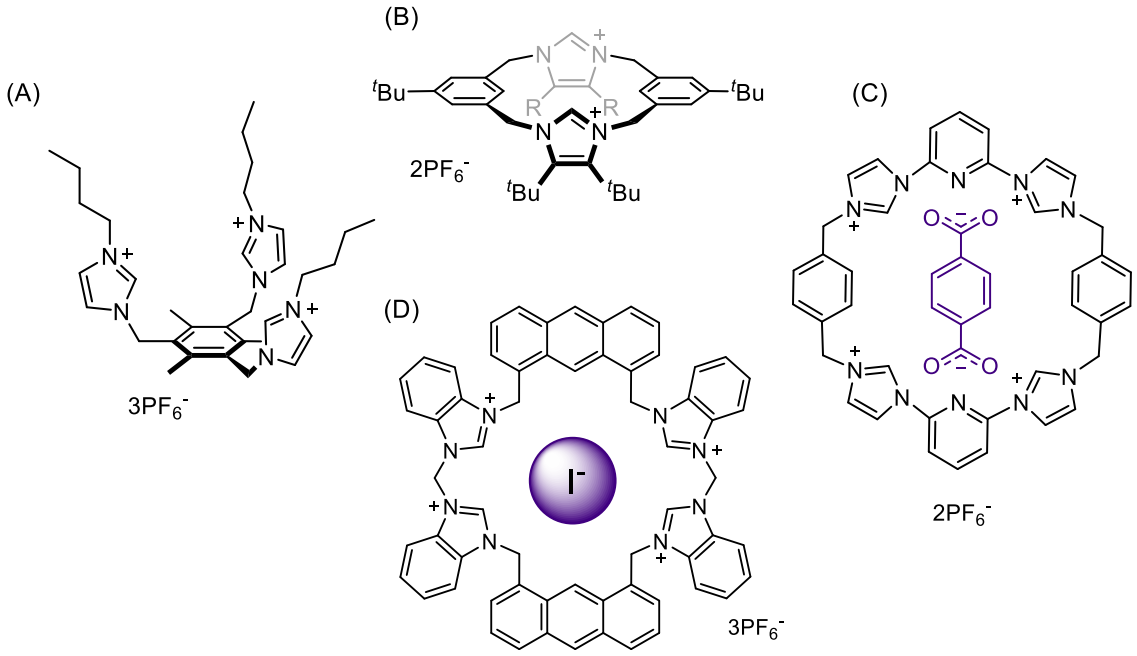


Figure 1.17: *Imidazolium-based anion receptors. (a) Sato[123] and (b) Alcalde's seminal hosts;[124] (c) Sessler's 'Texas-sized' molecular box capable of capable of carboxylate recognition;[125] (d) Kim's iodide-selective benzimidazolium-based cyclophane.[126]*

- **Triazolium-based receptors**

Similar to its imidazolium kin, the triazolium moiety also employs charge-assisted C-H hydrogen bonding to facilitate anion recognition. Following the reports of 1,2,3-triazole-based hosts (*vide infra*) and derived *via* alkylation at the N^3 junction of the latter, the anion binding properties of the resultant *triazolium* motif have been demonstrated to be much more enhanced in comparison to its neutral triazole predecessor.[127–130] Through functionalization of a *cholapod* steroidal scaffold, Kumar and Pandey prepared the first triazolium-based receptor (Figure 1.18A) which preferentially bound dihydrogen phosphate over the halides in $CDCl_3$.[131] Contrastingly, their subsequent macrocyclic *cholaphane* analogue (Figure 1.18B) displayed a reversal of the binding trend, which was attributed to the lessened flexibility of the cyclosteroidal framework, preventing it from adopting a complementary geometry to accommodate the tetrahedral guest.[132] Schubert and co-workers also described an acyclic bis-triazolium benzene receptor, which formed an orthogonal 2:1 host-guest complex with sulfate in CD_3CN.[133] More recently, Cyclodextrin click clusters (CCCs) appended with multiple triazolium units (Figure 1.18C), as reported by Kim and co-workers have

been shown to bind polyanions such as inositol-1,4,5-triphosphate and ATP in aqueous solution, at physiological pH[134] – the presence of a severely confined, hydrophobic microenvironment to aid the recognition of structurally related organophosphonate-based molecules is particularly noteworthy, and elaborated upon in Section 1.3.

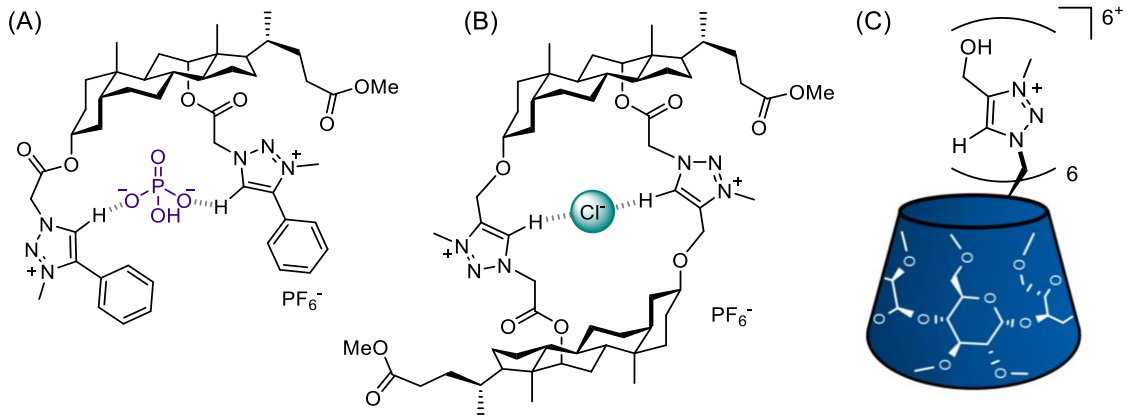


Figure 1.18: *Triazolium-based anion receptors. (A) Pandey's acyclic[131] and (B) cyclic bis-triazolium hosts;[132] (C) Kim's water-soluble β-cyclodextrin based host for biologically relevant polyanion recognition.[134]*

1.2.3 Neutral hydrogen bonding receptors

Lacking the assistance of charge *via* electrostatics, neutral hosts interact more weakly than their positively-charged analogues with anions in solution, and thus are usually confined to operating in low-polarity, organic media. Due to its directionality constraints, hydrogen bonding features as the most widely employed interaction in such hosts. Whilst the most popular motifs include amide, urea and thiourea, pyrrole and triazole functionalities, more recently, receptors containing alternate C-H hydrogen bond donor moieties have also surfaced and are expanded on below.

- **Amide-, urea- and thiourea-based receptors**

Reflecting their ubiquity in Nature's delicate protein-folding and molecular recognition processes, polarised N-H hydrogen bond donors have been widely employed as a universal ligation tool in a range of synthetic anion receptors. Amides were first incorporated into neutral host design by Pascal *et al.* in 1986, who demonstrated evidence for fluoride binding in d_6-DMSO by a tris-amide cyclophane.[135] However, it was Crabtree's later report of the isophthalamide moiety to complex

halides through simple non-preorganised acyclic receptors,[136] which propelled research efforts into the integration of this and other related motifs such as ureas and thioureas, into a variety of host structures. As alluded to earlier, a major caveat of neutral hydrogen bonding interactions, is their attenuated function in protic solvents - thus whilst there is an abundance of amido-receptors in the literature,[137] few examples exist capable of operating in aqueous solutions. Salient exceptions include Gale's macrocyclic amidourea host (Figure 1.19A) which binds acetate with high affinity in a d_6-DMSO/ D_2O 95:5 *v/v* mixture (K_a = 5170 M^{-1})[138] and Reinhoudt's saccharide-thiourea functionalised cavitand (Figure 1.19B) which exhibits chloride selectivity in a 1:1 MeCN/water solution (K_a = 250 M^{-1}).[139] Seminal contributions are further found in the works of Kubik who prepared a series of cyclic pseudo-peptide hosts *via* the integration of alternating aromatic and L-proline residues.[140] The bridged variant shown in Figure 1.19C displayed remarkable binding of sulfate (log K_a = 3.7) and iodide (log K_a = 3.96) in D_2O/ CD_3OD 95:5 *v/v* through a combination of convergent amide-NH hydrogen bonding and solvophobic interactions, resulting in the highly cooperative encapsulation of the guest between two cyclopeptides likened to a 'molecular oyster'.

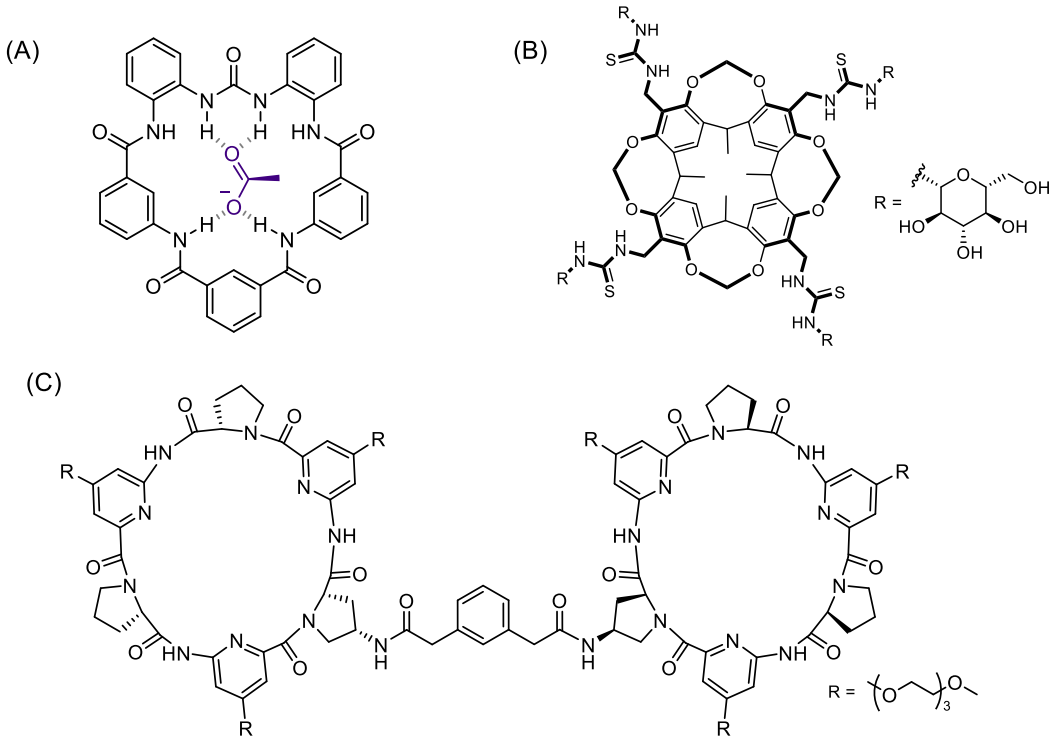


Figure 1.19: *Neutral amide and thiourea-based receptors capable of anion recognition in aqueous solution. (A) Gale's amide-urea macrocycle ;[138] (B) Reinhoudt's saccharide-thiourea functionalised cavitand;[139] (C) Kubik's water-soluble 'molecular oyster'[140]*

- **Pyrrole-based receptors**

Following the discovery of the anion binding properties of protonated sapphyrins (pentapyrrolic expanded porphyrins),[141] and influenced by the sulfate binding ability of the Trp residue in Nature's SBP[47] (*vide supra*), pyrrole has since been venerated as a robust N-H hydrogen bond donor motif whose attraction, in part, lies in its inability to self-associate. In contrast to the aforementioned amido- and urea entities which may do so *via* C=O···H-N interactions, the inherent lack of a hydrogen bond-acceptor functionality precludes pyrrolic systems from undergoing such processes which can compete alongside the anion. Nor, by itself, is it particularly acidic or basic, lending its use to a variety of conditions. Whilst it has been incorporated into a multitude of anion host frameworks,[142] the most distinguished class of macrocyclic pyrrole derivatives exist in the form of calix[4]pyrroles, which adopt a 'cone' conformation (with all four pyrroles participating in linear N-H···A^- hydrogen bonds) upon anion complexation.[143] Pioneered by Sessler, they are known to exhibit preferential binding of the smaller halides in polar organic solvents,[142,144] and when fashioned into more constrained 'strapped' architectures, shown to dramatically enhance anion binding. Indeed, Sessler's 'pyrrole-strapped' receptor (Figure 1.20A) demonstrated an up to 100-fold enhancement in chloride binding relative to the parent homologue in CH_3CN.[145]

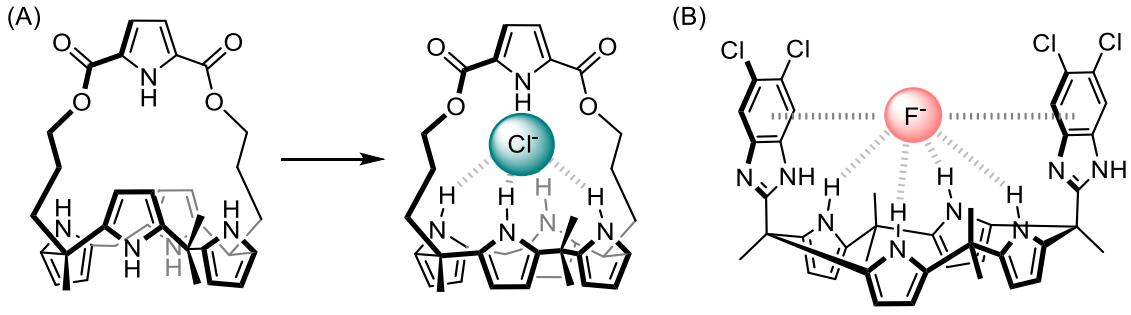


Figure 1.20: *Pyrrole-based receptors. (A) Sessler's pyrrole-strapped calix[4]pyrrole with basal pyrrole's adopting a cone conformation when binding to chloride;[145] (B) Lee's 'picket' calix[4]pyrrole cis-isomer.[147]*

Juxtapose to the 'strapping' method and given previous reports detailing the superior anion binding abilities of the *cis*-isomer of *meso*-disubstituted calix[4]pyrroles in comparison to its *trans*-counterpart,[146] Lee and co-workers recently reported a 'picket' calix[4]pyrrole isomer with two

diametrically opposed benzimidazole side-arms suspended above the core unit (Figure 1.20B).[147] The *cis*-isomer featuring hydrogen-bonding in concert with anion-pi interactions of the benzimidazole appendages resulted in the enhanced affinity for fluoride (K_a = 1.81 x 10^6 M^{-1} in CH_3CN), when compared to the parent system with no side-arms.

- **Triazole-based receptors**

Previously considered as auxiliaries in supplementing other stronger hydrogen bonding interactions, potent C-H hydrogen bond donors have become established for anion recognition, particularly in the form of 1,2,3-triazole groups. The highly polarised C^5-H bond, which arises due to the electron withdrawing nature of the sp^2-hybridised carbon and the three, contiguous, heterocyclic nitrogen atoms, presents triazole as a motif well-suited to anion coordination. Additionally, its popular use can be attributed to its facile synthesis *via* the Huisgen copper(I)-mediated azide–alkyne cycloaddition (CuAAC) reaction, which tolerates a substantial range of conditions and functionalities.[148–150] Following the communications of Meudtner and Hecht[151] and Craig[152] in 2008 where poly-triazole foldamers were demonstrated to exhibit a helical inversion upon binding of an achiral halide anion in 75% H_2O:CH_3CN, and helical folding (Figure 1.21A) from an open conformation in response to chloride in d_6-acetone respectively, triazoles have been incorporated into the frameworks of various anion receptors.[153]

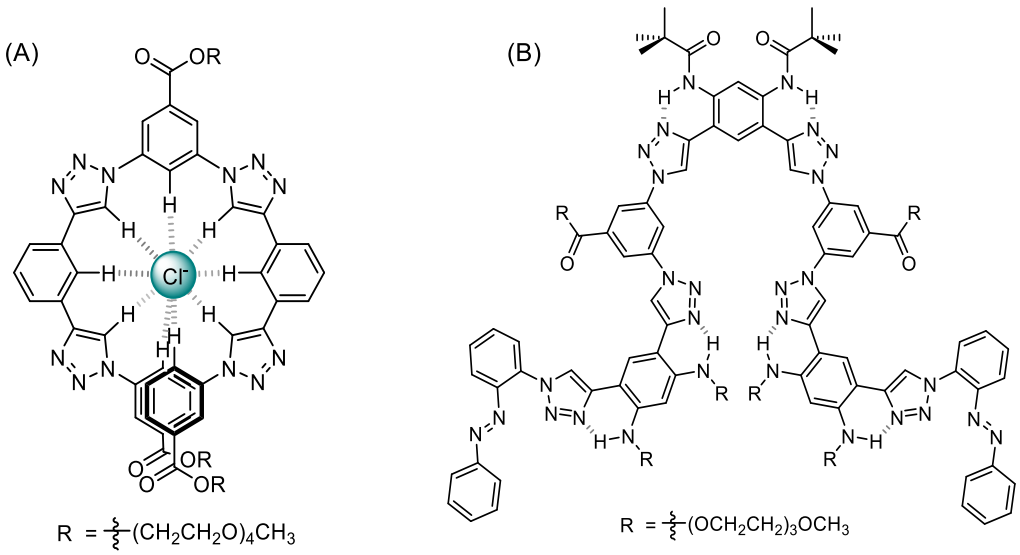


Figure 1.21: *Triazole-based receptors. (A) Craig's[152] and (B) Flood's poly-triazole foldamers.[154]*

Flood recently reported a preorganised polytriazole foldamer (Figure 1.21B) capable of functioning in CH_3CN/ H_2O 1:1 *v/v* solution.[154] Upon the addition of chloride, the formation of a double helical complex of 2:1 host:guest stoichiometry was observed with approximately 80% of the receptor's π-surfaces buried. Termed as a 'hydrophobic collapse', the conformational change shielded the bound halide from the organic-aqueous milieu, giving rise to a microenvironment favorable for chloride binding *via* multiple C-H triazole bonds.

- **Alternate C-H donor-based receptors**

Derived from the Latin term '*campester*' meaning 'flat' and characterised by their planar, highly-symmetric and shape-persistent form, *campestarenes* constitute a nascent class of neutral macrocyclic hosts comprised of (*n*) conjugated arene subunits which utilise an alternative C-H hydrogen bond-donor motif for anion binding – specifically, (*n*) Ar-H protons directed towards the central cavity of the macrocycle.[155,156] Eminent in the reports of Flood, the C_5-symmetric 'cyanostar' (Figure 1.22A) composed of repeating cyanostilbene monomers has been demonstrated to form 2:1 host-guest complexes with large anions (PF_6^- and ClO_4^- in CH_3OH/ CH_2Cl_2 4:6 *v/v*) through a sandwich arrangement of the two stacked macrocycles and *via* convergent hydrogen bonding interactions between them.[157] Most recently, an unprecedented tetrameric co-assembly of cyanostar was found to be threaded by a phosphate trimer in CD_2Cl_2 (Figure 1.22B).[158] Whilst phosphate oligomerisation has been evidenced in solution,[159,160] even without receptors and previously modelled in acetonitrile only as a simple monomer-dimer equilibrium (K_{dimer} = 2400 M^{-1}),[161] such complexation of multiple phosphates is rare. The unique 4:3 host-guest stoichiometry observed represents the first experimental evidence of solution-phase anion trimer encapsulation, where the stabilisation of the latter *via* multiple convergent HB interactions decorating the macrocyclic cavities was able to offset the electrostatic repulsion between them.

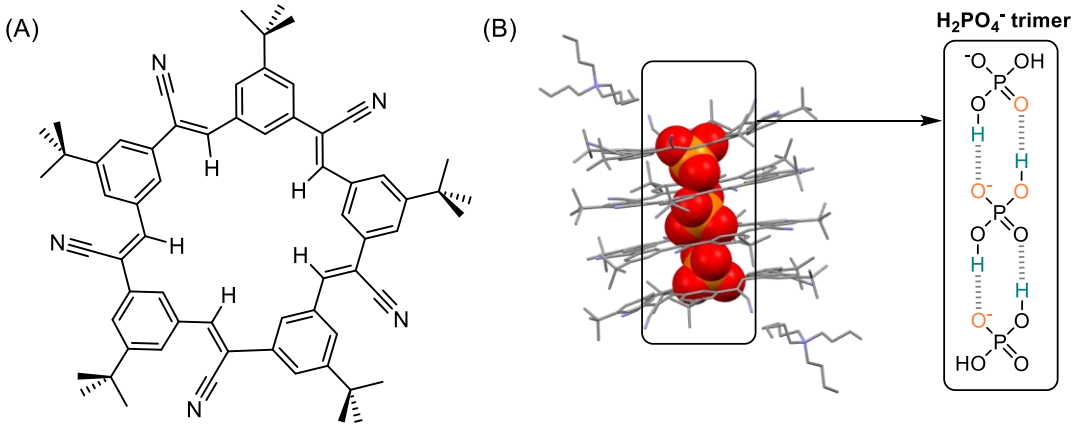


Figure 1.22: *Alternate C-H donor-based receptors. (A) Flood's cyanostar macrocycle[157] and (B) Flood's poly-triazole foldamer.[158]*

Also under the umbrella of neutral C-H hydrogen bond donors and pioneered by Sindelar and co-workers, the creatively-termed 'bambus[*n*]urils' represent a family of cyclic glycoluril oligomers shown to exhibit strong binding of the halides in organic solvents such as $CDCl_3$.[162,163] Characteristic of these macrocycles are deeply buried, electropositive interior cavities perfectly suited to form inclusion complexes with the guest anion. Given the continuous strive towards anion recognition in highly competitive aqueous environments, the authors further prepared a water-soluble analogue[164] (Figure 1.23) which displayed Hofmeister-type selectivity, impressively binding iodide and perchlorate over other inorganic anions in phosphate-buffered water (K_a = 1.0 x 10^7 and 5.5 x 10^7 M^{-1} respectively) – particularly admirable given the electrostatic repulsion between the carousel of solubilising carboxylate groups surrounding the hydrophobic cavity and the anionic guest. Moreover, thermodynamic investigations elucidated the associations as enthalpically driven. The observed complex stabilization *via* multiple C-H···A^- interactions, together with the concomitant release of high energy molecules forming superior hydrogen bonding networks in the bulk solution than when encapsulated in the binding pocket, is a neat example of the non-classical hydrophobic effect in operation (*cf.* Nau's δ-CD host and Gibb's octaacid-cavitand in Figure 1.14).

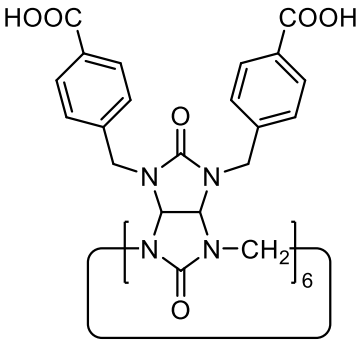


Figure 1.23: *Sindelar's water-soluble bambus[6]uril receptor.[164]*

1.2.4 Lewis acid and transition-metal based receptors

The integration of Lewis acidic fragments into a host's molecular skeleton can facilitate anion binding through various mechanisms: (1) the formation of a Lewis acid···A^- dative bond; (2) electrostatic interactions if cationic, and additionally polarising adjacent hydrogen or halogen bond donors; (3) preorganisation of the host structure for optimal anion binding and (4) operating as a non-coordinating optical or electrochemical reporter group. Following Shriver and Biallas' seminal report of the complex formed between methoxide and a bidentate boron derivative[165] and Lehn's subsequent examples of dicopper(II) cryptates,[166] a range of transition-metal and main group element Lewis acid based assemblies have been synthesised. In addition to Gabbaï's bidentate antimony(V) receptor for fluoride mentioned earlier[99] (Figure 1.13), salient metallo-hosts include Fabrizzi's dizinc(II) 'cascade complex' of a bistren cage (Figure 1.24A) capable of azide recognition in water (log K_a = 5.8, pH = 8)[167] and Reinaud's tris-pyridyl amine 'capped' Cu(II)-calix[6]arene receptor (Figure 1.24B) which exhibits an exceptionally high affinity for fluoride in water (log$K$ = 4.93, pH 6 - 7) – the association constant being the highest value known amongst monometallic systems described in the literature.[168]

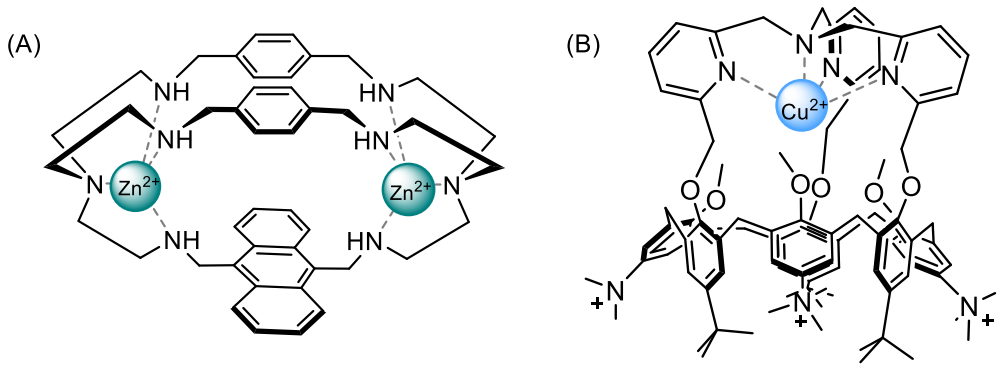


Figure 1.24: *Lewis acidic and Transition-metal based receptors. (a)Fabrizzi's diZinc(II) bistren cage;[167] (b) Reinaud's 'capped' Cu(II)-calix[6]arene.[168] (Counter-anions omitted for clarity)*

Inspired by the presence of metal cations in the binding sites of natural proteins,[169–173] transition-metal complexes of Zn(II) and Cu(II) in particular, have proved to be highly efficient receptors for oxoanion recognition in water.[174–176] These systems are discussed in more detail in Section 1.3, specifically in the context of the recognition and sensing of phosphate and its derivatives.

1.2.5 Halogen bonding (XB) receptors

The emergence of XB interactions for solution phase anion recognition was a seminal publication by Resnati and co-workers in 2005, where a heteroditopic tripodal receptor (Figure 1.11D) was demonstrated to impressively bind a NaI ion-pair, binding sodium in its polyether region and the iodide counter ion *via* a single iodoperfluoroarene mediated halogen bond (K_a = 2.6 x 10^5 M^{-1} in $CDCl_3$).[89] Since then, whilst there remains a marked disparity in the proportion of XB-donor anion hosts compared to their ubiquitous HB counterparts, a rapid expansion has occurred.[177,178] The highly directional nature of the halogen bond, coupled with the ability to tune the strength of interaction (see Section 1.1.5.2) adds to the appeal of XB-donors as versatile synthons in the design of host systems for anion recognition. Due to the formation of highly electrophilic σ-holes, the larger, more polarizable halogens (Br and I) are commonly exploited for strong XB interactions and thus feature in a variety of neutral and cationic XB-donor motifs. These can be categorised into three classes: haloperfluoroarene, haloimidazolium and halotriazole/triazolium. When used in a multivalent manner and/or in concert with other non-covalent interactions, the latter have been shown to dramatically enhance the strength and selectivity of anion binding, especially in comparison to their HB analogues and are expanded on below.

- **Neutral halogen bonding receptors**

Renowned as robust tectons in the field of solid-state crystal engineering,[179,180] electron-deficient haloperfluoroarenes have also found popular use in XB anion host systems as their facile functionalisation at any position with Br or I, enables the tuning of anion coordination geometries at will. In contrast to Resnati's divergent system where the *para*-substituted arrangement of all XB-donor atoms prevented them from cooperatively interacting with the bound iodide (Figure 1.11D), Taylor and co-workers further exploited the tripodal framework except incorporating *ortho*-substituted iodines to facilitate anion binding in a tridentate manner (Figure 1.25A).[181] The receptor displayed general selectivity for the halides ($Cl^- > Br^- > I^-$) over the oxoanions (TsO^-, HSO_4^- and NO_3^-

) in d_6-acetone, which was presumed to arise from an intrinsic preference of XB to interact with 'softer' halides over 'harder' oxoanions.

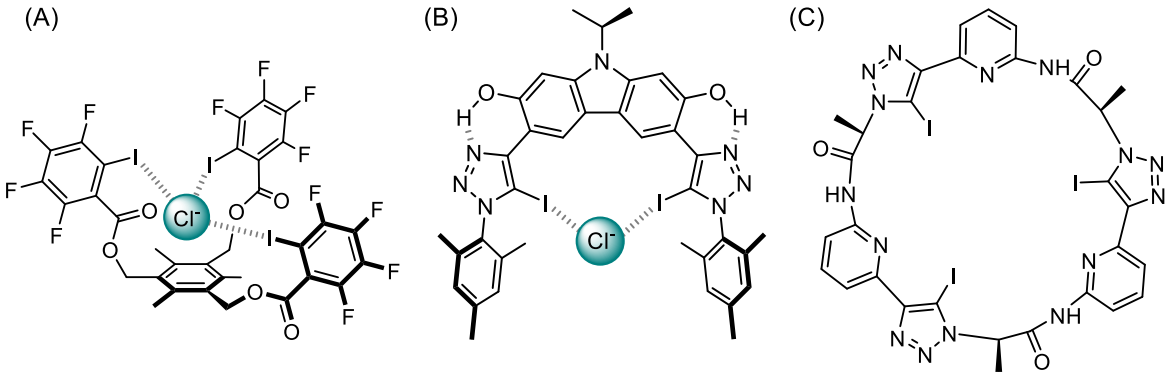


Figure 1.25: *Neutral XB receptors. (A) Taylor's tridentate iodotetrafluorobenzene host,[181] (B) Schubert's bidentate bis-iodotriazole host;[182] (C) Kubik's cyclic XB peptide.[183]*

Due to the synthetic accessibility of halotriazoles from CuAAC 'click' reactions using terminal azides and haloalkynes,[184,185] alongside Zhu's 'one-pot' iodo-variant[186], halotriazoles, specifically iodotriazoles due to their enhanced electron-withdrawing character, constitute versatile XB-donor motifs. For example, Schubert designed a pair of a cleft-type receptors (Figure 1.25B) symmetrically functionalised with XB iodotriazoles to enable bidentate coordination of halides.[182] Preorganisation of the phenolic carbazole-scaffold *via* intramolecular OH···*N*-(triazole) hydrogen bonding afforded the *syn*-s*yn* isomer, which bound chloride and bromide in THF through favourable enthalpic and entropic contributions to the binding energy, as indicated by isothermal titration calorimetry (ITC) measurements. In contrast, the phenol-lacking analogue exhibited reduced anion binding affinities due to the greater entropic penalty associated with the formation of the receptor-halide complex. Recently, Kubik and co-workers have reported the first example of a neutral macrocyclic pseudopeptide host decorated with three iodotriazoles (Figure 1.25C), which exhibited stronger halide binding than the HB analogue in 2.5% H_2O/ DMSO.[183]

- **Cationic halogen bonding receptors**

Akin to cationic HB receptors, the use of positive charge is often the prevailing strategy to increase the potency of XB hosts. Theoretical and experimental studies have demonstrated the halotriazolium motif to be a stronger XB donor than its charge neutral iodotriazole analogue,[187–189] due to the combined effects of greater C-X bond polarisation and charge-assistance. The latter also advantageously allows for binding in highly competitive solvent systems and has recently enabled the recognition of biologically and environmentally relevant anions. Beer's bis-iodotriazolium receptor (Figure 1.26A), rendered water-soluble *via* the attachment of tetra(ethylene glycol) substituents, was used to probe XB-driven anion recognition processes in aqueous solution.[190] Anion selectivity followed a Hofmeister bias in D_2O ($I^- > Br^- > Cl^-$), correlating with the relative ease of desolvation of the heavier halides. Impressively, the receptor also exhibited superior binding of perrhenate (an innocuous surrogate for the environmental pollutant pertechnetate) (K_a = 44 M^{-1} in D_2O), in contrast to the HB analogue which displayed no appreciable binding affinity. Additionally, in the first example of the application of XB interactions for enantioselective anion recognition, the authors further reported a (*S*)-BINOL receptor appended with two convergent iodotriazoliums (Figure 1.26B).[191] The latter was shown to recognise a range of chiral amino acid carboxylates and BINOL-phosphate anions with higher affinities and enhanced enantioselectivities compared to the bis-prototriazolium HB analogue in CD_3CN/ D_2O 99:1 *v/v*.

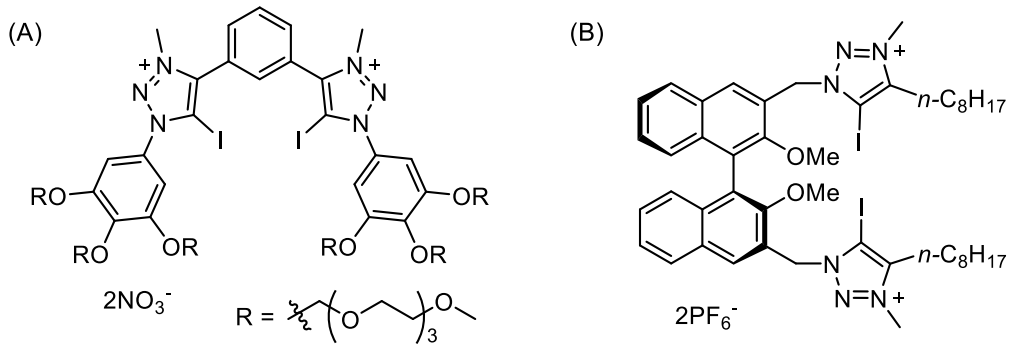


Figure 1.26: *Cationic XB receptors. (A) Beer's water-soluble bis-iodotriazolium receptor;[190] (B) Beer's (S)-BINOL based dicationic host for oxoanions.[191]*

Given the potency of imidazolium derivatives as charge-assisted C-H hydrogen bond donors in anion recognition processes (see Section 1.2.2), the potential of analogous 2-haloimidazoliums has also been investigated. As XB donors, the latter have been shown to exhibit almost identical Lewis acidities as halotriazoliums.[192–194] Following Resnati's 2-imidazolium appended anthracenyl receptor, which was demonstrated to form strong, linear XB interactions with the halides in the solid state,[195] haloimidazoliums have been incorporated into a variety of structures. Ghosh and co-workers reported a tripodal receptor (Figure 1.27A) which selectively sequestered bromide from a solution of competitive anions through crystallisation from CH_3CN.[196] Likewise, Beer's series of haloimidazoliophane macrocycles (Figure 1.27B) exhibited strong binding of the heavier halides in a competitive CH_3OH/ H_2O 9:1 *v/v* solvent system, of which bromide and iodide selectivity hinged on the nature of the XB-donor atom and the spacer group between them.[197,198] Furthermore, the potent XB donor ability of the iodoimidazolium motif has also been recently exploited for organocatalysis applications. Takeda's iodoimidazolium salt (Figure 1.27C) displayed very strong catalytic activity in the aza-Diels-Alder benchmark reaction between aldimines and Danishefsky dienes, producing an 85% yield, compared to no observed product for the HB analogue.[199]

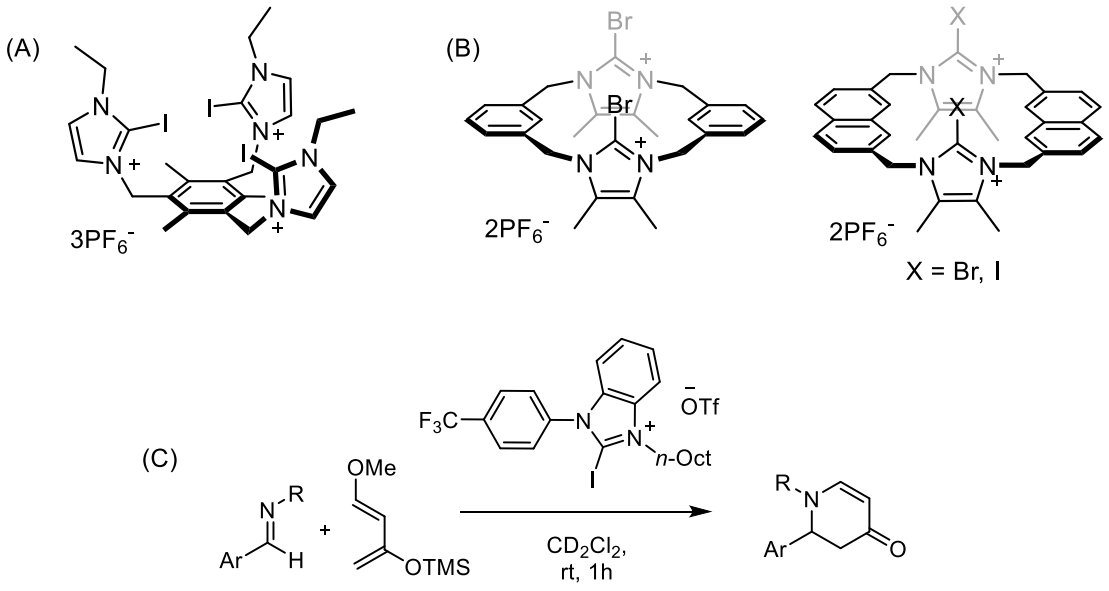


Figure 1.27: *Cationic XB receptors. (A) Ghosh's tripodal receptor for bromide;[196] (B) Beer's family of haloimidazoliophane macrocycles;[197,198] (C) Takeda's iodoimidazolium catalyst.[199]*

1.2.6 Anion sensing

Parallel to the advances in fundamental anion recognition are those related to anion *sensing*, which occurs when the presence of an anion causes a detectable change in the macroscopic properties (optical, electrochemical and more recently, changes in bulk sample viscosity) of a host molecule. The latter is a dynamic area of research and particularly applicable where anion detection is required in an environmental or industrial setting.[200] The three most common methodologies employed for anion sensing are depicted schematically below (Figure 1.28). The first and most fervently adopted 'receptor-reporter' approach involves the appendage of an optical or electrochemical reporter group to the anion receptor motif, which upon non-covalent anion binding perturbs its photo-physical or redox properties producing a measurable macroscopic response. To enable efficient electronic and spatial communication of the anion association event, reporter groups are typically covalently linked *in close proximity* to the binding cavity. Alternatively, the indicator displacement assay (IDA) methodology utilises a receptor pre-formed with a bound dye guest that is expelled from the cavity by the preferential binding of an anion; the concomitant change in the microenvironment of the indicator is signalled through the alteration of its optical properties.[201,202] Finally, the chemodosimeter approach relies on the receptor undergoing a specific irreversible chemical reaction with the analyte thereby inducing a change in the sensory properties of the original host.[203]

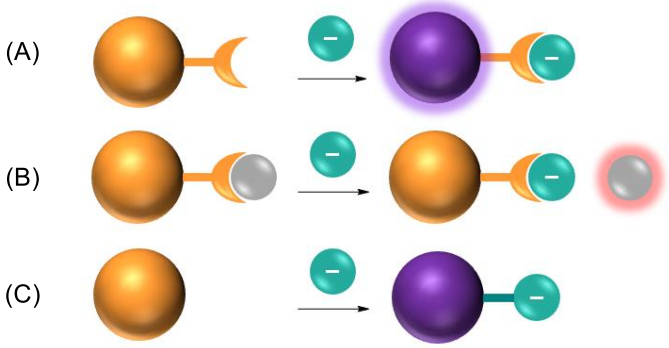


Figure 1.28: *Schematic representation of the general methods of anion sensing. (A) Reporter group attached to a receptor; (B) Displacement assay; (C) Chemodosimeter.*

High guest affinity and selectivity in unison with an easily detectable, sensitive response output constitute the basis of an ideal sensor, which in turn demands careful receptor and reporter design. Whilst IDA's are mentioned later, specifically in the context of phosphate recognition and sensing (Section 1.3), the following section provides a short survey of the wide structural variety of systems employing the other mentioned approaches for electrochemical and optical anion sensing in solution.

1.2.6.1 Electrochemical anion sensors

Since the early reports of Beer's cobaltocenium- and ferrocene-based anion receptors nearly three decades ago,[204,205] electrochemical anion sensing has been ardently demonstrated by various tripodal,[206] macrocyclic[207,208] and interlocked host systems[209,210] appended with similar redox-active reporter groups vicinal to the binding site. Owing to the stabilising effect of the bound anion, the voltammetric potential for the processes involving either oxidation (for example ferrocene to ferrocenium) or reduction (cobaltocenium to cobaltocene) of the redox couple is perturbed. For example, Molina and co-workers reported an acyclic bis-ferrocene-triazole receptor (Figure 1.29A) which sensed OAc^-, $H_2PO_4^-$ and $HP_2O_7^{3-}$ *via* a large cathodic shift in the ferrocene/ferrocenium redox couple (ΔE = ~200 mV in CH_3CN / 0.1 M $TBAPF_6$).[211] In addition to metallocenes, other redox-active auxiliaries such as tetrathiafulvalene (TTF) have been integrated into the structural frameworks of sensory hosts. Becher's TTF-appended calix[4]pyrrole (Figure 1.29B) detected chloride and bromide in CH_3CN solution *via* a ~460 mV cathodic perturbation of the first TTF oxidation potential for both anions.[212]

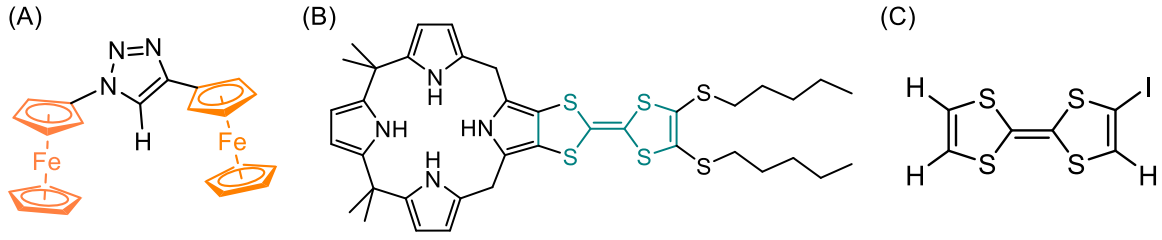


Figure 1.29: *Electrochemical anion sensors. (A)Molina's bis-ferrocene-triazole receptor;[211] (B) Becher's tetrathiafulvalene-appended calix[4]pyrrole;[212] (C) Schöllhorn's XB iodo-TTF receptor.[213]*

Furthermore, although the incorporation of XB donors into anion sensors is a relatively new field of research, Schöllhorn and co-workers have recently reported a redox-responsive XB *iodo*-TTF derivative (Figure 1.29C), which upon chloride addition in DMF displayed enhanced cathodic shifts of 37 mV and 50 mV for the first and second oxidation redox couples respectively, in comparison to the protic analogue.[213]

1.2.6.2 Optical anion sensors

Optical anion sensors are dichotomised as either *luminescent* or *colorimetric* depending upon their mode of signalling: anion complexation in the former perturbs the excited-state emission (from a singlet state in the case of *fluorescence*, or a triplet state in *phosphorescence*) whilst the latter display ground state absorbance changes in the visible spectrum (*vide infra*). Due to the highly sensitive nature of luminescence spectroscopy, receptors appended with luminescent reporter groups in proximity to the recognition site have proven particularly useful in the detection of anions at very low concentrations.

With anion binding signalled through a modulation in their emission profile *via* different transduction pathways such as (1) photoinduced electron transfer (PET), (2) monomer- excimer formation (or *vice versa*) and (3) the 'rigidity effect',[214] luminescent sensors feature widely in the literature, often with photo-active transition metal / lanthanide complexes incorporated into their host frameworks. For example, Ye reported an imidazole-based bimetallic Ru(II) receptor (Figure 1.30A) that selectively detected micromolar quantities of CN^- in water at pH 7, through a decrease in the metal-to-ligand charge transfer (MLCT) emission intensity.[215] In 2012, Pierre published a Tb(III)-based molecular probe (Figure 1.30B) capable of the luminescent detection of biologically relevant ATP^{4-}, in buffered aqueous solution at neutral pH.[216] Favourable π-π stacking interactions between the ATP^{4-} purine base and the host's aromatic phenanthrodine unit favoured PET quenching of the antenna necessary for lanthanide phosphorescence. More recently, Beer and co-workers have described a rare example of a XB luminescent sensor: the bimetallic Re(I) pyrimidine-based host shown in Figure 1.30C selectively bound I^- (K_a = $>10^4$ M^{-1}) in $CDCl_3/CD_3OD$ 1:1 *via* a

pronounced increase in the metal's MLCT absorption band and with almost three orders of magnitude greater affinity than the HB analogue.[217]

As an alternative to photo-active metallo-complexes, organic fluorophores have also been used for anion sensing. The propensity of pyrene to undergo monomer-excimer switching was exploited by Nam and co-workers, who described a pyrene-appended calix[6]arene for the detection of HSO_4^- in CH_3CN (Figure 1.30D).[218] Hydrogen bonding interactions between the anion and the urea moieties resulted in the separation of the pyrene units from the correct π-π stacked orientation prerequisite for excimer formation. Consequently, a quenching of the excimer emission and increase in the monomer emission band was observed, with the selectivity for HSO_4^- ascribed to shape and size complementarity effects between the anion and the receptor binding cavity.

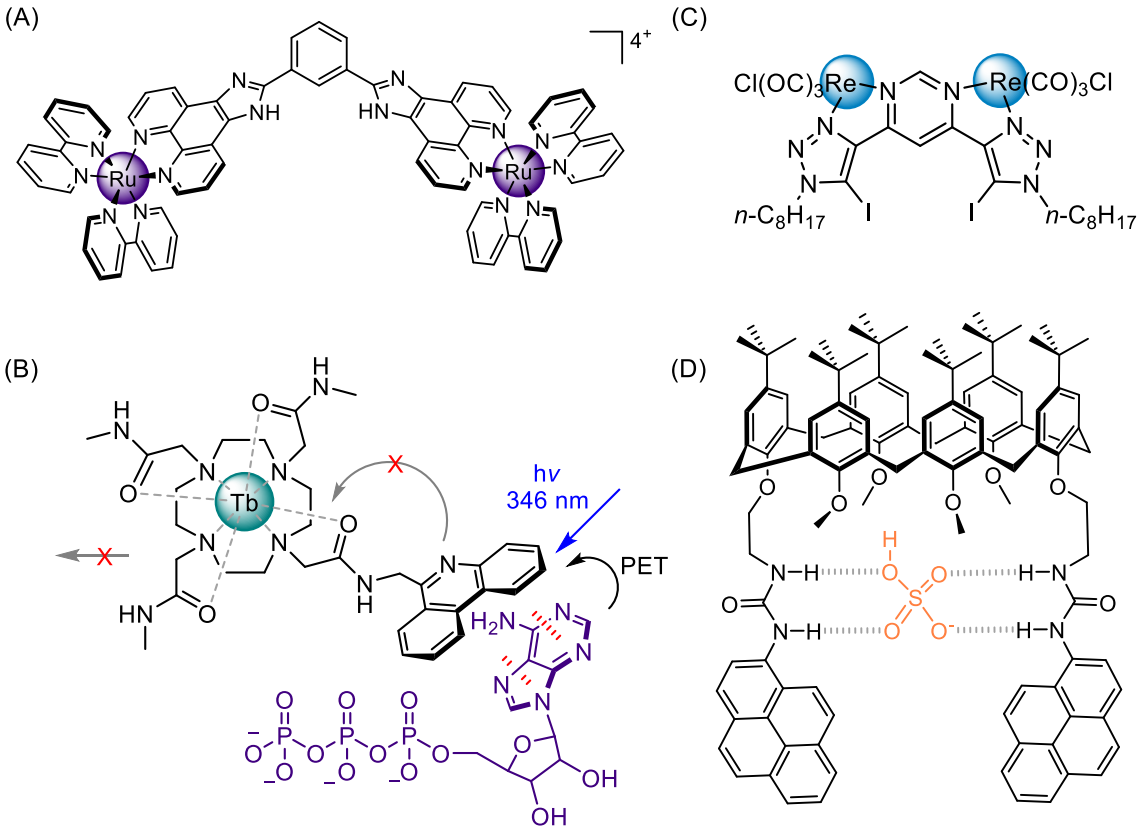


Figure 1.30: *Fluorescent / luminescent sensors. (A) Ye's bimetallic Ru(II) receptor;[215] (B) Pierre's Tb(III) based molecular probe for sensing phosphate nucleotides;[216] (C) Beer's XB sensor for iodide;[217] (D) Nam's pyrene appended calix[6]arene receptor for sulfate.[218]*

The anion-induced chromogenic responses of colorimetric anion sensors facilitate naked-eye detection of the analyte which heightens their appeal. The latter have proven to be particularly popular in the detection of highly basic anions, which give rise to visible colour changes often by deprotonating the receptor's acidic protons. For example, Sun and co-workers reported a diketopyrrolopyrrole-based system Figure (1.31A) that changed from orange to blue upon deprotonation of its hydrazine motif by fluoride in DMSO.[219] Similarly, Sessler described a series of chromophore-appended calix[4]pyrroles, such as the hydroxyl-anthraquinone host in Figure 1.31B, which exhibited anion-specific chromogenic changes for a range of basic anions in CH_2Cl_2 (turning from red to blue, and red to purple, upon the addition of F^- and Cl^- respectively).[220] Alternatively utilising the chemodosimeter approach, Isaad and El Achari's sensor based on trifluoroacetamide benzhydrol (Figure 1.31C) underwent a chromogenic change from colourless to yellow in the presence of CN^-, the strongest carbonyl affinity of which relative to the other anions examined, enabled cyanohydrin adduct formation with the host in aqueous solution.[221]

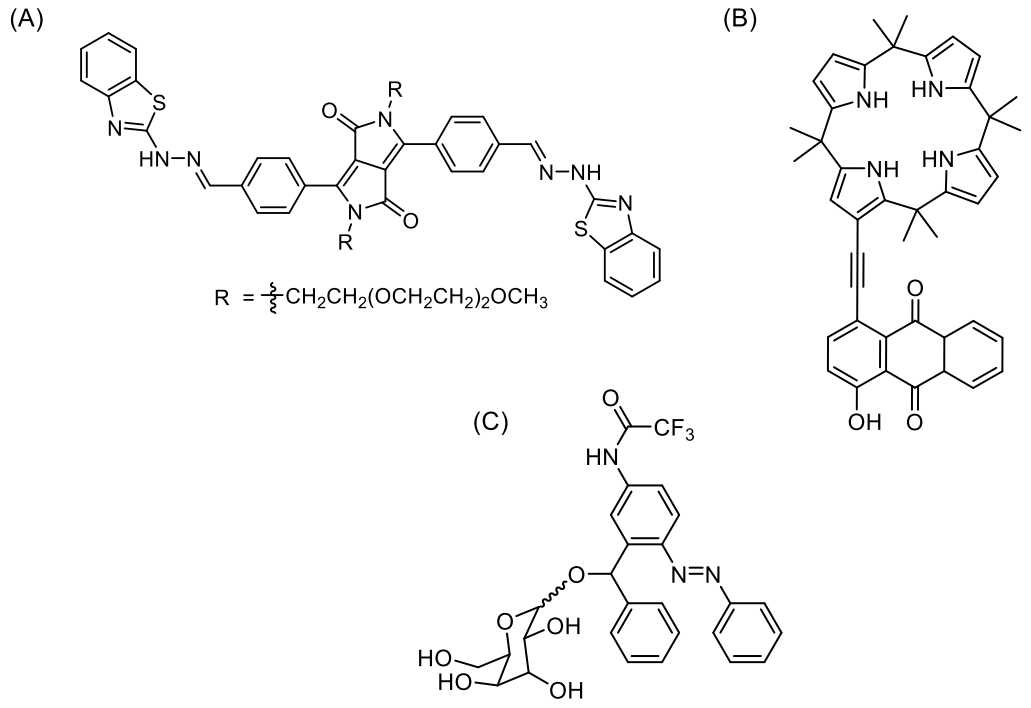


Figure 1.31: *Colorimetric anion sensors. (A) Sun's diketopyrrolopyrrole-based sensor for fluoride;[219] (B) Sessler's anthraquinone appended calix[4]pyrrole;[220] (C) Isaad and El Achari's chemodosimeter for cyanide.[221]*

1.3 Artificial receptors for the recognition of phosphate and its derivatives

1.3.1 The importance and challenges of phosphate recognition

Given the crucial role of phosphate-based anions in various biological processes discussed earlier (see Section 1.1.2), it is unsurprising that the last century has witnessed extensive efforts of researchers to achieve the selected binding of phosphate and its derivatives. Indeed, the significance of the latter is far-reaching with further environmental and medical implications. Whilst phosphorylated molecules are key components of industrial fertilisers akin to nitrates, they are also in part responsible for the eutrophication of natural water sources.[222,223] Additionally, the adverse effects of hyperphosphatemia, a condition that arises from an abnormally high concentration of blood phosphate levels, include the development of hyperthyroidism, soft-tissue calcification and cardiovascular complications.[224–229] Moreover, neurotoxic chemical warfare agents (CWAs) which constitute one of the greatest threats in the modern world are essentially organophosphonate-derived compounds[230–232] (Figure 1.33C) that irreversibly inhibit the activity of cholinergic enzymes within the body, resulting in several deleterious effects in the victim and ultimately death.[233,234] Consequently, the importance of this class of anions as well as the need for receptors capable of their selective recognition, extraction and transport cannot be stressed enough.

Historically, the selective binding of phosphate was investigated by Taylor and Miller in 1914, who established the first colorimetric method for the estimation of phosphorous in biological material.[235] Utilising a coloured molybdenum (IV) phosphate complex to assay inorganic phosphate, their method (now much improved)[235–240] involved a time-consuming procedure, generated toxic metal waste and suffered from interference. Since then, although other assays for phosphorylated molecules have been developed, they involve either lengthy derivatization-based protocols[241–243] or highly-sensitive enzymatic recognition elements that often necessitate careful handling, suffer from poor stability and complicated, costly production procedures.[244–246] Accordingly, the design and synthesis of abiotic phosphate receptors seeks to overcome these

limitations. Whilst this has been extensively pursued, the sensitive and selective recognition of phosphate species however remains a challenging area of research due to a number of key factors. As indicated by the speciation curve of its parent orthophosphoric acid (Figure 1.32A), phosphate can exist in various charged states in aqueous media depending on pH, with two dominant mono- ($H_2PO_4^-$) and di-basic (HPO_4^{2-}) forms present at physiological pH 7.4.[247] This adds a level of complexity to receptor design as the system must accommodate the favourable binding of one or the other protonated forms or, ideally both. The large size and tetrahedral shape of phosphate (Figure 1.32B) places further size and geometric constraints upon the design of a suitable host, especially where structurally more elaborate polyphosphate or phosphate-derived guests are concerned. Furthermore, the highly hydrophilic nature of phosphate as reflected by its position near the bottom of the Hofmeister series (Figure 1.5), with the Gibbs free energy of hydration increasing substantially with increasing charge (ΔG_{hydr} of $H_2PO_4^-$ = -465 kJ mol^{-1} and ΔG_{hydr} of PO_4^{3-} = -2765 kJ mol^{-1}),[248] makes the prospect of binding this elusive species in biologically relevant aqueous media most certainly an arduous task.

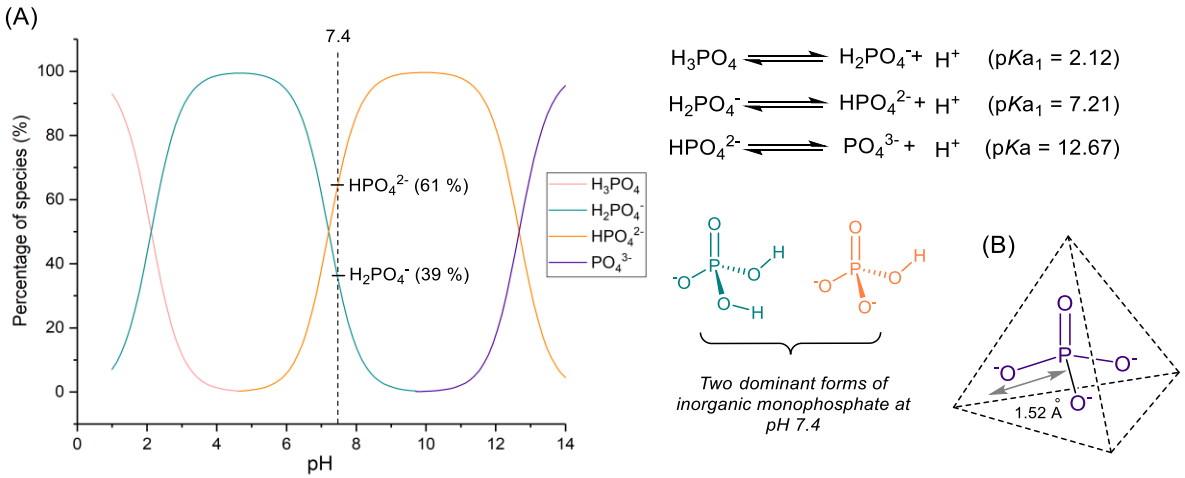


Figure 1.32: *General properties of phosphate. (A) (left) the speciation curve of orthophosphoric acid with percentage abundances determined using 'Hyperquad simulation and speciation' (HySS) software[249] and (right) the associated acid-base equilibria;[247] (B) schematic geometry of phosphate and associated r(P-O) bond length determined from X-ray data.[247]*

Despite these challenges, a large repertoire of artificial hosts for phosphates have been developed capable of functioning in both organic and aqueous solvents.[247,250,251] Whilst a few examples have been previously mentioned in a rather general manner under the 'umbrella' of anion receptors, this section aims to provide a more detailed summary of the wider efforts channelled in these pursuits. There is particular emphasis on the design strategies and fundamental molecular recognition processes involved, with brief mention of the potential and realised applications of phosphate binding interspersed throughout the discussion. Importantly, given that a diversity of phosphates exist, only those most commonly targeted in anion supramolecular chemistry will be examined here. For convenience, these are sub-divided into three categories (Figure 1.33): (A) classical inorganic phosphates (*i.e.* monophosphate (the conjugate base species of orthophosphoric acid) and polyphosphates (arising from the polymerization of phosphoric acid derivatives), (B) organophosphate-derivatives (*i.e.* the esters of phosphoric acid) and (C) organophosphonate-compounds (*i.e.* the esters of phosphonic acid derivatives) and organophosphinate-compounds (*i.e.* the esters of phosphinic acid derivatives).

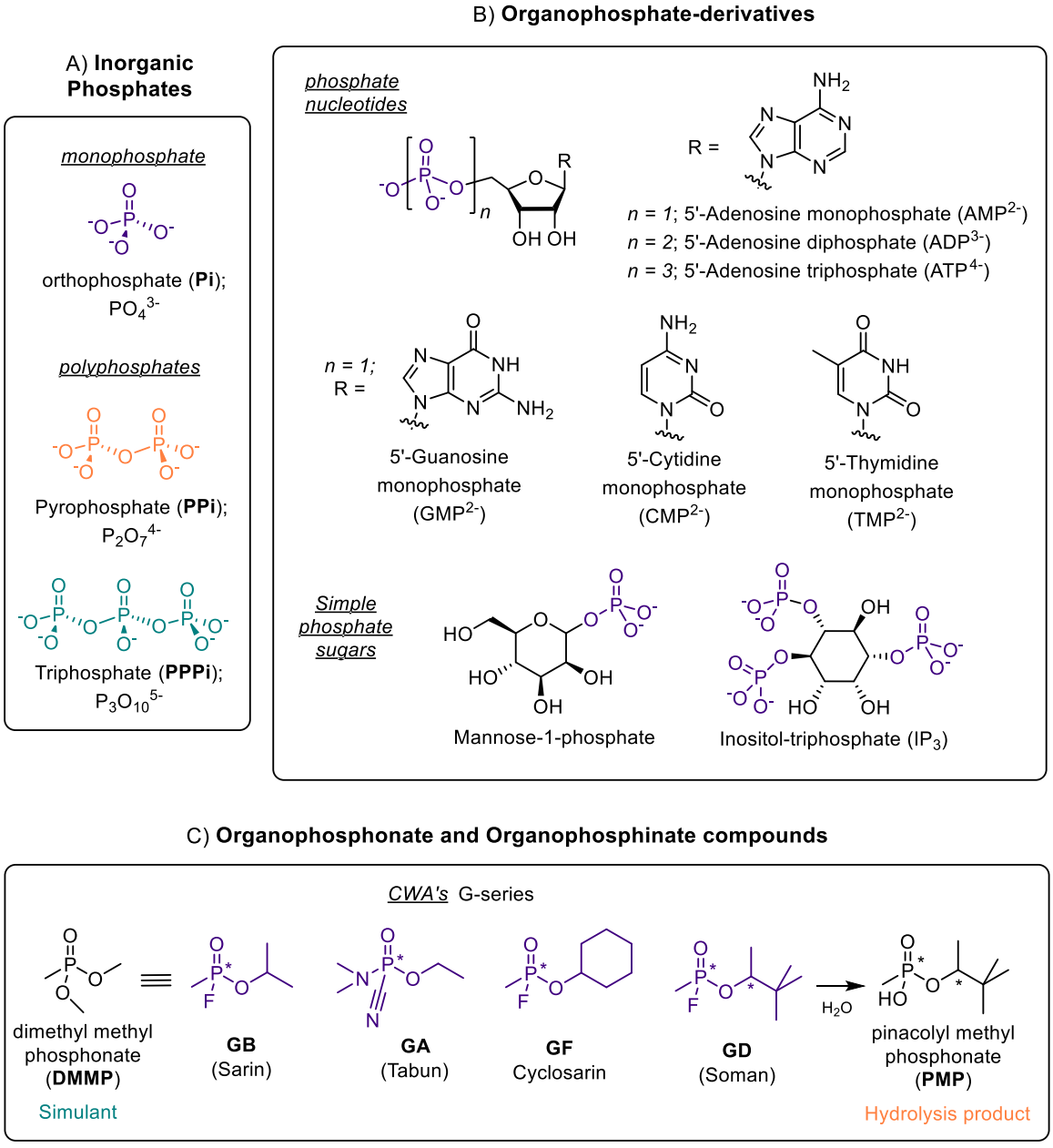


Figure 1.33: *Classifications of phosphates. (A) Classical inorganic phosphates (B) Common organophosphate- and (C) organophosphonate and organophosphinate compounds mentioned in this section. (Chiral centres are marked with an asterisk).*

1.3.2 Receptors for inorganic phosphates

Guided by the design principles from Nature's PBP examined earlier (Section 1.1.4),[46] it is apparent that encapsulation and topological complementarity, achieved *via* optimised electrostatic and hydrogen bonding interactions are critical for successful phosphate recognition. Consequently,

these themes are also common amongst synthetic phosphate selective receptors which have been developed as either (1) metal-free hosts, or (2) metallo-complexes, mostly transition metal or lanthanide based, in which the metal ion is the anchoring point for the anionic species.

1.3.2.1 Metal-free hosts

- **Acyclic structures**

Proceeding the discovery of the oligophosphate binding capabilities of naturally occurring putrescine, spermidine and spermine compounds (Figure 1.34A) over forty years ago,[252,253] the earliest synthetic receptors for phosphates to be described in the literature were aliphatic polyamines. Able to be protonated in aqueous solution at physiological pH (although strictly speaking, they adopt a fully protic form in water only at very low pH values), such hosts function essentially as polycations and in addition to hydrogen bonding and the extent of 'geometric fit' between host-guest species, owe their efficacy in large measure to the strong electrostatic interactions generated between the anionic phosphate and polyammonium functionalities. Hence, the stability of their adducts increases with the increasing charge of the interacting partners and the phosphate binding trend they display follows the order monophosphate << pyrophosphate < triphosphate.

Open chain alkyl polyamines such as those in Figure 1.34A represent the simplest receptors in terms of design.[251] Whilst flexible, upon protonation they stiffen into rod-like structures of *anti* conformation in order to minimise any electrostatic repulsions between neighbouring polyammonium groups and thus bind the inorganic phosphates in a linear manner. As evidenced in the layered X-ray crystal structure of spermidine phosphate trihydrate (Figure 1.34B), the anions are embedded within the polycationic matrix in an arrangement parallel to the rigidified ligands.[254] Indeed, ^{1}H and ^{13}C NMR spectra performed with solutions of these ligands at various pH values have shown that the formation of complexes with the inorganic phosphates does not alter the protonation patterns or the topology of the charged groups in the ligands and does not modify significantly the overall conformation of the protonated receptors.[255,256] Relative to the other

polyammonium hosts which follow, they offer the least geometric complementarity to the inorganic phosphates and consequently, the association constants for the formation of their 1:1 host-guest adducts are generally rather low. For example, tetraprotonated spermine was demonstrated to bind HPO_4^{2-} and $HP_2O_7^{3-}$ in water (pH 7.4) with log K_a =2.23 and 2.56 respectively.[35]

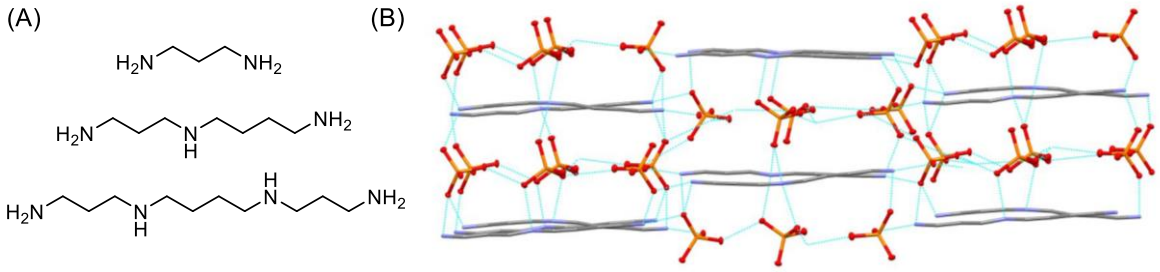


Figure 1.34: *Open chain polyamine receptors. (A) top to bottom, putrescine, spermidine and spermine (B) layer structure of spermidine phosphate trihydrate.[254] Atoms of the phosphate atoms shown as spheres, with hydrogen atoms omitted for clarity. Light blue dashed lines indicate hydrogen bonds.*

Tripodal polyamines lie a rung above their linear acyclic analogues on the ladder of pre-organised hosts for phosphate binding, with the most prominent class of these being tris(2-aminoethyl)amine (TREN) derived (Figure 1.35A). Due to the C_{3v} symmetric conformation of convergent binding groups, they are better able to chelate to phosphate and thus afford adducts of higher stability. For example, triprotonated TREN bound HPO_4^{2-}, $P_2O_7^{4-}$ and $P_3O_{10}^{5-}$ in aqueous solution with log K_a =2.66, 5.78 and 6.70 respectively, in accordance with the increasing charge density of the anionic species.[257] As elucidated from the X-ray crystal structure of Bowman-James' benzyl-appended tripodal receptor with $H_2PO_4^-$ (Figure 1.35B),[258] the typical binding mode of the TREN subunit involves the chelation of all three protonated amine termini to an oxygen atom of the phosphate anion, enabling multiple electrostatic and hydrogen-bonding contacts between the host-guest species. Owing to the formation of a similar complex with HPO_4^{2-} in water (pH 6), Czarnik's anthracenyl-appended tris(3-aminopropyl)amine sensor (Figure 1.35C) exhibited a 145% increase in its chelation-enhanced fluorescence (CHEF) intensity.[259] It was proposed that whilst the benzylic nitrogen lone pair quenched the fluorescence of the naphthalene motif (*via* PET) in the unbound state, anion complexation led to a change in the protonation state of the nitrogen and attenuated the quenching process, thus turning on the fluorescence response.

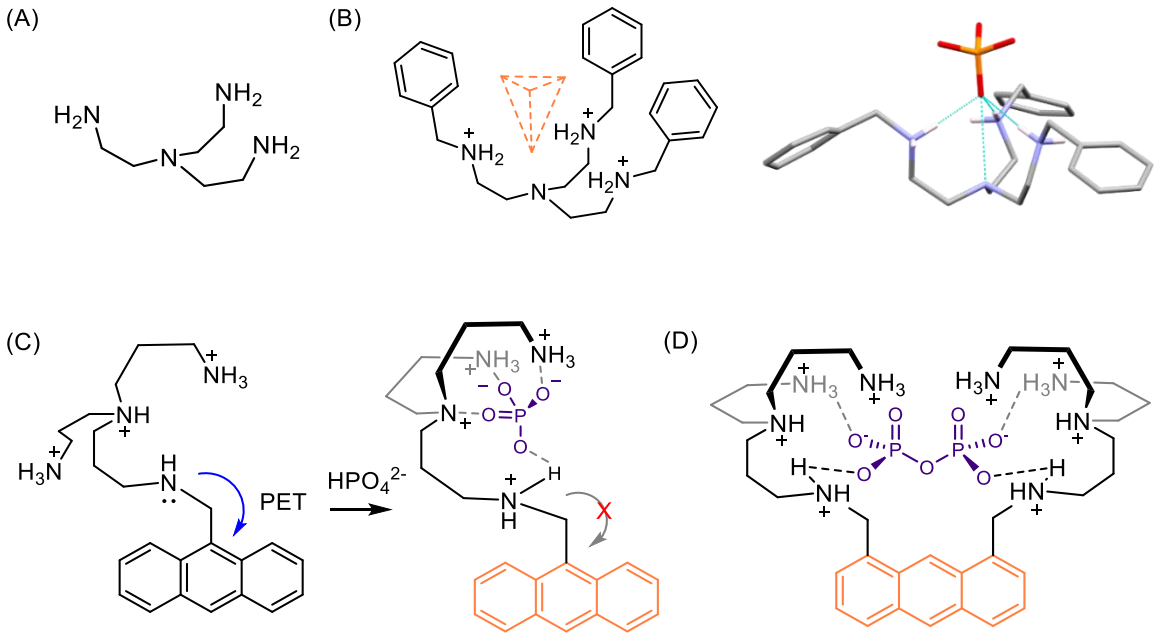


Figure 1.35: *Tripodal polyamine receptors. (A) TREN subunit; (B) (left) Bowman-James' benzyl-appended tripod and (right) the corresponding crystal structure of its adduct with inorganic monophosphate.*[258] *Hydrogen atoms, except those on protonated nitrogens omitted for clarity. Light blue dashed lines indicate hydrogen bonds. (C) Czarnik's anthracenyl-appended phosphate sensor;*[259] *(D) Czarnik's anthrylpolyamine sensor for pyrophosphate.*[260]

Structurally related to the above, 'conjoined' tripodal polyamine receptors in particular have enabled the discrimination between the inorganic monophosphate and polyphosphate species. Due its constituent tripodal host groups being geometrically disposed at the right distance to fit the stereochemical requirements of pyrophosphate, Czarnik's expanded anthrylpolyamine receptor (Figure 1.35D) was found to bind $P_2O_7^{4-}$ over 2000-fold more strongly than HPO_4^{2-} in aqueous solution (pH 7, 50 mM HEPES).[260]

- **Macrocyclic receptors**

In comparison to the previous rigid open chain and tripodal polyamine systems, polyazacycloalkanes conceptually represent a step further in the design of even more pre-organised hosts for inorganic phosphates. Seminal work in developing polyammonium macrocyclic receptors was carried out by the groups of Lehn and Kimura who, aware of the spacing of the nitrogen atoms in the natural phosphate binding polyamines (*vide supra*), suggested that structures similarly containing multiple (i) 1,3-propylenediamine or (ii) ethylenediamine moieties would represent

effective phosphate binding systems.[261,262] In principle, still flexible protonated forms of these macrocycles would be able to wrap around the bulky phosphates according to their ring size, and self-adapt to the stereochemical requirements of the anionic guests, thus forming highly stable adducts. Indeed, both the 'first' and 'second' generation of macrocyclic polyamines to be synthesised (Figure 1.36) were found to form strong 1:1 stoichiometric complexes with the inorganic phosphates in solution. For example, the tetraprotonated BMXD macrocycle (Figure 1.36B) bound HPO_4^{2-}, $P_2O_7^{4-}$ and $P_3O_{10}^{5-}$ with log K_a = 2.87, 5.73 and 6.47 respectively in aqueous media, as inferred from potentiometric measurements.[263] Single-crystal X-ray diffraction analysis of the BMXD/Pyrophosphate complex (Figure 1.36D) revealed the anion to be disposed perpendicular to the mean plane of the twisted chair-type receptor and encapsulated within its cavity *via* multiple ion-pairing and hydrogen bonding interactions. Contrastingly, a 'nesting-type' complex of 1:2 host-guest stoichiometry was observed in the pyrophosphate adduct of the smaller tetraprotonated [18]aneN_6 host (Figure 1.36C), with two $H_2P_2O_7^{2-}$ anions facially bound to the cyclic cation in *endo* conformation.[256]

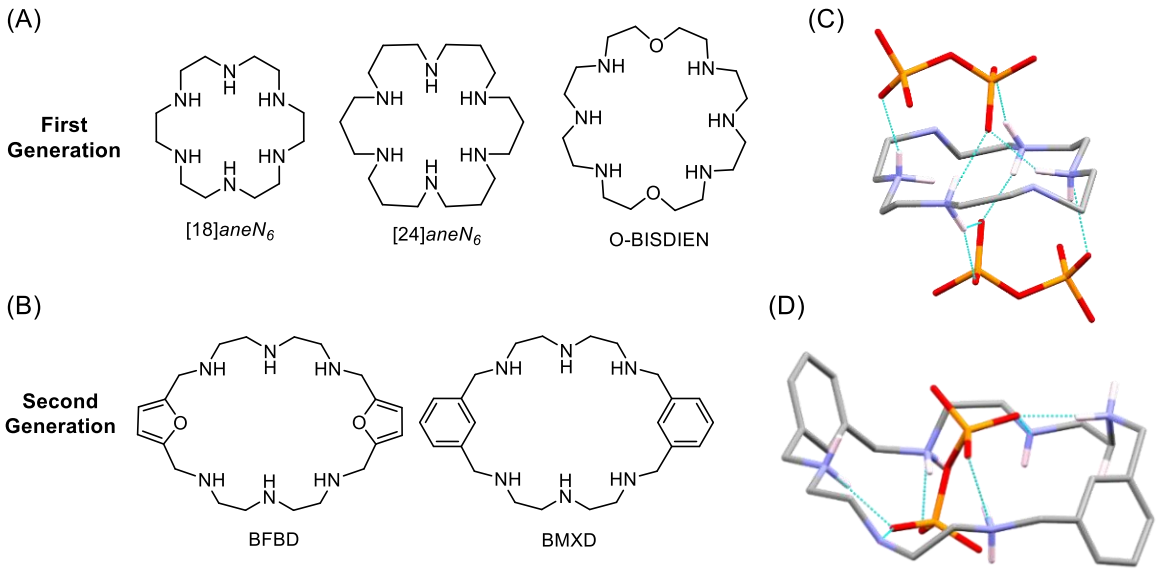


Figure 1.36: *Macrocyclic polyamine phosphate receptors. (A) First and (B) Second generation polyamines;[247] (C) crystal structure of the tetraprotonated BMXD and;[263] (D) tetraprotonated [18]aneN₆ macrocycle with PPi.[256] HB interactions shown as blue dashed lines. (H atoms, except those on protonated nitrogens have been omitted for clarity).*

Termed so due to the integration of aromatic spacer units within their macrocyclic framework, 'second generation' polyamines such as the latter have been widely utilised for the recognition of phosphate nucleotides[264–266] and are expanded on later in Section 1.3.3.1.

Despite the strong binding of the inorganic phosphates generally exhibited by cyclic polyamines, it is worth noting that they are also capable of binding other oxoanions such as sulfate and various carboxylates with association constants very similar to those of monophosphate. For example, in the case of the pentaprotonated BMXD macrocycle in acidic aqueous solution, log K_a (SO_4^{2-})/ log K_a (HPO_4^{2-}) = 0.66.[267] Structurally more elaborate host molecules with greater shape and size complementarity for phosphates are thus needed to achieve better selectivity over other oxoanions.

- **Cryptand-like receptors**

Due to their shielded cavities which offer the possibility of *complete* guest encapsulation, three dimensional receptors such as cryptands and interlocked structures represent the epitome of pre-organised hosts for anion binding. Whilst they have been shown to bind halides strongly,[268–271] the inclusion of phosphate species has proven more difficult due to their geometric and steric demands. Of the few rare examples, the octaprotonated bicyclic TREN derived cryptand in Figure 1.37A was demonstrated by Lu and co-workers to form an encapsulated complex with $H_2PO_4^-$ in aqueous solution (pH 1).[272] Solid state analysis (Figure 1.37B) revealed the anion tightly fixed within the cavity through two strong hydrogen-bonds between the two unprotonated oxygen atoms of dihydrogen phosphate and the two protonated bridgehead nitrogen atoms of the cage. Interestingly, upon deprotonation of the latter (at pH 2), the guest was easily released from the receptor's internal binding pocket and evidenced to reside within the clefts between the 'arms' of the cryptand instead (Figure 1.37C).[273] This pH dependent 'swelling' of the receptor which effectively widens the 'windows' between the phenyl rings to facilitate phosphate entry into the (enlarged) cavity, crucially demonstrates the further intricacies involved with the encapsulation of such guests. Sessler, Vögtle and co-workers have also reported a bipyrrole-based [2]catenane (Figure 1.37D) that exhibited a high selectivity for $H_2PO_4^-$ ($K_a > 10^7$ M^{-1}) over the halides and OAc^- in d_6-DMSO.[274]

This was attributed to arise from the encapsulation of the anion within the geometrically complementary tetrahedral cavity between the two rings.

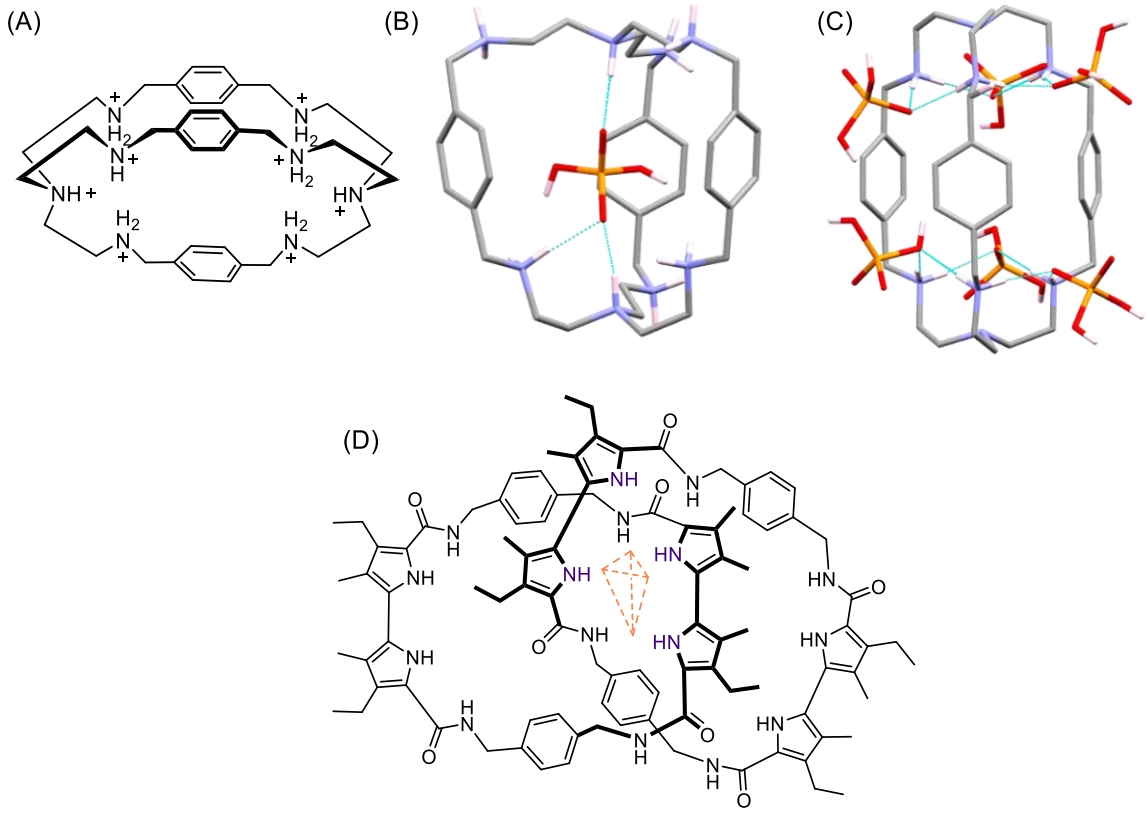


Figure 1.37: *(A) A bicyclic TREN derived cryptand and (B) the crystal structure of its complex with inorganic monophosphate;[272] (C) Peripheral phosphate binding observed with the hexaprotonated receptor.[273] HB interactions shown as blue dashed lines. (hydrogen atoms, except those on protonated nitrogens have been omitted for clarity). (D) Sessler's bipyrrole-based [2]catenane.[274]*

1.3.2.2 Metallo-complexes for inorganic phosphates

Metal cations feature widely in the active sites of several natural phosphate-binding proteins[275–277] and hence their presence, as well as the interactions they sustain have inspired the synthesis of numerous abiotic metallo-receptors for phosphates. These are typically designed around organic scaffolds that chelate metals with high kinetic and thermodynamic stability such that at least one coordination site on the metal centre remains vacant or coordinated to a weakly bound substrate (as in an IDA, Figure 1.28B) and thus available for anion binding. In such systems expanded on below, phosphate recognition is largely directed by the dative coordinate bond formed between the receptor's metal cation and a negatively charged oxygen atom present on the phosphate group of

interest. Whilst extra functionalities have been incorporated to increase specificity, metal coordination of the anion is generally the greatest contributor to the stability of the complexes formed from this class of receptors. Additionally, although numerous metal-based hosts have been reported,[278–280] they are largely dominated by Cu(II) and Zn(II) (and to a lesser extent, trivalent lanthanide) cations, which by virtue of their charge also facilitate phosphate recognition in water.

Given the phosphate binding abilities of Kimura and Lehn's early polyammonium macrocycles, a natural extension towards further improving their efficiency (and that of other structurally-related systems) has involved the incorporation of metals into the receptor framework. For example, the mono-Cu(II) complexes of the O-BISDIEN and BMXD macrocycles in their deprotonated states (Figure 1.36) were demonstrated to bind orthophosphate much more strongly than the corresponding free ligands in aqueous solution.[281] Whilst these systems have been shown to function as effective phosphate receptors up until in their triply protonated state (the log K_a's for orthophosphate, pyrophosphate and triphosphate being 12.10, 10.68 and 11.28 respectively, in the case of BMXD.Cu^{2+}.$3H^+$), as stated previously, extremely high selectivity is generally not observed with similar receptor designs based on polyaza macrocycles which often complement phosphate oxoanions in charge but not geometry. Employing a more strategic 'lock and key' approach towards monophosphate binding, Anslyn developed a series of tripodal receptors derived from the coordination of tris-functionalised TREN and tris(2-pyridylmethyl)amine (TPMA) ligands to a central Cu(II) core (Figure 1.38).[282]

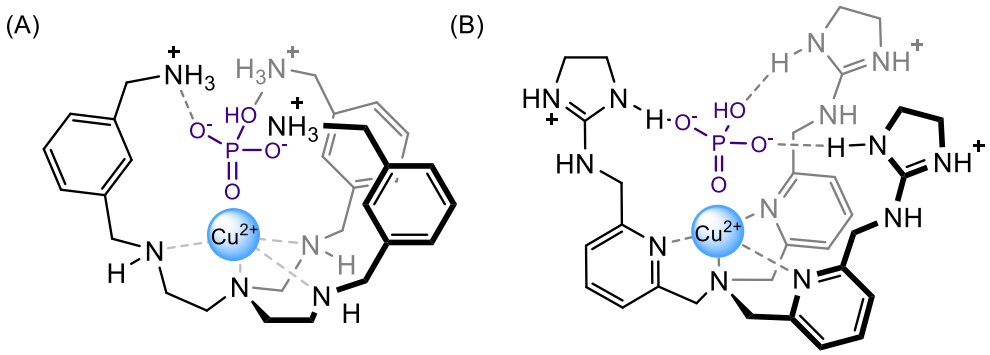


Figure 1.38: *Metallo-complexes for phosphate binding. (A) Anslyn's TREN- and (B) TPMA derived Cu(II)- tripods.*[282]

Featuring highly pre-organised C_{3v} symmetric cavities which offer exact shape and size complementarity to accommodate the tetrahedral guest, they were demonstrated to selectively bind HPO_4^{2-} over structurally similar oxyanions ReO_4^- and SO_4^{2-}, in aqueous solution (H_2O/ CH_3OH 98:2 *v/v*). To date, the reported binding constants (K_a = 2.5 x 10^4 M^{-1} and 1.5 x 10^4 M^{-1}) are amongst the largest known for phosphate binding to a synthetic receptor in water at neutral pH. These high affinities can be ascribed to the combined multiple charge pairing interactions of the ammonium/guanidinium appendages and the Cu(II) center with the oxygens of the target phosphate.

Perhaps more familiar of the metal-based phosphate-binding motifs, Zn(II)-dipicolylamine (Zn(II)DPA)-based hosts have been found to be selective for polyphosphorylated species over other anions, especially when multiple Zn(II)DPA functionalities are incorporated into the receptor framework.[283,284] In particular, complexes bearing two suitably positioned Zn(II)DPA units were shown to selectively bind pyrophosphate (PPi) *via* a two-point interaction, where the oxoanion binds to the two metals in a bridging mode, with one or two oxygen atoms bound to each Zn(II). Hence, in these systems, the distance between the two metallo-centers is key to controlling their selectivity. For example, the *meta*-xylyl derivative in Figure 1.39A exhibited a twenty-fold enhancement in the binding of PPi (K_a = 152 x 10^5 M^{-1}) compared to its shorter Pi monomer (K_a = 7.3 x 10^5 M^{-1}) in buffered aqueous media, due to the Zn(II)DPA groups positioned at an appropriate distance complementary to the size and geometry of the phosphate dimer.[285] Consequently, many structurally similar bis-Zn(II)DPA acyclic hosts have been reported in the literature, and often coupled to a range of fluorophores to facilitate applications in PPi sensing and detection.[284] Hong's naphthalene appended phenoxide receptor (Figure 1.39B) exhibited a 9.5 fold increase in fluorescence intensity upon the addition of one equivalent of PPi (in 10 mM HEPES, pH 7.4), whereas the addition of four equivalents of ATP^{4-} only resulted in a two-fold fluorescence enhancement.[286] The selectivity for PPi over ATP^{4-} was proposed to arise from the difference in the total anionic charge density of the four O-P oxygen atoms of the phosphate species involved in the complexation, being greatest in the case of PPi.

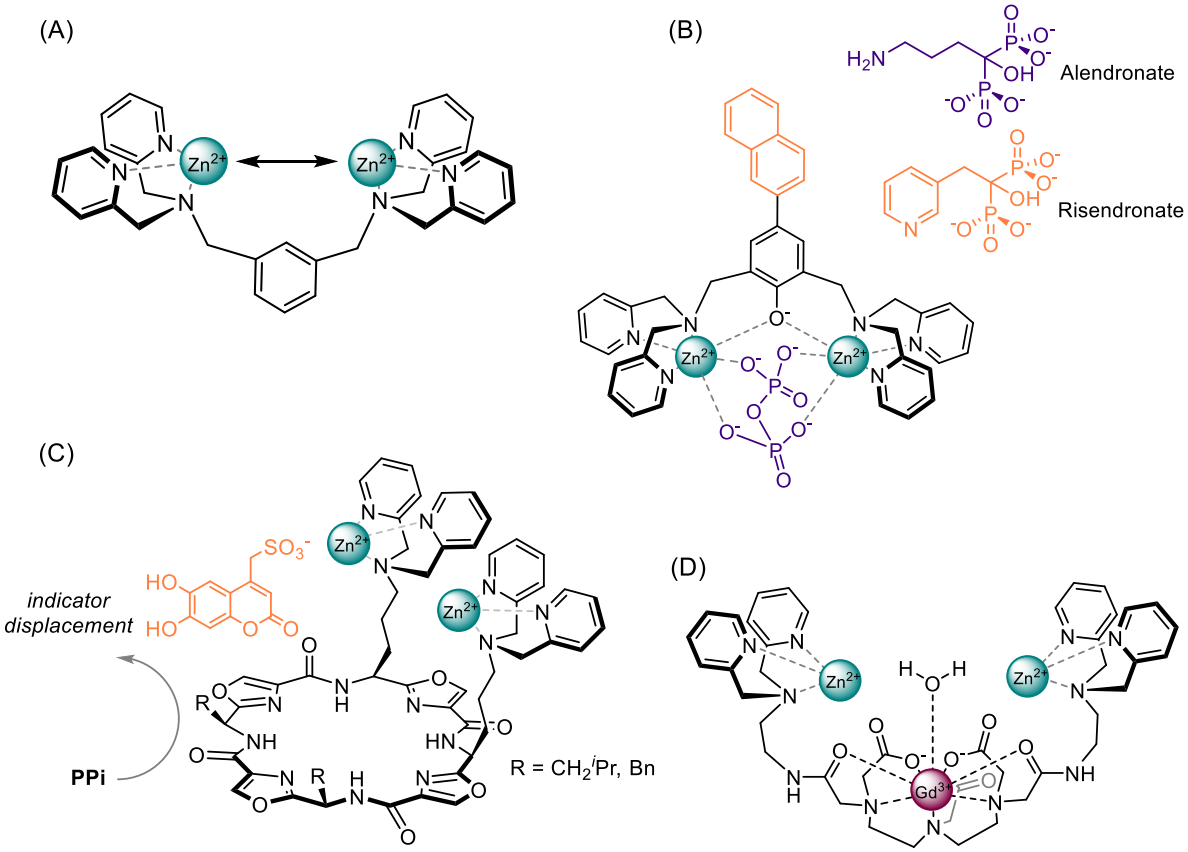


Figure 1.39: *Metallo-complexes for PPi. (A) Smith's meta-xylyl derivative;[285] (B) Hong's naphthalene appended sensor.[286] (C) Joliffe's Zn(II)DPA macrocycle (coumarin methylsulfonate indicator in orange);[287] (D) Vilar's Gd(III) complex.[288]*

Interestingly, the same receptor was also used to detect the levels of structurally related alendronate and risendronate, which are used as treatments for osteoporosis in blood plasma. Similar to PPi, both bisphosphonates were bound with a 1:1 host:guest stoichiometry, and calibration curves allowed the accurate determination of their concentrations in the range 0.5-2.0 μg mL^{-1}.[289] More recently and inspired by the *Lissoclinum* family of heterocyclic peptides, the Joliffe group have synthesised a range of bis-Zn(II)DPA appended macrocycles (Figure 1.39C) and demonstrated their ability to selectively bind PPi in the presence of other polyphosphate species (in 5 mM HEPES, pH 7.4, 145 mM NaCl).[175,287] Utilising a fluorescent coumarin methylsulfonate IDA, improved discrimination between PPi, ATP and ADP was achieved when the Zn(II)-DPA pendant arms were brought into close proximity, whereas the selectivity was lost when the steric bulk of the non-binding side chains was increased.

In comparison to the transition metal-based hosts previously mentioned, far fewer examples of lanthanide-based receptors for the complexation and detection of phosphates exist.[290,291] The latter typically rely on changes in the emissive properties of the cation that arise when anions displace water molecules from the metal center. Having coupled the aforementioned Zn(II)DPA moieties with a Gd(III) complex, Vilar and co-workers reported a PPi-selective receptor (Figure 1.39D) which was able to act as a magnetic resonance imaging (MRI) contrast reagent.[288] The binding of PPi in water solution at physiological pH modulated the relaxivity of the Gd(III) complex sufficiently to be observed in imaging experiments.

1.3.3 Receptors for organophosphate derivatives

1.3.3.1 Phosphate-nucleotides and simple phosphate sugars

Akin to their inorganic precursors, organic phosphate derivatives such as AMP^{2-}, ADP^{3-} and ATP^{4-} (Figure 1.33B), are also amongst the most targeted anionic species on account of their essential role in many biological processes spanning from metabolism to biosynthesis, gene regulation, signal transduction and muscle contraction.[292] In contrast to the previous inorganic phosphates which have been demonstrated to interact with synthetic receptors essentially *via* electrostatics and hydrogen bonding interactions, the aforementioned nucleotides (and indeed, other phosphate-containing metabolites / oligonucleotides) have other functionalities attached, the most common being nitrogenous nucleobases and sugar moieties, which can also participate in the binding process. Accordingly, the design of host molecules for such phosphate derivatives incorporate binding sites within the receptor framework, which target not only the inorganic 'phosphate tail' (*e.g. via* a (poly)cationic or Lewis-acidic binding site), but also the 'organic' sections of these guests - most commonly utilising functional groups capable of interacting *via* HB with the sugar moieties and/or aromatic or heteroaromatic units capable of donor-acceptor π-pairing with the nucleobases.

Exemplary of the latter are Lehn's early cyclo-intercaland-type cyclophanes (*i.e.* 'second generation' polyamine macrocycles), designed to encapsulate nucleotide phosphates in acidic

aqueous media (pH 6):[293–295] the aza-acridine receptor in Figure 1.40A was observed to bind ATP *via* a dual binding mode in which the triphosphate group was bound to the polyammonium macrocycle while the adenine nucleobase formed favourable π-stacking interactions with the acridine subunits.[294] Due to the reliance on electrostatic interactions governing the binding, the binding trend followed the order $AMP^{2-} < ADP^{3-} < ATP^{4-}$ in line with the increasing charge of the phosphate species. Indeed, this sequence can be considered a general rule in nucleotide binding by polyammonium guests, as already observed for their inorganic counterparts. Furthermore, the selectivity for phosphate tethered to a particular nucleobase can be tuned through judicious selection of the aromatic receptor unit.[216] For example, the extended π-surface of the pyrene subunit in Inouye's receptor (Figure 1.40B) favoured the binding of purine phosphates (ATP^{4-}, GTP^{4-}) over their pyrimidine analogues (CTP^{4-}, TTP^{4-}) in water, due to the maximised π-stacking interactions with the larger aromatic surfaces of the purine derivatives.[296]

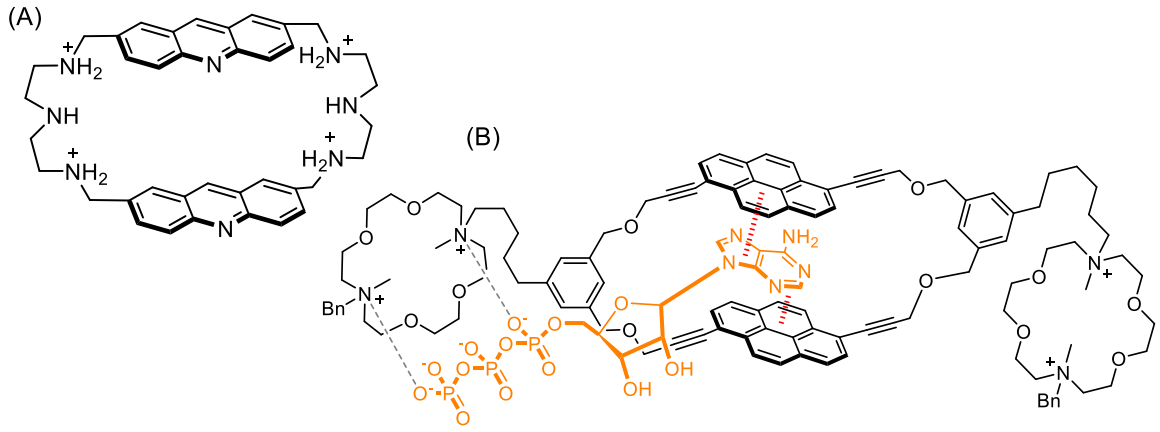


Figure 1.40: *Artificial hosts for phosphate nucleotides. (A) Lehn's aza-acridine macrocycle for ATP (shown in its major tetraprotonated form at pH 6);[294] (B) Inouye's pyrene receptor with the proposed mode of ATP binding.[296] (Non-covalent interactions shown by dashed lines).*

Such extended π-surfaces have also been used to promote the encapsulation of pairs of nucleotides in aqueous solution (possibly associated through traditional Watson-Crick (Figure 1.9A) or nonclassical homo-base[297] pairings), as exemplified by Lehn's quinacridine receptor (Figure 1.41A) which bound a range of nucleotide monophosphates with 1:2 host:guest stoichiometry.[295] Interestingly, the crystal structure of a structurally similar tetraprotonated terpy-

based host and its thymidine triphosphate (TTP) adduct revealed that in addition to π-stacking and multiple charge-charge contacts, several weak forces work cooperatively to hold together the two partners in these systems.[298] Shown in Figure 1.41B, the complex is further stabilised by a variety of weak interactions (indicated by the green dashed lines), including HB between one carbonyl oxygen of thymidine and an ammonium group, CH···π contacts involving the methyl group of thymine and the 5'-methylene of the thymidine moiety and pyridine rings and a C=O···π contact between the second carbonyl group of thymine and a pyridine ring.

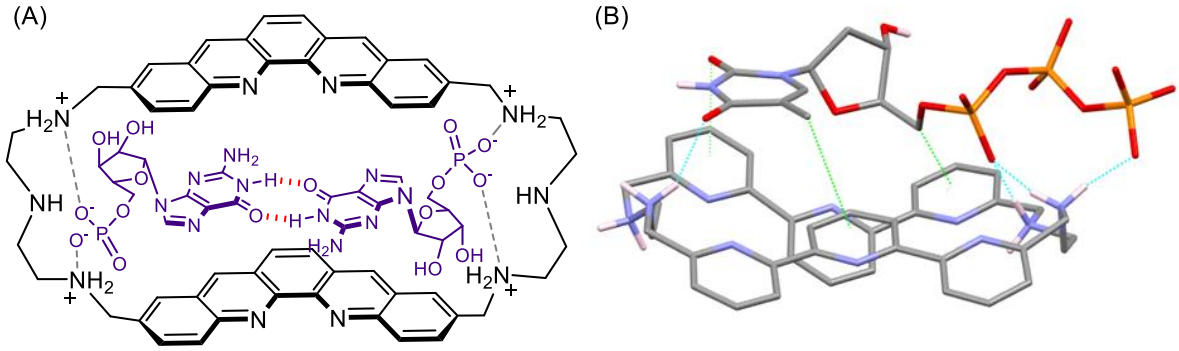


Figure 1.41: *Other cyclophane Hosts for phosphate nucleotides. (A) Lehn's quinacridine receptor for monophosphate nucleotide pairing, shown encapsulating two GMP anions (proposed nonclassical homo-base pairing interactions highlighted in red);[295] (B) Crystal structure of the TTP adduct of a terpy-based cyclophane showing multivalent interactions between host-guest species.[298] (hydrogen atoms, except those on protonated nitrogens have been omitted for clarity).*

In contrast to the above polyammonium-based hosts, several guanidinium receptors that contain additional functionalities have also been investigated for the complexation of other small organic phosphate sugars. In particular, pre-organised C_{3v} symmetric 'pinwheel' scaffolds have proven popular for this purpose having been designed to achieve geometric complementarity in addition to allowing for hydrogen bonding, electrostatic interactions and metal coordination.[299–303] For example, Shmuck and Schwegmann's tripodal receptor (Figure 1.16C) was found to exhibit a two-fold preference for mannose-1-phosphate (K_a = 1.25 x 10^{-3} M^{-1}) over carboxylated sugars in aqueous DMSO (30% water); molecular modelling analyses led to the suggestion that the anionic phosphate interacted with the guanidiniums, whereas the hydroxy units of the sugar participated in hydrogen bonds with the basal pyrrole and amide units.[299] In a similar manner except utilising the IDA methodology, Anslyn's polyguanidinium complex with 5-carboxyfluorescin dye (Figure 1.42A)

was shown to selectively bind IP_3 (and structurally similar benzene-1,3,5-triphosphate) more strongly than a variety of other phosphorylated molecules, including ATP and fructose-1,6-diphosphate in an aqueous medium (10 mM HEPES, pH 7.4).[301] The addition of IP_3 to the host solution led to dye displacement and a concomitant fluorescence quenching whereas with the other anions tested, little or no fluorescence changes were observed. More recently, Kuchelmeister and Schmuck have also exploited the unique coordination geometry of guanidinium for nucleotide binding, reporting a 'tweezer-like' host (Figure 1.42B) which bound AMP^{2-} ($K_a = 10^4\ M^{-1}$) with an unprecedented selectivity over ADP^{3-} and ATP^{4-} in water at neutral pH, with binding occurring through a combination of electrostatics, hydrogen bonding and π-π stacking interactions with the receptor's central aromatic core.[300] The rare selectivity for AMP was ascribed to the distinct binding mode of the receptor, which is less well suited to wrap around substrates with a larger phosphate hinge and hence are bound less optimally at the periphery of the cavity.

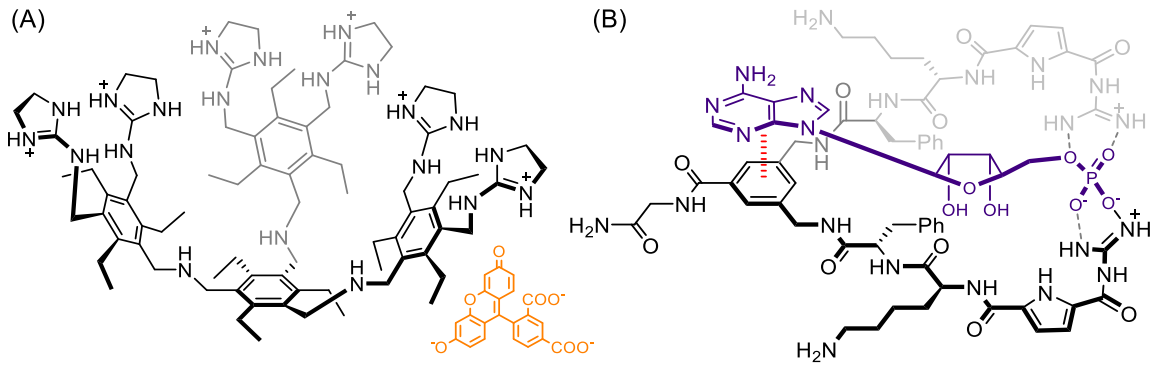


Figure 1.42: *Guanidinium receptors for phosphate sugars. (A) Anslyn's tripodal IDA for IP_3 (5-carboxyfluorescin dye in orange);[301] (B) Kuchelmeister and Schmuck's 'molecular tweezer' for AMP where the Y-shaped' geometry of the guanidinium functionality offers ideal complementarity to the phosphate 'head'.[300]*

Closely resembling those of their inorganic counterparts, a number of metal-containing receptors have also been reported for organic phosphate derivatives,[304,305] further incorporating additional functionalities to optimise interactions with the extended phosphate frameworks. Having utilised to similar effect the design principles underlying Anslyn's tripodal Cu(II) complexes, Butler described the preparation of a trisquinolyl-based Zn(II) receptor (Fig 1.43A) which was demonstrated to selectively bind ATP^{4-} over a range of non-nucleoside phosphates in aqueous solution (log K_a =

5.21 in 25 mM HEPES, pH 7.4).[176] This was due to favourable: (i) metal-ligand and (ii) urea-based hydrogen bonding interactions between the receptor and the 'phosphate tail', as well as multiple π-π stacking interactions between the terminal aromatic groups and the adenosine moiety of ATP^{4-}. Interestingly, the latter was also used to monitor the apyrase catalysed hydrolysis of ATP in real time *via* a decrease in the excimer emission of the Zn(II)host-ATP complex. The same author has also recently reported an ATP-responsive tetraazacyclododecane-Eu(III) complex (Figure 1.43B) which was used to visualise the real-time fluctuations in mitochondrial ATP in mammalian (NIH-3T3) cells *via* modulations in the emission intensity of the bright europium-based luminescence.[306]

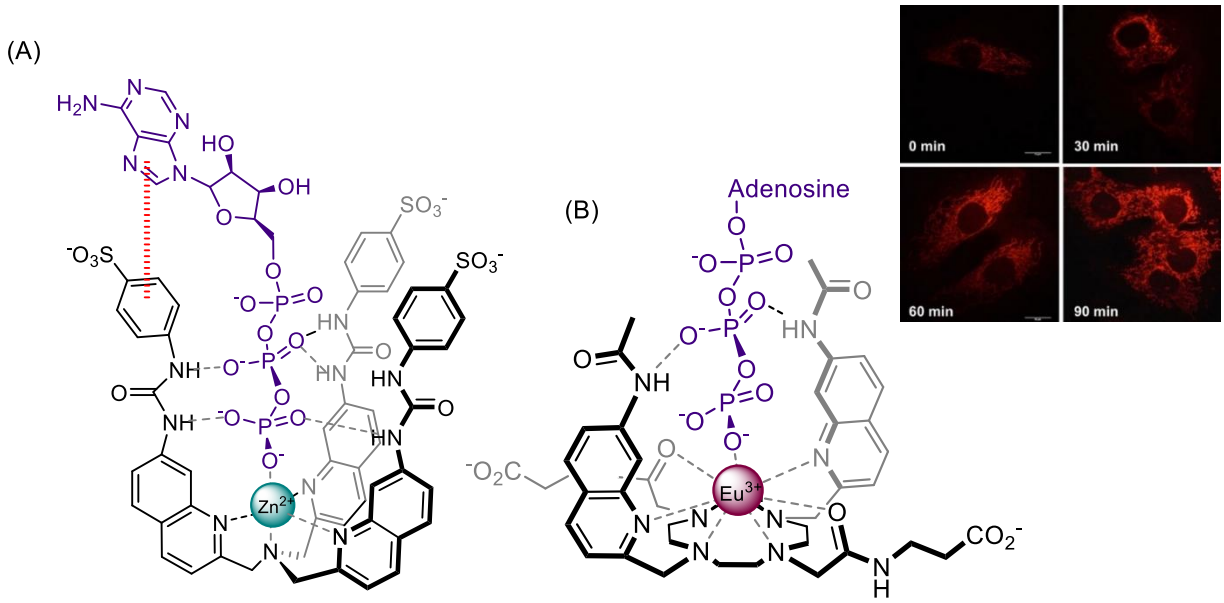


Figure 1.43: *Metallo-complexes for organophosphates. (A) Butler's Zn(II) tripodal receptor;[176] (B) (left) Butler's Eu(III) complex, for ATP; (right) Time-lapsed LSCM images of the NIH-3T3 cells stained with the uncomplexed receptor and staurosporine, a potent inhibitor of protein kinases.[306] Red regions indicate elevated levels of ATP. (Images reprinted with permission from ref 306. Copyright 2018 John Wiley and Sons). (Both receptors shown with the proposed mode of ATP binding).*

1.3.3.2 Receptors for organophosphorous (OP) chemical warfare agents (CWA's)

The first world war marked the advent of modern chemical warfare and sadly, with time fuelled the development of a range of weaponised compounds in the form of choking gases, vesicants and neurotoxic nerve agents (NAs).[307] Developed in the 1940's, the organophosphorous-based 'G-series' NAs (G designating German) depicted in Figure 1.33C represent a particular class of the latter, whose lethality arises from their potent ability to inhibit acetylcholinesterase (AChE) within

the body.[233] The high lability of the NAs' P-F bond enables robust phosphoester formation with a nucleophilic serine (S203) residue in the active site of AChE, rendering it incapable of the breakdown of endogenous ACh neurotransmitters – the accumulation of which can cause death by asphyxiation. Indeed, the release of GB (sarin) on the Tokyo subway in 1995[308] and more recently in Syria,[309] demonstrates the severe threat posed by these materials. Therefore, with noble motives in mind many groups have applied substantial effort into the design of hosts for the recognition and degradation of G-agents, largely utilising their innocuous hydrolysis products or physico-chemically related 'simulant' compounds (Figure 1.33C) as target guests for self-evident reasons.[231,310] The paucity of chemoreceptors for this purpose however, attests to the many challenges associated with the selective binding of these species.

Whilst long-range, strong electrostatic interactions have undoubtedly been the workhorse in driving phosphate *anion* binding in the examples discussed so far, the charge neutrality of the G-series NAs negates the use of such interactions to aid their association. Additionally, when compared to other OP-based molecules, for example the sugar nucleotides, the functionalities available for the non-covalent binding of the G-agents are limited and instead, the attention is primarily focused on the apolar 'alkyl side chain' and phosphoryl double bond (Figure 1.44).

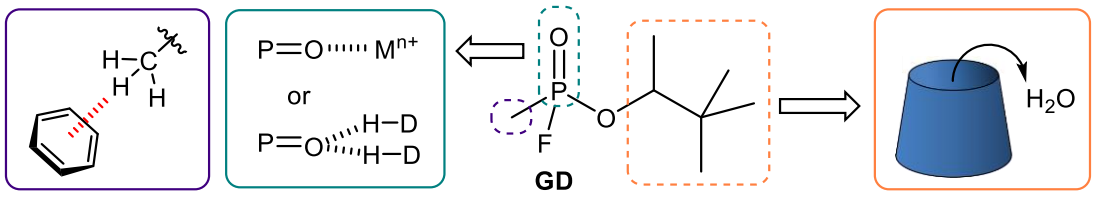


Figure 1.44: *A supramolecular consideration of the agent GD, indicating the challenges of OP CWA recognition.*

For the former, binding strategies point towards hydrophobically driven encapsulation and thus concave cavitands such as calixarenes and cyclodextrins[311,312] which feature shielded microenvironments present themselves as ideal hosts. Particularly when functionalised with suitably positioned HB donor moieties for secondary interactions with the phosphoryl bond (which also gives rise to the possibility for cooperative interactions), these can lead to host-guest complexes

of enhanced stability. For example, Dalcanale and co-workers have reported a solid-state structure of the inclusion complex of a monofunctionalised calix[4]arene with DMMP (Figure 1.45A) where an attractive (a) C–H···π interaction between the simulants -OCH_3 group and the host cavity (green dashed line), and (b) HB contact between the upper rim carboxylic OH and phosphoryl oxygen were observed (blue dashed line).[313] When immobilised onto a gold surface, the host was able to detect DMMP vapours of concentration as low as 16 ppb, thus highlighting the promise of such functional cavitands as effective sensors for the unambiguous detection of toxic G-series substances. Moreover, similarly monofunctionalised cyclodextrins except with nucleophilic groups at the wide and narrow rims have been shown to promote the degradation of the G-agents *via* cleavage of the NAs P-F (or P-CN) bond. Worek and co-workers stated the ability and velocity of the iodosobenzyl (IBA) β-CD host shown in Figure 1.45B to detoxify the NAs (in water, TRIS buffer), which decreased in the following order GF > GB > GA, driven by the increasing hydrophobic nature of the guest's phosphorous-alkyl group.[314]

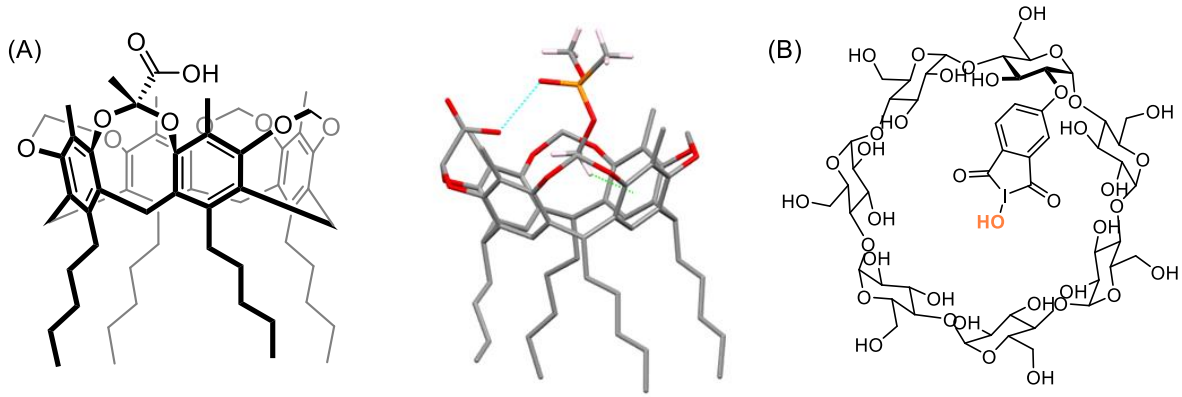


Figure 1.45: *Concave hosts for the molecular recognition of organophosphonates. (A) (left) Dalcanale's monofunctionalised calix[4]arene;[313] (right) the solid state structure of the DMMP adduct (with the host's lower rim alkyl chins omitted for clarity);[313] (B)Worek's IBA β-CD host capable of G-agent degradation (phosphonate ester forming functional group in orange).[314]*

Finally, with a view of binding OP compounds in a more geometrically optimal manner, Haddad and Badjić recently prepared a series of deep-cavity, C_{3v} symmetric 'molecular baskets' designed to promote the topological matching of phosphonates, in addition to hydrophobic effects.[315–317] The histamine-appended receptor in Figure 1.46A was demonstrated to 'trap' DMMP (K_a = 321 M^{-1} in 10 mM phosphate-buffered water, pH 2.5) *via* an induced-fit mechanism, with ^{1}H-NMR and

computational studies indicating the C−H···π interaction between the guest's P-CH_3 group and the host's cyclohexyl base as key to the association.[315] Interestingly, through studies of analogous dialkyl methylphosphonates with increasingly large alkoxy side chains (K_a's = 87 - 242 M^{-1}), a correlation was found between the strength of this interaction and the opening of the host molecule to accommodate the guest. Being the smallest in size, DMMP was found to be particularly effective at accessing the aromatic core of the cavitand (Figure 1.46B), thus resulting in the expansion of the arms, whereas larger guests were not able to access this as effectively and the host molecule was perturbed to a lesser extent.

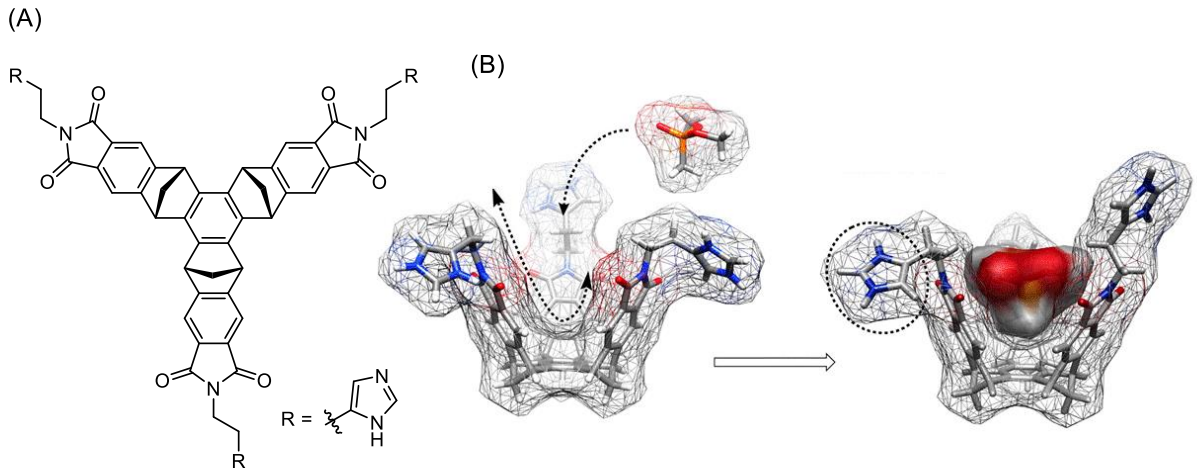


Figure 1.46: *Haddad and Badjić's tripodal 'basket'. (A) structure of cavitand with histamine apertures;[315] (B) van der Waal's surfaces of the same cavitand and DMMP indicating complementary size and shape fit.[315] (Spartan, MMFFs), (Images reprinted with permission from ref 315. Copyright 2013 American Chemical Society).*

1.4 Project Aims

Having emerged as the leitmotif for tetrahedral guest binding from the previous discussion and inspired by the strength of XB···anion interactions evidenced in the rare examples of the XB acyclic and macrocyclic host molecules reported to date, the broad aims of the project are to develop a series of C_{3v} symmetric halogen bonding metallo-tripodal receptors for the selective recognition and sensing of phosphate and phosphate ester anionic species.

Chapter Two initially details the development of a general synthetic protocol for a family of tris(iodotriazole) containing XB Zn(II)-based tripodal receptors (including redox-active hosts) and their respective inorganic monophosphate binding abilities are examined in comparison to the HB counterparts in competitive organic-aqueous solution. To further probe the XB-mediated molecular recognition properties of these systems in biologically relevant media, the preparation of a series of water-soluble XB Cu(II)-based analogues with poly(ethylene glycol) and permethylated-*β*-cyclodextrin appendages is also described and their anion binding abilities investigated *via* calorimetric, optical and electrochemical analyses.

Chapter Three extends this work and explores the application of XB metallo-tripodal receptors for the enantioselective recognition of the chiral phosphate ester species BINOL-PO_4^- as well as other biologically relevant carboxylate oxo-anions. Novel chiral XB Zn(II)-based hosts are prepared *via* an alternative synthetic strategy and their enantioselective anion binding behaviour studied in competitive organic-aqueous solution.

Chapter Four expands the use of the XB Zn(II)-tripodal motif recurrent in Chapters Two and Three, in the construction of a diZn(II) XB supramolecular cage envisioned for the recognition of inorganic *poly*phosphates. Specifically, dimetallic cryptate formation is attempted using a di-amine based [2 + 3] Schiff base synthetic strategy.

1.5 References

1 J.-M. Lehn, *Angew. Chem. Int. Ed. Engl.*, 1988, **27**, 89–112.
2 G. R. Desiraju, *Angew. Chem. Int. Ed. Engl.*, 1995, **34**, 2311–2327.
3 J. Steed and J. L. Atwood, *Supramolecular Chemistry, 2nd Edition*, Wiley, Chichester, UK, 1999.
4 E. R. Kay and D. A. Leigh, *Angew. Chem. Int. Ed.*, 2015, **54**, 10080–10088.
5 J. F. Stoddart, *Angew. Chem. Int. Ed.*, 2014, **53**, 11102–11104.
6 R. Dong, Y. Zhou, X. Huang, X. Zhu, Y. Lu and J. Shen, *Adv. Mater.*, 2015, **27**, 498–526.
7 M. J. Webber, E. A. Appel, E. W. Meijer and R. Langer, *Nat. Mater.*, 2016, **15**, 13–26.
8 E. Mattia and S. Otto, *Nat. Nanotechnol.*, 2015, **10**, 111–119.
9 E. Fischer, *Berichte Dtsch. Chem. Ges.*, 1894, **27**, 2985–2993.
10 D. E. Koshland, *Proc. Natl. Acad. Sci.*, 1958, **44**, 98–104.
11 D. E. Koshland, *Angew. Chem. Int. Ed. Engl.*, 1999, **33**, 2375–2378.
12 C. J. Pederson, *J. Am. Chem. Soc.*, 1967, **89**, 7017–7036.
13 J. M. Lehn, *Acc. Chem. Res.*, 1978, **11**, 49–57.
14 D. J. Cram, T. Kaneda, R. C. Helgeson and G. M. Lein, *J. Am. Chem. Soc.*, 1979, **101**, 6752–6754.
15 D. J. Cram, *Angew. Chem. Int. Ed. Engl.*, 1986, **25**, 1039–1057.
16 C. H. Park and H. E. Simmons, *J. Am. Chem. Soc.*, 1968, **90**, 2431–2432.
17 N. Busschaert, C. Caltagirone, W. Van Rossom and P. A. Gale, *Chem. Rev.*, 2015, **115**, 8038–8155.
18 J.-M. Lehn, *Angew. Chem. Int. Ed.*, 2002, **52**, 2836–2850.
19 J. J. Danon, A. Krüger, D. A. Leigh, J.-F. Lemonnier, A. J. Stephens, I. J. Vitorica-Yrezabal and S. L. Woltering, *Science*, 2017, **355**, 159–162.
20 K. S. Chichak, S. J. Cantrill, A. R. Pease, S.-H. Chiu, G. W. V. Cave, J. L. Atwood and J. F. Stoddart, *Science*, 2004, **304**, 1308–1312.
21 R. P. Feynman, *Caltech Engineering and Science.*, 1960, **23**, 22–36.
22 J. F. Stoddart, *Nat. Chem.*, 2009, **1**, 14–15.
23 *Nat. Nanotechnol.*, 2009, **4**, 781–781.
24 P. M. Proulx-Curry and N. D. Chasteen, *Coord. Chem. Rev.*, 1995, **144**, 347–368.
25 R. K. Watt, *BioMetals*, 2011, **24**, 489–500.
26 J. Boekhoven and S. I. Stupp, *Adv. Mater.*, 2014, **26**, 1642–1659.
27 F. A. Aldaye and H. F. Sleiman, *Pure Appl. Chem.*, 2009, **81**, 2157–2181.
28 P. Chidchob and H. F. Sleiman, *Curr. Opin. Chem. Biol.*, 2018, **46**, 63–70.
29 S. Erbas-Cakmak, D. A. Leigh, C. T. McTernan and A. L. Nussbaumer, *Chem. Rev.*, 2015, **115**, 10081–10206.
30 B. L. Feringa, *Angew. Chem. Int. Ed.*, 2017, **56**, 11060–11078.
31 I. Bertini, D. Lalli, S. Mangani, C. Pozzi, C. Rosa, E. C. Theil and P. Turano, *J. Am. Chem. Soc.*, 2012, **134**, 6169–6176.
32 B. Alberts, A. Johnson, J. Lewis, D. Morgan, M. Raff, K. Roberts and P. Walter, *Molecular Biology of the Cell, Sixth Edition*, Garland Science, New York, 2014.
33 P. Chakrabarti, *J. Mol. Biol.*, 1993, **234**, 463–482.
34 F. Delange, *Thyroid*, 1994, **4**, 107–128.
35 J. L. Sessler, P. Gale and W.-S. Cho, *Anion Receptor Chemistry*, The Royal Society of Chemistry, 2006.
36 W. D. McArdle, V. L. Katch and F. I. Katch, *Essentials of Exercise Physiology*, Lippincott Williams & Wilkins, London, 2011.
37 E. O'Dell, S. M. Tibby, A. Durward and I. A. Murdoch, *Crit. Care Med.*, 2007, **35**, 2390.
38 M. P. Anderson, R. J. Gregory, S. Thompson, D. W. Souza, S. Paul, R. C. Mulligan, A. E. Smith and M. J. Welsh, *Science*, 1991, **253**, 202–205.

39 L. Puljak and G. Kilic, *Biochim. Biophys. Acta BBA - Mol. Basis Dis.*, 2006, **1762**, 404–413.
40 R. F. Follett and J. F. Hatfield, *Nitrogen in the Environment: Sources, Problems and Management*, Elsevier, New York, 2001.
41 K. Yoshihara and T. Omori, Eds., *Technetium and Rhenium: Their Chemistry and Its Applications*, Springer-Verlag, Berlin Heidelberg, 1996.
42 A. R. Allen, L. Booker and G. A. Rockwood, in *Toxicology of Cyanides and Cyanogens*, Wiley-Blackwell, 2016.
43 R. D. Shannon, *Acta Crystallogr. Sect. A.*, 1976, **32**, 751–767.
44 F. Hofmeister, *Arch. Für Exp. Pathol. Pharmakol.*, 1888, **24**, 247–260.
45 K. H. G. Verschueren, F. Seljee, H. Rozeboom, K. Kalk and B. W. Dijkstra, *Nature*, 1993, **363**, 693–698.
46 H. Luecke and F. A. Quiocho, *Nature*, 1990, **347**, 402–406.
47 J. W. Pflugrath and F. A. Quiocho, *J. Mol. Biol.*, 1988, **200**, 163–180.
48 D. J. Cram, *Angew. Chem. Int. Ed. Engl.*, 1988, **27**, 1009–1020.
49 C. A. Hunter and H. L. Anderson, *Angew. Chem. Int. Ed.*, 2009, **48**, 7488–7499.
50 R. Breslow, S. Belvedere, L. Gershell and D. Leung, *Pure Appl. Chem.*, 2000, **72**, 333–342.
51 A. E. Martell, R. D. Hancock and R. J. Motekaitis, *Coord. Chem. Rev.*, 1994, **133**, 39–65.
52 Y. Li and A. H. Flood, *Angew. Chem. Int. Ed.*, 2008, **47**, 2649–2652.
53 P. Atkins and J. de Paula, *Atkins' Physical Chemistry*, OUP Oxford, 2010.
54 H.-J. Schneider, *Angew. Chem. Int. Ed.*, 2009, **48**, 3924–3977.
55 A. J. Wilson, *Nat. Chem.*, 2011, **3**, 193–194.
56 T. Steiner, *Angew. Chem. Int. Ed.*, 2002, **41**, 48–76.
57 J. A. K. Howard, V. J. Hoy, D. O'Hagan and G. T. Smith, *Tetrahedron*, 1996, **52**, 12613–12622.
58 J. Emsley, *Chem. Soc. Rev.*, 1980, **9**, 91–124.
59 P. Politzer, J. S. Murray and T. Clark, *Phys. Chem. Chem. Phys.*, 2013, **15**, 11178–11189.
60 J. Y. C. Lim and P. D. Beer, *Chem*, 2018, **4**, 731–783.
61 G. R. Desiraju, P. S. Ho, L. Kloo, A. C. Legon, R. Marquardt, P. Metrangolo, P. Politzer, G. Resnati and K. Rissanen, *Pure Appl. Chem.*, 2013, **85**, 1711–1713.
62 F. Guthrie, *J. Chem. Soc.*, 1863, **16**, 239–244.
63 O. Hassel and J. Hvoslef, *Acta Chem. Scand.*, 1954, **8**, 873.
64 O. Hassel and K. O. Strømme, *Acta Chem. Scand.*, 1958, **12**, 1146.
65 O. Hassel and K. O. Strømme, *Acta Chem. Scand.*, 1959, **13**, 1781–1786.
66 O. Hassel and C. Rømming, *Q Rev Chem Soc*, 1962, **16**, 1–18.
67 J.-M. Dumas, M. Gomel and M. Guerin, in *Molecular interactions involving organic halides*, John Wiley & Sons, Ltd., 1983, pp. 985–1020.
68 T. Clark, M. Hennemann, J. S. Murray and P. Politzer, *J. Mol. Model.*, 2007, **13**, 291–296.
69 L. P. Wolters, P. Schyman, M. J. Pavan, W. L. Jorgensen, F. M. Bickelhaupt and S. Kozuch, *Wiley Interdiscip. Rev. Comput. Mol. Sci.*, 2014, **4**, 523–540.
70 P. Metrangolo, H. Neukirch, T. Pilati and G. Resnati, *Acc. Chem. Res.*, 2005, **38**, 386–395.
71 P. Metrangolo, F. Meyer, T. Pilati, G. Resnati and G. Terraneo, *Angew. Chem. Int. Ed.*, 2008, **47**, 6114–6127.
72 D. Cinčić, T. Friščić and W. Jones, *Chem. – Eur. J.*, 2008, **14**, 747–753.
73 K. Rissanen, *CrystEngComm*, 2008, **10**, 1107.
74 F. Meyer and P. Dubois, *CrystEngComm*, 2013, **15**, 3058–3071.
75 G. Berger, J. Soubhye and F. Meyer, *Polym. Chem.*, 2015, **6**, 3559–3580.
76 J.-P. Gliese, S. H. Jungbauer and S. M. Huber, *Chem. Commun.*, 2017, **53**, 12052–12055.
77 O. Coulembier, F. Meyer and P. Dubois, *Polym. Chem.*, 2010, **1**, 434–437.
78 F. Kniep, S. H. Jungbauer, Q. Zhang, S. M. Walter, S. Schindler, I. Schnapperelle, E. Herdtweck and S. M. Huber, *Angew. Chem. Int. Ed.*, 2013, **52**, 7028–7032.

79 N. Houbenov, R. Milani, M. Poutanen, J. Haataja, V. Dichiarante, J. Sainio, J. Ruokolainen, G. Resnati, P. Metrangolo and O. Ikkala, *Nat. Commun.*, 2014, **5**, 4043.
80 E. Corradi, S. V. Meille, M. T. Messina, P. Metrangolo and G. Resnati, *Angew. Chem. Int. Ed.*, 2000, **39**, 1782–1786.
81 P. M. J. Szell, A. Siiskonen, L. Catalano, G. Cavallo, G. Terraneo, A. Priimagi, D. L. Bryce and P. Metrangolo, *New J. Chem.*, 2018, **42**, 10467–10471.
82 L. Meazza, J. A. Foster, K. Fucke, P. Metrangolo, G. Resnati and J. W. Steed, *Nat. Chem.*, 2013, **5**, 42–47.
83 A. Pizzi, L. Lascialfari, N. Demitri, A. Bertolani, D. Maiolo, E. Carretti and P. Metrangolo, *CrystEngComm*, 2017, **19**, 1870–1874.
84 R. Wilcken, M. O. Zimmermann, A. Lange, A. C. Joerger and F. M. Boeckler, *J. Med. Chem.*, 2013, **56**, 1363–1388.
85 L.-Y. You, S.-G. Chen, X. Zhao, Y. Liu, W.-X. Lan, Y. Zhang, H.-J. Lu, C.-Y. Cao and Z.-T. Li, *Angew. Chem. Int. Ed.*, 2012, **51**, 1657–1661.
86 P. Auffinger, F. A. Hays, E. Westhof and P. S. Ho, *Proc. Natl. Acad. Sci.*, 2004, **101**, 16789–16794.
87 Y. Lu, T. Shi, Y. Wang, H. Yang, X. Yan, X. Luo, H. Jiang and W. Zhu, *J. Med. Chem.*, 2009, **52**, 2854–2862.
88 R. D. Carpenter, A. Natarajan, E. Y. Lau, M. Andrei, D. M. Solano, F. C. Lightstone, S. J. DeNardo, K. S. Lam and M. J. Kurth, *Cancer Res.*, 2010, **70**, 5448–5456.
89 A. Mele, P. Metrangolo, H. Neukirch, T. Pilati and G. Resnati, *J. Am. Chem. Soc.*, 2005, **127**, 14972–14973.
90 D. Quiñonero, C. Garau, A. Frontera, P. Ballester, A. Costa and P. M. Deyà, *Chem. Phys. Lett.*, 2002, **359**, 486–492.
91 O. B. Berryman, V. S. Bryantsev, D. P. Stay, D. W. Johnson and B. P. Hay, *J. Am. Chem. Soc.*, 2007, **129**, 48–58.
92 M. Albrecht, C. Wessel, M. de Groot, K. Rissanen and A. Lüchow, *J. Am. Chem. Soc.*, 2008, **130**, 4600–4601.
93 A. Frontera, P. Gamez, M. Mascal, T. J. Mooibroek and J. Reedijk, *Angew. Chem. Int. Ed.*, 2011, **50**, 9564–9583.
94 C. Estarellas, A. Bauzá, A. Frontera, D. Quiñonero and P. M. Deyà, *Phys. Chem. Chem. Phys.*, 2011, **13**, 5696–5702.
95 J. Mareda and S. Matile, *Chem. – Eur. J.*, 2009, **15**, 28–37.
96 O. B. Berryman, F. Hof, M. J. Hynes and D. W. Johnson, *Chem. Commun.*, 2006, **0**, 506–508.
97 T. K. Ronson, J. Fisher, L. P. Harding, P. J. Rizkallah, J. E. Warren and M. J. Hardie, *Nat. Chem.*, 2009, **1**, 212–216.
98 Q.-F. Sun, J. Iwasa, D. Ogawa, Y. Ishido, S. Sato, T. Ozeki, Y. Sei, K. Yamaguchi and M. Fujita, *Science*, 2010, **328**, 1144–1147.
99 M. Hirai and F. P. Gabbaï, *Angew. Chem. Int. Ed.*, 2014, **54**, 1205–1209.
100 F. Biedermann, W. M. Nau and H.-J. Schneider, *Angew. Chem. Int. Ed.*, 2014, **53**, 11158–11171.
101 M. S. Cubberley and B. L. Iverson, *J. Am. Chem. Soc.*, 2001, **123**, 7560–7563.
102 M. Fernández-Vidal, S. H. White and A. S. Ladokhin, *J. Membr. Biol.*, 2011, **239**, 5–14.
103 M. Lisbjerg, B. E. Nielsen, B. O. Milhøj, S. P. A. Sauer and M. Pittelkow, *Org. Biomol. Chem.*, 2014, **13**, 369–373.
104 K. I. Assaf, D. Gabel, W. Zimmermann and W. M. Nau, *Org. Biomol. Chem.*, 2016, **14**, 7702–7706.
105 P. Sokkalingam, J. Shraberg, S. W. Rick and B. C. Gibb, *J. Am. Chem. Soc.*, 2016, **138**, 48–51.
106 J. M. Lehn, E. Sonveaux and A. K. Willard, *J. Am. Chem. Soc.*, 1978, **100**, 4914–4916.
107 B. Dietrich, J. Guilhem, J.-M. Lehn, C. Pascard and E. Sonveaux, *Helv. Chim. Acta*, 1984, **67**, 91–104.

108 B. Dietrich, J.-M. Lehn, J. Guilhem and C. Pascard, *Tetrahedron Lett.*, 1989, **30**, 4125–4128.
109 B. Dietrich, B. Dilworth, J.-M. Lehn, J.-P. Souchez, M. Cesario, J. Guilhem and C. Pascard, *Helv. Chim. Acta*, 1996, **79**, 569–587.
110 A. Bencini, C. Coluccini, A. Garau, C. Giorgi, V. Lippolis, L. Messori, D. Pasini and S. Puccioni, *Chem. Commun.*, 2012, **48**, 10428–10430.
111 F. P. Schmidtchen, *Angew. Chem. Int. Ed. Engl.*, 1977, **16**, 720–721.
112 F. P. Schmidtchen, *Chem. Ber.*, 1981, **114**, 597–607.
113 K. Worm, F. P. Schmidtchen, A. Schier, A. Schäfer and M. Hesse, *Angew. Chem. Int. Ed. Engl.*, 1994, **33**, 327–329.
114 K. Worm and F. P. Schmidtchen, *Angew. Chem. Int. Ed. Engl.*, 1995, **34**, 65–66.
115 D. W. Christianson and W. N. Lipscomb, *Acc. Chem. Res.*, 1989, **22**, 62–69.
116 T. H. Wirth and N. Davidson, *J. Am. Chem. Soc.*, 1964, **86**, 4325–4329.
117 F. A. Cotton, V. W. Day, E. E. Hazen and S. Larsen, *J. Am. Chem. Soc.*, 1973, **95**, 4834–4840.
118 D. M. Perreault, L. A. Cabell and E. V. Anslyn, *Bioorg. Med. Chem.*, 1997, **5**, 1209–1220.
119 P. Blondeau, M. Segura, R. Pérez-Fernández and J. de Mendoza, *Chem. Soc. Rev.*, 2007, **36**, 198–210.
120 B. Dietrich, T. M. Fyles, J.-M. Lehn, L. G. Pease and D. L. Fyles, *J. Chem. Soc. Chem. Commun.*, 1978, 934.
121 M. Berger and F. P. Schmidtchen, *J. Am. Chem. Soc.*, 1999, **121**, 9986–9993.
122 C. Schmuck and M. Schwegmann, *J. Am. Chem. Soc.*, 2005, **127**, 3373–3379.
123 K. Sato, S. Arai and T. Yamagishi, *Tetrahedron Lett.*, 1999, **40**, 5219–5222.
124 E. Alcalde, N. Mesquida, L. Pérez-García, C. Alvarez-Rúa, S. García-Granda and E. García-Rodriguez, *Chem. Commun.*, 1999, **0**, 295–296.
125 H.-Y. Gong, B. M. Rambo, E. Karnas, V. M. Lynch and J. L. Sessler, *Nat. Chem.*, 2010, **2**, 406–409.
126 N. Ahmed, B. Shirinfar, I. S. Youn, M. Yousuf and K. S. Kim, *Org. Biomol. Chem.*, 2013, **11**, 6407–6413.
127 K. Ohmatsu, M. Kiyokawa and T. Ooi, *J. Am. Chem. Soc.*, 2011, **133**, 1307–1309.
128 L. C. Gilday, N. G. White and P. D. Beer, *Dalton Trans.*, 2012, **41**, 7092–7097.
129 N. Mesquida, I. Dinarès, A. Ibáñez and E. Alcalde, *Org. Biomol. Chem.*, 2013, **11**, 6385–6396.
130 J. M. Aizpurua, R. M. Fratila, Z. Monasterio, N. Pérez-Esnaola, E. Andreieff, A. Irastorza and M. Sagartzazu-Aizpurua, *New J. Chem.*, 2014, **38**, 474–480.
131 A. Kumar and P. S. Pandey, *Org. Lett.*, 2008, **10**, 165–168.
132 R. K. Chhatra, A. Kumar and P. S. Pandey, *J. Org. Chem.*, 2011, **76**, 9086–9089.
133 B. Schulze, C. Friebe, M. D. Hager, W. Günther, U. Köhn, B. O. Jahn, H. Görls and U. S. Schubert, *Org. Lett.*, 2010, **12**, 2710–2713.
134 H. T. Le, S. C. Park, C. Kang, C. W. Lim and T. W. Kim, *Org. Biomol. Chem.*, 2015, **13**, 8291–8297.
135 R. A. Pascal, J. Spergel and D. Van Engen, *Tetrahedron Lett.*, 1986, **27**, 4099–4102.
136 K. Kavallieratos, S. R. de Gala, D. J. Austin and R. H. Crabtree, *J. Am. Chem. Soc.*, 1997, **119**, 2325–2326.
137 C. R. Bondy and S. J. Loeb, *Coord. Chem. Rev.*, 2003, **240**, 77–99.
138 S. J. Brooks, P. A. Gale and M. E. Light, *Chem. Commun.*, 2006, **0**, 4344–4346.
139 G. V. Oshovsky, W. Verboom, R. H. Fokkens and D. N. Reinhoudt, *Chem. – Eur. J.*, 2004, **10**, 2739–2748.
140 S. Kubik, R. Kirchner, D. Nolting and J. Seidel, *J. Am. Chem. Soc.*, 2002, **124**, 12752–12760.
141 J. L. Sessler, M. J. Cyr, V. Lynch, E. McGhee and J. A. Ibers, *J. Am. Chem. Soc.*, 1990, **112**, 2810–2813.
142 P. A. Gale, *Chem. Commun.*, 2008, 4525.

143 I. Saha, J. T. Lee and C.-H. Lee, *Eur. J. Org. Chem.*, 2015, **2015**, 3859–3885.
144 P. A. Gale, J. L. Sessler, V. Král and V. Lynch, *J. Am. Chem. Soc.*, 1996, **118**, 5140–5141.
145 D.-W. Yoon, D. E. Gross, V. M. Lynch, J. L. Sessler, B. P. Hay and C.-H. Lee, *Angew. Chem. Int. Ed.*, 2008, **47**, 5038–5042.
146 K.-C. Chang, T. Minami, P. Koutnik, P. Y. Savechenkov, Y. Liu and P. Anzenbacher, *J. Am. Chem. Soc.*, 2014, **136**, 1520–1525.
147 E. Mulugeta, R. Dutta, Q. He, V. Lynch, J. Sessler and C.-H. Lee, *Eur. J. Org. Chem.*, 2017, **2017**, 4891–4895.
148 H. C. Kolb, M. G. Finn and K. B. Sharpless, *Angew. Chem. Int. Ed.*, 2001, **40**, 2004–2021.
149 F. Himo, T. Lovell, R. Hilgraf, V. V. Rostovtsev, L. Noodleman, K. B. Sharpless and V. V. Fokin, *J. Am. Chem. Soc.*, 2005, **127**, 210–216.
150 V. V. Rostovtsev, L. G. Green, V. V. Fokin and K. B. Sharpless, *Angew. Chem. Int. Ed.*, 2002, **41**, 2596–2599.
151 R. M. Meudtner and S. Hecht, *Angew. Chem. Int. Ed.*, 2008, **47**, 4926–4930.
152 H. Juwarker, J. M. Lenhardt, D. M. Pham and S. L. Craig, *Angew. Chem. Int. Ed.*, 2008, **47**, 3740–3743.
153 J. Cai and J. L. Sessler, *Chem. Soc. Rev.*, 2014, **43**, 6198–6213.
154 Y. Hua, Y. Liu, C.-H. Chen and A. H. Flood, *J. Am. Chem. Soc.*, 2013, **135**, 14401–14412.
155 S. Guieu, A. K. Crane and M. J. MacLachlan, *Chem. Commun.*, 2011, **47**, 1169–1171.
156 Y. Liu, A. Singharoy, C. G. Mayne, A. Sengupta, K. Raghavachari, K. Schulten and A. H. Flood, *J. Am. Chem. Soc.*, 2016, **138**, 4843–4851.
157 S. Lee, C.-H. Chen and A. H. Flood, *Nat. Chem.*, 2013, **5**, 704–710.
158 E. M. Fatila, M. Pink, E. B. Twum, J. A. Karty and A. H. Flood, *Chem. Sci.*, 2018, **9**, 2863–2872.
159 M. K. Cerreta and K. A. Berglund, *J. Cryst. Growth*, 1987, **84**, 577–588.
160 F. Rull, A. D. Valle, F. Sobron and S. Veintemillas, *J. Raman Spectrosc.*, 1989, **20**, 625–631.
161 N. Bregović, N. Cindro, L. Frkanec, K. Užarević and V. Tomišić, *Chem. – Eur. J.*, 2014, **20**, 15863–15871.
162 J. Svec, M. Necas and V. Sindelar, *Angew. Chem. Int. Ed.*, 2010, **49**, 2378–2381.
163 V. Havel, J. Svec, M. Wimmerova, M. Dusek, M. Pojarova and V. Sindelar, *Org. Lett.*, 2011, **13**, 4000–4003.
164 M. A. Yawer, V. Havel and V. Sindelar, *Angew. Chem. Int. Ed.*, 2015, **54**, 276–279.
165 D. F. Shriver and M. J. Biallas, *J. Am. Chem. Soc.*, 1967, **89**, 1078–1081.
166 R. J. Motekaitis, A. E. Martell, B. Dietrich and J. M. Lehn, *Inorg. Chem.*, 1984, **23**, 1588–1591.
167 L. Fabbrizzi and I. Faravelli, *Chem. Commun.*, 1998, **0**, 971–972.
168 A. Brugnara, F. Topić, K. Rissanen, A. de la Lande, B. Colasson and O. Reinaud, *Chem. Sci.*, 2014, **5**, 3897–3904.
169 M. M. Harding, M. W. Nowicki and M. D. Walkinshaw, *Crystallogr. Rev.*, 2010, **16**, 247–302.
170 D. Duda, L. Govindasamy, M. Agbandje-McKenna, C. Tu, D. N. Silverman and R. McKenna, *Acta Crystallogr. D Biol. Crystallogr.*, 2003, **59**, 93–104.
171 G. R. Hemsworth, E. J. Taylor, R. Q. Kim, R. C. Gregory, S. J. Lewis, J. P. Turkenburg, A. Parkin, G. J. Davies and P. H. Walton, *J. Am. Chem. Soc.*, 2013, **135**, 6069–6077.
172 M. A. Hough and S. S. Hasnain, *J. Mol. Biol.*, 1999, **287**, 579–592.
173 T. Haikarainen, C. Frioux, L.-Q. Zhnag, D.-C. Li and A. C. Papageorgiou, *Biochim. Biophys. Acta BBA - Proteins Proteomics*, 2014, **1844**, 422–429.
174 S. L. Tobey and E. V. Anslyn, *J. Am. Chem. Soc.*, 2003, **125**, 14807–14815.
175 S. J. Butler and K. A. Jolliffe, *Org. Biomol. Chem.*, 2011, **9**, 3471–3483.
176 S. J. Butler, *Chem. – Eur. J.*, 2014, **20**, 15768–15774.

177 L. C. Gilday, S. W. Robinson, T. A. Barendt, M. J. Langton, B. R. Mullaney and P. D. Beer, *Chem. Rev.*, 2015, **115**, 7118–7195.
178 A. Brown and P. D. Beer, *Chem. Commun.*, 2016, **52**, 8645–8658.
179 T. Caronna, R. Liantonio, T. A. Logothetis, P. Metrangolo, T. Pilati and G. Resnati, *J. Am. Chem. Soc.*, 2004, **126**, 4500–4501.
180 G. Marras, P. Metrangolo, F. Meyer, T. Pilati, G. Resnati and A. Vij, *New J. Chem.*, 2006, **30**, 1397–1402.
181 M. G. Sarwar, B. Dragisic, S. Sagoo and M. S. Taylor, *Angew. Chem. Int. Ed.*, 2010, **49**, 1674–1677.
182 R. Tepper, B. Schulze, H. Görls, P. Bellstedt, M. Jäger and U. S. Schubert, *Org. Lett.*, 2015, **17**, 5740–5743.
183 D. Mungalpara, S. Stegmüller and S. Kubik, *Chem. Commun.*, 2017, **53**, 5095–5098.
184 B. H. M. Kuijpers, G. C. T. Dijkmans, S. Groothuys, P. J. L. M. Quaedflieg, R. H. Blaauw, F. L. van Delft and F. P. J. T. Rutjes, *Synlett*, 2005, **2005**, 3059–3062.
185 J. E. Hein, J. C. Tripp, L. B. Krasnova, K. B. Sharpless and V. V. Fokin, *Angew. Chem. Int. Ed.*, 2009, **48**, 8018–8021.
186 W. S. Brotherton, R. J. Clark and L. Zhu, *J. Org. Chem.*, 2012, **77**, 6443–6455.
187 B. Nepal and S. Scheiner, *Chem. – Eur. J.*, 2015, **21**, 13330–13335.
188 R. Tepper, B. Schulze, M. Jäger, C. Friebe, D. H. Scharf, H. Görls and U. S. Schubert, *J. Org. Chem.*, 2015, **80**, 3139–3150.
189 B. Nepal and S. Scheiner, *J. Phys. Chem. A*, 2015, **119**, 13064–13073.
190 J. Y. C. Lim and P. D. Beer, *Chem. Commun.*, 2015, **51**, 3686–3688.
191 J. Y. C. Lim, I. Marques, L. Ferreira, V. Félix and P. D. Beer, *Chem. Commun.*, 2016, **52**, 5527–5530.
192 B. Nepal and S. Scheiner, *ChemPhysChem*, 2016, **17**, 836–844.
193 S. M. Walter, F. Kniep, E. Herdtweck and S. M. Huber, *Angew. Chem. Int. Ed.*, 2011, **50**, 7187–7191.
194 S. M. Walter, S. H. Jungbauer, F. Kniep, S. Schindler, E. Herdtweck and S. M. Huber, *J. Fluor. Chem.*, 2013, **150**, 14–20.
195 M. Cametti, K. Raatikainen, P. Metrangolo, T. Pilati, G. Terraneo and G. Resnati, *Org. Biomol. Chem.*, 2012, **10**, 1329–1333.
196 S. Chakraborty, R. Dutta and P. Ghosh, *Chem. Commun.*, 2015, **51**, 14793–14796.
197 A. Caballero, N. G. White and P. D. Beer, *Angew. Chem. Int. Ed.*, 2011, **50**, 1845–1848.
198 F. Zapata, A. Caballero, N. G. White, T. D. W. Claridge, P. J. Costa, V. Félix and P. D. Beer, *J. Am. Chem. Soc.*, 2012, **134**, 11533–11541.
199 Y. Takeda, D. Hisakuni, C.-H. Lin and S. Minakata, *Org. Lett.*, 2015, **17**, 318–321.
200 N. Busschaert, C. Caltagirone, W. Van Rossom and P. A. Gale, *Chem. Rev.*, 2015, **115**, 8038–8155.
201 B. T. Nguyen and E. V. Anslyn, *Coord. Chem. Rev.*, 2006, **250**, 3118–3127.
202 X. Lou, D. Ou, Q. Li and Z. Li, *Chem. Commun.*, 2012, **48**, 8462–8477.
203 J. Du, M. Hu, J. Fan and X. Peng, *Chem. Soc. Rev.*, 2012, **41**, 4511–4535.
204 P. D. Beer and A. D. Keefe, *J. Organomet. Chem.*, 1989, **375**, C40–C42.
205 P. D. Beer, A. R. Graydon, A. O. M. Johnson and D. K. Smith, *Inorg. Chem.*, 1997, **36**, 2112–2118.
206 X. Huang, B. Wu, C. Jia, B. P. Hay, M. Li and X.-J. Yang, *Chem. – Eur. J.*, 2013, **19**, 9034–9041.
207 N. G. White and P. D. Beer, *Beilstein J. Org. Chem.*, 2012, **8**, 246–252.
208 C.-T. Li, Q.-Y. Cao, J.-J. Li, Z.-W. Wang and B.-N. Dai, *Inorganica Chim. Acta*, 2016, **449**, 31–37.
209 N. H. Evans, C. J. Serpell and P. D. Beer, *Chem. Commun.*, 2011, **47**, 8775–8777.
210 J. Y. C. Lim, M. J. Cunningham, J. J. Davis and P. D. Beer, *Dalton Trans.*, 2014, **43**, 17274–17282.
211 T. Romero, R. A. Orenes, A. Tárraga and P. Molina, *Organometallics*, 2013, **32**, 5740–5753.

212 K. A. Nielsen, J. O. Jeppesen, E. Levillain and J. Becher, *Angew. Chem. Int. Ed.*, 2003, **42**, 187–191.
213 R. Oliveira, S. Groni, C. Fave, M. Branca, F. Mavré, D. Lorcy, M. Fourmigué and B. Schöllhorn, *Phys. Chem. Chem. Phys.*, 2016, **18**, 15867–15873.
214 R. Martínez-Máñez and F. Sancenón, *Chem. Rev.*, 2003, **103**, 4419–4476.
215 H.-J. Mo, Y. Shen and B.-H. Ye, *Inorg. Chem.*, 2012, **51**, 7174–7184.
216 E. A. Weitz, J. Y. Chang, A. H. Rosenfield and V. C. Pierre, *J. Am. Chem. Soc.*, 2012, **134**, 16099–16102.
217 T. K. Mole, W. E. Arter, I. Marques, V. Félix and P. D. Beer, *J. Organomet. Chem.*, 2015, **792**, 206–210.
218 N.-J. Jeon, B.-J. Ryu, B.-H. Lee and K.-C. Nam, *Bull. Korean Chem. Soc.*, 2009, **30**, 1675–1677.
219 X. Yang, G. Zhang, Y. Li, Z. Liu, X. Gong, B. Gao, G. Zhang, Y. Cui and G. Sun, *RSC Adv.*, 2015, **5**, 22455–22462.
220 H. Miyaji, W. Sato and J. L. Sessler, *Angew. Chem. Int. Ed.*, 2000, **39**, 1777–1780.
221 J. Isaad and A. El Achari, *Tetrahedron*, 2011, **67**, 4196–4201.
222 *Phosphorus in The Global Environment: Transfers, Cycles and Management*, Wiley, New York, 1995.
223 C. F. Mason, *Biology of freshwater pollution.*, Longman, New York, 1991.
224 J. A. Delmez and E. Slatopolsky, *Am. J. Kidney Dis.*, 1992, **19**, 303–317.
225 G. Block, T. Hulbert-Shearon, N. Levin and F. Port, *Am. J. Kidney Dis.*, 1998, **31**, 607–617.
226 G. A. Block and F. K. Port, *Am. J. Kidney Dis.*, 2000, **35**, 1226–1237.
227 A. E. Timms, Y. Zhang, R. G. G. Russell and M. A. Brown, *Rheumatology*, 2002, **41**, 725–729.
228 R. Dhingra, L. M. Sullivan, C. S. Fox, T. J. Wang, R. B. D'agostino, J. M. Gaziano and R. S. Vasan, *Arch. Intern. Med.*, 2007, **167**, 879–885.
229 F. Albaaj and A. J. Hutchison, *Drugs*, 2003, **63**, 577–596.
230 R. T. Delfino, T. S. Ribeiro and J. D. Figueroa-Villar, *J. Braz. Chem. Soc.*, 2009, **20**, 407–428.
231 K. Kim, O. G. Tsay, D. A. Atwood and D. G. Churchill, *Chem. Rev.*, 2011, **111**, 5345–5403.
232 R. M. Black and J. M. Harrison, in *The Chemistry of Organophosphorus Compounds*, Wiley, Chichester (UK), 1996, vol. 4, pp. 781–840.
233 J. Bajgar, *Adv. Clin. Chem.*, 2004, **38**, 151–216.
234 J. Bajgar, K. Kuca, D. Jun, L. Bartosova and J. Fusek, *J. Curr. Drug. Metab.*, 2007, **8**, 803–809.
235 A. E. Taylor and C. W. Miller, *J. Biol. Chem.*, 1914, **18**, 215–224.
236 J. B. Martin and D. M. Doty, *Anal. Chem.*, 1949, **21**, 965–967.
237 A. Gee and V. R. Deitz, *Anal. Chem.*, 1953, **25**, 1320–1324.
238 H. Baadenhuijsen, H. E. Seuren-Jacobs and A. P. Jansen, *Clin. Chem.*, 1977, **23**, 1275–1280.
239 A. Muñoz, F. M. Torres, J. M. Estela and V. Cerda, *Anal. Chim. Acta*, 1997, **350**, 21–29.
240 S. D. Katewa and S. S. Katyare, *Anal. Biochem.*, 2003, **323**, 180–187.
241 E. Diacu, P. C. Ioannou, C. K. Polydorou and C. E. Efstathiou, *Analyst*, 1995, **120**, 2613–2616.
242 J. Estela and V. Cerda, *Talanta*, 2005, **66**, 307–331.
243 A. T. Law al and S. B. Adeloju, *Talanta*, 2013, **114**, 191–203.
244 K. Ikebukuro, H. Wakamura, I. Karube, I. Kubo, M. Inagawa, T. Sugawara, Y. Arikawa, M. Suzuki and T. Takeuchi, *Biosens. Bioelectron.*, 1996, **11**, 959–965.
245 N. Gajovic, K. Habermüller, A. Warsinke, W. Schuhmann and F. W. Scheller, *Electroanalysis*, 1999, **11**, 1377–1383.
246 C. Solscheid, S. Kunzelmann, C. T. Davis, J. L. Hunter, A. Nofer and M. R. Webb, *Biochemistry*, 2015, **54**, 5054–5062.

247 E. A. Katayev, Y. A. Ustynyuk and J. L. Sessler, *Coord. Chem. Rev.*, 2006, **250**, 3004–3037.
248 Y. Marcus, *Biophys. Chem.*, 1994, **51**, 111–127.
249 L. Alderighi, P. Gans, A. Ienco, D. Peters, A. Sabatini and A. Vacca, *Coord. Chem. Rev.*, 1999, **184**, 311–318.
250 A. E. Hargrove, S. Nieto, T. Zhang, J. L. Sessler and E. V. Anslyn, *Chem. Rev.*, 2011, **111**, 6603–6782.
251 C. Bazzicalupi, A. Bencini and V. Lippolis, *Chem. Soc. Rev.*, 2010, **39**, 3709–3728.
252 C. Nakai and W. Glinsmann, *Biochemistry*, 1977, **16**, 5636–5641.
253 S. Bunce and E. S. W. Kong, *Biophys. Chem.*, 1978, **8**, 357–368.
254 C. A. Ilioudis, D. G. Georganopoulou and J. W. Steed, *CrystEngComm*, 2002, **4**, 26–36.
255 E. García-España, P. Díaz, J. M. Llinares and A. Bianchi, *Coord. Chem. Rev.*, 2006, **250**, 2952–2986.
256 C. Bazzicalupi, A. Bencini, A. Bianchi, M. Cecchi, B. Escuder, V. Fusi, E. Garcia-España, C. Giorgi, S. V. Luis, G. Maccagni, V. Marcelino, P. Paoletti and B. Valtancoli, *J. Am. Chem. Soc.*, 1999, **121**, 6807–6815.
257 C. Bazzicalupi, A. Bencini, A. Bianchi, A. Danesi, C. Giorgi and B. Valtancoli, *Inorg. Chem.*, 2009, **48**, 2391–2398.
258 M. A. Hossain, J. A. Liljegren, D. Powell and K. Bowman-James, *Inorg. Chem.*, 2004, **43**, 3751–3755.
259 M. E. Huston, E. U. Akkaya and A. W. Czarnik, *J. Am. Chem. Soc.*, 1989, **111**, 8735–8737.
260 D. H. Vance and A. W. Czarnik, *J. Am. Chem. Soc.*, 1994, **116**, 9397–9398.
261 B. Dietrich, M. W. Hosseini, J. M. Lehn and R. B. Sessions, *J. Am. Chem. Soc.*, 1981, **103**, 1282–1283.
262 E. Kimura, A. Sakonaka, T. Yatsunami and M. Kodama, *J. Am. Chem. Soc.*, 1981, **103**, 3041–3045.
263 D. A. Nation, J. Reibenspies and A. E. Martell, *Inorg. Chem.*, 1996, **35**, 4597–4603.
264 Q. Lu, A. E. Martell and R. J. Motekaitis, *Inorganica Chim. Acta*, 1996, **251**, 365–370.
265 D. A. Nation, Q. Lu and A. E. Martell, *Inorganica Chim. Acta*, 1997, **263**, 209–217.
266 C. Anda, A. Llobet, V. Salvado, J. Reibenspies, R. J. Motekaitis and A. E. Martell, *Inorg. Chem.*, 2000, **39**, 2986–2999.
267 T. Clifford, A. Danby, J. M. Llinares, S. Mason, N. W. Alcock, D. Powell, J. A. Aguilar, E. García-España and K. Bowman-James, *Inorg. Chem.*, 2001, **40**, 4710–4720.
268 S. W. Robinson, C. L. Mustoe, N. G. White, A. Brown, A. L. Thompson, P. Kennepohl and P. D. Beer, *J. Am. Chem. Soc.*, 2015, **137**, 499–507.
269 B. R. Mullaney, A. L. Thompson and P. D. Beer, *Angew. Chem. Int. Ed.*, 2014, **53**, 11458–11462.
270 M. Mascal, I. Yakovlev, E. B. Nikitin and J. C. Fettinger, *Angew. Chem. Int. Ed.*, 2007, **46**, 8782–8784.
271 M. A. Hossain, P. Morehouse, D. Powell and K. Bowman-James, *Inorg. Chem.*, 2005, **44**, 2143–2149.
272 L.-Z. Yang, Y. Li, L. Jiang, X.-L. Feng and T.-B. Lu, *CrystEngComm*, 2009, **11**, 2375–2380.
273 Y. Li, L. Jiang, X.-L. Feng and T.-B. Lu, *Cryst. Growth Des.*, 2008, **8**, 3689–3694.
274 A. Andrievsky, F. Ahuis, J. L. Sessler, F. Vögtle, D. Gudat and M. Moini, *J. Am. Chem. Soc.*, 1998, **120**, 9712–9713.
275 K. D. Karlin, *Science*, 1993, **261**, 701–708.
276 S. Hansen, E. Hough, L. A. Svensson, Y.-L. Wong and S. F. Martin, *J. Mol. Biol.*, 1993, **234**, 179–187.
277 S. Karthikeyan, Q. Zhou, F. Mseeh, N. V. Grishin, A. L. Osterman and H. Zhang, *Structure*, 2003, **11**, 265–273.
278 N. A. Chaniotakis, K. Jurkschat and A. Rühlemann, *Anal. Chim. Acta*, 1993, **282**, 345–352.

279 J. A. Tovilla, R. Vilar and A. J. P. White, *Chem. Commun.*, 2005, 4839–4841.
280 K. M. K. Swamy, S. K. Kwon, H. N. Lee, S. M. Shantha Kumar, J. S. Kim and J. Yoon, *Tetrahedron Lett.*, 2007, **48**, 8683–8686.
281 A. E. Martell, R. J. Motekaitis, Q. Lu and D. A. Nation, *Polyhedron*, 1999, **18**, 3203–3218.
282 S. L. Tobey, B. D. Jones and E. V. Anslyn, *J. Am. Chem. Soc.*, 2003, **125**, 4026–4027.
283 H. T. Ngo, X. Liu and K. A. Jolliffe, *Chem. Soc. Rev.*, 2012, **41**, 4928–4965.
284 S. Lee, K. K. Y. Yuen, K. A. Jolliffe and J. Yoon, *Chem. Soc. Rev.*, 2015, **44**, 1749–1762.
285 R. G. Hanshaw, S. M. Hilkert, H. Jiang and B. D. Smith, *Tetrahedron Lett.*, 2004, **45**, 8721–8724.
286 D. H. Lee, S. Y. Kim and J.-I. Hong, *Angew. Chem. Int. Ed.*, 2004, **43**, 4777–4780.
287 S. J. Butler and K. A. Jolliffe, *Chem. – Asian J.*, 2012, **7**, 2621–2628.
288 A. J. Surman, C. S. Bonnet, M. P. Lowe, G. D. Kenny, J. D. Bell, É. Tóth and R. Vilar, *Chem. – Eur. J.*, 2011, **17**, 223–230.
289 Y.-S. Jeong, S.-Y. Kim, G.-W. Jin, S.-H. An, J.-H. Lee, A.-R. Jeong, Y.-S. Chio, J.-I. Hong and J.-S. Park, *Bull. Korean Chem. Soc.*, 2010, **31**, 2561–2564.
290 J. I. Bruce, R. S. Dickins, L. J. Govenlock, T. Gunnlaugsson, S. Lopinski, M. P. Lowe, D. Parker, R. D. Peacock, J. J. B. Perry, S. Aime and M. Botta, *J. Am. Chem. Soc.*, 2000, **122**, 9674–9684.
291 R. S. Dickins, S. Aime, A. S. Batsanov, A. Beeby, M. Botta, J. I. Bruce, J. A. K. Howard, C. S. Love, D. Parker, R. D. Peacock and H. Puschmann, *J. Am. Chem. Soc.*, 2002, **124**, 12697–12705.
292 R. L. P. Adams, J. T. Knowler and D. P. Leader, *The biochemistry of the nucleic acids*, *10th ed*, Chapman and Hall, New York, 1986.
293 M. Dhaenens, J.-M. Lehn and J.-P. Vigneron, *J. Chem. Soc. Perkin Trans. 2*, 1993, **0**, 1379–1381.
294 M.-P. Teulade-fichou, J.-P. Vigneron and J.-M. Lehn, *Supramol. Chem.*, 1995, **5**, 139–147.
295 O. Baudoin, F. Gonnet, M.-P. Teulade-Fichou, J.-P. Vigneron, J.-C. Tabet and J.-M. Lehn, *Chem. – Eur. J.*, 1999, **5**, 2762–2771.
296 H. Abe, Y. Mawatari, H. Teraoka, K. Fujimoto and M. Inouye, *J. Org. Chem.*, 2004, **69**, 495–504.
297 J. Pranata, S. G. Wierschke and W. L. Jorgensen, *J. Am. Chem. Soc.*, 1991, **113**, 2810–2819.
298 C. Bazzicalupi, A. Bencini, A. Bianchi, E. Faggi, C. Giorgi, S. Santarelli and B. Valtancoli, *J. Am. Chem. Soc.*, 2008, **130**, 2440–2441.
299 C. Schmuck and M. Schwegmann, *Org. Lett.*, 2005, **7**, 3517–3520.
300 H. Y. Kuchelmeister and C. Schmuck, *Chem. – Eur. J.*, 2011, **17**, 5311–5318.
301 K. Niikura, A. Metzger and E. V. Anslyn, *J. Am. Chem. Soc.*, 1998, **120**, 8533–8534.
302 C. Schmuck and M. Heller, *Org. Biomol. Chem.*, 2007, **5**, 787–791.
303 S. E. Schneider, S. N. O'Nei and E. V. Anslyn, *J. Am. Chem. Soc.*, 2000, **122**, 542–543.
304 T. Zhang and E. V. Anslyn, *Org. Lett.*, 2006, **8**, 1649–1652.
305 M. D. Best and E. V. Anslyn, *Chem. – Eur. J.*, 2003, **9**, 51–57.
306 R. Mailhot, T. Traviss-Pollard, R. Pal and S. J. Butler, *Chem. – Eur. J.*, 2018, **24**, 10745–10755.
307 L. Szinicz, *Toxicology*, 2005, **214**, 167–181.
308 A. T. Tu, *Toxin Rev.*, 2007, **26**, 231–274.
309 E. Dolgin, *Nat. Med.*, 2013, **19**, 1194–1195.
310 M. R. Sambrook and S. Notman, *Chem. Soc. Rev.*, 2013, **42**, 9251–9267.
311 M. R. Sambrook, J. C. Vincent, J. A. Ede, I. A. Gass and P. J. Cragg, *RSC Adv.*, 2017, **7**, 38069–38076.
312 S. Letort, S. Balieu, W. Erb, G. Gouhier and F. Estour, *Beilstein J. Org. Chem.*, 2016, **12**, 204–228.

313 S. M. Daly, M. Grassi, D. K. Shenoy, F. Ugozzoli and E. Dalcanale, *J. Mater. Chem.*, 2007, **17**, 1809–1818.
314 T. Wille, O. Tenberken, G. Reiter, S. Müller, R. Le Provost, O. Lafont, F. Estour, H. Thiermann and F. Worek, *Toxicology*, 2009, **265**, 96–100.
315 Y. Ruan, H. A. Taha, R. J. Yoder, V. Maslak, C. M. Hadad and J. D. Badjić, *J. Phys. Chem. B*, 2013, **117**, 3240–3249.
316 S. Chen, Y. Ruan, J. D. Brown, C. M. Hadad and J. D. Badjić, *J. Am. Chem. Soc.*, 2014, **136**, 17337–17342.
317 S. Chen, M. Yamasaki, S. Polen, J. Gallucci, C. M. Hadad and J. D. Badjić, *J. Am. Chem. Soc.*, 2015, **137**, 12276–12281.

Chapter Two

Halogen bonding metallo-tripodal receptors for the recognition and sensing of inorganic monophosphate and simple phosphate-ester anionic species

2 Halogen bonding metallo-tripodal receptors for the recognition and sensing of inorganic monophosphate and simple phosphate-ester anionic species

2.1 Introduction

Vital to any molecular recognition project concerned with the selective binding of a certain guest, is the adoption of a fundamental strategy in the design of a potential host which serves '*as a compass on an otherwise unchartered sea full of synthesizable target complexes…for host-guest chemistry'*.[1] With this concept in mind and having previously detailed the virtues of the halogen bond in mediating anion-recognition processes (see Section 1.2.5), this chapter focuses on the design and synthesis of halogen bonding (XB) metallo-tripodal receptors for the selective recognition and sensing of inorganic monophosphate and simple phosphate-ester anionic species (*i.e.* PMP, Figure 1.33C), specifically where a 'lock and key' approach is utilised in host design. In particular, the facile metal coordination properties of appropriately functionalised, tris-*iodo*triazole containing, tertiary amine-derived ligands are exploited to generate a family of preorganised, C_{3v} symmetric XB Zn(II)- and Cu(II)-based sensory hosts whose anion binding and sensing properties are investigated relative to their protic HB counterparts - foremost in a competitive organic-aqueous solvent mixture and subsequently in wholly aqueous media.

2.1.1 XB receptors for the selective recognition of inorganic monophosphate

Despite the superb ability of XB receptors to outperform their HB analogues in the realm of anion recognition (see Section 1.2.5), very few examples exist capable of selectively binding and sensing inorganic monophosphate, especially in protic media. As stated previously, this may be attributed to the XB donor groups' inherent hydrophobicities and proclivity towards binding 'softer' anions (*e.g.* I^-, Br^-). Thus, the cases in which 'harder' oxoanions are preferentially bound are scarce and represent exceptions to the general trend rather than the norm. At the inception of this project, those present amongst the dearth of such XB hosts were Resnati's 2-iodoimidazolium derivative[2] (Figure 2.1A) which displayed an enhanced affinity for $H_2PO_4^-$ (K_a = 1100 M^{-1}) over the halides in

d_6-DMSO and Ghosh's 5-iodo-,1,2,3-triazole containing bis-heteroleptic Ru(II) receptor (Figure 2.1B), which was similarly capable of selective phosphate sensing in up to 20% H_2O/MeCN mixtures *via* perturbations in the MLCT luminescent intensities of the metallo-complex.[3] As evidenced in the crystal structures of its corresponding adducts with $H_2PO_4^-$ (Figure 2.1B) and $H_2P_2O_7^{2-}$, the anions are bound by strong XB interactions (81% vdW) (blue dashed lines) of near linearity between the iodine atom of the iodotriazole moiety and the oxygen atoms of the respective phosphate species, with the latter also involved in the hydrogen-bonded (green dashed lines) polymeric assemblies of the anions - giving rise to an infinite monophosphate chain and a pyrophosphate dimer respectively.

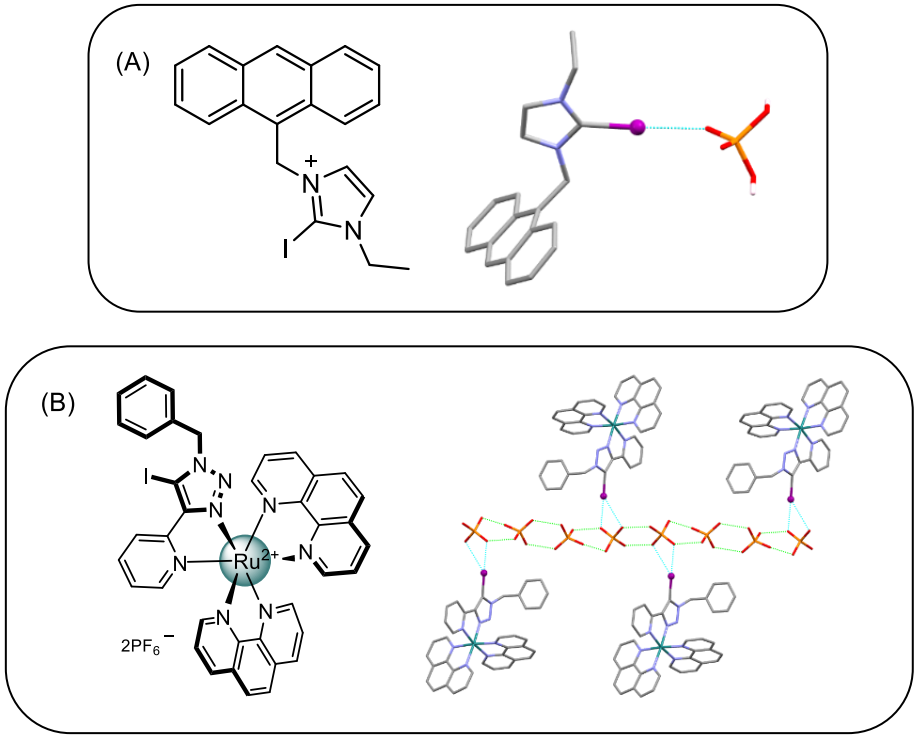


Figure 2.1: *Phosphate selective XB receptors. (A) (left) Resnati's 2-iodoimidazolium derivative (furnished as the iodide salt) and (right) the crystal structure of the adduct with dihydrogen monophosphate;[2] (B) (left) Ghosh's XB bis-heteroleptic Ru(II) receptor and (right) the crystal structure of its adduct with dihydrogen monophosphate.[3] (XB interactions shown as blue dashed lines).*

Most recently and as previously evidenced in the case of Flood's cyanostar tetramer (Figure 1.22 in Chapter One), the multivalent, selective binding of inorganic phosphate has also been utilised to drive the anion-templated self-assembly of XB supramolecular materials. In the presence of oxoanions such as $H_2PO_4^-$ and $H_2P_2O_7^{2-}$, Molina's iodotriazolium-appended naphthalene monomer[4]

generated novel intertwined polymeric assemblies in 9:1 CD_3CN/CD_3OD solution *via* cooperative XB (Figures 2.2A and 2.2B). Contrastingly, ^{1}H-NMR titrations of the proto-triazolium analogue with the same anions did not show any evidence of polymer formation, thus attesting to the versatility of these robust XB synthons in guiding oxoanion-mediated self-assembly processes. The same author also reported a bidentate triferrocene-bis(iodotriazole) host[5] (Figure 2.2C) which exhibited the largest cathodic perturbations of the two peripheral and internal ferrocene/ferrocenium redox couples in the presence of $H_2PO_4^-$ (ΔE = -76 and -327 mV respectively) in 1:1 CH_2Cl_2/MeCN (0.15 M $TBAPF_6$ supporting electrolyte) when compared to other oxoanions (OAc^- and $HP_2O_7^{3-}$) tested. Shortly thereafter, Beer and co-workers further reported a novel pyrrole-containing, dicationic cleft-type receptor (Figure 2.2D) that displayed a marked selectivity for tetrahedral oxoanions including $H_2PO_4^-$ (K_a = 3460 M^{-1}) over the halides in 9:1 MeCN/H_2O.[6]

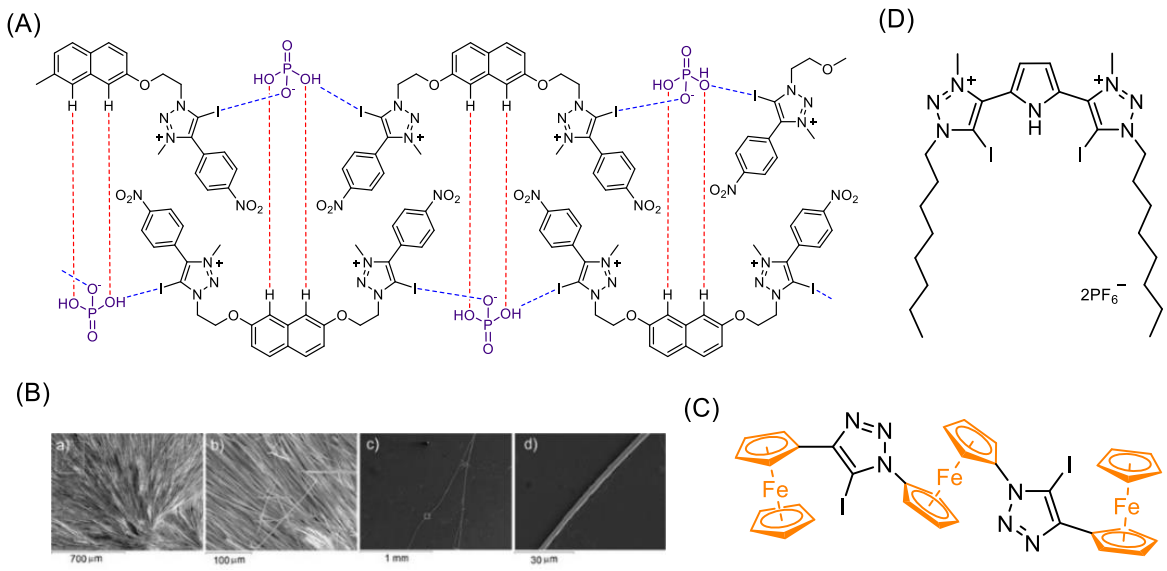


Figure 2.2: *Phosphate selective XB receptors. (A) Schematic representation of Molina's phosphate-templated iodotriazolium-appended naphthalene polymer (XB represented by blue dashed lines and resultant HB as red dashed lines);*[4] *(B) SEM images of the self-assembled compounds formed from the phosphate-templated polymeric assemblies*[4] *(Images reprinted with permission from ref 4, Copyright 2018 American Chemical Society); (C) Molina's bidentate triferrocene-bis(iodotriazole) host;*[5] *(D) Beer's dicationic, pyrrole-containing cleft-type receptor.*[6]

Rather apparent in the case of the above XB hosts however, is the absence of a fundamental design strategy for the targeted recognition of inorganic monophosphate. As such, they do not offer any clear geometric match to the oxoanionic species of interest and altogether lack a definitive

three-dimensional binding pocket aimed for tetrahedral guest recognition. Learning from these examples, XB hosts with greater structural complementarity congruent to the tetrahedral geometry of the anion should be designed to explicitly bias their selectivity towards phosphate.

2.1.2 A rational approach to phosphate host design: C_{3v} symmetric metallo-tripodal receptors

In this regard and from amongst the diversity of phosphate-selective receptors surveyed in Section 1.3, most salient are the C_{3v} symmetric hosts such as Anslyn's TREN-based and TPMA-based Cu(II)-tripods[7] (Figures 1.38A and 1.38B respectively) whose tetrahedral cavities undoubtedly provide the best topological match for phosphate guest species. Surprisingly, this potent rationale of incorporating a metal cation within an appropriately functionalised organic tripodal framework (Figure 2.3) has not yet been applied to the design of potential phosphate-selective XB hosts and thus provides impetus for the work described herein.

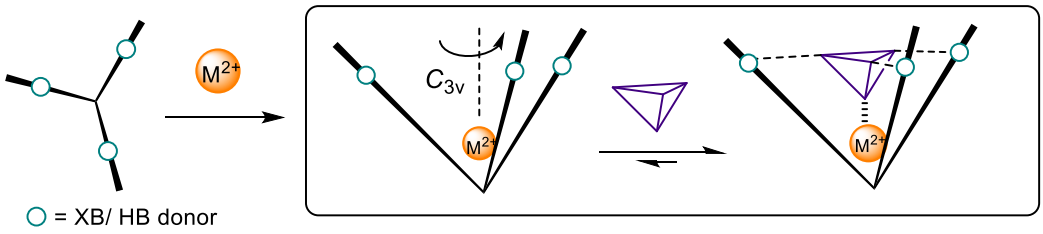


Figure 2.3: *Schematic representation of the specific metallo-tripodal design principle to accommodate tetrahedral oxoanions.*[7]

2.1.3 Chapter aims

Accordingly, this chapter aims to fulfil the following goals:

- To prepare a series of novel metallo-tripodal anion host systems containing a triad of convergent XB-donor moieties (specifically, 5-iodo-,1,2,3-triazoles) for the selective recognition and sensing of inorganic monophosphate and simple phosphate-ester species, in competitive organic-aqueous solvent mixtures and aqueous solvent media.

- To investigate and compare the fundamental anion recognition properties of these XB hosts (*i.e.* binding affinities and trends) with their tris-1,2,3-triazole-containing, HB metallo-tripodal counterparts.

Harnessing the aforementioned design principle to specifically accommodate tetrahedral oxoanions (Figure 2.3), this chapter initially introduces the 'general XB metallo-tripodal motif' (*vide infra*) which serves as the structural foundation for the family of novel, C_{3v} symmetric XB metallo-hosts prepared during the course of this study. Through the modification of the motif's tripodal '*arm*' fragments with various octyl-chain, ferrocene, poly(ethylene glycol) and permethylated-*β*-cyclodextrin appendages, as well as the nature of the metallo-centre itself, a cadre of redox-active and water-soluble XB Zn(II)- and Cu(II)-tripodal hosts are constructed, and their anion binding properties examined using a range of ^{1}H NMR, voltammetric, calorimetric and optical titration techniques.

2.2 The '*general* XB metallo-tripodal Motif'

The pervasive 'general XB metallo-tripodal motif' (Figure 2.4) features a cavity complementary to that of a tetrahedron, with a single M^{2+} cation positioned along the C_3 axis for effective phosphate binding. Venerated as one of the archetypal ligands in coordination chemistry and similar to compounds studied by Canary[8] and Karlin[9], the tripodal platform is derived from a tetradentate chelating tris(2-pyridylmethyl)amine (TPMA) subunit functionalised with three convergent 5-iodo-1,2,3-triazoles, positioned to (1) provide additional XB interactions to supplement the Lewis acidic metallocentre for potent anion binding and (2) afford the additional versatility of conveniently appending appropriate reporter- or solubilising R-groups (highlighted in the black box, Figure 2.4) to facilitate anion sensing capability and/or anion recognition in aqueous media, respectively.

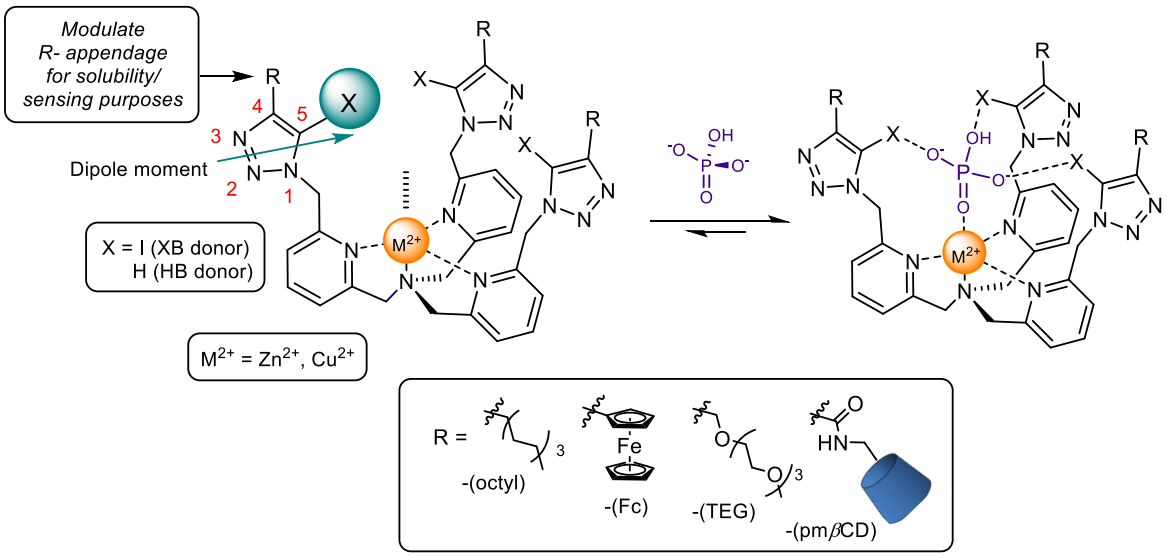
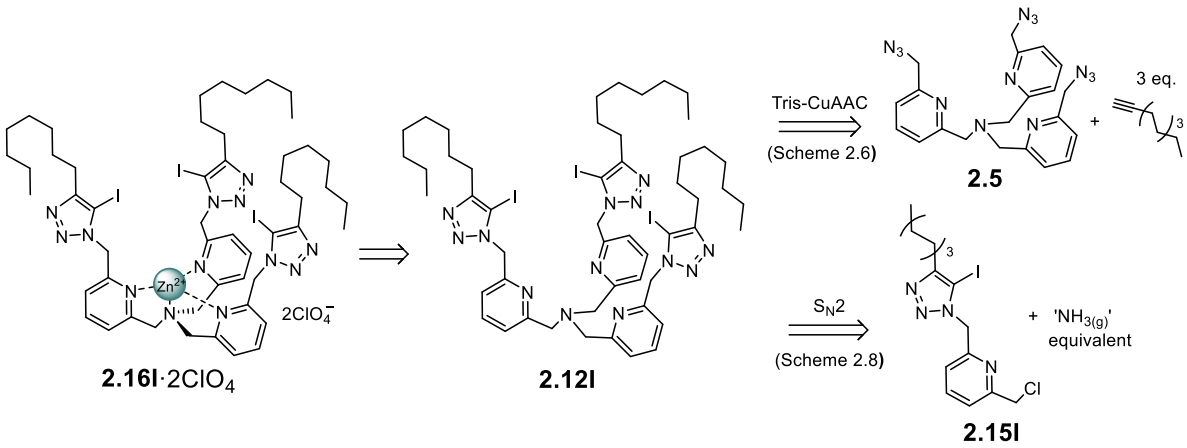


Figure 2.4: *Specific design features of the 'general XB-metallo tripodal motif'.*

2.3 A tris(octyl-chain)-appended XB Zn(II) tripod

2.3.1 Synthesis and characterisation of **2.16I**·$2ClO_4$ and **2.16H**·$2ClO_4$

Derived from the retrosynthetic analysis of the intital target tris(octyl-chain)-appended XB Zn(II)-tripodal receptor **2.16I**·$2ClO_4$, two synthetic pathways were undertaken to prepare its precursor XB ligand **2.12I** either by (i) a 'tris' Cu(I) catalysed [3+2] Azide-Alkyne cycloaddition (CuAAC), so called 'Click', reaction between the tris-azide appended subunit **2.5** and three three equivalents of the relevant terminal acetylene or *via* (ii) reaction of an appropriately functionalised 2-chloromethyl-6-methylpyridyl iodotriazole '*arm*' precursor **2.15I** with ammonia or a source of its equivalent (Scheme 2.1).

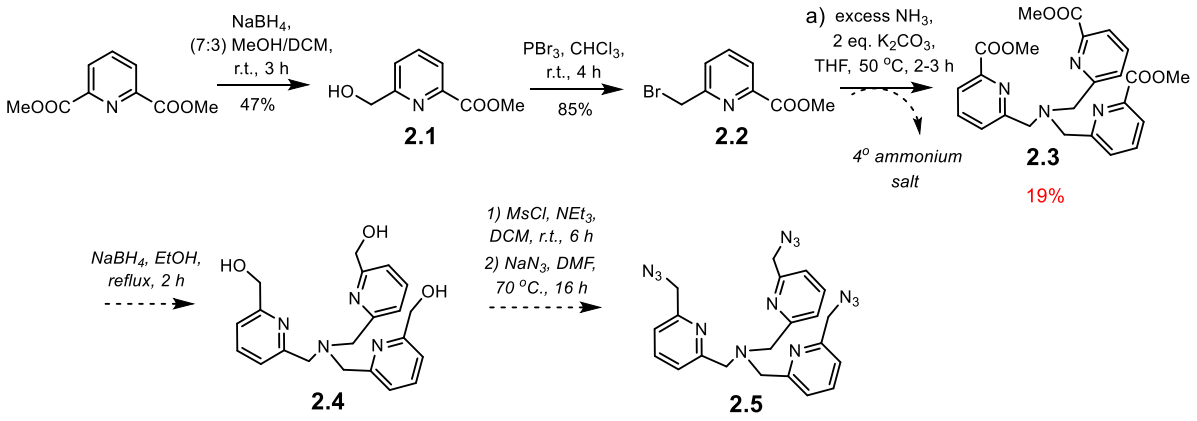


Scheme 2.1: *Retrosynthetic analysis of the initial target Zn(II)-tripodal receptor* ***2.16I****·2ClO₄.*

2.3.1.1 Investigation of the 'tris-CuAAC' strategy

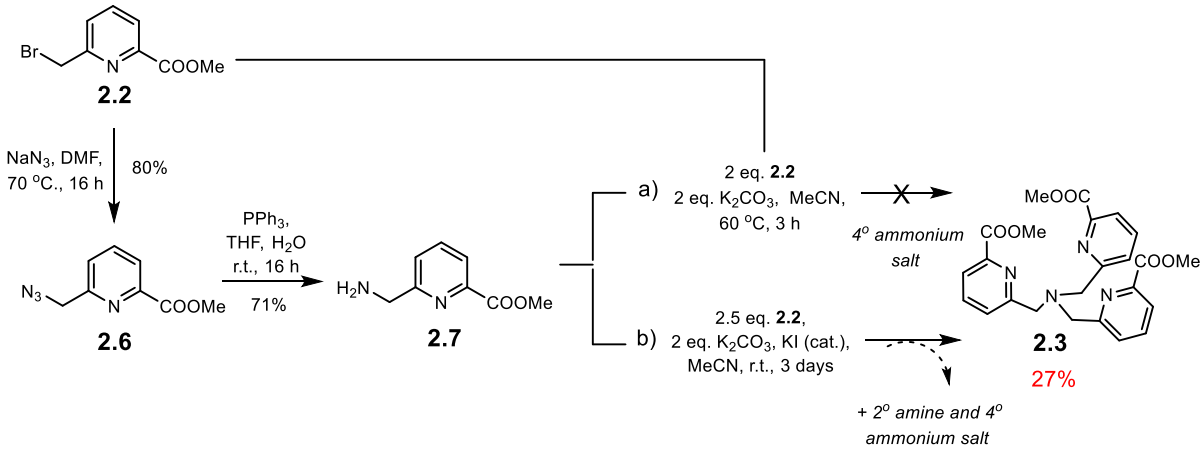
The 'tris-CuAAC' strategy was initially investigated with the synthesis of tris-azide **2.5** according to modified literature procedures previously reported by Jabin and co-workers (Scheme 2.2).[10] 6-Bromomethyl pyridyl ester derivative **2.2** was prepared in two successive steps *via* the $NaBH_4$ reduction of commercially available dimethyl pyridine 2,6-dicarboxylate to produce alcohol **2.1**, followed by treatment with PBr_3 to afford the corresponding brominated compound in good yield. The subsequent reaction of **2.2** in a saturated solution of ammonia with K_2CO_3 in THF at 50 °C to produce tris-ester **2.3** proved extremely problematic however, as the concomitant over-

alkylation to the corresponding quaternary ammonium salt was observed. Consequently, purification was challenging, and chromatographic separation was repeated multiple times to obtain **2.3** in a modest 19% isolated yield.



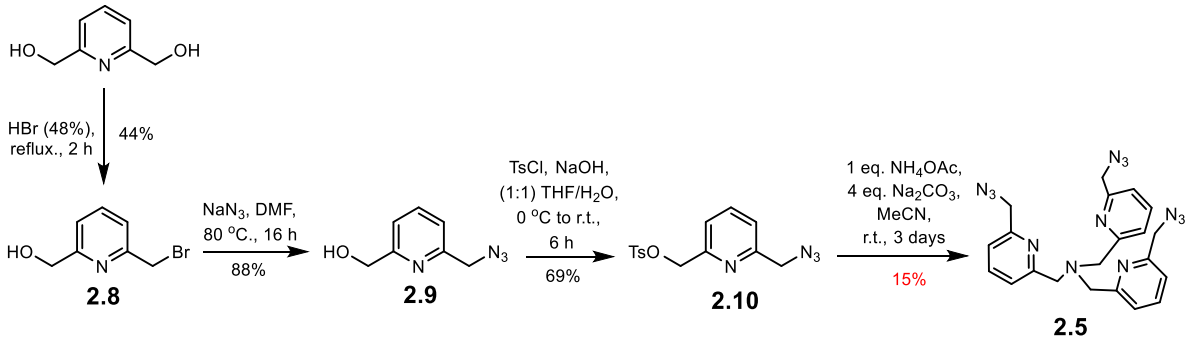
Scheme 2.2: *Initially followed synthetic route to the tris-azide subunit* ***2.5****, building upon Jabin's protocol.*[10]

Given the poor yield of the tris-ester moiety **2.3**, an alternative alkylation route was undertaken using primary amine **2.7** prepared *via* the reaction of **2.2** with NaN_3 to form azide **2.6**, followed by a Staudinger reduction (Scheme 2.3). The reaction of **2.7** with stoichiometric quantities of **2.2** however did not result in significant improvements in tris-ester yield.



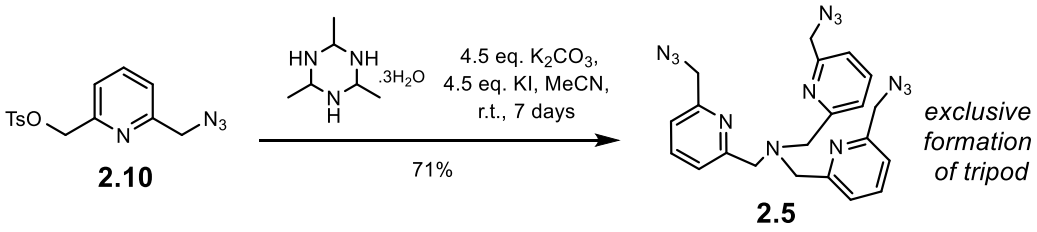
Scheme 2.3: *Alternate primary amine-based N-alkylation pathway to the tris-ester subunit.*

Similarly, reacting the tosylate **2.10** with NH_4OAc under the basic conditions stated in Scheme 2.4 afforded the crucial tris-azide **2.5** in low yield.



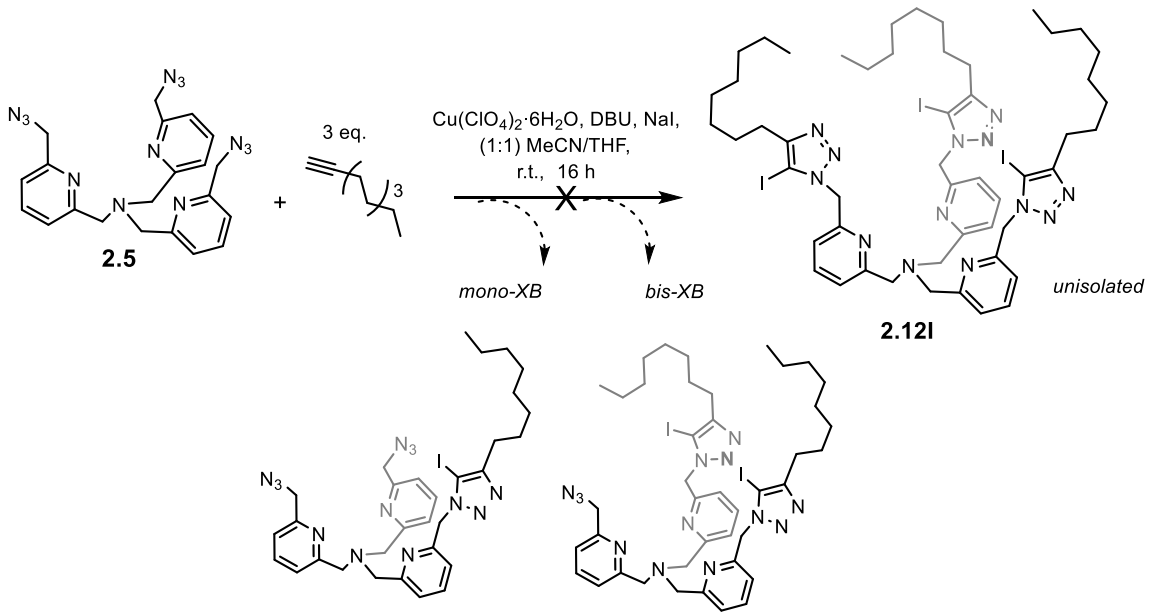
Scheme 2.4: *Alternate synthetic pathway to directly afford tris-azide* ***2.5*** *from a single N-alkylation step.*

Finally, **2.10** was reacted with the acetaldehyde trimer trihydrate under modified conditions[11] and ligand **2.5** isolated *via* chromatographic purification in a commendable 71% yield (Scheme 2.5). Evidently, the nitrogenous trimer compound proved to be the most efficient reagent for the generation of tripodal derivatives - most likely due to the existence of a favourable equilibrium between the acetaldehyde and trimeric species permitting the *slow*-release of ammonia. Critically aided by the modified temperature conditions, the latter thus prevented the rapid over *N*-alkylations observed in earlier efforts.



Scheme 2.5: *Utilisation of the acetaldehyde trimer trihydrate to form tris-azide* ***2.5****.*

Preparation of the target derivative **2.12I** was attempted by mixing 3 equivalents of 1-decyne and tris-azide **2.5** in the presence of sodium iodide and copper(II) perchlorate hexahydrate in 1:1 MeCN/THF (Scheme 2.6), utilising Zhu's one-pot 'iodo-Click' CuAAC methodology[12] (the corresponding catalytic cycle of which is illustrated in Figure 2.5A).



Scheme 2.6: *the initial 'one-pot tris-CuAAC' reaction attempted towards tripodal ligand* ***2.12I****.*

Notably, tris(benzyltriazolylmethyl)amine (TBTA) (Figure 2.5B), the canonical ancillary rate accelerating ligand (RAC) fervently utilised in 'Click' protocols to stabilise the oxidation state and modulate the catalytic activity of the Cu(I) metal center was omitted from the initial 'tris-CuAAC' procedure. Instead, tripodal-azide **2.5** bearing the robust metal-chelating TPMA moiety as part of its 'substrate' skeleton was envisaged to (i) itself stabilise the *in-situ* generated Cu(I) species and hence (ii) self-catalyse the ensuing multiple cycloaddition reaction (Figure 2.5C). Interestingly, this concept, otherwise known as 'chelation-assisted metal catalysis', has only in recent years been incorporated into the design of highly-reactive azides[13–15] which, through the inclusion of a proximal copper-chelating auxiliary as part of their complete structure, have been demonstrated to promote the formation of the metalla-cycle intermediate (**iv** in the catalytic cycle) and thus cycloaddition by effectively (i) increasing the 'concentration' of Cu(I) at the reactive site, as well as (ii) augmenting the electrophilicity of the azido group (thereby increasing the overall rate and efficiency of the respective CuAAC also).

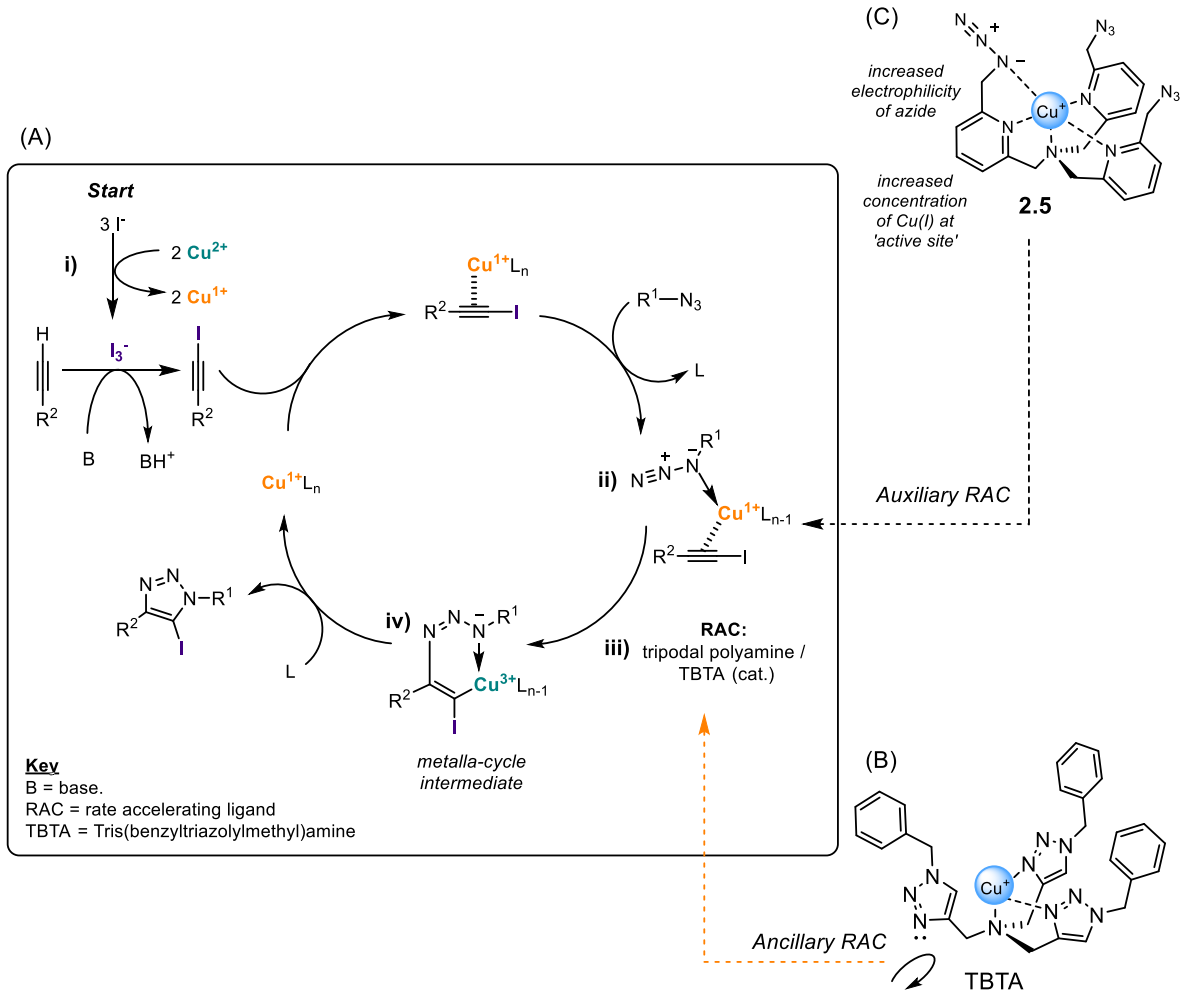
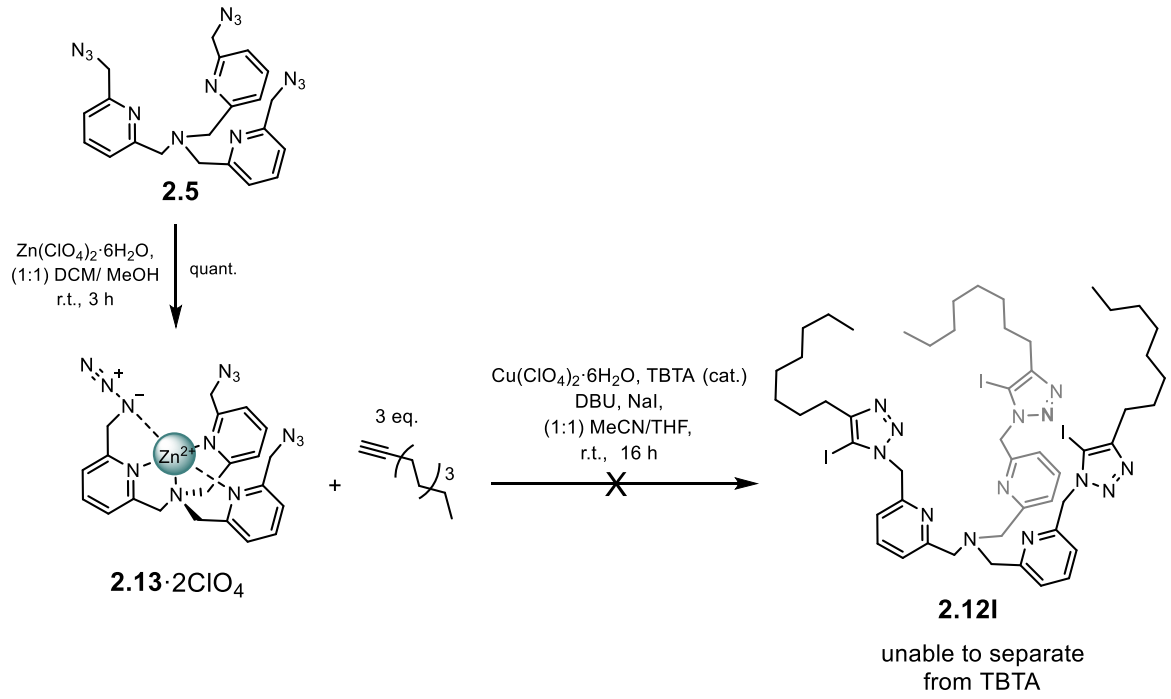


Figure 2.5: *(A) Catalytic cycle of the 'one-pot iodo-Click' reaction involving a 1-iodoalkyne intermediate;*[16] *(B) the structure of TBTA;*[17] *(C) Schematic representation of Cu(I) stabilisation by compound* ***2.5****.*

Despite these factors however, ESI-MS analysis of the crude reaction mixture revealed distinct peaks at *m/z* = 720.3 $[M + H]^+$, 984.2 $[M + H]^+$ and 1248.3 $[M + H]^+$ corresponding to the formation of the mono, bis- and tris-XB derivatives respectively. Subsequent purification efforts *via* preparative TLC unfortunately failed to separate the components.

Consequently, as an alternative to the previous 'substrate as catalyst' reaction, TBTA was re-incorporated into the one-pot iodo-Click protocol and the tris-CuAAC procedure repeated with the Zn(II)-complex **2.13**·2ClO_4 (Scheme 2.7). Gratifyingly, a single ESI-MS peak corresponding to the desired cavity (*vide supra*) was detected from the crude reaction mixture which signalled the sole formation of the tris-XB assembly.



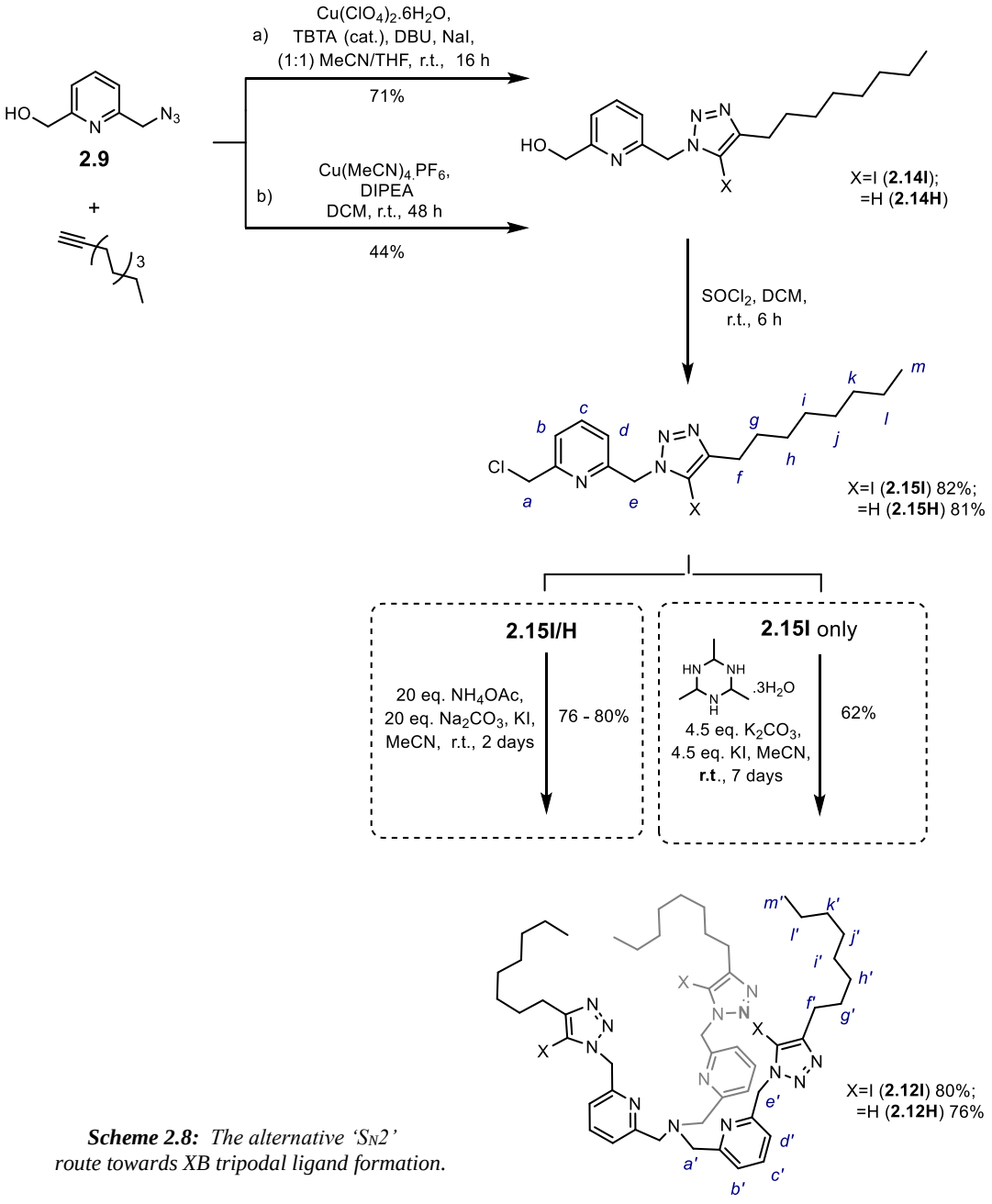
Scheme 2.7: *the second 'one-pot tris-CuAAC' reaction attempted inclusive of TBTA.*

Yet again, purification proved extremely difficult, this time however due to the presence of the canonical RAC, whose inherent tripodal structure comprising triazole and aromatic linkages reminiscent of the target XB ligand afforded it an identical R_f value. Thus, disappointingly **2.12I** remained unisolated.

2.3.1.2 Investigation of the XB 'arm' formation strategy

The alternate strategy using a 2-chloromethyl-6-methylpyridyl iodotriazole '*arm*' pecursor proved to be much more successful (Scheme 2.8). The one-pot iodo-CuAAC reaction between azide precursor **2.9** and 1-decyne produced the XB-donor containing synthon **2.14I** in 71% yield after chromatographic purification. Chlorination with $SOCl_2$ afforded the relevant '*arm*' derivative **2.15I**, which upon reaction with the acetaldehyde ammonia trimer trihydrate in the presence of 4.5 equivalents of K_2CO_3 and KI as per modified literature procedures[11] gave the desired XB ligand **2.12I** in a 62% isolated yield. Pleasingly, the lengthy reaction time of 7 days was reduced significantly to 2 days using excess NH_4OAc and Na_2CO_3 (20 equivalents of each) and **2.12I** produced in an improved yield of 80%. Notably, a distinct upfield shift of the singlet signal (4.67 ppm) corresponding to the relevant H_a methylene protons of the '*arm*' precursor **2.15I**, to the diagnostic tertiary *N*-amine region *ca*. 3.86 ppm was evidenced in the comparative ^1H NMR of ligand **2.12I** (Figure 2.6), which along with ESI-MS analysis, affirmed the successful transformation to the appropriate XB tripodal assembly.

Finally, complexation with a stoichiometric quantity of zinc(II) perchlorate hexahydrate quantitively afforded the pre-organised XB metallo-tripodal receptor **2.16I**·$2ClO_4$ (Scheme 2.9) which was fully characterised *via* ^1H and ^{13}C NMR spectroscopy and high resolution ESI-MS methods. The corresponding stacked ^1H-NMR spectra of the respective metal-free ligand and metal-containing entity in $CDCl_3$ are shown in Figure 2.7A. Pronounced downfield shifts in the aromatic pyridyl proton signals $H_{b'-d'}$ and proximal aliphatic -CH_2 proton $H_{a'}$ were observed upon coordination to the diamagnetic metal, whilst the methylene protons $H_{f'}$ and $H_{g'}$ of the peripheral octyl-chain appendages displayed minor upfield perturbations.



Scheme 2.8: *The alternative 'SN2' route towards XB tripodal ligand formation.*

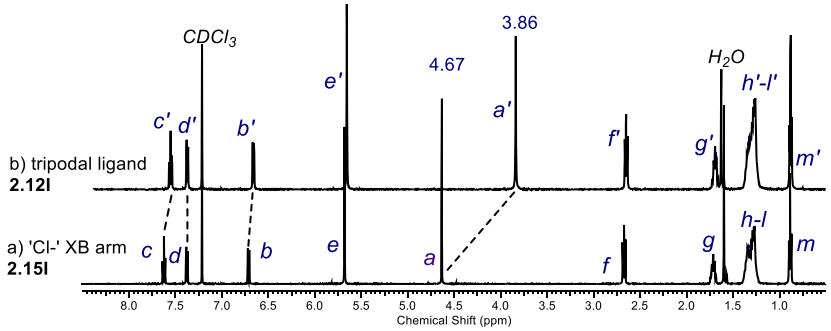
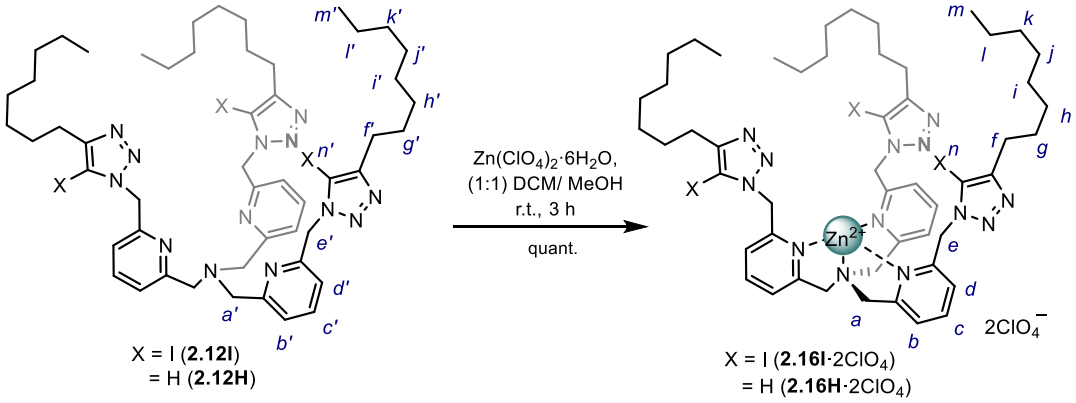


Figure 2.6: *^{1}H NMR spectra of (a) the tripodal 'arm' **2.15I**. (b) XB tripodal ligand **2.12I** ($CDCl_3$, 500 MHz, T = 298 K) Assignments follow those in Scheme 2.8.*



Scheme 2.9: *Metal complexation of the XB ligand* ***2.12I*** *to afford the pre-organised Zn(II)-metallo receptor* ***2.16I****.2ClO4*

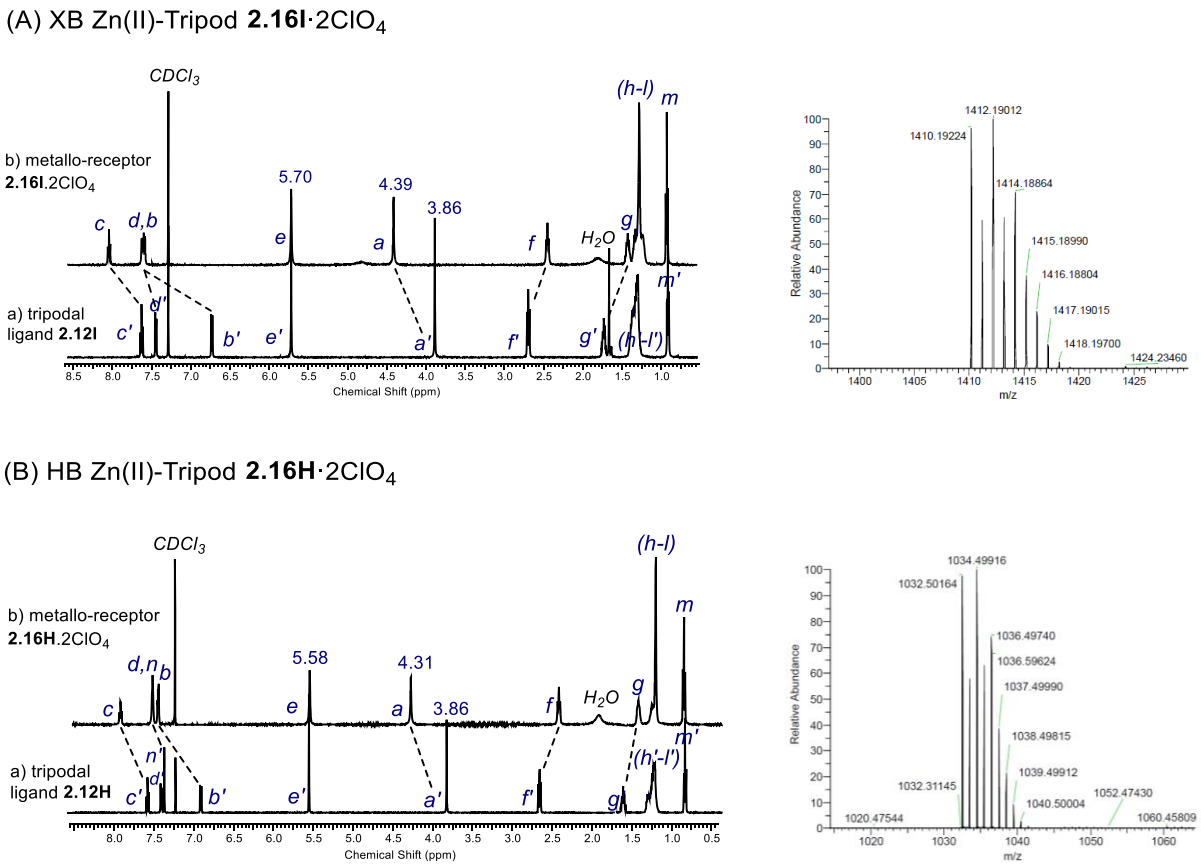


Figure 2.7: *[1]H NMR (Left row) and high-resolution ESI-MS (Right row) characterisation of the octyl-chain appended Zn(II)-tripodal receptors (A)* ***2.16I****·2ClO4 and (B)* ***2.16H****·2ClO4. All NMR spectra were obtained in CDCl3 (500 MHz, T = 298 K). Assignments follow those in Scheme 2.9.*

The HB tripod derivative **2.12H** was synthesised *via* an analogous multi-step procedure using the HB '*arm*' precursor **2.15H** (Scheme 2.8) and also complexed with a stoichiometric quantity of

zinc(II) perchlorate salt to afford the protic metallo-host **2.16H**·2ClO_4 (Scheme 2.9). Mirroring the behaviour of its skeletal XB counterpart, the halogen-free ligand **2.12H** exhibited marked downfield perturbations of its central tris-pyridyl proton signals $H_{b',-d'}$ and methylene proton $H_{a'}$ as well as that of the triazole proton $H_{n'}$ when complexed to the Zn(II)-center (Figure 2.7B). It is worth noting that the chemical shift of the medial protons $H_{e'}$ bridging the TPMA subunit and the anion binding triazole moieties is further downfield in the case of the XB ligand **2.12I** (5.70 ppm) compared to that of **2.12H** (5.58 ppm) which is indicative of the electron-withdrawing iodotriazole units polarising the tripodal core to a greater extent than their prototriazole analogues - thereby producing a more electron-deficient XB tripodal scaffold and hence also, giving rise to a more electron-deficient binding cavity of the metallo-host **2.16I**·2ClO_4 for anion recognition.

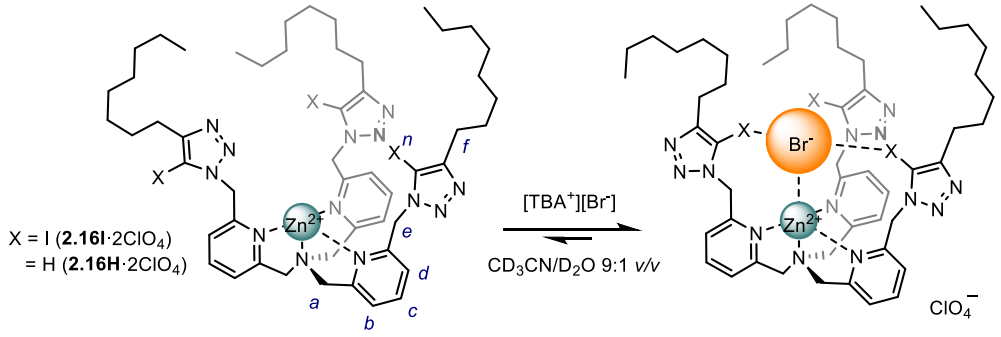
Additionally, through ESI-MS analyses both isolated XB and HB metallo-tripodal receptors were identified as their mono-perchlorate counteranion containing adducts (*i.e. m/z*= 1410.1 [M - ClO_4]$^+$ for **2.16I**·2ClO_4 and *m/z* = 1032.5 [M - ClO_4]$^+$ for **2.16H**·2ClO_4) and thus displayed the characteristic isotopic distributions arising from the multiple stable isotopes of Zn in each of their corresponding high-resolution ESI spectra (Figure 2.7).

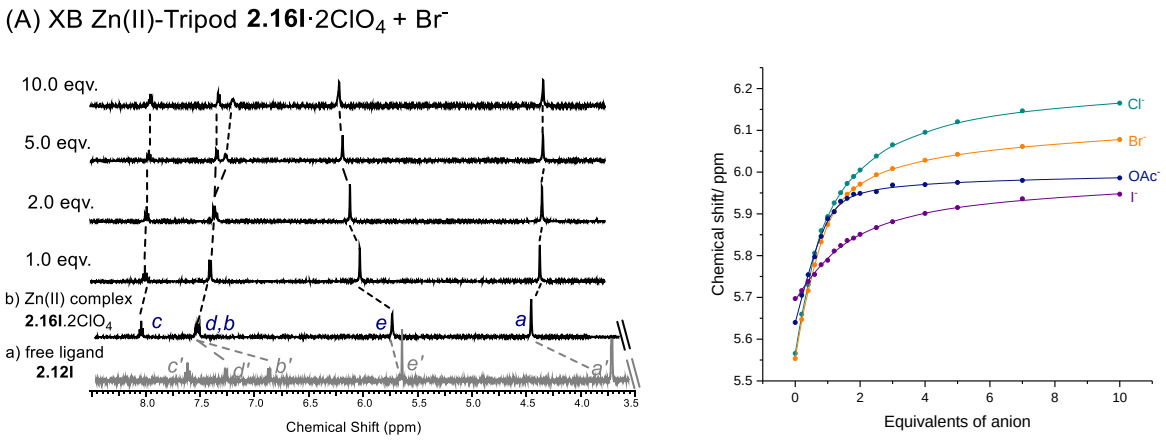
2.3.2 ^{1}H NMR anion binding studies with **2.16I**·2ClO_4 and **2.16H**·2ClO_4

The anion recognition properties of the XB Zn(II)-tripodal receptor **2.16I**·2ClO_4 were probed *via* a series of ^{1}H-NMR titration experiments and subsequently compared to its HB analogue **2.16H**·2ClO_4 to reveal the important influences of XB interactions on anion association. In a typical titration procedure, increasing aliquots of anions (in the form of their non-coordinating tetrabutylammonium (TBA) salt were added to separate 1.5 mM solutions of each metallo-host in a competitive CD_3CN/D_2O 9:1 *v/v* solvent system and the resultant chemical shifts of selected proton signals proximal to the anion binding cavity monitored as a function of anion concentration.

As an illustrative example, the perturbations of the various proton environments of the XB tripod **2.16I**·2ClO_4 upon addition of Br^- are displayed in Figure 2.8A. Over the addition of 10 equivalents of the halide, discernible upfield shifts were exhibited in the signals of the aromatic pyridyl protons

$H_{b\text{-}d}$ (with H_b and H_d initially co-resonant) and methylene H_a protons ($\Delta\delta$ = 0.14 ppm) surrounding the metallo-center, whilst conversely significant downfield perturbations of the iodotriazole adjacent aliphatic H_e ($\Delta\delta_e$ = 0.4 ppm) and H_f ($\Delta\delta_f$ = 0.14 ppm) protons were observed indicating anion binding within the designated tripodal interior.





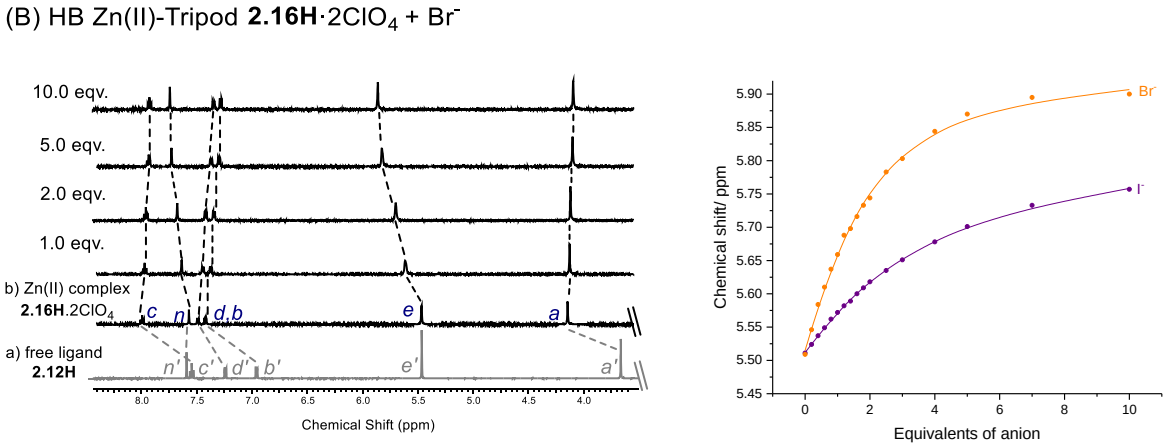


Figure 2.8: *(Left row) Partial ^{1}H NMR spectra of Zn(II) tripodal receptors (A)* ***2.16I***·*2ClO₄ and (B)* ***2.16H***·*2ClO₄ in the presence of 0.0, 1.0, 2.0, 5.0 and 10.0 equivalents of Br⁻ at T = 298 K. (Right row) Titration isotherms: plots of the medial methylene proton's (H_e) chemical shifts of tripod as a function of anion concentration. ([metallo-host] = 1.5 mM, CD₃CN/ D₂O 9:1 v/v, 500 MHz). All proton assignments follow those in Scheme 2.9.*

Similarly, the addition of anions to the analogous protic metallo-host **2.16H**·2ClO_4 typically caused downfield perturbations of the characteristic prototriazole proton H_n ($\Delta\delta$ = 0.18 ppm with 10 equivalents of Br^-, Figure 2.8B), signalling direct involvement in anion coordination *via* HB interactions. Importantly, the overall retention of one set of signals in these titration spectra indicated the anion recognition process was fast on the ^{1}H NMR timescale where the triad of XB-/ HB-donor arms are able to effectively chelate the anion guest in a cooperative convergent manner.

By contrast, in the case of $H_2PO_4^-$ with **2.16I**·2ClO_4, anion association was found to occur in slow exchange on the NMR timescale (Figure 2.9): two sets of resonances were observed in the spectra of the host containing less than one equivalent of $H_2PO_4^-$, relating to the respective uncomplexed and complexed host species. The complete disappearance of the free host's proton signals by the addition of 1.0 equivalent of the anion was indicative of a stable, C_{3v}symmetric, host-guest complex of 1:1 stoichiometry whose association constant of $>10^4$ M^{-1} was determined from the relative integrals of the '*bound*' and '*unbound*' (H_a) proton resonances.[18] Similar to the fast-exchange regime of Br^- (Figure 2.7A), the phosphate complex of **2.16I**·2ClO_4 exhibited pronounced upfield perturbations ($\Delta\delta$ = 0.18 – 0.34 ppm) of the core pyridyl protons $H_{b\text{-}d}$ as well as a modest downfield shift ($\Delta\delta$ = 0.1 ppm) of the iodotriazole vicinal H_e proton. In stark contrast however, was the marked *downfield* shift ($\Delta\delta$ = 0.3 ppm) of the aliphatic H_a proton proximal to the Zn(II)-center.

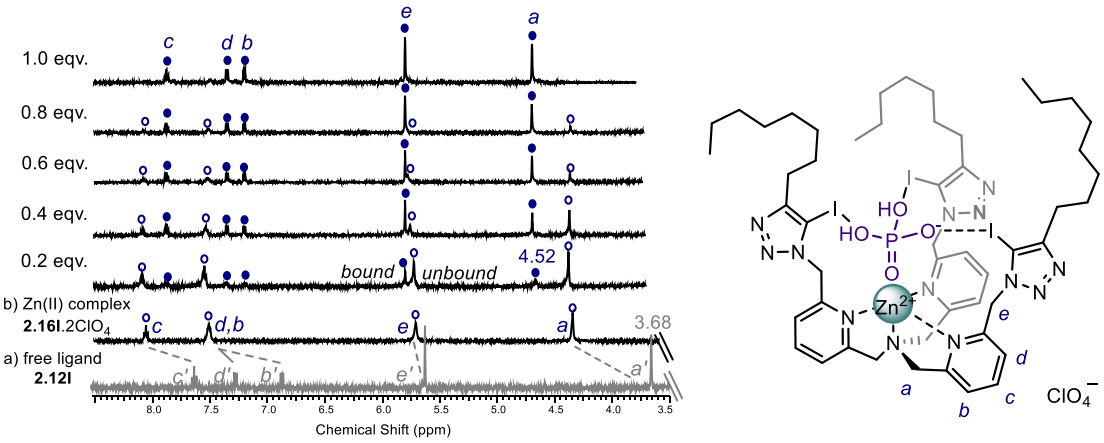


Figure 2.9: *Changes in the (partial) ^{1}H NMR spectra of the Zn(II) tripodal receptor* ***2.16I***·*2ClO_4 upon the addition of 1.0 equivalent of $H_2PO_4^-$ at T = 298 K. ([metallo-host] = 1.5 mM, CD_3CN/ D_2O 9:1 v/v, 500 MHz). All proton assignments follow those in Scheme 2.9.*

Whilst the reason for this could not be definitively ascertained, a comparison of this '*bound*' H_a resonance (δ = 4.52 ppm) with the equivalent $H_{a'}$ (δ = 3.68 ppm) signal of the *apo*-Zn(II) ligand **2.12I** (highlighted in grey, also in Figure 2.9) negated the possibility of metal abstraction by the highly basic oxoanion, and thus upheld the notion of the symmetric, 'in-cavity' binding of the tetrahedral guest.

Non-linear regression analysis of the fast-exchange titration data (monitoring the shifts of the medial methylene proton H_e as a function of anion concentration) using WinEQNMR2[19] determined association constant data for **2.16I**·2ClO_4 and **2.16H**·2ClO_4 shown in Table 2.1. Both receptors were found to bind anions in a 1:2 host-guest stoichiometry (with the exception of $H_2PO_4^-$, *vide supra*), however the magnitude of the second binding constant (K_{12}) was much smaller than the first (K_{11}) in all cases, suggesting weak peripheral association of the second anion with the bound complex likely driven by the electrostatic attraction of the host's *divalent* Zn(II)-metallocentre.

Inspection of the anion binding affinities revealed the tetrahedral, tripodal binding cavity of the XB host **2.16I**·2ClO_4 to be highly selective for $H_2PO_4^-$ over other anions, with an association constant (> 10^4 M^{-1}) too strong to quantify in the CD_3CN/D_2O 9:1 *v/v* solvent medium. Compared to the monocharged oxoanions investigated, the $H_2PO_4^-$ selectivity over OAc^- (K_{11} = 7980 M^{-1}) was particularly noteworthy, despite the latter anion being two orders of magnitude more basic (Table 2.1). In addition, no binding was observed with ReO_4^- and NO_3^- anions giving clear evidence of the tripodal XB metallo-receptor's binding pocket being of complementary size and geometric match to the tetrahedral $H_2PO_4^-$ anion. The halide binding trend of Br^- > Cl^- > I^- is also noteworthy and rare amongst XB-donor containing hosts functioning in aqueous media, which have a proclivity towards binding the relatively 'softer' and less hydrated I^-.[20,21] In contrast, whilst a similar halide selectivity trend (Br^- > I^-) was observed with **2.16H**·2ClO_4, the HB analogue exhibited much weaker relative binding. These results suggest that the influence of XB has a profound effect in enhancing anion binding relative to HB. Importantly, the $H_2PO_4^-$ selectivity of **2.16I**·2ClO_4 not only served to highlight the crucial role the unique C_{3v} symmetric XB donor cavity played in achieving

shape selectivity for the tetrahedral phosphate anion, but also demonstrated the rare preference of a XB receptor for binding a 'harder' oxoanion over the heavier halides.

Table 2.1: Anion association constants (K_a/ M^{-1}) of the Zn(II)-tripodal hosts **2.16I**·2ClO_4 and **2.16H**·2ClO_4.[a]

Anion[b]	pK_aH[h]	CD_3CN/ D_2O 9:1 *v/v*	
		2.16I·2ClO_4 **XB** K_a/ M^{-1} [a]	**2.16H**·2ClO_4 **HB** K_a/ M^{-1} [a]
Cl^-	-7.0	K_{11} = 2920 (58) K_{12} = 59 (5)	-[c]
Br^-	-9.0	K_{11}= 4054 (364) K_{12} = 32 (3)	K_{11} = 1468 (25) K_{12} = 348 (15)
I^-	-10.0	K_{11} = 1327 (84) K_{12} = 203 (8)	K_{11} = 883 (86) K_{12} = 129 (6)
CN^-	9.2	-[d]	-[c]
NO_3^-	-1.38	NB[e]	NB[e]
OAc^-	4.75	K_{11} = 7980 (599) K_{12} = 77 (2)	-[f]
$H_2PO_4^-$	2.12	K_{11} = >10^4 [g]	-[c]
ReO_4^-	-1.25	NB[e]	NB[e]

[a]Obtained by fitting the binding isotherms to a host-guest 1:2 stoichiometric binding model using WINEQNMR2[19] software, monitoring the perturbations of the methylene protons H_e for both XB and HB hosts (Scheme 2.8); errors (±) in parenthesis (<10%); [host] = 1.5 mM, T = 298 K. [b]Anions added as their TBA salts. [c]Precipitation of host-anion adducts occurred. [d]Slight decomposition of receptor as well as abstraction of Zn(II) from tripodal cavity observed. [e]NB: No binding, $\Delta\delta$ <0.05 ppm. [f]Multiple complex binding equilibria. Data could not be fit to 1:1 / 1:2 host-guest models. [g]Bound in slow-exchange. Association constant of 1:1 host-guest stoichiometry calculated using with the relative bound/ unbound integrals of proton H_a[18]. [h]pK_aH values represent the pK_a values for the respective conjugate acids, reported in water by Smith and March.[22]

2.4 A tris(ferrocene)-appended XB Zn(II) tripod

Encouraged by the augmented anion recognition properties of the previous XB Zn(II)-tripodal host **2.16I**·2ClO_4 compared to its protic counterpart **2.16H**·2ClO_4, a redox-active ferrocene-appended XB metallo-receptor **2.20I**·2ClO_4 was prepared to investigate the *sensing* of anions electrochemically *via* the ferrocene/ ferrocenium (Fc/ Fc^+) redox couple (Scheme 2.10).

2.4.1 XB-mediated redox anion sensing

As briefly mentioned in Sections 1.2.6.1 and 1.2.6.2 of Chapter One, the development of XB anion sensor molecules, let alone electrochemically proficient ones, is a field still in its infancy.

Given that the enhanced covalent character of the XB interaction[23] advantageously provides a conduit to facilitate effective electronic communication with a suitable reporter group, it is somewhat surprising this property has not been fully exploited for XB-mediated anion sensing. Indeed, Beer and co-workers reported the first XB electrochemical anion sensory host, an acyclic bidentate 1,1'-bis-iodotriazole ferrocene derivative (Figure 2.10A), which exhibited larger magnitudes of cathodic shifts of the Fc/ Fc^+ redox potential in the presence of Cl^- and Br^- ($\Delta E_{1/2}$ = - 30 mV and -18 mV respectively) in CH_3CN than the HB analogue ($\Delta E_{1/2}$ = - 6 mV and - 10 mV respectively).[24] Subsequently, by appending iodotriazole units on the 1,3-positions of the same cyclopentadienyl ring of ferrocene, the same group demonstrated the unprecedented use of XB in the selective redox sensing of the highly toxic and environmentally hazardous N_3^- anion.[25] Impressively, the electrochemically-active XB receptor shown in Figure 2.10B displayed a larger redox potential cathodic shift of $\Delta E_{1/2}$ = - 40 mV with 10 equiv. of N_3^- in CH_3CN/ H_2O 99:1 *v/v* than the $\Delta E_{1/2}$ = - 18 mV observed with the analogous HB host, clearly conveying the importance of XB interactions for enhancing the sensitivity of redox anion detection even in the presence of water. Shortly thereafter, the incorporation of XB donor groups into other various redox-active (ferrocene and TTF) functionalities were also reported by the groups of Molina (Figure 2.2C, Section 2.2.1) and Schöllhorn (Figure 1.29C, Section 1.2.6.1) as highlighted previously. Very recently, Beer and co-workers also studied the use of iodotriazole-substituted diquat derivatives (Figure 2.10C) for XB-mediated sensing of the halides.[26] The present rarity of such amperometric XB hosts thus provided further motivation for the synthetic endeavour outlined in this section.

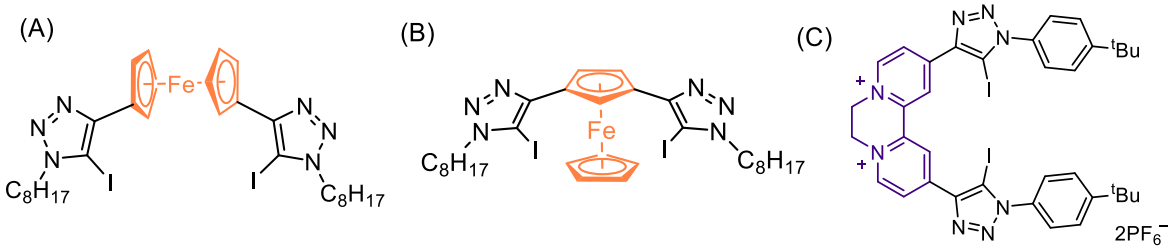
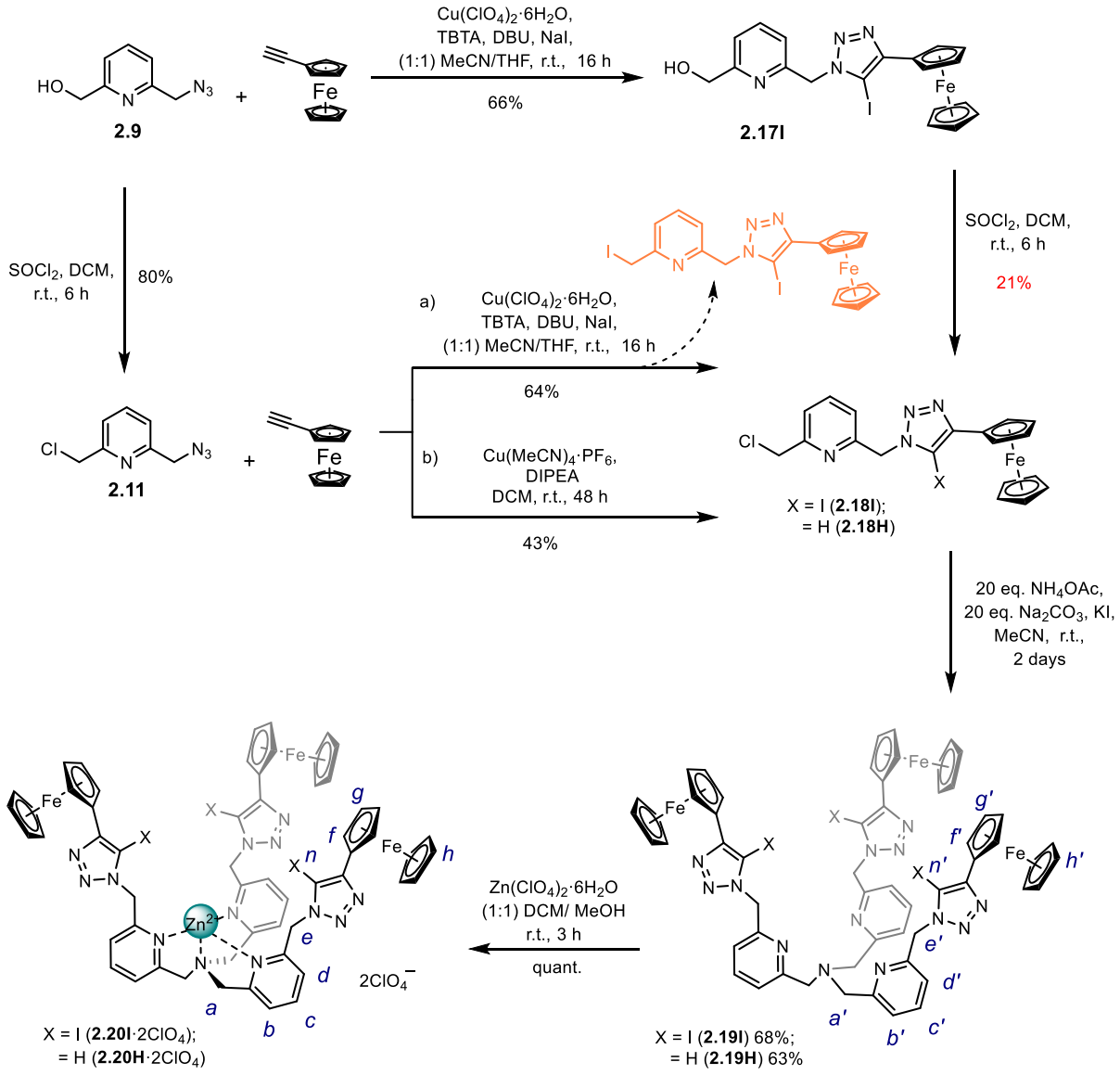


Figure 2.10 *XB-donor redox-active molecules for anion sensing: Beer's (A) 1,1'-bis-iodotriazole ferrocene derivative;[24] (B) 1,3-bis-iodotriazole ferrocene host[25] and (C) bis-iodotriazole diquat sensor.[26]*

2.4.2 Synthesis and characterisation of **2.20I**·2ClO_4 and **2.20H**·2ClO_4

The target tris-ferrocene appended host compound **2.20I**·2ClO_4 was prepared *via* adaption of the synthetic methodology used to prepare the tris-octyl appended XB tripod **2.I6**·2ClO_4 (Scheme 2.10). Commercially available ethynylferrocene was first reacted with the azide **2.9** under one-pot 'iodo-Click' conditions to afford the ferrocene-appended XB synthon **2.17I** in 66% yield. Further treatment with $SOCl_2$ to give the chlorinated '*arm*' **2.18I** proved problematic however due to decomposition of by-products and **2.18I** was isolated only in a modest 21% yield after chromatographic purification.



Scheme 2.10: *Synthetic pathway followed to obtain the ferrocene-appended XB Zn(II)-tripodal host* ***2.27I****.2ClO_4*

Hence, the synthetic route was modified by first reacting **2.9** with $SOCl_2$ to quantitatively afford the chlorinated azide **2.11** and subsequent iodo-CuAAC with ethynylferrocene followed by chromatographic purification gave the desired product in good 64% yield.* Reaction of **2.18I** with excess NH_4OAc and Na_2CO_3 (20 equivalents of each) in MeCN at room temperature afforded the ferrocene tripodal XB ligand **2.19I** in 68% yield after purification *via* preparative TLC. Subsequent complexation with a stoichiometric quantity of zinc(II) perchlorate hexahydrate furnished the XB tetra-metallo-host **2.20I**·$2ClO_4$ as a lustrous orange powder, which was fully characterised *via* ^{1}H and ^{13}C NMR spectroscopy, high resolution ESI-MS and solid-state structural analyses. The HB counterpart **2.20H**·$2ClO_4$ was synthesised using an analogous multi-step procedure involving standard 'proto-Click' conditions (Scheme 2.10).

The ^{1}H-NMR spectra of both ferrocene-appended Zn(II)-hosts **2.20I**·$2ClO_4$ and **2.20H**·$2ClO_4$ compared to their respective zinc-free ligands (in Acetone-d_6) are displayed in Figure 2.11. XB tripod **2.20I**·$2ClO_4$ displayed pronounced downfield shifts of its core pyridyl proton $H_{b\text{-}d}$ and methylene proton H_a signals which confirmed ligation of the TPMA cavity to the Zn(II) center, whilst the distal Fe-Cp proton H_f and H_h signals of the ferrocene appendages experienced comparatively minor upfield shifts.

*During the purification process, a second compound was found to partly co-elute with **2.18I** and later identified by ESI-MS (peak at *m/z* = 610.8 $[M + H]^+$) as the '6-(iodomethyl)pyridine-*arm*' (highlighted in orange, in Scheme 2.11). This was presumed to have formed due to the use of excess NaI in the respective iodo-CuAAC and simply re-combined with the chlorinated analogue **2.18I** for further use in the tripodal ligand formation step.

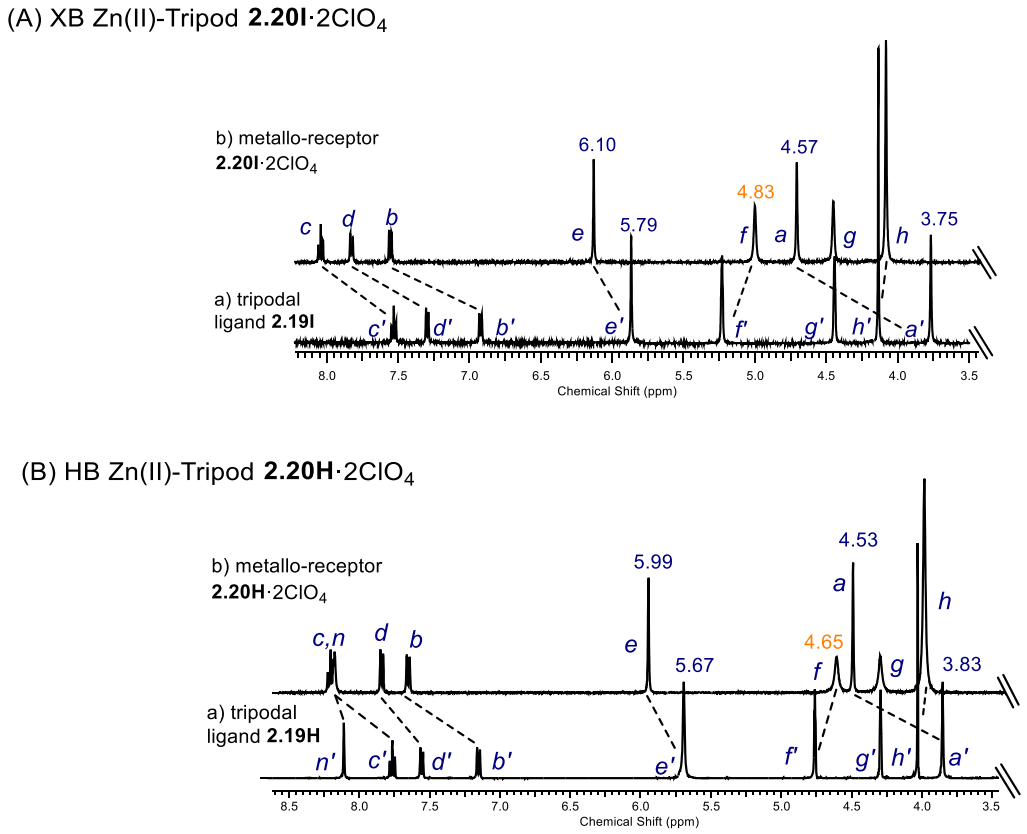


Figure 2.11: *^{1}H-NMR characterisation of the ferrocene appended Zn(II)-tripodal receptors (A)* ***2.20I***·$2ClO_4$ *and (B)* ***2.20H***$.2ClO_4$*. All spectra were obtained in Acetone- d_6 (T = 298 K, 500 MHz). Assignments follow those in Scheme 2.10.*

Curiously and in contrast to the ^{1}H-NMR spectrum of **2.16I**·$2ClO_4$ (Figure 2.7A) where the respective medial methylene H_e protons' resonance (δ = 5.70 ppm) remained unperturbed in the presence of the Zn(II) cation, with **2.20I**·$2ClO_4$ the same signal was shifted noticeably downfield (δ = 6.10 ppm). Similarly, **2.20H**·$2ClO_4$ displayed analogous shifts of its proton resonances, except with a minor downfield shift of the characteristic prototriazole H_n proton. Finally, a comparison of the ferrocene H_f proton signals *directly conjugated* to each XB/ HB metallo-receptors' triazoles revealed the relevant chemical shifts (highlighted in orange) to be more downfield in the case of **2.20I**·$2ClO_4$ ($\Delta\delta$ = 0.18 ppm) relative to that of **2.20H**·$2ClO_4$, which further served to highlight the greater polarising ability and hence greater electron-withdrawing capacity of the all-important XB-donor iodotriazole moieties.

2.4.3 Crystal structures of **2.20I**·$2ClO_4$ and **2.20H**·$2ClO_4$

Block-shaped, deep orange crystals of **2.20I**·$2ClO_4$ obtained by slow evaporation of saturated solutions of the compound in CD_3CN were subjected to single crystal X-ray diffraction structural analysis. The structure, determined by Dr Christopher Durr, shows the XB tripod to be crystallised in the $P2_1/c$ (monoclinic) space group with two perchlorate counteranions, as well as one molecule of acetonitrile in the asymmetric unit (Figure 2.12A). The Zn(II) center exhibits a hexacoordinate preference in the solid state and was found to adopt a distorted octahedral configuration, with four coordination sites satisfied by the proximal pyridyl nitrogens (N(10), N(11), N(12) and N(13)) of the TPMA subunit of the ligand and the remaining two being supplied by the medial nitrogens (N(2) and N(5)) of two of the iodotriazole moieties. The former basal subunit of the ligand maintains a helical twist in which the dihedral angle between the plane of each pyridine ring and the axis of the Zn(1)-N(13) bond is between 34.9(4) and 47.9(4) degrees. Thus, the overall shape of the cationic portion of the molecule elegantly resembles a propeller, whose adjoining iodotriazoles are additionally twisted out in converse planes (presumably due to the steric bulk of the voluminous iodine atoms which point 'out' from the tripodal binding pocket in the most energetically-favourable conformation for crystallisation). A comparison of the relevant Zn(1)-N bond lengths summarised in Figure 2.12A, conveys the distance of one iodotriazole (Zn(1)-N(2)) N^2-ligated to the metallocentre to be much longer than the other (Zn(1)-N(5)) which suggests a weaker interaction of the former in the solid state, likely imposed by the steric clash of their respective conjugated ferrocene termini due to close packing.[†‡] Notably, a distinct, highly linear short contact between the remaining, 'non Zn-coordinating' iodotriazole's I(3) atom and $O(1)^-$ oxygen atom of one of the perchlorate counteranions (highlighted in green, $D_{I(3)\cdots O(1)^-}$ = 2.978(6) Å) can be

[†] The display of C_3 symmetry in the prior ^{1}H-NMR of **2.20I**·$2ClO_4$ (Figure 2.11A), affirms that this solid state iodotriazole N^2-coordination behaviour is highly 'fluxional' in solution. Accordingly, the interior cavity of the XB metallo-host is still 'open' to dynamically accommodate and bind exogenous anions in the envisioned tetradentate manner in solution.

[‡] This fluxional iodotriazole N^2-coordination is presumably also responsible for the previously unrationalised marked downfield shift of the adjacent methylene H_e protons upon metal complexation (see Figure 2.11A) which are consequently deshielded.

discerned, which is shorter than the sum of their respective van der Waal's (vdW) radii (85%) and indicative of a strong, perchlorate anion···iodotriazole halogen bond.

Interestingly, given that Zn(II) metal coordination would effectively render them more electron-deficient and thus superior XB donors, one might reasonably expect the dyad of N^2-ligated iodotriazoles to be 'better suited' for such an interaction with the respective counter-anion in the solid state compared to their 'non Zn-coordinating' analogue. Indeed, further inspection of the solid-state packing in the crystal lattice of **2.20I**·$2ClO_4$ (Figure 2.12C) revealed the formation of a 3-D network in which the I(2) atom of a Zn(II)-coordinated iodotriazole of an *adjacent* metallo-tripodal entity was also found to exhibit a similar short contact of near linearity (highlighted in orange) with the O(4) oxygen atom of the same 'bound' perchlorate counteranion ($D_{I(2)\cdots O(4)}$ = 3.004(8) Å, 86% vdW radii), thus distinguishing a second, robust, perchlorate anion···iodotriazole halogen bond.

The structure of **2.20H**·$2ClO_4$ was also determined crystallographically, with isomorphous crystals suitable for X-ray diffraction structural analysis acquired in the exact same manner as its halogenated counterpart (*vide supra*). The conformation of the triply ferrocene-appended protic Zn(II) tripod (Figure 2.12B) matched that of **2.20I**·$2ClO_4$, except with the notable absence of a corresponding HB interaction between any of the prototriazoles and perchlorate counteranions in the solid state.

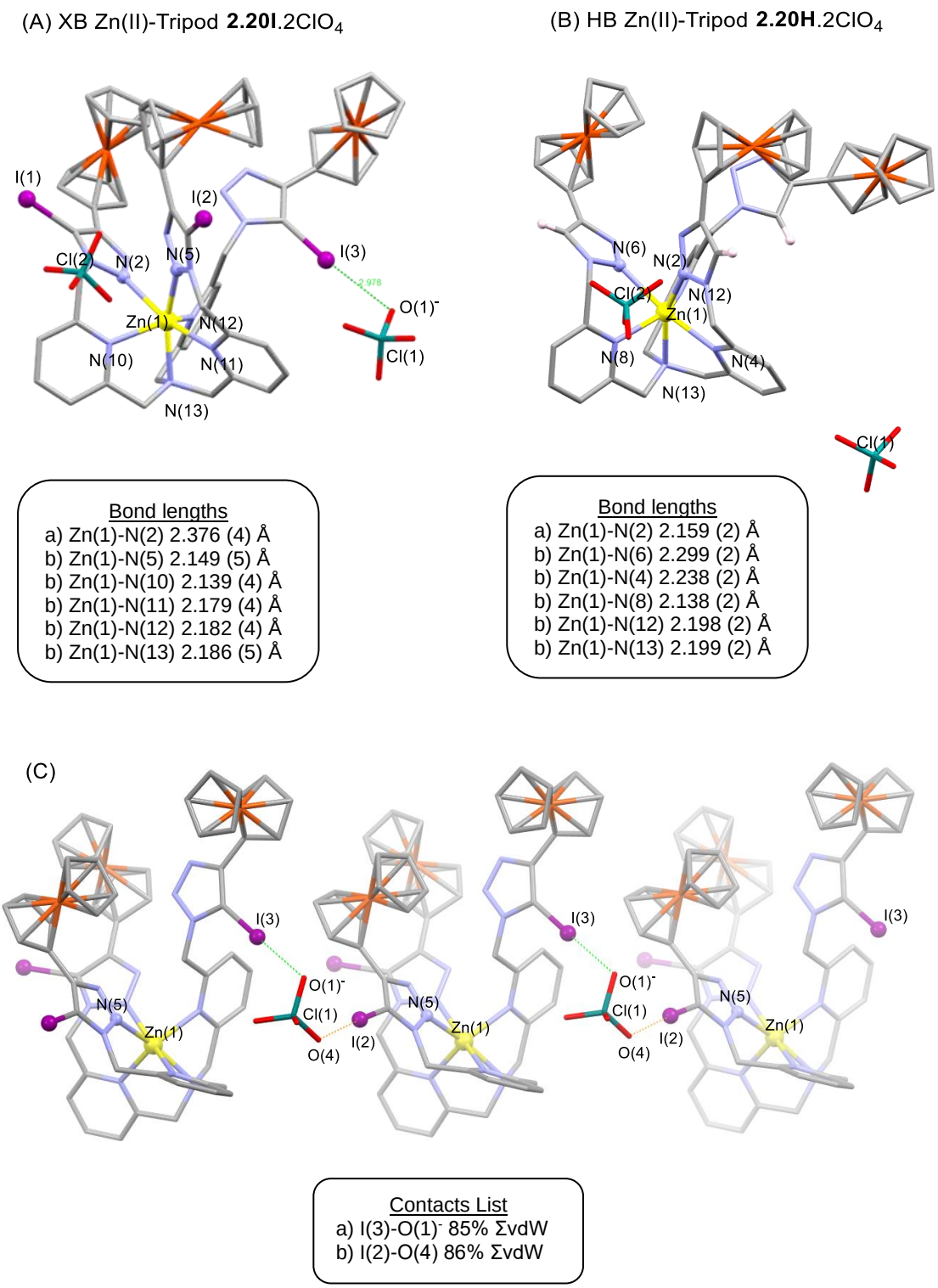


Figure 2.12: *Crystal structures of (A)* ***2.20I****·2ClO4 and (B)* ***2.20H****·2ClO4 with list of relevant bond lengths. Both receptors are drawn as capped sticks with the Zn(II) centre, coordinating triazole-N² atoms and halides as spheres. The iodotriazole-I···O⁻ halogen bond with an oxygen atom of one of the perchlorate counteranions is indicated as a green dashed line. (CD3CN solvent molecules and most hydrogen atoms are omitted for clarity). C) Side view of the solid-state packing structure in the crystal lattice of* ***2.20I****·2ClO4, distinguishing a second N²-coordinated iodotriazole-I···O⁻ halogen bond (orange dashed line).(Non-coordinated second perchlorate counteranions omitted for clarity).*

2.4.4 ^{1}H NMR binding studies with **2.20I**·2ClO$_4$ and **2.20H**·2ClO$_4$

Following the same titration protocol outlined in Section 2.3.2, the solution-phase anion recognition properties of the ferrocene-appended Zn(II) receptors were initially studied *via* ^{1}H NMR titration experiments also in CD_3CN/D_2O 9:1 *v/v*. Similar anion binding induced proton perturbations observed with the octyl-appended Zn(II)-tripodal receptors were seen with the ferrocene Zn(II)-receptor systems.

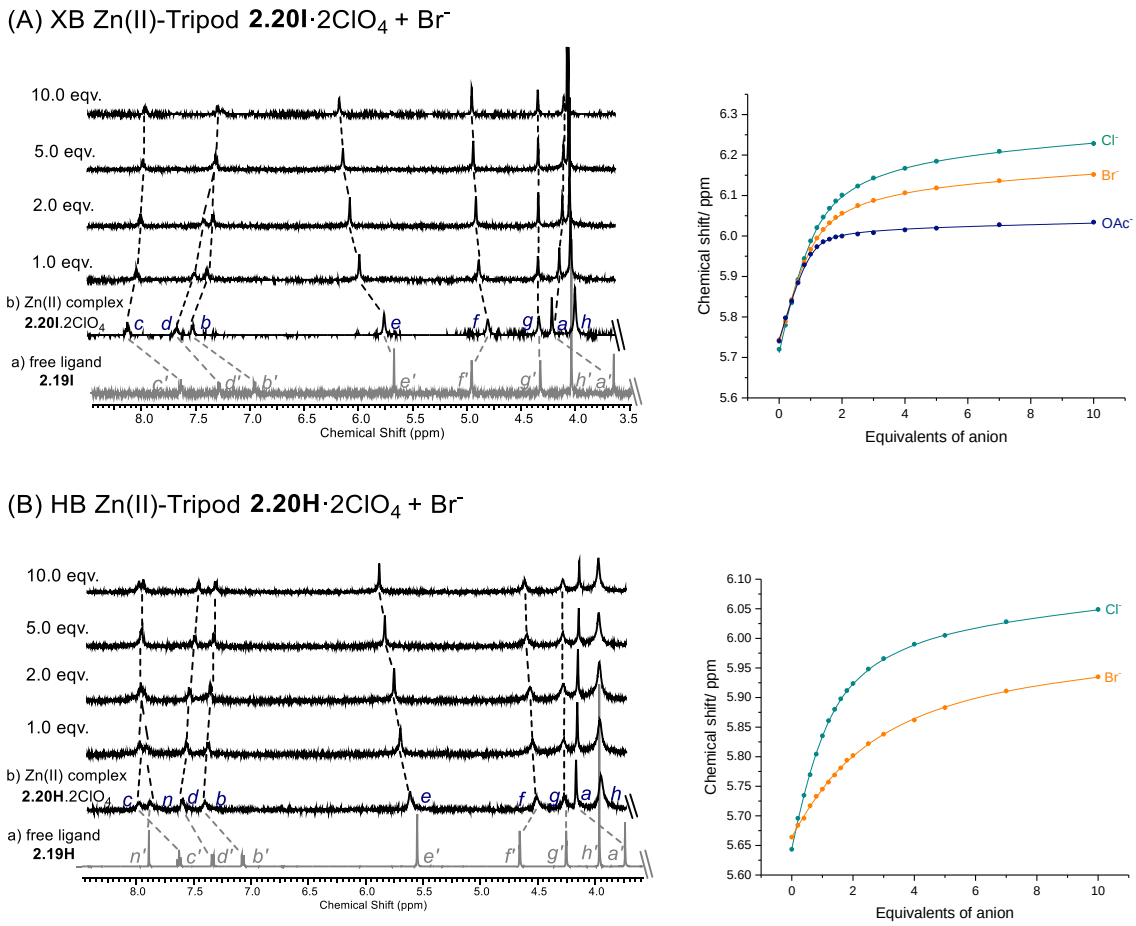


Figure 2.13: *(Left row) ^{1}H NMR spectra of Zn(II) tripodal receptors (A)* ***2.20I***·*2ClO$_4$ and (B)* ***2.20H***·*2ClO$_4$ in the presence of 0.0, 1.0, 2.0, 5.0 and 10.0 equivalents of Br$^-$ at T = 298 K. (Right row) Titration isotherms: Plots of the medial methylene proton's (H_e) chemical shifts of tripod as a function of anion concentration. ([metallo-host] = 1.5 mM, CD_3CN/ D_2O 9:1 v/v, 500 MHz). All proton assignments follow those in Scheme 2.10.*

From Figure 2.13A, the addition of 10 equivalents of Br$^-$ to **2.20I**·2ClO$_4$ (as well as **2.20H**·2ClO$_4$, Figure 2.13B) resulted in discernible successive upfield perturbations of the TPMA pedestal's $H_{a\text{-}d}$ proton resonances, as well as a comparatively larger downfield shift of the proximal

methylene H_e proton ($\Delta\delta$ = 0.41 ppm). Additionally, smaller yet significant downfield perturbations of the Fc-Cp proton H_f ($\Delta\delta$ = 0.14 ppm) immediately adjacent to the triazole moieties and a modest upfield shift of H_g, clearly indicated that effective electronic communication between the bound anion and the ferrocene reporter motifs was occurring. Similar notable perturbations of these proton environments were also evidenced with the titrations performed with Cl^- and OAc^-, whilst the addition of ReO_4^- elicited no appreciable signal shifts.

Notably, upon addition of $H_2PO_4^-$ to **2.20I**·2ClO_4, and as previously observed with the octyl-appended tripod **2.16I**·2ClO_4, two distinct sets of 'unbound' and 'bound' host resonances were evidenced in the titration spectra indicative of slow-exchange kinetics on the ^{1}H-NMR timescale (Figure 2.14). Likewise, the resonances of the ferrocene appended Zn(II)-host's aromatic pyridyl protons $H_{b\text{-}d}$ appeared further upfield, whilst the methylene H_a proton signal was dramatically shifted further downfield (δ = 4.54 ppm). In contrast however, was the slight *upfield* resonance of the iodotriazole adjacent H_e protons (δ = 5.69 ppm), possibly suggestive of a minor conformational rearrangement of the XB-donor arms to accommodate the tetrahedral guest.

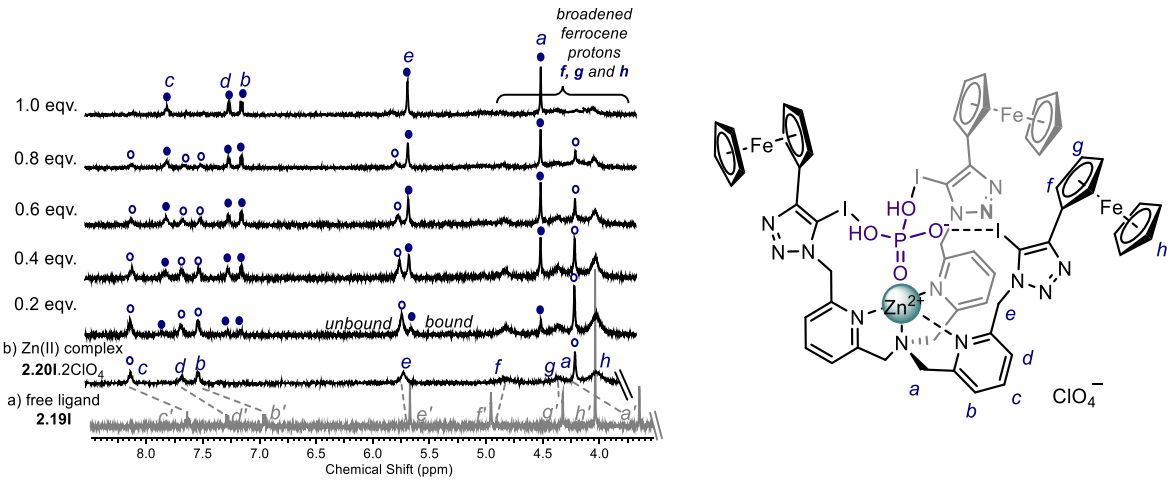


Figure 2.14: *Changes in the ^{1}H NMR spectra of the Zn(II) tripodal receptor* ***2.20I***·*2ClO_4 upon the addition of 1.0 equivalent of $H_2PO_4^-$ at T = 298 K. ([metallo-host] = 1.5 mM, CD_3CN/ D_2O 9:1 v/v, 500 MHz). All proton assignments follow those in Scheme 2.10.*

Anion association constants of 1:2 host:guest stoichiometry for both ferrocene-appended XB and HB Zn(II)-hosts were determined by WinEQNMR2[19] analysis of the titration data (monitoring the

shifts of the medial methylene proton H_e as a function of anion concentration, see Figures 2.13A and 2.13B) summarised in Table 2.2.

Table 2.2: Anion association constants (K_a/ M^{-1}) of the ferrocene Zn(II)-tripodal hosts **2.20I**·2ClO_4 and **2.20H**·2ClO_4.[a]

Anion[b,c]	CD_3CN/ D_2O 9:1 *v/v*	
	2.20·2ClO_4 **XB** K_a/ M^{-1} [a]	**2.20H**·2ClO_4 **HB** K_a/ M^{-1} [a]
Cl^-	K_{11} = 2544 (292) K_{12} = 70 (6)	K_{11} = 1580 (89) K_{12} = 62 (3)
Br^-	K_{11} = 3685 (16) K_{12} = 60 (4)	K_{11} = 903 (86) K_{12} = 134 (4)
OAc^-	K_{11} = 9323 (374) K_{12} = 12 (1)	-[d]
$H_2PO_4^-$	K_{11} = >10^4 [e]	-[f]
ReO_4^-	NB[g]	NB[g]

[a]Obtained by fitting the binding isotherms to a host-guest 1:2 stoichiometric binding model using WINEQNMR2 software[19], monitoring the perturbations of the methylene protons H_e for both XB and HB hosts (Scheme 2.10); errors (±) in parenthesis (<12%); [host] = 1.5 mM, T = 298 K. [b]Anions added as their TBA salts. [c]The binding of Iodide was not investigated *via* ^{1}H-NMR titration as it is not possible to perform complementary electrochemical anion titrations with the anion due to its low oxidation potential. [d]Multiple complex binding equilibria. Data could not be fit to 1:1 / 1:2 host-guest models. [e]Bound in slow-exchange till 1 equivalent of anion. Anion association constant of 1:1 host-guest stoichiometry calculated using with the relative bound/ unbound integrals of proton H_c [f]Titration not performed. [g]NB: No binding, $\Delta\delta$ <0.05 ppm.

The anion binding trend of **2.20I**·2ClO_4 exactly mirrored that of **2.16I**·2ClO_4 (see Table 2.1). The XB ferrocene receptor exhibited a clear selectivity for $H_2PO_4^-$ over the other anions, with the enhanced association constant > 10^4 M^{-1} attributed to the excellent size and geometric complementarity of the XB ferrocene receptor's tetrahedral binding cavity. Similarly, very strong binding of OAc^- was observed followed by a distinct Hofmeister preference for Br^- > Cl^- in the case of the halides. Again, the halide binding trend further served to highlight the influential effects of the size and shape of the host's binding cavity in dictating anion binding as the less basic and larger Br^- was preferentially bound over the smaller, charge-dense Cl^-. Conversely, the protic host analogue **2.20H**·2ClO_4 displayed a reversal in selectivity for the two halides, binding Cl^- with a larger affinity than Br^- - presumably, the size of the tripodal cavity flanked instead by three prototriazoles complemented the smaller ionic radii of Cl^- and hence afforded the larger association constant. Notably, both halides were bound much more strongly to the XB receptor than the HB

counterpart and thus, the superiority of XB over HB for solution-phase anion recognition was clearly demonstrated once more.

2.4.5 Electrochemical anion sensing studies with **2.20I**·2ClO$_4$ and **2.20H**·2ClO$_4$

Having investigated the anion binding behaviour of the ferrocene Zn(II)-hosts by ^{1}H NMR titrations, their redox anion sensing properties were further probed. With the aid of Dr Jason Lim, at the time a D.Phil. student in the group, electrochemical reversibility studies of the **2.20I**·2ClO$_4$ and **2.20H**·2ClO$_4$ were first conducted *via* cyclic voltammetry (CV) in the electrolyte solution of 0.1 M TBAClO$_4$ in CH$_3$CN/ H$_2$O 9:1 *v/v*. A standard three electrode electrochemical cell was used, with a glassy carbon working electrode, a Pt wire auxiliary electrode and a Ag/AgNO$_3$ non-aqueous reference electrode.[27] Both XB and HB receptors displayed a single, quasi-reversible redox-wave (Figure 2.15) indicative of all three ferrocene centres being oxidised at the same potential with $E_{1/2}$ values of + 188 and + 173 mV respectively.[§] Notably, the more anodic $E_{1/2}$ value of the XB host **2.20I**·2ClO$_4$ compared to the HB counterpart **2.20H**·2ClO$_4$ reflected its more electron-deficient nature by virtue of the electronegative iodine atoms thermodynamically disfavouring oxidation of the ferrocene units, and thus corroborating prior observations from ^{1}H-NMR characterisation (Figure 2.11).

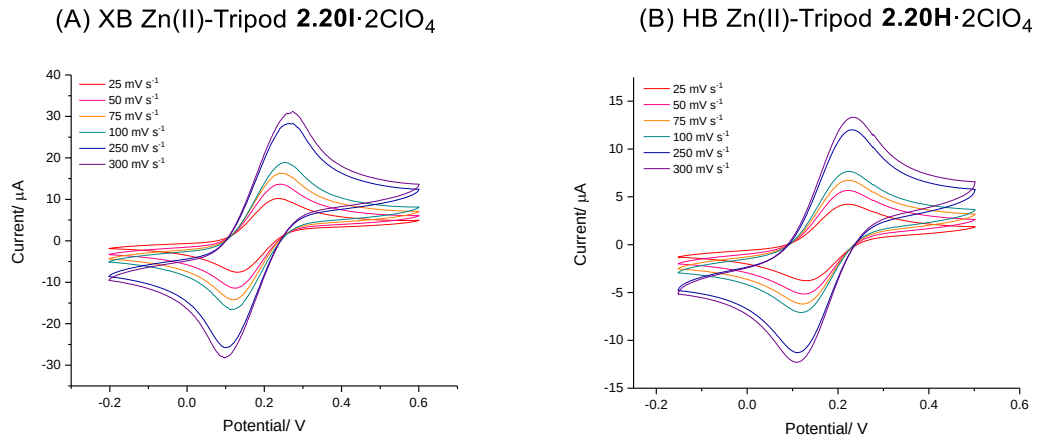


***Figure 2.15**: Electrochemical reversibility studies: Cyclic voltammograms (CVs) of the ferrocene-appended Zn(II)-tripodal hosts (A) **2.20I**·2ClO$_4$ and (B) **2.20H**·2ClO$_4$, recorded at various scan rates of 25, 50, 75, 100, 250 and 300 mV s^{-1}. Potentials compared to the Ag/AgNO$_3$ reference electrode. ([metallo-host] = 0.5 mM, electrolyte: 0.1 M TBAClO$_4$ in CH$_3$CN/ H$_2$O 9:1 v/v, T = 293 K)*

[§] Details of the reversibility studies performed on all the redox-active host systems studied in this thesis, as well as the relevant theory of electrochemical anion sensing are provided in Appendices B and C.

Electrochemical anion titrations were carried out using differential pulse voltammetry (DPV) in the analogous electrochemical solvent system, as summarised in Table 2.3. Upon the addition of 10.0 equivalents of Cl^-, Br^- and OAc^-, significant cathodic perturbations of the respective ferrocene/ferrocenium redox couples were manifest for both XB and HB electrochemically active receptors (Figure 2.16), arising from the anion binding stabilising the ferrocenium oxidation state. In the case of **2.20I**·$2ClO_4$, the observed cathodic shifts were all of a comparable magnitude, indicating that the halides and acetate anions were able to stabilise ferrocenium to a similar degree, whereas by contrast, Cl^- induced the largest $\Delta E_{1/2}$ perturbation with **2.20H**·$2ClO_4$. Importantly, the XB receptor exhibited an enhanced voltammetric response for Br^- and OAc^- in comparison to its protic counterpart. These differences in electrochemical behaviour between **2.20I**·$2ClO_4$ and **2.20H**·$2ClO_4$ indicated that the XB-donor atoms of the former host were facilitating through-bond electronic communication between the conjugated binding site and the redox-active ferrocene motif, ostensibly owing to the greater degree of covalency in the XB-anion interaction.[23]

Table 2.3: Cathodic Shifts ($\Delta E_{1/2}$/ mV) of the ferrocene/ ferrocenium redox couples of **2.20I**·$2ClO_4$ and **2.20H**·$2ClO_4$ upon addition of 10 equivalents of various anions.

Anion[a]	CH_3CN/ H_2O 9:1 *v/v*	
	2.20I·$2ClO_4$ **XB** $\Delta E_{1/2}$/ mV [b]	**2.20H**·$2ClO_4$ **HB** $\Delta E_{1/2}$/ mV [b]
Cl^-	-26	-30
Br^-	-25	-17
OAc^-	-29	-14
$H_2PO_4^-$	- [c]	- [d]
ReO_4^-	0	0

[a]Anions added as their TBA salt. Electrolyte: 0.1 M $TBAClO_4$ in CH_3CN/ H_2O 9:1 *v/v*. Reference electrode: $Ag/AgNO_3$; Working electrode: glassy carbon; Counter electrode: platinum. [b]Error estimated to be ±5 mV. ([receptor] = 0.5 mM, T = 293 K). [c] precipitation occurred. [d]loss of redox reversibility as well as precipitation.

With regards to $H_2PO_4^-$, whilst a large cathodic perturbation of $\Delta E_{1/2}$ = -20 mV was initially evidenced upon addition of 1 equivalent of the anion with **2.20I**·$2ClO_4$ (Figure 2.16A), unfortunately upon subsequent anion addition precipitation occurred. Similar solubility issues as well as a loss of electrochemical reversibility was encountered with $H_2PO_4^-$ and **2.20H**·$2ClO_4$,

suggesting electron transfer-chemical (EC) reactions between the oxoanion and the ferrocenium oxidation state of the protic receptor.[28] Finally, there was no electrochemical response upon the addition of ReO_4^- with either receptor, corroborating the ^1H NMR titration results where no binding was observed.

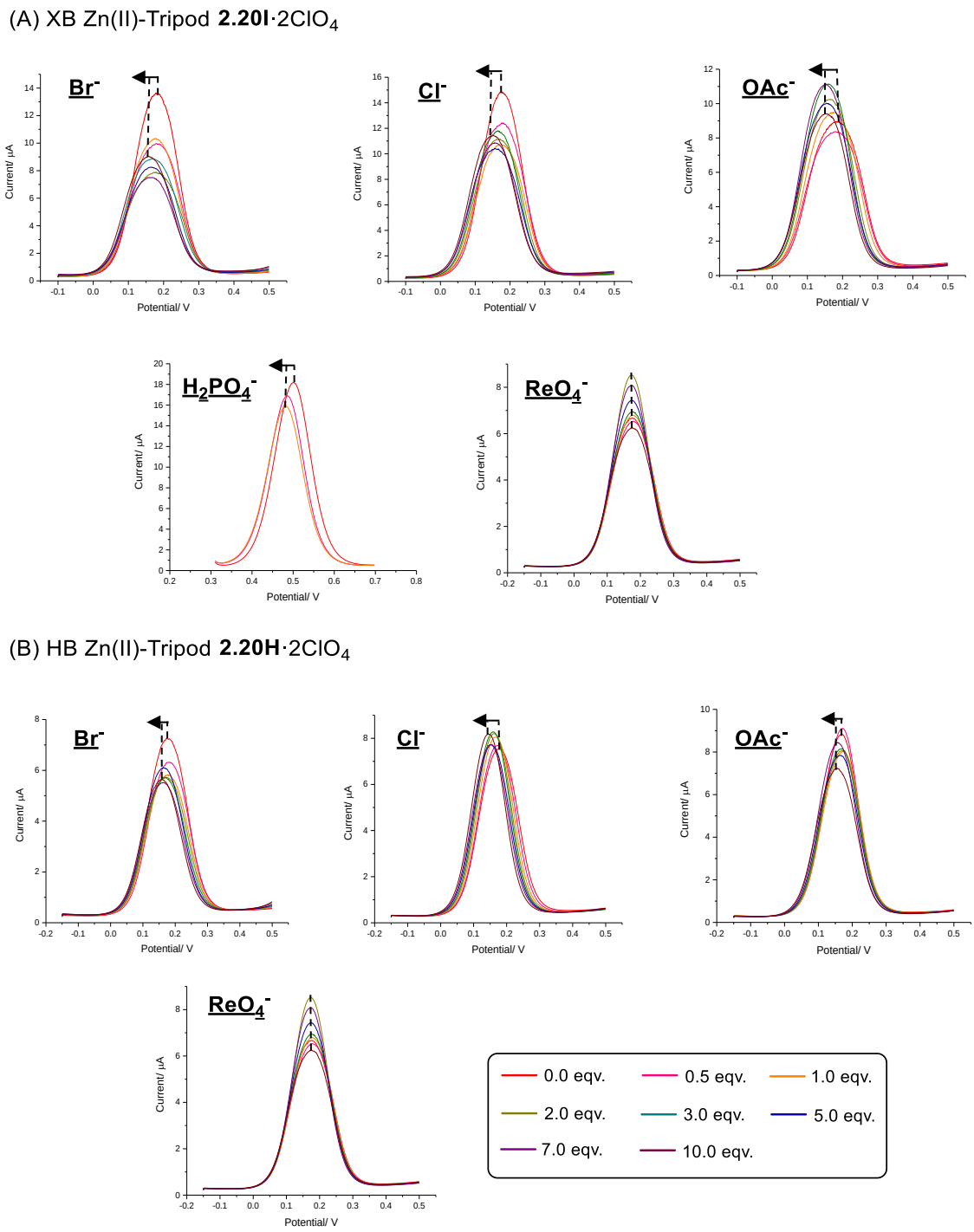


Figure 2.16: *Electrochemical anion titrations. DPV's of receptors (A)* ***2.20I***·$2ClO_4$ *and (B)* ***2.20H***·$2ClO_4$ *with incremental quantities of various anions; Potentials compared to the Ag/AgNO₃ reference electrode. ([metallo-host] = 0.5 mM, electrolyte: 0.1 M TBAClO₄ in CH₃CN/ H₂O 9:1 v/v, T = 293 K).*

2.5 A water soluble, tris(triethylene glycol)-appended XB Zn(II) tripod

Having evidenced the potent anion recognition properties of the XB octyl- and ferrocene-appended Zn(II)-tripods (**2.16I**·2ClO_4 and **2.20I**·2ClO_4 respectively) in the competitive CD_3CN/D_2O 9:1 *v/v* solvent mixture and motivated by the goal of *quantifying* the strong ($K_a > 10^4$ M^{-1}) binding of inorganic monophosphate observed with each host, a XB metallo-tripodal receptor **2.25I**·2ClO_4 with hydrophilic poly(ethylene glycol) (PEG) groups, specifically tri(ethylene glycol) (TEG)-based appendages was next prepared to explore the binding of anions in *pure water* (Scheme 2.11). As briefly mentioned in Section 1.2.1 of Chapter One, there is increasing focus towards the development of synthetic anion receptors capable of functioning under 'real-world' conditions,[29,30] which is vital given that their proposed applications lie overwhelmingly in biological, medical and environmental arenas and therefore require aqueous conditions. In light of this and considering the significance of phosphate within each of these domains (Section 1.3.1), the segue to 100% water (as a more competitive solvent system) in which to conduct XB-mediated anion binding seemed particularly fitting.

2.5.1 XB-mediated anion recognition in water

Given its exotic nature, XB has only very recently been demonstrated as an effective interaction for anion recognition in 100% water and thus examples of wholly-aqueous performing XB hosts are exceptionally rare, with those exhibiting an increased affinity for oxo-anions rarer still.[20,21,31,32] In 2014, a seminal study by Beer and co-workers reported a series of permethylated-*β*-cyclodextrin functionalised XB acyclic and interlocked host structures which were demonstrated to bind the heavier halides in pure water with superior affinity compared to their HB counterparts.[20] In particular, van't Hoff analysis of the impressive and selective I^- binding (K_a = 2200 M^{-1}) exhibited by a dicationic [2]rotaxane incorporating a pyridinium bis-iodotriazole XB-donor motif revealed the association to be enthalpically-favoured and entropically-disfavoured, suggesting the complexation to be driven by strong XB-anion interactions. By contrast, the HB analogue displayed negligible I^- association. More recently, the same group also reported a novel acyclic host comprising a pair of diametrically-opposed, pendant XB-donor arms appended onto a central

perbenzylated, α-cyclodextrin scaffold (Figure 2.17)[33] that exhibited a high selectivity for ReO_4^- (K_a = 950 M^{-1}) in unbuffered D_2O, over the other more hydrophobic I^- and ClO_4^- anions investigated. Compared with its HB analogue and native (unfunctionalised) α-cyclodextrin, the XB assembly showed superior binding of ReO_4^-, again not only affirming the dominant role of XB but its ability to also augment *oxo*anion binding interactions in water. The paucity of such XB receptors capable of potent and selective anion binding in an all-aqueous environment provided further motive for the challenging endeavour detailed in this section.

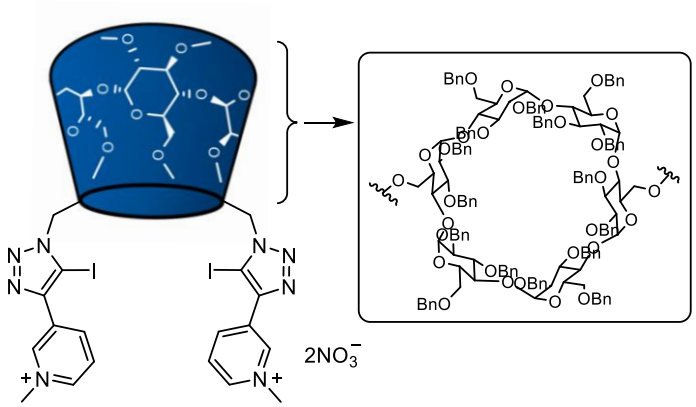
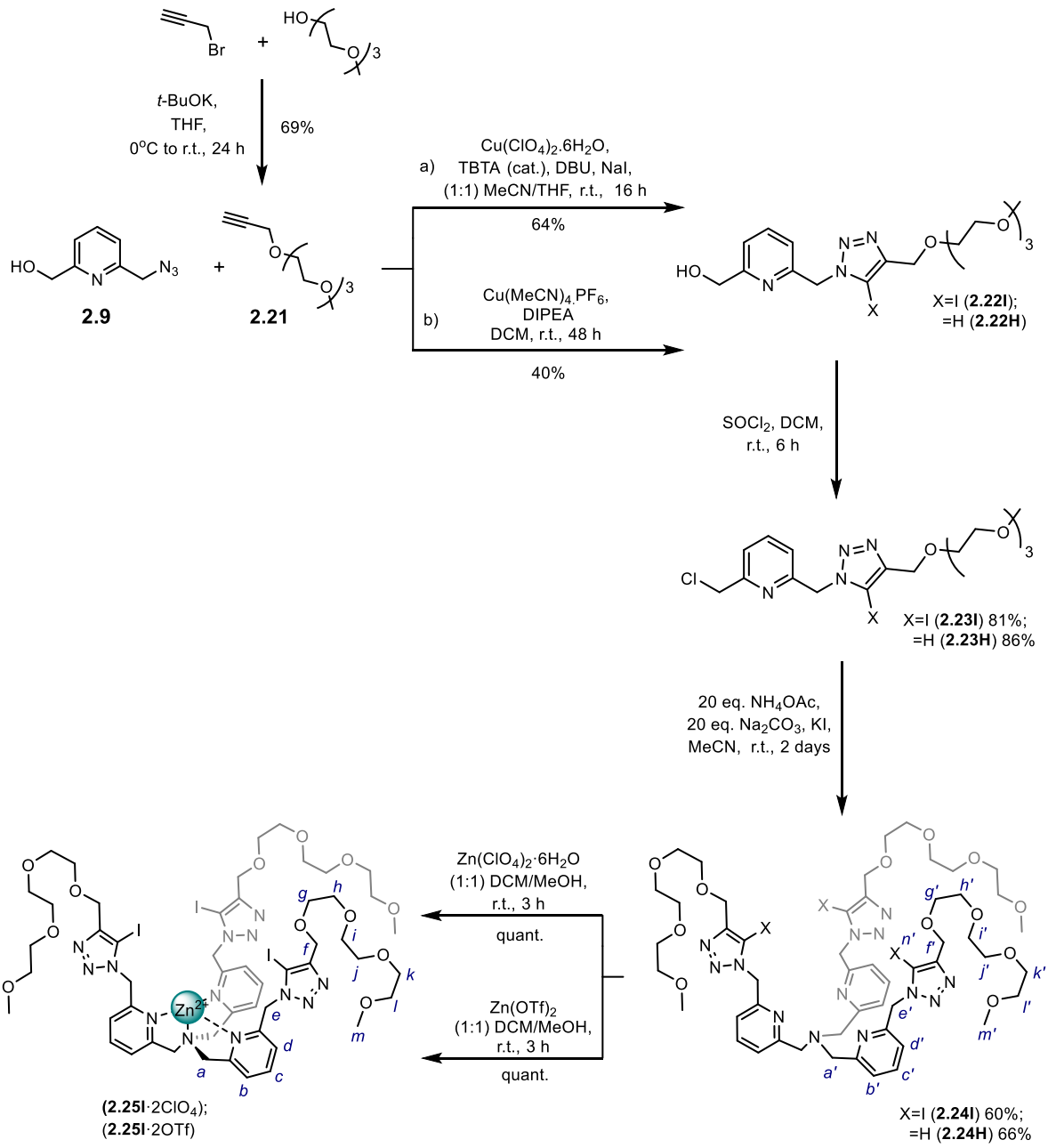


***Figure 2.17**: Beer's XB-decorated perbenzylated α-cyclodextrin receptor for ReO_4^- in water.*[33]

2.5.2 Synthesis and characterisation of **2.25I**·2ClO_4

The target tris-TEG appended host **2.25I**·2ClO_4 was prepared utilising a synthetic procedure similar to that used to construct metallo-receptors **2.16I**·2ClO_4 and **2.20I**·2ClO_4 (Scheme 2.11). The appropriate TEG-based terminal alkyne **2.21** was first synthesised by treating commercially-available TEG monomethyl ether with propargyl bromide under basic conditions as per literature procedures[34] and reacted with azide **2.9** using Zhu's 'one-pot' iodo-CuAAC protocol[12] to afford the iodotriazole-containing precursor **2.22I** in good 64% yield after chromatographic purification. Through treatment with $SOCl_2$, the corresponding chlorinated '*arm*' derivative **2.23I** was produced and reacted with excess portions of NH_4OAc and Na_2CO_3 (20 equivalents of each) in MeCN at room temperature. The water-soluble XB tripodal ligand **2.24I** was isolated in 60% yield *via* preparative TLC and subsequent complexation with a stoichiometric quantity of zinc(II) perchlorate

hexahydrate yielded the tris-TEG appended host metallo-host **2.25I**·2ClO_4 as a deep yellow oil, which was characterised *via* ^1H and ^{13}C NMR spectroscopy and high resolution ESI-MS methods.



Scheme 2.11: *Synthetic pathway followed to obtain the TEG-appended XB Zn(II)-tripodal host* ***2.25I****.2*ClO_4

The comparative ^1H NMR spectra of **2.25I**·2ClO_4 and the precursor *apo*-Zn(II) ligand (in $CDCl_3$) are illustrated in Figure 2.18. Characteristic marked downfield perturbations of the respective host's pyridyl protons $H_{b\text{-}d}$ and methylene proton H_a signals confirmed the coordination

of the TPMA subunit to the Zn(II) center, whilst the distal H_f protons of the TEG appendages exhibited an appreciable upfield shift. Notably and as previously observed with **2.16I**·2ClO$_4$ and **2.20I**·2ClO$_4$, the retention of one set of resonances of the ligands core proton $H_{a\text{-}e}$ environments upon Zn(II) complexation affirmed the equivalence of all three XB tripodal *'arms'* and hence the all-important C_{3v} symmetry of the resultant metallo-host.

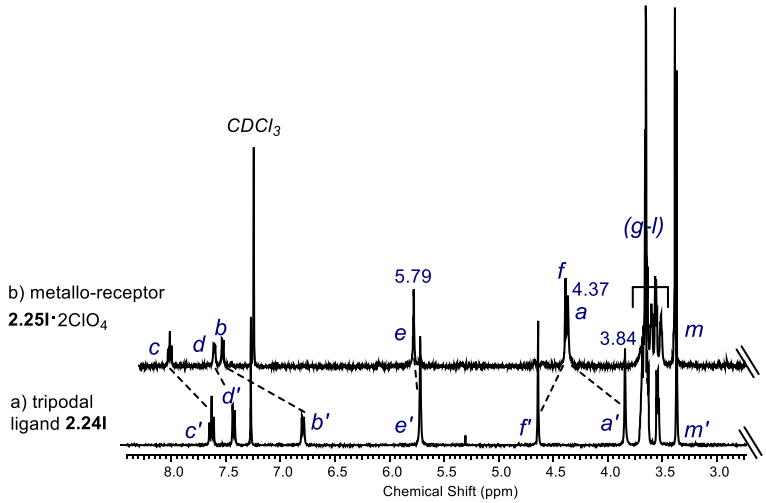


Figure 2.18: *^{1}H-NMR characterisation of the TEG appended Zn(II)-tripodal receptor **2.25I**·2ClO$_4$. All spectra were obtained in CDCl$_3$ (T = 298 K, 400 MHz). Assignments follow those in Scheme 2.11.*

2.5.3 Isothermal calorimetry and ^{1}H NMR binding studies with 2.25I·2ClO$_4$ in water

Preliminary investigations into the anion binding properties of the XB host **2.25I**·2ClO$_4$ were conducted using isothermal titration calorimetry (ITC) in buffered water at physiological pH (with 10 mM 4-(2-hydroxyethyl)-1-piperazineethanesulfonic acid (HEPES), pH 7.4).[**] In a typical titration procedure, aliquots of 20 mM solutions of various anions (in the form of their sodium salts) were added to a 0.2 mM solution of the metallo-host at regular intervals, with the heat pulses generated (Figures 2.19A-C) integrated with respect to time to produce plots of ΔH vs. concentration of anion (Figures 2.19D-F). Importantly in each case, control experiments were also

[**] Given the complex protonation equilibria that inorganic monophosphate exhibits in aqueous media (see Figure 1.32A in Chapter One for the relevant speciation diagram), any binding of this oxoanion in water inevitably involves the binding of a *mixture* of species. At the working pH 7.4 maintained in these studies, two forms exist: HPO_4^{2-} (61%) and $H_2PO_4^-$ (39%). Therefore, whilst the former, dominant dibasic analogue is referred to here, the simultaneous presence and interactions of the latter protonated counterpart should also be kept in mind. As such, any K_a values reported would actually represent the apparent binding affinities for the total phosphate species present in solution.

undertaken where the individual anions were titrated into a cell absent of the XB host, to account for any heat exchange from the interaction between the anion and zwitterionic buffer as well as their heats of dilution. (Further details of the experimental conditions used in the ITC titrations can be found in Chapter Six).

Under the ITC conditions described however, no significant interaction was detected between **2.25I**·2ClO_4 and any of the HPO_4^{2-}, Br^- and I^- anions investigated, as evident from their respective integrated heat plots which indicated there to be negligible heat changes evolved, suggestive of the lack of binding.

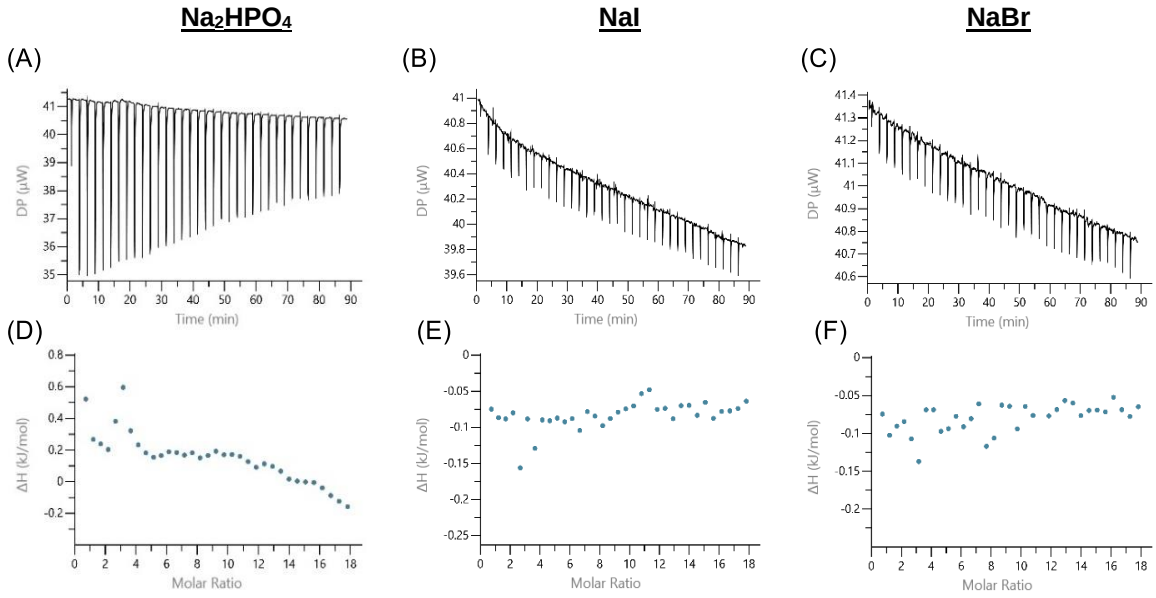


Figure 2.19: *ITC data of preliminary titrations performed upon* ***2.25I***·*2ClO_4 in water (buffered at pH 7.4 with 10 mM HEPES, 298 K). (Above) Raw thermograms for the sequential additions of a) Na_2HPO_4, b) NaI and c) NaBr. (below) Integrated heat plots obtained from the corresponding thermograms with d) Na_2HPO_4, e) NaI and f) NaBr.*

An investigative ^{1}H-NMR titration was further performed with **2.25I**·2ClO_4 and NaI in unbuffered D_2O (Figure 2.20).[††] However upon addition of the hydrophobic halide (up to 100 equivalents), no shifts were observed corroborating the observation from the prior corresponding ITC titration (Figure 2.19E). Closer inspection of the XB host's ^{1}H-NMR spectrum in D_2O (Figure 2.21) although curiously revealed a second set of upfield resonances matching the host's original

[††] The water suppression ^{1}H-NMR pulse sequence *NOESYGPPR1d*, set up by Dr. Nick Rees, was used to perform the binding study to improve the signal-to-noise ratio of the resulting spectra in D_2O.

core $H_{a\text{-}e}$ signals (indicated by the hollow and filled dots respectively), which was in contrast to the characterisation spectrum of **2.25I**·2ClO_4 in $CDCl_3$ (Figure 2.18) and thus suggested a change in the C_{3v} symmetric conformation previously adopted in organic media.

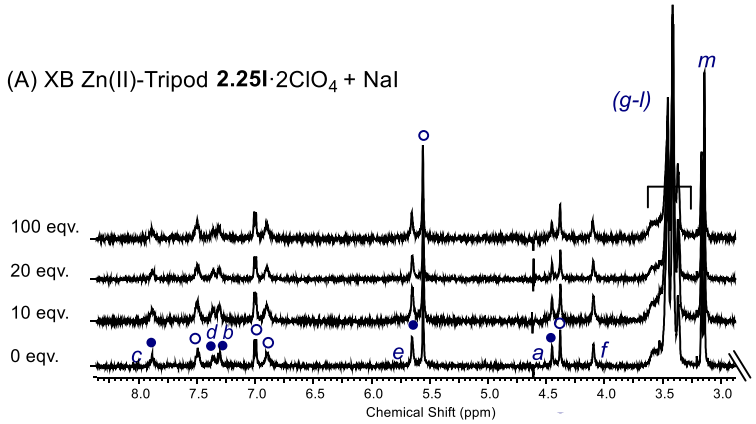


Figure 2.20: *^{1}H NMR titration spectra of **2.25I**·2ClO_4 upon the addition of 100 equivalents of NaI at T = 298 K. ([metallo-host] = 1.0 mM, unbuffered D_2O, 500 MHz). All proton assignments follow those in Scheme 2.11.*

.

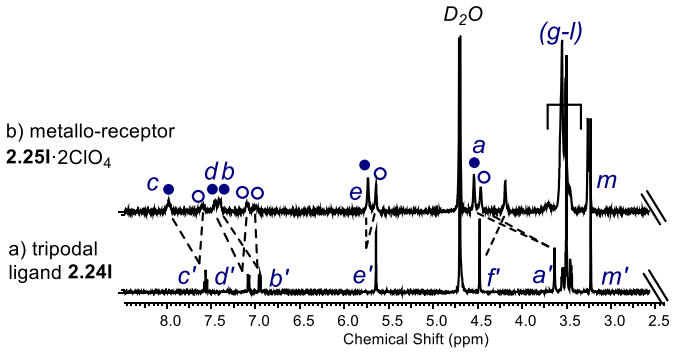


Figure 2.21: *Further ^{1}H-NMR inspection of the TEG appended Zn(II)-tripodal receptor **2.25I**·2ClO_4. All spectra were obtained in D_2O (T = 298 K, 500 MHz). Assignments follow those in Scheme 2.11.*

Consequently, and considering the essentially hydrophobic nature of the XB receptor's binding pocket, it was postulated that self-association of the host (possibly *via* dimerization, which has been previously observed in structurally-related tripodal Zn(II)-picolyl compounds[35,36]) or alternatively, coordination of the relatively hydrophobic perchlorate counteranions (ΔH_{hyd} ClO_4^- = - 245 kJ mol $^{-1}$)[37] might be the underlying reasons for the duplicate proton resonances of **2.25I**·2ClO_4 observed in water and were thus further investigated.

2.5.4 Investigation of the duplicate ^{1}H NMR resonances of **2.25I**·2ClO$_4$ in D$_2$O

To first examine the possibility of host aggregation in aqueous solution, a series of 2D-diffusion order spectroscopy (DOSY) experiments were performed to obtain the diffusion coefficient (*D*) of the Zn(II)-receptor **2.25I**·2ClO$_4$ in D$_2$O, from which the corresponding hydrodynamic radius (r_H) could be calculated (using the Stokes-Einstein equation[38]) and compared with that of the *apo*-Zn(II) XB ligand **2.24I**. With the aid of Dr Nick Rees, convection compensated measurements were conducted on individual 2 mM sample solutions of **2.25I**·2ClO$_4$ and **2.24I** prepared in D$_2$O and also in CDCl$_3$ which served as the experimental standard. The acquired DOSY spectra are illustrated in Figure 2.22 and the determined *D* and r_H values summarised in Table 2.4.

All proton signals in the DOSY spectrum of **2.25I**·2ClO$_4$ in D$_2$O displayed the same diffusion co-efficient indicating the presence of a single molecular species (Figure 2.22); a comparison of the corresponding r_H (8.19 Å) against that of the metal-free ligand **2.24I** (8.44 Å) in the analogous solvent revealed only a very modest decrease in the size of the Zn(II)-complexed species which thus made the likelihood of host dimerization (or any other, higher-order aggregate formation) in water extremely unlikely. A further comparison of their respective hydrodynamic radii in CDCl$_3$ (Table 2.4) showed there to be a similarly negligible decrease in size of the C_{3v} symmetric Zn(II)-tripodal receptor compared to the precursor ligand, further negating the notion of **2.25I**·2ClO$_4$ self-associating in water.

Subsequently, the TEG-appended Zn(II)-host **2.25I**·2OTf with alternative hydrophilic triflate counteranions (ΔH_{hyd} OTf$^-$ > - 460 kJ mol^{-1})[39] was prepared *via* complexation of **2.24I** with a stoichiometric quantity of zinc(II) triflate (Scheme 2.11). However, the ^{1}H-NMR spectrum of **2.25I**·2OTf in D$_2$O resembled that of **2.25I**·2ClO$_4$ (Figure 2.24), similarly displaying a duplicate set of resonances corresponding to the core H$_{a\text{-}e}$ protons and thus also ruled out the possibility of any counteranion coordination effects in water.

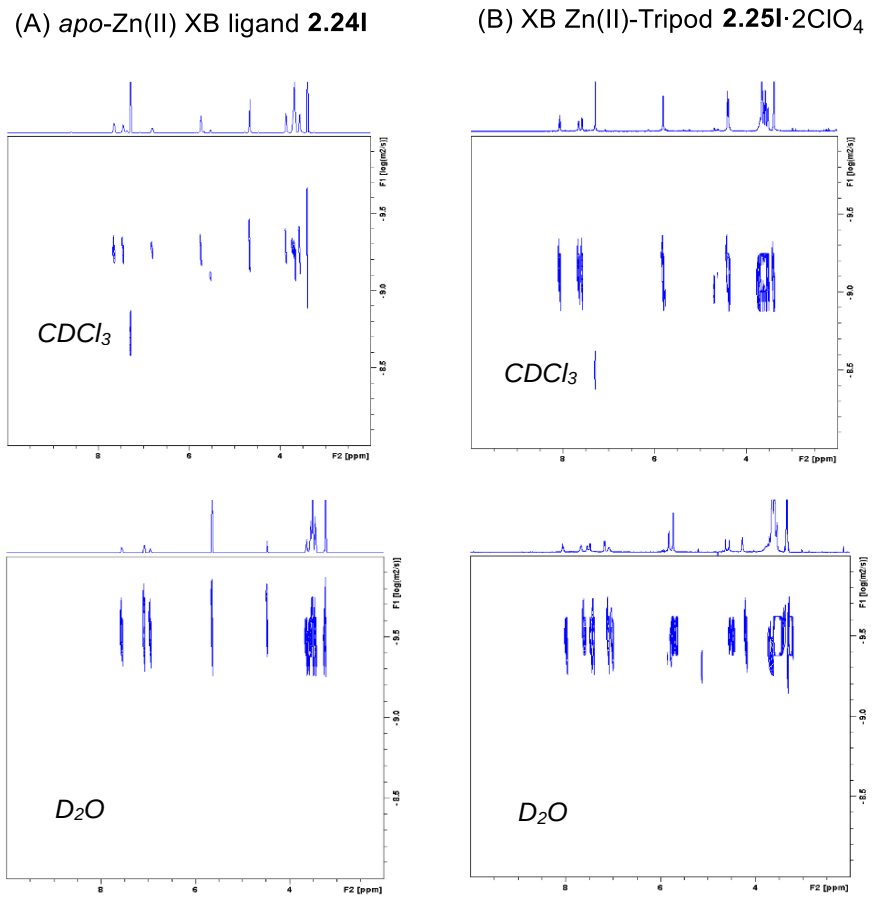


Figure 2.22: *^{1}H 2D-DOSY NMR spectra of the (A) apo-Zn(II) XB ligand* ***2.24I and*** *(B) Zn(II)-receptor* ***2.25I***·*2ClO$_4$ in (top row) CDCl$_3$ and (bottom row) D$_2$O at T = 298 K. ([sample] = 2.0 mM, solvent as listed, 500 MHz).(Water suppression ^{1}H-NMR pulse sequence NOESYGPPR1d utilised for all spectra in D$_2$O).*

Table 2.4: Comparison of the experimentally determined diffusion co-efficient (*D*) and corresponding hydrodynamic radius (r_H) values of **2.25I**·2ClO$_4$ and **2.24I** in organic and aqueous media.

Solvent[a]	*apo*-Zn(II) XB ligand **2.24I**		XB Zn(II)-tripod **2.25I**.2ClO$_4$	
	D x 10 $^{-10}$/ m^2 s^{-1}	r_H / Å [b]	*D* x 10^{-10}/ m^2 s^{-1}	r_H / Å [b]
CDCl$_3$	5.26	7.86	5.68	7.27
D$_2$O	2.35	8.44	2.42	8.19

[a]Solvent viscosities utilised in the Stokes-Einstein equation obtained from the Landolt-Börnstein online database (for CDCl$_3$) and as reported by Matteoli[] (for D$_2$O); [b] r_H calculated using the Stokes-Einstein equation[38] assuming hard sphere radius of receptor.

Together the above observations pointed towards the remaining prospect of two of the iodotriazole encompassing '*arms*' *N*^{2}-coordinating to the host's hydrophobic Zn(II)-core in a *static* manner in aqueous solution, as previously observed in the solid state crystal structure of the

ferrocene-appended Zn(II) analogue **2.20I**·2OTf (Figure 2.12A). This would lead to the 'inequivalence' of the uncoordinated third XB '*arm*' and thus explain the double set of proton resonances observed. Moreover, this water-induced '4+2 locking' of the Zn(II)-coordination sphere further substantiates the lack of anion binding observed with **2.25I**·2ClO_4, given that the structurally-related Cu(II)-TPMA subunit (lacking of additionally coordinating triazoles) has been reported to bind inorganic monophosphate with an affinity of K_a = 300 M^{-1} in pure water.[40‡‡]

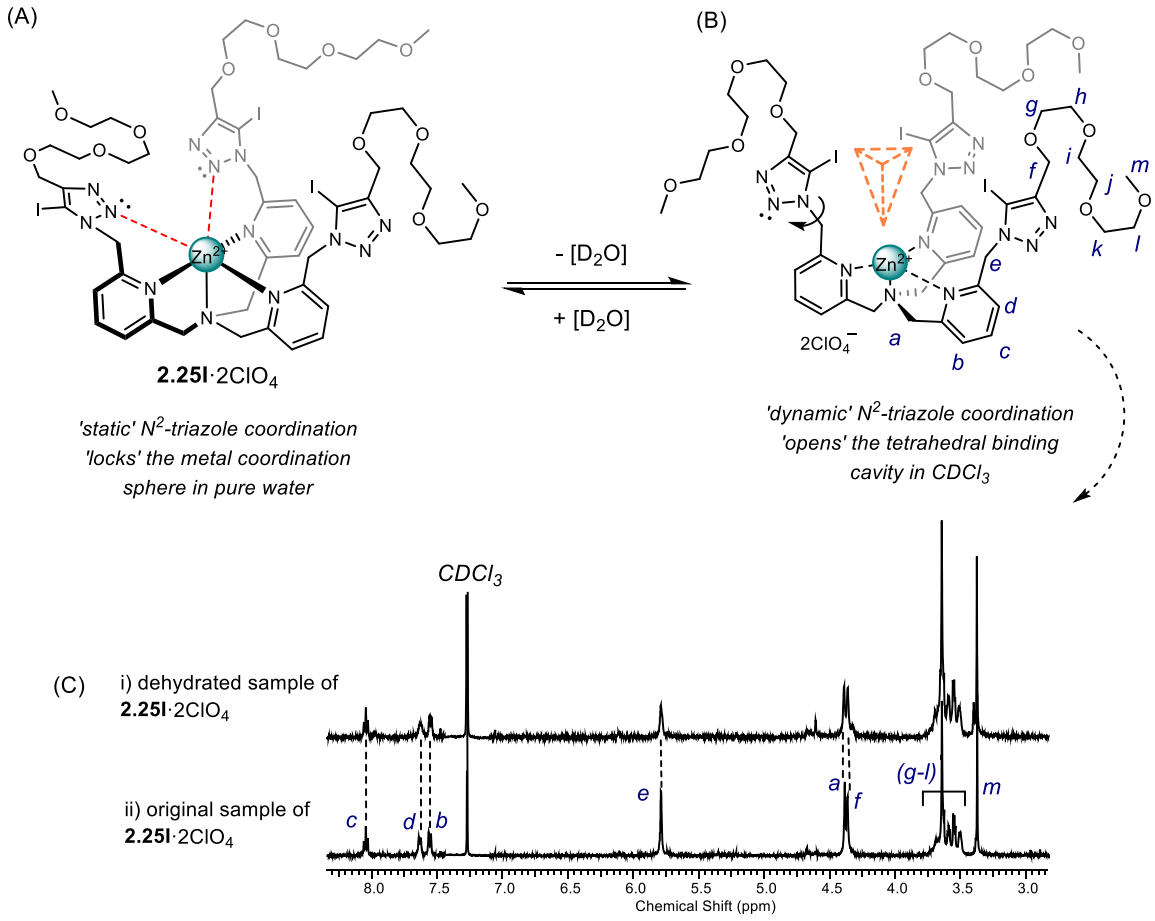


Figure 2.23: *Schematic representation of (A)the 'static' N^2-coordination' of iodotriazoles to the Zn(II)-center of* ***2.25I***·*2ClO_4 in pure water and (B)'unlocking' of the tetrahedral anion binding cavity in $CDCl_3$. (C) ^{1}H NMR spectra of the (top row) dehydrated sample of host and (bottom row) original sample of host in $CDCl_3$. (T = 298 K, 500 MHz).*

‡‡ This low binding affinity further demonstrates that alongside the 'availability' of a vacant coordination site on the metal center in such tripodal host systems, the use of *substantial* positive electrostatic charge, as employed in Anslyn's pentacationic Cu(II)-tripods (Figure 1.38), is vital for achieving the strong binding of the hydrophilic inorganic monophosphate species (ΔG_{hydr} of $H_2PO_4^-$ = -465 kJ mol^{-1}) in a wholly aqueous milieu.

Indeed a final investigative experiment, where the same sample of **2.25I**·2ClO_4 in D_2O was dehydrated and re-dissolved in $CDCl_3$, suggested a switch back to the seemingly 'fluxional' N^2coordination behaviour of the iodotriazoles and hence the re-generation of the tetrahedral binding cavity, as the resultant ^{1}H NMR spectrum exhibited a reversal back to a single set of core $H_{a\text{-}e}$ proton resonances that exactly matched those of the original ^{1}H NMR of the host in $CDCl_3$ (Figures 2.23B-C).

Accordingly, ^{1}H-NMR spectra of **2.25I**·2ClO_4 in various CD_3CN/D_2O mixtures revealed the optimal organic-aqueous solvent ratio to be 6:4 *v/v* in which the host's C_{3v} symmetry remained unperturbed (*i.e.* the second set of host resonances were not apparent) (Figure 2.24) and hence anion binding was pursued in this solvent mixture instead. Furthermore, given the renowned ability of Cu(II) to form the most thermodynamically stable metal-ligand complexes amongst the first-row divalent transition metals,[41] as well as serve as a signal transduction entity by virtue of its $3d^9$ electronic configuration, the nature of the metal epitope was switched from Zn(II) to Cu(II) and anion binding next probed *via* UV-Vis spectroscopy.

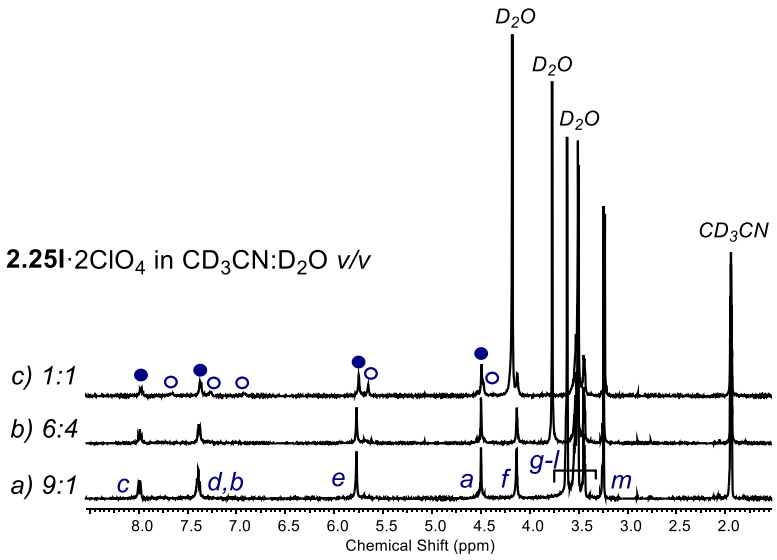


Figure 2.24: *^{1}H-NMR spectra of **2.25I**·2ClO_4 in various CD_3CN; D_2O v/v solvent mixtures. (a) 9:1, (b) 6:4 and (c) 1:1. (All spectra recorded at T = 298 K, 500 MHz). Assignments follow those in Figure 2.23*

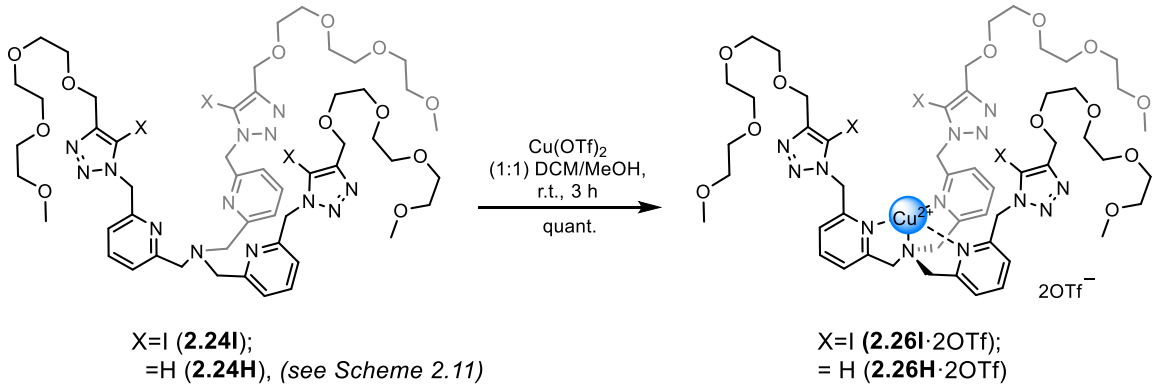
2.6 A tris(triethylene glycol)-appended XB Cu(II) tripod analogue

2.6.1 Synthesis and characterisation of **2.26I**·2OTf and **2.26H**·2OTf

The alternative TEG-appended Cu(II)-host **2.26I**·2OTf was prepared *via* complexation of **2.24I** with a stoichiometric quantity of copper(II) triflate and subsequently isolated as a dark blue oil (Scheme 2.12). UV-Vis spectroscopy was utilised to observe the absorbance in CH_3CN as aliquots of the copper salt were added to a 2 mM solution of **2.24I**, with the appearance of a broad peak $\lambda_{abs,max}$ (ε/ M^{-1} cm^{-1}) at 640 nm (161) and shoulder peak at 766 nm (98) attributed to arise from the characteristic splitting of the metal's *d-d* envelope upon chelation of the XB ligand (Figure 2.25A).[42] The change in absorbance at 640 nm was used to generate a mole ratio plot which verified the expected 1:1 stoichiometry for ligand to metal binding (Figure 2.25B). The latter isotherm was not curve fit however as the binding affinity was too high to generate an association constant with reasonable error. Thus, an ITC titration was conducted in unbuffered water, with aliquots of a 4 mM solution of the respective metal salt added to a 0.5 mM solution of **2.24I** at regular intervals (Figure 2.25C). Fitting the data from the resulting integrated heat plot to a one-site binding model using a non-linear least squares regression method (Figure 2.25D) afforded an association constant of K_a = 1.55 x 10^6 M^{-1}, as well as the relevant thermodynamic parameters revealing metal complexation in aqueous solution to be predominantly enthalpically (ΔH = -29.8 kJ mol^{-1}) but also entropically ($-T\Delta S$ = -5.56 kJ mol^{-1}) driven. This large association constant is not unusual given that a stability constant for Cu(II) complexation to TPMA itself has previously been reported by Rorabacher[43] to be as high as 10^{17} M^{-1} similarly in unbuffered water. Interestingly, under the same ITC experimental conditions, a further titration was also conducted with the analogous zinc(II) triflate salt to compare the ligand's Cu(II) *vs*. Zn(II) metal binding affinities, however, no evidence could be obtained for the complexation of the Zn(II) cation with **2.24I**

The HB counterpart **2.26H**·2OTf was synthesised using analogous procedures outlined in Schemes 2.12 and 2.11 and both paramagnetic Cu(II)-tripodal XB/ HB receptors characterised *via* electron paramagnetic resonance (EPR) spectroscopy (*vide infra*), optical- (Section 2.6.2) and electrochemical- methods (Section 2.6.3). Additionally, through ESI-MS analyses, both

2.26I·2OTf and **2.26H**·2OTf were identified as their dicationic Cu(II) adducts [M - $2ClO_4$]$^{2+}$ and thus showed distinct peaks at *m/z* = 751.0916 and 562.2471 in their corresponding high-resolution ESI spectra respectively (not shown here).



Scheme 2.12: *Cu(II)-complexation of **2.24I/H** to obtain the TEG-appended XB & HB Cu(II)-tripodal hosts **2.26I/H**.2OTf*

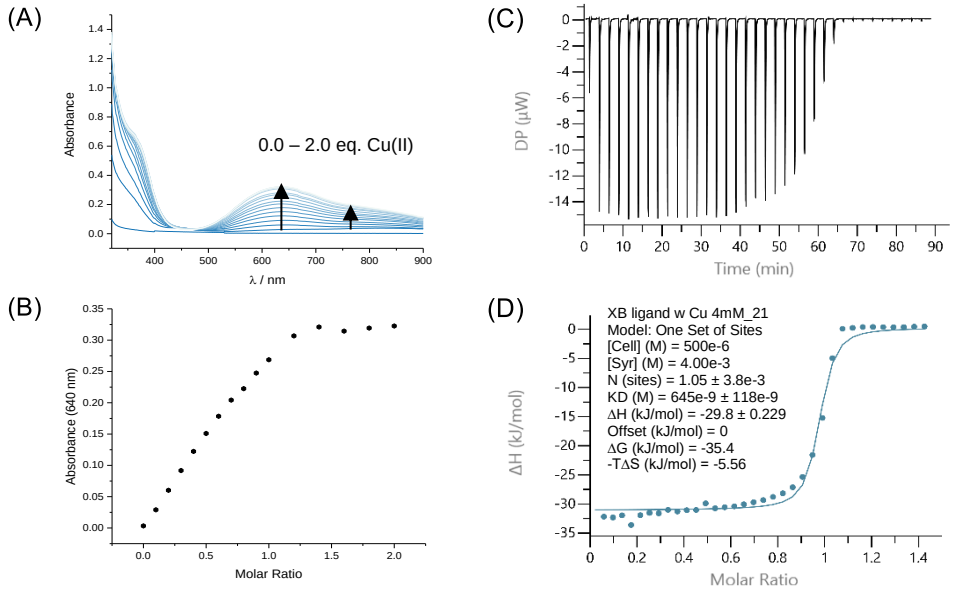


Figure 2.25: *(A) UV-Vis spectra of **2.24I** upon addition of molar increments of $CuOTf_2$ up to 2.0 equivalents.([**2.24I**] = 2 mM, CH_3CN, T = 293 K) and (B) the corresponding mole ratio plot.(C) Raw ITC data for the sequential addition of $CuOTf_2$ to **2.24I** (unbuffered H_2O, 298 K) and (D) corresponding integrated heat plot.*

2.6.1.1 EPR characterisation of Cu(II)-tripods 2.26I·2OTf and 2.26H·2OTf

With the aid of Dr Will Myers at the Centre for Advanced Electron Spin Resonance (CAESR) Oxford, the X-band continuous wave (CW) EPR spectra of both XB and HB Cu(II)-receptors were recorded at 95 K in CH_3CN and are shown in Figure 2.26. The XB host displayed an axial signature

characterised by the principal *g* values of $g\parallel$ = 2.225 and $g\perp$ = 2.065 ($A\parallel$ = 183.0 x 10^{-4} cm^{-1}), with the classic four-line splitting pattern arising from the hyperfine interactions between the unpaired Cu(II) electron and the two principle ^{63}Cu and ^{65}Cu paramagnetic nuclei (I = 3/2, $2I + 1 = 4$). Notably, these $g\parallel > g\perp$ values are quite unusual for TPMA based Cu(II)-complexes which typically present $g\perp > g\parallel$ values that denote a 5-coordinate Cu(II) environment, where the metal cation is ligated by four nitrogen atoms of the tetradentate TPMA subunit and also one solvent molecule (either CH_3CN or H_2O), predominantly in a trigonal bipyramidal (TBP) geometry.[44–46] The obtained $A\parallel$ value is also much larger than the ones classically encountered for TBP Cu(II)-centers ($A\parallel$ < 80 x 10^{-4} cm^{-1}).[47] With these observations in mind and having evidenced the additional N^2-coordination of two of the iodotriazoles to the Zn(II) center in the solid state crystal structure of the ferrocene-appended analogue **2.20I**·2ClO_4 (see Figure 2.12A), a similar 6-coordinate Cu(II) centre of **2.26I**·2OTf in frozen solution thus seems likely.[§§] Due to the lack of spectroscopic characterisation of such '4+2' coordinated Cu(II)-TPMA complexes in the literature however, the unambiguous assignment of an octahedral coordination geometry is rather complicated.

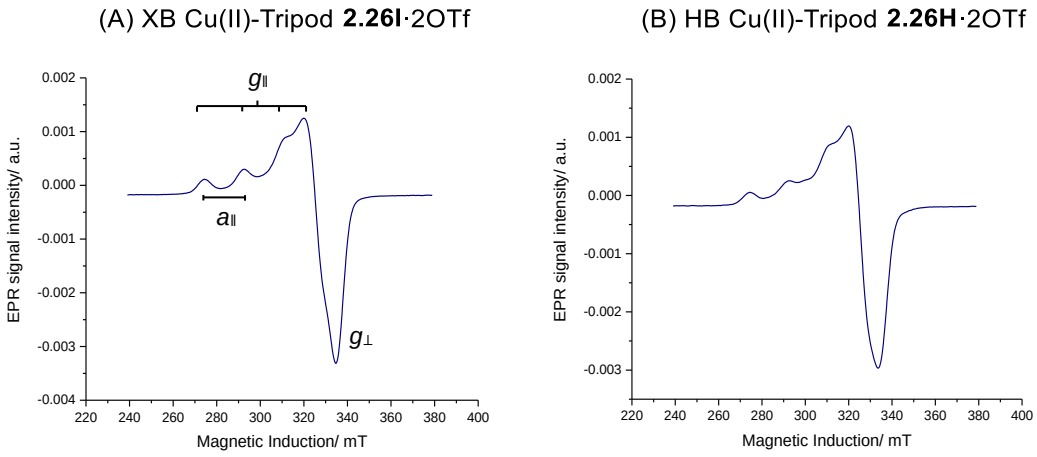


Figure 2.26: *Frozen solution EPR spectra of (A)* ***2.26I****·2OTf and (B)* ***2.26H****·2OTf in CH_3CN at 95 K. ([Cu(II)-host] = 2 mM). (microwave freq. 9.3871 GHz, modulation freq. 100 kHz, modulation amplitude 8 G, microwave power 0.633 mW).*

[§§]*N.B.* The very fast relaxation times of the two *dynamic* T_1 (spin-lattice) and T_2 (spin-spin) relaxation processes often observed at room temperature (*e.g.* for transition-metal complexes) and crucial in the EPR experiment, inevitably lead to extensive broadening of the acquired spectrum such that effectively no EPR signal is observed (half linewidth = $1/T_2 + 1/2T_1$, as also dictated by Heisenberg's uncertainty principle).[48] Consequently, EPR measurements are routinely undertaken at cryogenic temperatures (*i.e.* in frozen solution) to increase the T_1 and T_2 times of such 'fast relaxing systems' thus leading to better-resolved EPR spectra.

The HB host exhibited virtually identical EPR parameters of $g\parallel = 2.225$ and $g\perp = 2.065$ apart from a very small difference of the $A\parallel$ value ($A\parallel = 182.0 \times 10^{-4}$ cm^{-1}) suggesting little influence of the iodotriazoles on the hyperfine coupling and hence degree of delocalisation of the unpaired d-electron from the respective paramagnetic Cu(II) center.

2.6.2 UV-Vis anion binding studies with **2.26I**·2OTf and **2.26H**·2OTf

Quantitative UV-Vis titration experiments were performed by adding increasing quantities of anions as their TBA salts to 2mM solutions of **2.26I**·2OTf and **2.26H**·2OTf accordingly in the CH_3CN/ H_2O 6:4 *v*/*v* solvent mixture (buffered with 10 mM HEPES at pH 6.3). Both receptors exhibited very similar molar extinction coefficients and peak absorption wavelengths $\lambda_{abs,max}$ (ε/ M^{-1} cm^{-1}) at 647 nm (117) and 775 nm (91) (shoulder) for **2.26I**·2OTf and 639 nm (125) and 760 nm (98) (shoulder) for **2.26H**·2OTf, suggesting, yet again, that the more electron-deficient, iodotriazole encompassing tripodal ligand framework of **2.26I**·2OTf did not significantly affect the electronic energy levels of the respective Cu(II) core in mixed organic-aqueous media.

With both **2.26I**·2OTf and **2.26H**·2OTf, the interactions of the Br^-, Cl^-, OAc^- and $H_2PO_4^-$ anions and the Cu(II) center led to visible colour changes of the host solution from light blue to green, as well as an observed decrease in intensity of the absorption band at *ca.* 640 nm and simultaneous increase in intensity of the broad shoulder peak at *ca.* 770 nm in their corresponding UV-Vis spectra, presumably due to ligand field effects and further implying a similar mode of anion binding within the XB/ HB tripodal host interior (Figure 2.27). In the case of the halides, particularly Br^-, the spectral changes of the latter, lower energy band were greater than the former, higher energy band whereas with the respective oxo-anions, both bands exhibited comparable spectral perturbations. In contrast, negligible spectral changes were seen during the titrations of NO_3^- indicating that the anion was not interacting appreciably with either receptor. Global spectral fitting of the UV-Vis titration data was performed using the BindFit[49] software monitoring the change in absorbance as a function of anion concentration (Figure 2.28) and the calculated association

constants are summarised in Table 2.5. All the anions were found to bind predominantly *via* a 1:2 host:guest stoichiometry with K_{12} being of much lower magnitude than K_{11}.

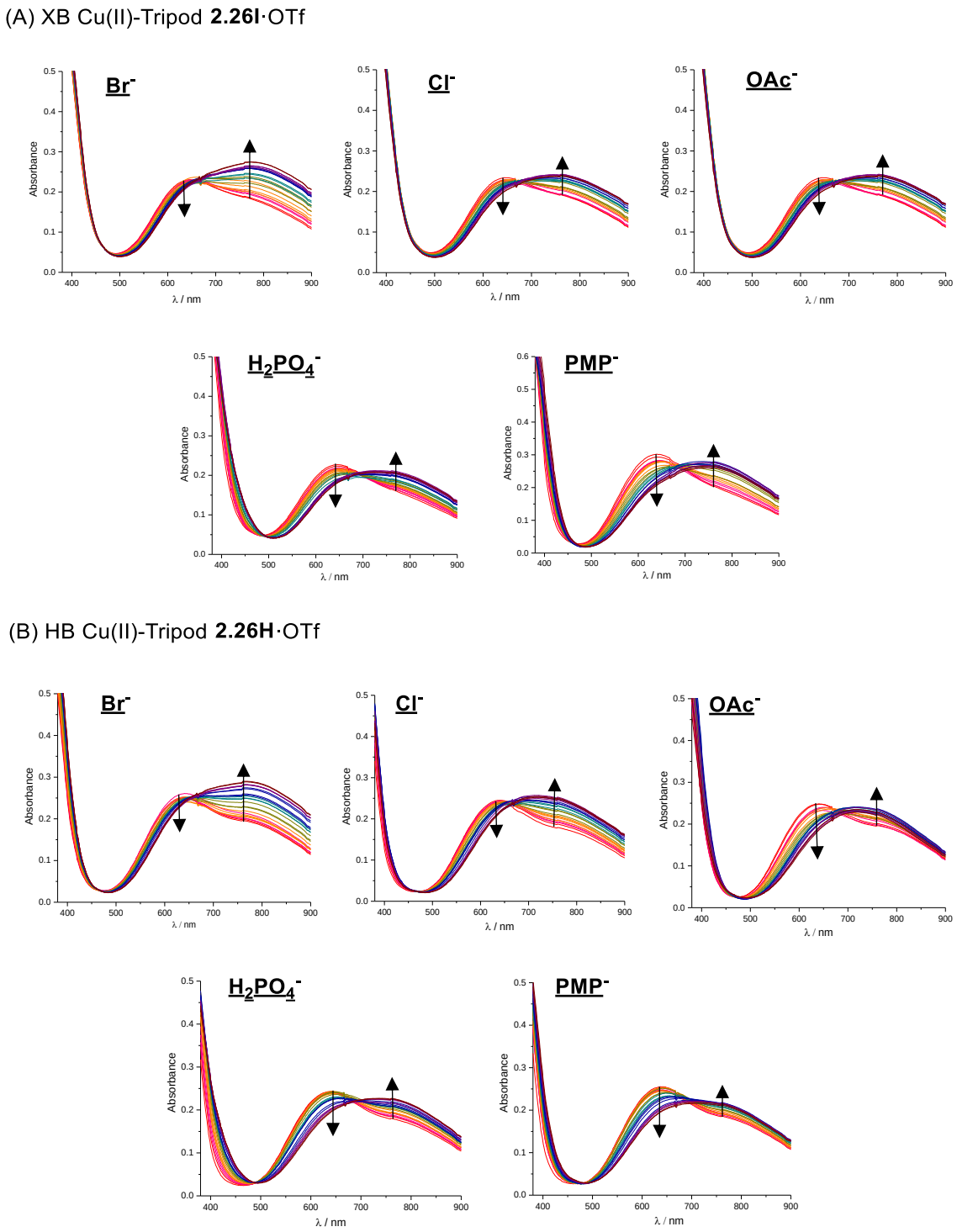


Figure 2.27: *UV-Vis titrations showing the spectra of the Cu(II)-tripodal receptors (A)**2.26I**·2ClO₄ and (B) **2.26H**·2ClO₄ in the presence of increasing quantities of various halide and oxoanions added as their TBA salts. ([metallo-host] = 2.0 mM, CH₃CN/ H₂O 6:4 v/v buffered with 10 mM HEPES at pH 6.3, T = 293 K).*

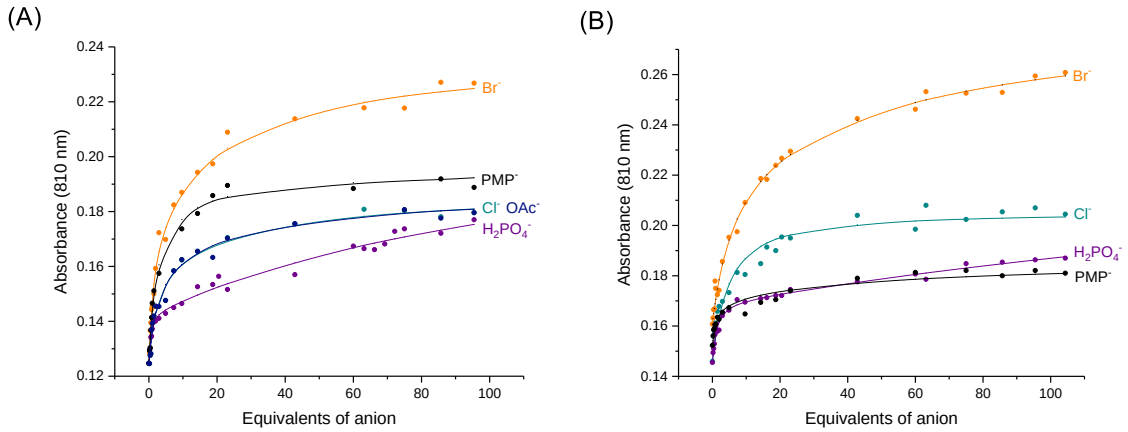


Figure 2.28: *UV-Vis titration isotherms: Plot of peak absorbance (λ_{abs} = 810 nm) of (A) XB Cu(II)-host* ***2.26I***·*2OTf and (B) HB Cu(II)-host* ***2.26H***·*2OTf against equivalents of anion added. ([metallo-host] = 2.0 mM, CH_3CN/ H_2O 6:4 v/v buffered with 10 mM HEPES at pH 6.3, T = 293 K)*

Table 2.5: Anion association constants (K_a/ M^{-1}) of various anions with the TEG-appended Cu(II)-tripodal receptors **2.26I**·2OTf and **2.26H**·2OTf.[a]

Anion[b]	ΔG_{hyd}/ kJ mol^{-1} [c]	CH_3CN/ H_2O 6:4 *v/v* (10 mM HEPES at pH 6.3)	
		2.26I·2OTf **XB** K_a/ M^{-1} [a]	**2.26H**·2OTf **HB** K_a/ M^{-1} [a]
Cl^-	-340	K_{11} = 379 (15) K_{12} = 16.1 (0.4)	K_{11} = 121 (3)
Br^-	-315	K_{11} = 834 (38) K_{12} = 23.9 (0.2)	K_{11} = 108 (2) K_{12} = 7.64 (0.1)
I^-	-275	-[d]	-[d]
NO_3^-	-300	NB[e]	NB[e]
OAc^-	-365	K_{11} = 435 (20) K_{12} = 21.3 (0.7)	-[f]
$H_2PO_4^-$	-465	K_{11} = 2816 (309) K_{12} = 3.82 (0.03)	K_{11} = 745 (25) K_{12} = 1.2 (0.1)
PMP^-	n/a	K_{11} = 1094 (68) K_{12} = 73.6 (2.9)	K_{11} = 772 (63) K_{12} = 11.1 (0.6)
PPi^{3-}	-1848 [g]	-[f]	-[h]

[a]A 1:2 host-guest binding model, unless otherwise stated, was used to determine the association constants from global fitting of the UV-Vis titration spectra (monitoring the change in absorption from 800-850 nm) using BindFit[49], errors (±) in parenthesis (<11%); ([Metallo-host] = 2mM, T = 293 K). [b]Anions added as their TBA salts at T = 298 K. [c] Values reported by Marcus[50]. [d]Titration not performed as I^- is easily oxidised in the presence of Cu(II). [e]NB: No binding. Spectral changes too little to accurately determine association constants. [f]Multiple complex binding equilibria. Unable to fit data to 1:1, 1:2 or 2:1 host-guest models. [g]Value obtained *via* conversion of the theoretical solvation energy of PPi^{3-} (ΔG_{solv} = -441 kcal mol^{-1}) as calculated by Colvin and co-workers[51]. [h]Titration not performed.

Inspection of the binding data revealed the association constant value for $H_2PO_4^-$ with **2.26I**·2OTf to be significantly larger than the other anions, being bound with an affinity over six times greater than the weakest bound Cl^-. Given that the hydration energy of $H_2PO_4^-$ is the largest of all the anions tested (Table 2.5), the observed selectivity was thus credited to the favourable size and shape match of the TEG-appended XB tripodal receptor's binding pocket with the tetrahedral guest (Figure 2.29A). The effects of increasing the water content four-fold can clearly be seen comparing the anion affinities of Br^- and OAc^- as the former, less basic halide with a lower hydration energy was bound nearly twice as strongly as the latter more hydrophilic oxyanion. Notably, this represents a reversal of the $OAc^- > Br^-$ trend previously evidenced with **2.16I**·2ClO_4 (Table 2.1) and **2.20I**·2ClO_4 (Table 2.2) in CD_3CN/ D_2O 9:1 *v/v* where the binding was in accordance with their respective anion basicities. Similarly however, **2.26I**·2OTf exhibited a distinct Hofmeister preference for $Br^- > Cl^-$. Importantly, the HB receptor **2.26H**·2OTf displayed attenuated anion binding in all cases, with the very modest discrimination between Br^- and Cl^-. The large difference between the magnitudes of the $H_2PO_4^-$ association constants of the two receptors in particular, provides a rare demonstration of the superior ability of XB to enhance oxo-anion recognition in the competitive aqueous-acetonitrile CH_3CN/ H_2O 6:4 *v/v* solvent mixture, with the value calculated for the XB host over three-times greater than the HB counterpart.

In comparison to the handful of receptors mentioned in Section 2.1.1, **2.26I**·2OTf therefore constitutes a potent XB host capable of discriminating inorganic monophosphate in comparatively more polar protic media, exceeding Ghosh's XB bis-heteroleptic Ru^{II} complex[3] (Figure 2.1B) which functions similarly in CH_3CN/ H_2O mixtures but with the percentage water content, at best, 20%.

2.6.2.1 Binding of a simple phosphate-ester and a higher-order inorganic polyphosphate species

The successful display of selective inorganic monophosphate binding by the TEG-appended Cu(II)-hosts **2.26I/H**·2OTf prompted further investigation into their ability to bind simple phosphate-ester and higher-order inorganic polyphosphate species, specifically pinacolyl methyl

phosphonate (PMP) (Figure 1.33C), the innocuous hydrolysis product of the nerve agent Soman (GD) (see Section 1.3.3.2) and pyrophosphate (PPi) (Figure 1.33A) respectively.

Accordingly, UV-Vis titrations were performed by addition of increasing quantities of the TBAPMP[***] and TBA_3PPi salts to separate solutions of both XB/ HB hosts under the same experimental conditions (*vide supra*). Pronounced optical perturbations analogous to those elicited with $H_2PO_4^-$ were evidenced in the individual absorption spectra of **2.26I**·2OTf and **2.26H**·2OTf with PMP^- (Figures 2.26A and 2.26B respectively) and the organophosphonate found to associate with the host similarly with a 1:2 host-guest stoichiometry (Table 2.5). Yet again, the XB receptor proved to be the stronger complexant, binding PMP^- with a much larger affinity than the protic counterpart thus highlighting the applicability of XB as potent supramolecular interaction to exploit for the enhanced recognition of toxic G-series substances (see Section 1.3.3.2). The lower association constant value of PMP^- with **2.26I**·2OTf compared to $H_2PO_4^-$ is unsurprising given the steric demands of the much larger aliphatic phosphonate, resulting in a less complementary fit within the XB host's tetrahedral cavity: possibly, the *α*-methylene protons of the organophosphonate's phosphate 'head' might impose a steric clash with one of the voluminous iodine atoms of a convergent iodotriazole binding unit (red lines, Figure 2.29B), whereas when the binding pocket is flanked by much smaller prototriazoles this effect is less pronounced as reflected by the very similar association constant values of each of the respective phosphate species with **2.26H**·2OTf.

In contrast, the interaction of PPi^{3-} with **2.26I**·2OTf elicited explicitly larger spectral changes with a dramatic intensity decrease in *both* of the absorption bands of the XB Cu(II)-host (not shown here). Compared to the other anions tested, only unidirectional changes were observed with the respective inorganic polyphosphate suggesting that it was being bound *via* a different coordination stoichiometry perhaps simultaneously bridging the metal centers of two individual XB hosts, in a

[***] The TBA salt of the stated nerve agent hydrolysis product was prepared according to a general procedure described in Chapter Six, using TBAOH and from the commercially available neutral pinacolyl methylphosphonic acid solution.

similar manner as when binding to the bimetallic Zn(II)DPA compounds mentioned in Section 1.3.2.2 (Figure 1.39) and structurally related di-nuclear Cu(II) tripodal amine complexes[52]. Nonetheless, attempts to fit the titration data to various models of 2:1 as well as 1:1 and 1:2 host-guest stoichiometries were unsuccessful and hence no association constant values could be determined for any binding process.

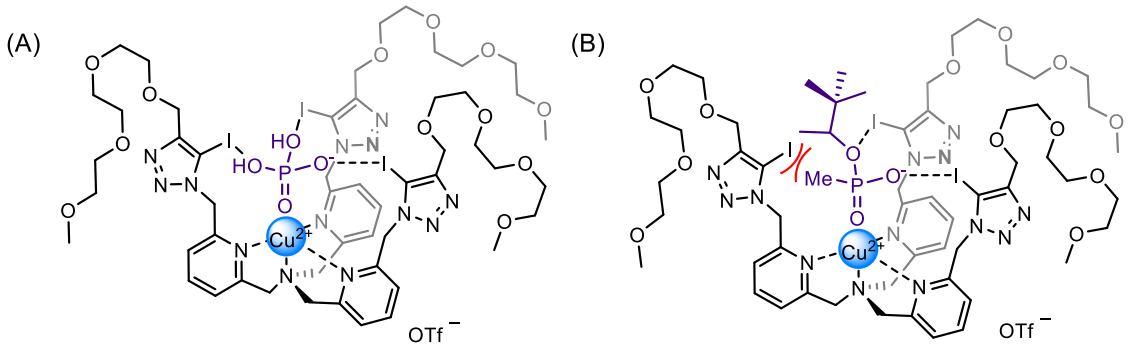


Figure 2.29: *The envisaged 'lock and key' binding mode of (A) $H_2PO_4^-$ and (B) PMP^- species with* ***2.26I****·2OTf.*

2.6.3 Electrochemical anion sensing studies with 2.26I·2OTf and 2.26H·2OTf

Having examined the anion recognition properties of **2.26I**·2OTf and **2.26H**·2OTf by UV-Vis titrations, the possibility of exploiting the Cu^{I}/Cu^{II} redox couple of the host's metal centre for electrochemical anion sensing was next explored *via* CV and square-wave voltammetry (SWV). The appropriate voltammetric measurements were carried out by Robert Hein, a joint D.Phil. student between the Beer and Davis groups.

2.6.3.1 Electrochemical characterisation

The electrochemical properties of **2.26I**·2OTf and **2.26H**·2OTf were first investigated *via* CV and SWV in anhydrous CH_3CN (0.1 M $TBAClO_4$ supporting electrolyte solution) and pure water (0.05 M KPF_6 supporting electrolyte solution) solvents as well as in various intermediate CH_3CN/H_2O mixtures, where both receptors displayed explicit solvent dependent redox behaviour. A standard three-electrode electrochemical cell, comprising of a glassy carbon working electrode, a Pt wire auxiliary electrode and a Ag/AgCl leak-free reference electrode was used in all cases.

In anhydrous CH_3CN, both **2.26I**·2OTf and **2.26H**·2OTf were electrochemically-active (see Appendix B) and displayed a well-defined, single quasi-reversible one-electron wave in their CV's attributed to the Cu^{I}/Cu^{II} redox couple (Figure 2.30), with the more anodic $E_{1/2}$ value of + 74 mV of the XB host versus - 179 mV of the HB counterpart (both vs. Fc/ Fc^{+}) derived from the corresponding SWV's (Figure 2.31) consistent with the increased electron-withdrawing nature of the iodotriazoles disfavouring oxidation of the Cu center. The marked 253 mV difference between the two $E_{1/2}$ values is particularly impressive and as previously suggested by the EPR measurements (*vide supra*), indicates the N^2-coordination of the XB/ HB-triazoles to the metal core, which are thus able to *directly* exert their electronic influences on the redox properties of the Cu center in organic media.[†††]

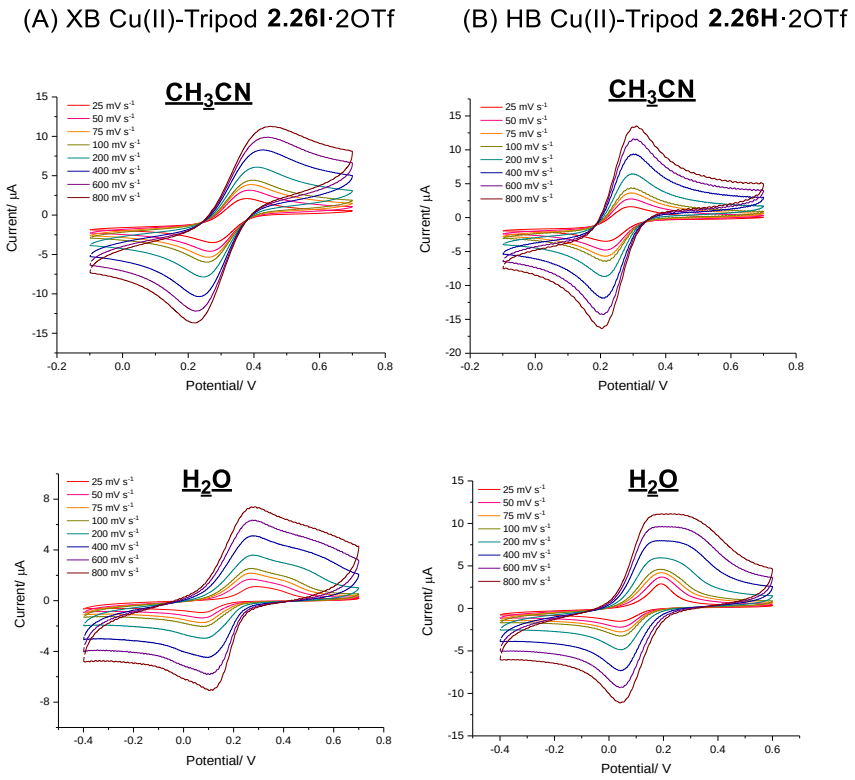


***Figure 2.30**: Electrochemical reversibility studies: CVs of the Cu(II)-tripodal hosts (A) **2.26I**·2OTf and (B) **2.26H**·2OTf in (top row) anhydrous CH_3CN and (bottom row) H_2O, recorded at various scan rates of 25, 50, 75, 100, 200, 400, 600 and 800 mV $s^{-1}$and vs. Ag/AgCl leak-free reference electrode).(in CH_3CN: [metallo-host] = 0.5 mM, supp. electrolyte 0.1 M $TBAClO_4$, T = 293 K) (in H_2O: [metallo-host] = 0.25 mM, supp. electrolyte 0.05 M KPF_6, T = 293 K).*

[†††] In retrospect, this evidenced N^2triazole-metal ligation behaviour also validates the comparatively smaller difference (15 mV) between the respective $E_{1/2}$ values of the Fc/ Fc^{+} couple of the ferrocene hosts **2.20I**·$2ClO_4$ and **2.20H**·$2ClO_4$ (Section 2.2.7); presumably the Zn(II)-center renders the electronic influences of the N^2-coordinated XB/HB-triazole moieties less apparent in their through-bond polarisation of the coupled ferrocene electrochemical reporter groups.

Contrastingly, whilst the XB and HB receptors retained redox quasi-reversibility in various CH_3CN/H_2O solvent mixtures, a significantly distorted anodic peak was observed in their CV's in each case, particularly at higher scan rates. This was exacerbated in pure H_2O (Figure 2.30) and postulated to arise from the 'static' N^2-ligation of the XB/ HB-triazoles to the Cu center, as strongly suggested by previous investigative ^{1}H-NMR experiments with the Zn(II)-analogue **2.25I**·2ClO_4 (see Section 2.5.4). Indeed, the more anodic SWV $E_{1/2}$ values of + 174 mV of the XB host and + 98 mV of the HB counterpart (both vs. Ag/AgCl) in pure water compared to those in MeCN (where the triazole coordination is 'dynamic') lend credence to this hypothesis. Additionally, the much smaller 76 mV discrepancy between these $E_{1/2}$ values likely results from the better stabilisation of the dicationic vs. monocationic Cu state due to the increased polarity of the all-aqueous solvent medium.

2.6.3.2 Preliminary electrochemical anion sensing studies

Owing to the complex voltammetric behaviour exhibited by **2.26I**·2OTf and **2.26H**·2OTf in aqueous media, their redox anion sensing properties were probed using SWV in anhydrous CH_3CN containing 0.1 M $TBAClO_4$ as supporting electrolyte. Preliminary electrochemical anion titrations with the addition of Br^- (up to 100 equivalents) induced significant cathodic perturbations of the respective Cu^I/Cu^{II} redox couples of both XB and HB electrochemically active receptors (Figure 2.31), arising from anion binding stabilising the oxidation of the Cu center. Notably, the XB host exhibited a much larger magnitude of cathodic shift (- 140 ± 5 mV) at saturation compared to the protic analogue (- 80 ± 5 mV) clearly highlighting the dominant role played by the XB donor groups for redox anion sensing. In both cases, a swift plateauing of the voltammetric response was observed further indicative of strong binding (Figure 2.32).

Quantitative analysis of the respective titration isotherms according to eqn 1[53]:

$$\Delta E = - \frac{RT}{nF} \ln \frac{(1 + K_{ox}[G])}{(1 + K_{red}[G])} \qquad \text{Eqn. 1}$$

revealed that the anion association constant of the oxidised metallo-receptor (K_{ox}) with the halide was, as expected, larger than the reduced form ($K_{ox} > K_{red}$) and that indeed, the XB receptor demonstrated a magnified switching on of Br^- binding (K_{ox}/ K_{red} = 65 074/ 289 M^{-1}) compared to the HB analogue (K_{ox}/ K_{red} = 15 734/ 581 M^{-1}). In particular, these amplified anion-induced voltammetric responses of **2.26I**·2OTf and **2.26H**·2OTf compared to the ferrocene Zn(II)-counterparts **2.20I**·2ClO_4 and **2.20H**·2ClO_4 (Table 2.3) convey not only the efficacy of the Cu^I/Cu^{II} redox couple as an electrochemical transduction entity but also the potency of utilising the host's metal epitope as a *direct* probe for the anion binding event – which for self-evident reasons, exhibits a greater sensitivity to the recognition process as opposed to the through-bond communicative pathways between the anion binding cavity and redox reporter group explored previously (see Section 2.4.5). The use of this XB Cu(II)-tripodal motif for electrochemical anion sensing is unprecedented and hence further studies are currently under investigation.

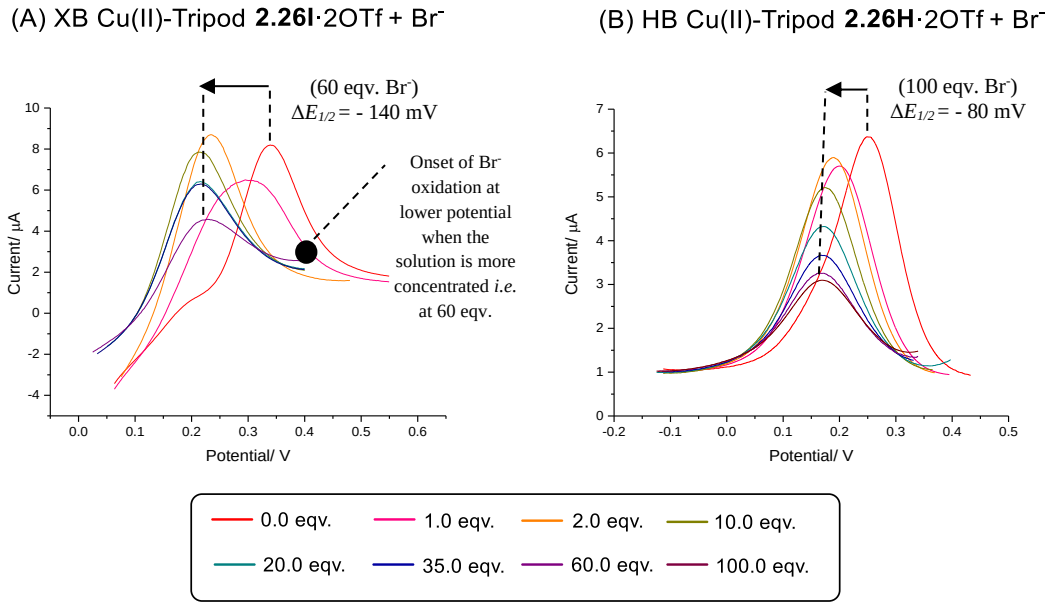


***Figure 2.31**: Preliminary electrochemical anion titrations. Square wave voltammograms (SWV's) of (A) **2.26I**·2OTf and (B) **2.26H**·2OTf with incremental quantities of TBABr; Potentials compared to the Ag/AgCl reference electrode (leak-free). ([metallo-host] = 0.5 mM, supp. electrolyte: 0.1 M $TBAClO_4$ in anhydrous CH_3CN, T = 293 K). (N.B. the distorted red baseline in (A) arises from the need of having to adjust the potential range during the titration to prevent Br^- oxidation)*

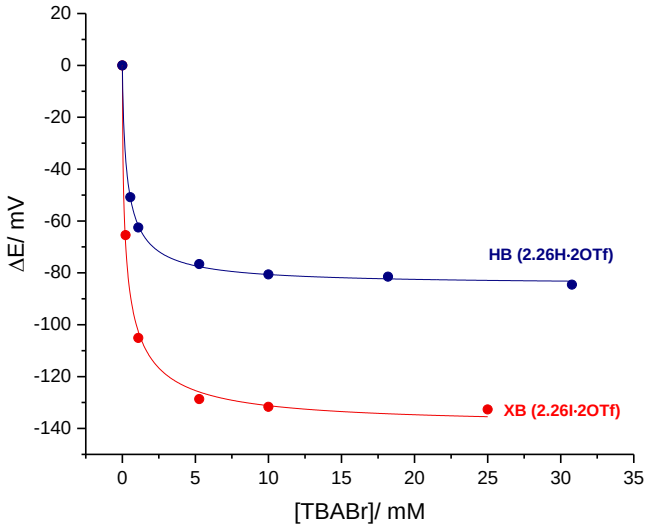


***Figure 2.32**: Electrochemical anion titration isotherms. Shift of half-wave potential ($\Delta E_{1/2}$) of the Cu^{I}/Cu^{II} redox couple of **2.26I**·2OTf and **2.26H**·2OTf in the presence of Br^- ([metallo-host] = 0.5 mM, supp. electrolyte: 0.1 M $TBAClO_4$ in anhydrous CH_3CN, T = 293 K).*

2.7 An alternative tris(permethylated-*β*-cyclodextrin)-appended XB Cu(II) tripod

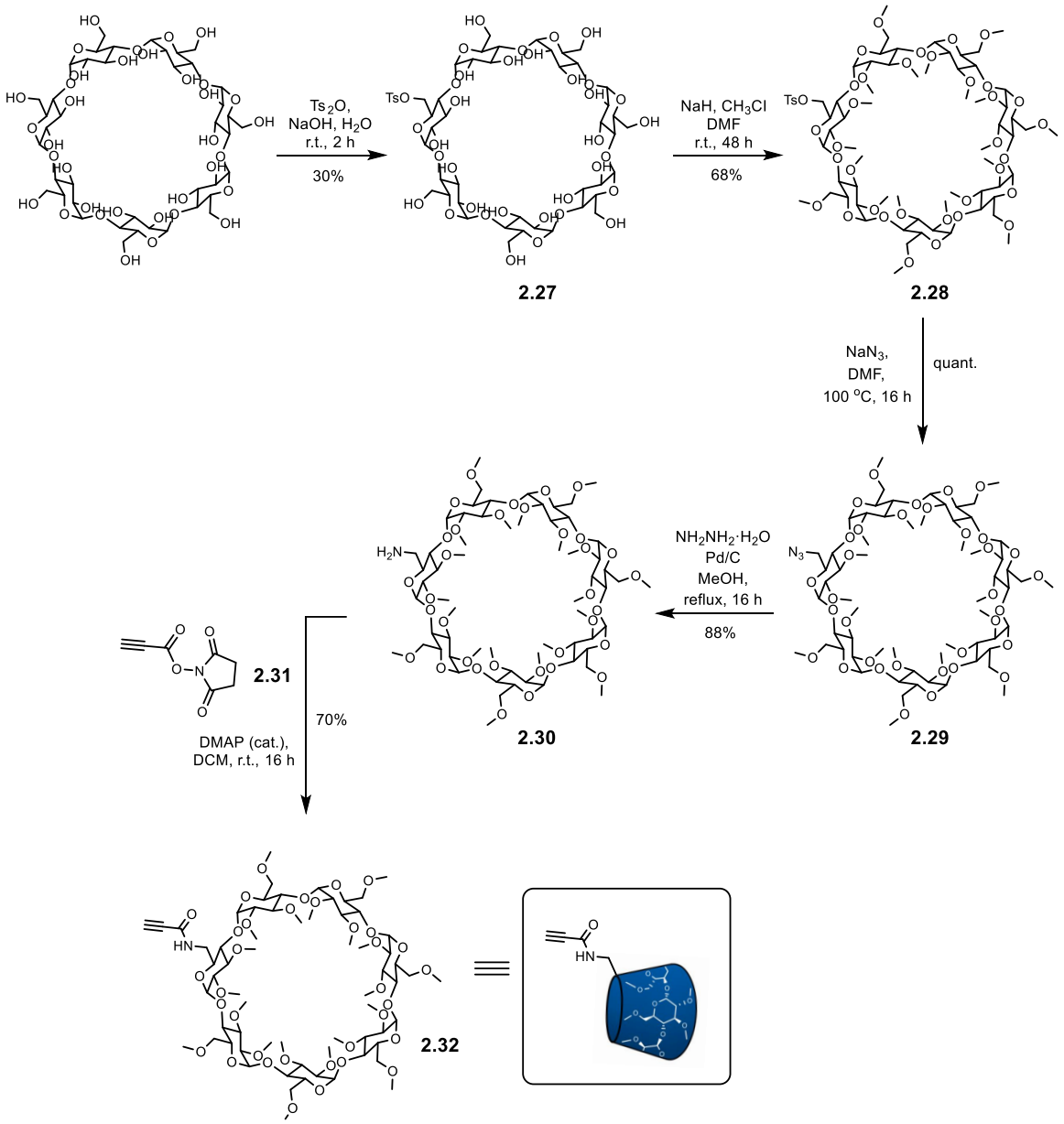
During the initial design process of an appropriate water-soluble XB metallo-tripodal receptor earlier on in Section 2.5, a second structurally-related XB tripodal framework **2.35I** featuring alternative hydrophilic, mono-functionalised permethylated-*β*-cyclodextrin (pm*β*CD)-derived appendages was also prepared in conjunction with the original tris(TEG)-appended Zn(II)-host **2.25I**·$2ClO_4$ (Scheme 2.14). Whilst the lack of anion binding in pure water exhibited by **2.25I**·$2ClO_4$ unfortunately precluded the use of **2.35I** for similar purposes, by complexing the ligand to a Cu(II) metal centre and following suit of the counterpart Cu(II)-receptor **2.26I**·2OTf, the resultant XB metallo-host **2.36I**·2OTf was utilised for optical anion sensing similarly in the CH_3CN/ H_2O 6:4 *v/v* solvent mixture (Scheme 2.15).

2.7.1 Synthesis and characterisation of 2.36I·2OTf

The water-soluble XB metallo-receptor **2.36I**·2OTf was prepared *via* adaption of the synthetic methodology used to construct **2.26I**·2OTf (Schemes 2.14 and 2.15). The appropriate pm*β*CD-derived terminal alkyne **2.32** was first synthesised using a multi-step procedure outlined in Scheme 2.13, involving a series of mono-functionalisation reactions at the 'narrow rim' of *β*-cyclodextrin

according to modified literature synthetic procedures.[54–56] *β*-Cyclodextrin was suspended in water in the presence of *p*-toluenesulfonic anhydride for 2 hours and subsequent addition of a 2.5 M $NaOH_{(aq)}$ solution afforded the monotosylate **2.27** in 30% yield after recrystallization in hot $MeOH/H_2O$. Methylation with iodomethane and NaH under strict dilution conditions afforded **2.28** in a 68% yield after chromatographic purification, which was then subjected to NaN_3 in DMF at 100 °C under N_2 quantitatively producing **2.29**. Thereafter, reduction of the mono-azide with hydrazine monohydrate in the presence of Pd/C in MeOH at 60 °C gave amine **2.30** which was further reacted with the activated ester *N*-hydroxysuccinimidyl propiolate **2.31** (separately prepared) and a catalytic amount of 4-dimethylaminopyridine (DMAP) in DCM overnight.[‡‡‡] Purification *via* column chromatography afforded the desired terminal alkyne **2.32** in 70% yield (Scheme 2.13).

[‡‡‡]Full experimental procedures for the synthesis of *β*-CD compounds **2.27** – **2.30** can be found in the thesis of Dr Sean Robinson[57], a previous D.Phil. student within the Beer group.



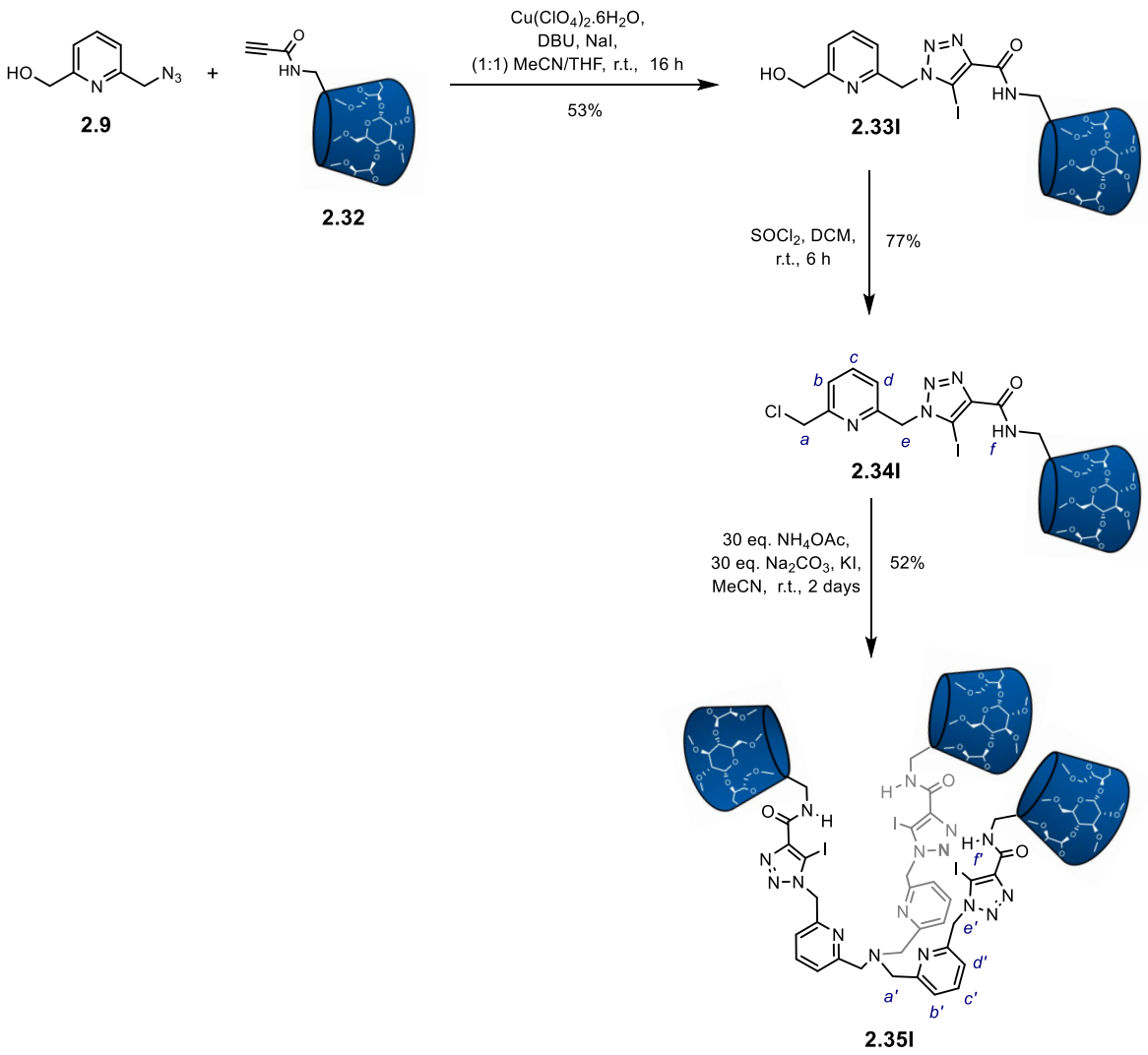
Scheme 2.13: *Synthetic pathway followed to obtain the pmβCD-derived terminal alkyne* ***2.32***

A subsequent 'one-pot iodo-Click' reaction between **2.32** and azide precursor **2.9** following Zhu's protocol[12] (omitting catalytic TBTA) produced the XB-donor containing synthon **2.33I** in a 53% isolated yield. Through treatment with $SOCl_2$, the corresponding chlorinated '*arm*' derivative **2.34I** was obtained and reacted with excess portions of NH_4OAc and Na_2CO_3 as well as an equivalent of

KI in MeCN at room temperature over two days.[§§§] The water-soluble tripodal ligand **2.35I** was obtained in a 52% isolated yield *via* preparative TLC. Notably, a diagnostic, significant upfield shift of the singlet signal (4.64 ppm) of the key H_a methylene protons of the '*arm*' precursor **2.34I** to the main pm*β*CD region was evidenced in the comparative ^{1}H NMR of ligand **2.35I** as shown in Figure 2.33, which along with ESI-MS analysis (*m/z* = 2626.9 $[M + Na + H]^{2+}$), affirmed the successful transformation to the appropriate XB tripodal assembly (*cf.* Figure 2.6). Noteworthy also are the respective methylene H_e protons of the '*arm*' and tripodal framework which are diastereotopic and hence appear as an AB quartet signal.

Finally complexation of **2.35I** with a stoichiometric quantity of copper(II) triflate quantitatively afforded the tris(pm*β*CD)-appended cupric host **2.36I**·2OTf which was isolated as a fine, pale blue crystalline powder (Scheme 2.15). Using a similar ITC titration protocol outlined in Section 2.6.1, the Cu(II)-binding properties of the *apo*-Cu(II) ligand **2.35I** were studied in unbuffered water (Figure 2.34) with data fitting of the resultant integrated heat plot using a non-linear least squares regression method verifying the expected 1:1 stoichiometry for ligand to metal binding and affording a large association constant of K_a = 1.26 x 10^5 M^{-1}. Additionally, the relevant thermodynamic parameters obtained from the one-site binding model revealed the Cu(II) complexation in aqueous solution to be, yet again, predominantly enthalpically (ΔH = -28.9 kJ mol^{-1}) but also marginally entropically ($-T\Delta S$ = -0.27 kJ mol^{-1}) driven.

[§§§] *N.B.* the usual 20 equivalents of NH_4OAc utilised in previous tripodal ligand formation procedures (see Schemes 2.6, 2.10 and 2.11) was increased to 30 equivalents, given the propensity of reagents to form inclusion complexes with the *β*-cyclodextrin 'cone'.



Scheme 2.14: *Synthetic pathway followed to obtain the pmβCD-appended XB tripodal framework* ***2.35I***

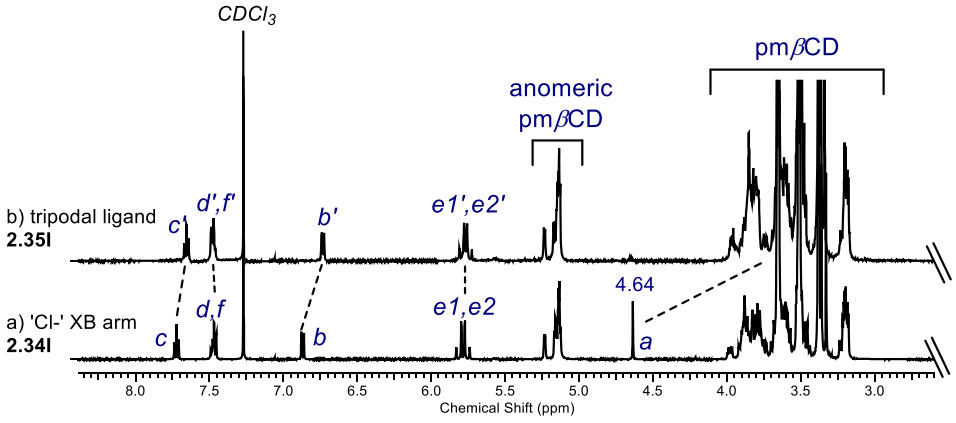
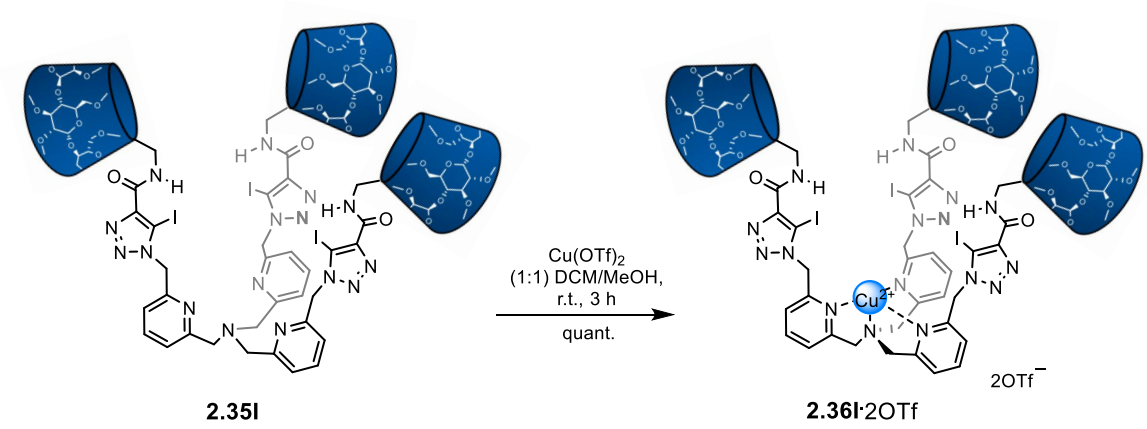


Figure 2.33: *^{1}H NMR spectra of the (a) tripodal 'arm'* ***2.34I*** *and (b) XB tripodal ligand* ***2.35I*** *($CDCl_3$, 500 MHz, T = 298 K) Assignments follow those in Scheme 2.14*



Scheme 2.15: *Cu(II)-complexation of* ***2.35I*** *to obtain the tris(pmβCD)-appended XB Cu(II)-tripodal host* ***2.23I****.2OTf*

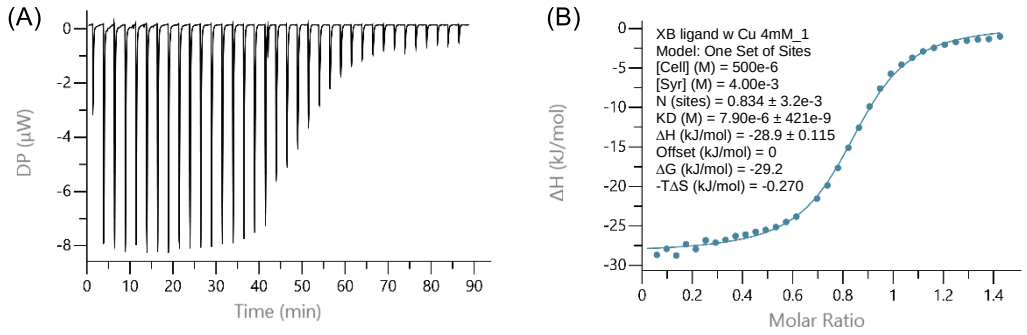


Figure 2.34: *(A) Raw ITC data for the sequential addition of* $CuOTf_2$ *to* ***2.35I*** *([XB ligand] = 0.5 mM, unbuffered* H_2O*, 298 K) and (B) corresponding integrated heat plot.*

The metallo-receptor was characterised by optical UV-Vis, EPR and high resolution ESI-MS methods. The electronic spectrum of **2.36I**·2OTf in CH_3CN/ H_2O 6:4 *v/v* (red dashed line, Figure 2.35A) displays a pronounced maximum absorption peak λ_{max} (ε/ M^{-1} cm^{-1}) at 645 nm (182) with a much broader shoulder peak at *ca.* 770 nm (119) attributed to arise from the relevant *d-d* transitions of the XB ligand chelated Cu(II) center. Additionally, through ESI-MS analyses, **2.36I**·2OTf was identified as the dicationic Cu(II) adduct (*i.e. m/z* = 2646.4 $[M - 2OTf]^{2+}$) and thus displayed the characteristic isotopic peak distributions arising from the multiple stable isotopes of Cu in the corresponding high-resolution ESI-MS spectrum.

2.7.2 UV-Vis anion binding studies with 2.36I·2OTf

Following the same UV-Vis anion titration protocol described in Section 2.6.2, the interaction of **2.36I**·2OTf with inorganic monophosphate was investigated in CH_3CN/ H_2O 6:4 *v/v* (buffered

with 10 mM HEPES at pH 6.3). Similar spectral perturbations of the host's aforementioned *d-d* bands were observed upon the addition of aliquots of $TBAH_2PO_4$ to **2.36I**·2OTf (Figure 2.35A) as **2.26I**·2OTf (*cf.* Figure 2.27A), with a progressive decrease in intensity of the initial higher energy absorption band and comparable increase in intensity of the initial lower energy shoulder peak suggestive of a similar mode of anion binding within the XB tripodal cavity. Global spectral fitting of the UV-Vis titration data using the BindFit[49] software monitoring the change in absorbance as a function of anion concentration (Figure 2.35B) pleasingly revealed an enhancement in the binding of inorganic monophosphate with **2.36I**·2OTf, with the determined 1:2 host:guest stoichiometric association constants of K_{11} = 9442 ± 944 M^{-1} and K_{12} = 40 ± 2 M^{-1} being *ca.* thrice as large in magnitude compared to the counterpart XB Cu(II)-host **2.26I**·2OTf (*cf.* Table 2.5). The observed increased anion affinity was postulated to arise from the multiple convergent interactions of the XB donor iodotriazoles and neighbouring N-H HB donor amide functionalities of the host's pm*β*CD-derived '*arms*' promoting the synergistic binding of the tetrahedral monophosphate guest (Figure 2.35C).

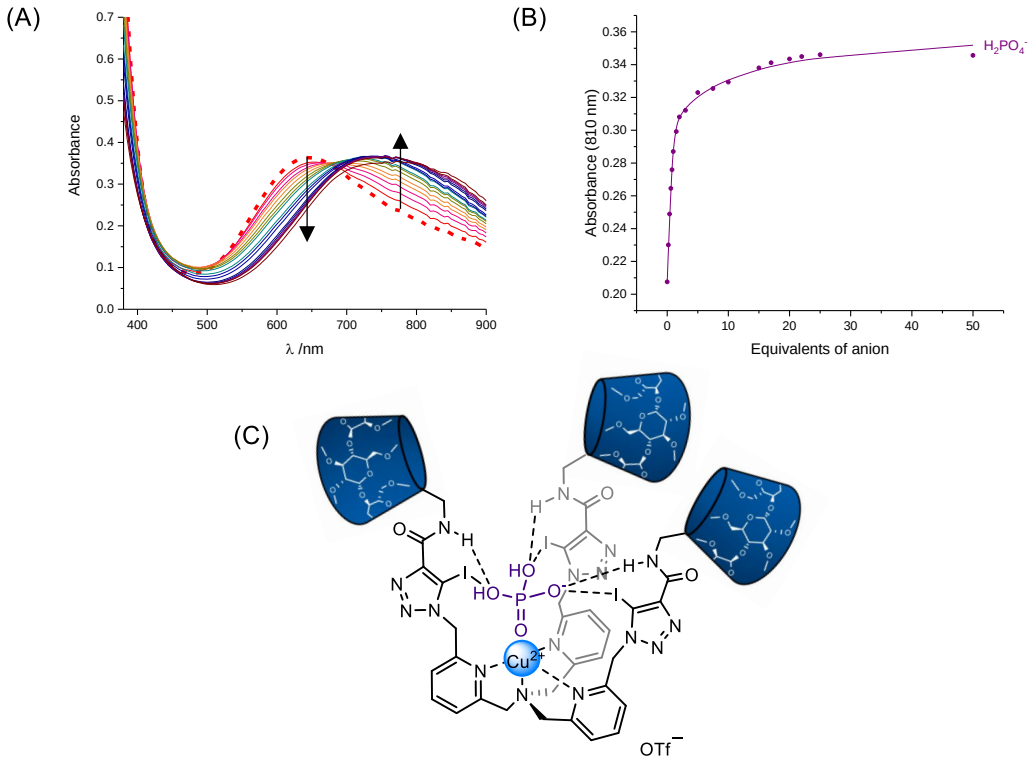


Figure 2.35: *(A) UV-Vis titration of* ***2.36I****·2OTf in the presence of increasing quantities of* $TBAH_2PO_4$*. ([metallo-host] = 2.0 mM,* CH_3CN*/* H_2O *6:4 v/v buffered with 10 mM HEPES at pH 6.3, T = 293 K) and (B) the corresponding isotherm. (C) The envisaged 'lock and key' binding mode of* $H_2PO_4^-$ *within the tetrahedral cavity of* ***2.36I****·2OTf.*

2.8 Conclusions

To conclude, the work presented in this chapter has demonstrated the power of rationally designed, XB metallo-tripodal host systems to achieve the *rare* selectivity for inorganic monophosphate and simple phosphate-ester *oxo*anionic guest species in competitive aqueous media. The adopted 'general XB metallo-tripodal motif' in particular, has been shown to be an effective structure for tetrahedral anion guest binding (Figure 2.4).

In the first section, a pair of novel tris(octyl chain)-appended and tris(ferrocene)-appended XB Zn(II)-hosts, **2.16I**·2ClO_4 and **2.20I**·2ClO_4 respectively, were synthesised alongside their HB analogues (**2.16H**·2ClO_4 and **2.20H**·2ClO_4) and their anion recognition properties determined in CD_3CN/D_2O 9:1 *v/v*. ^{1}H NMR titration experiments showed that both of the XB hosts displayed strong and selective binding of $H_2PO_4^-$ ($K_a > 10^4$ M^{-1}) over the more basic, OAc^- oxoanion as well as the halides, which was attributed to the shape and size complementarity of their unique C_{3v} symmetric XB donor cavities for the tetrahedral guest. In contrast, their HB counterparts displayed much weaker binding of the halides demonstrating the power of XB to enhance anion recognition in competitive organic-aqueous media. The influences of XB on electrochemical anion sensing was further probed utilising the Fc/ Fc^+ redox couples of **2.20I**·2ClO_4 and **2.20H**·2ClO_4. Generally amplified anion-induced cathodic shift perturbation magnitudes were exhibited by the electrochemically-active XB host compared to the HB counterpart, credited to the enhanced degree of covalency of XB···anion interactions facilitating through-bond communicative pathways between the conjugated binding site and the redox-active ferrocene reporter moiety.

In the second section, efforts to quantify the strong inorganic monophosphate binding exhibited by **2.16I**·2ClO_4 and **2.20I**·2ClO_4 led to the preparation of the water soluble, tris(TEG)-appended XB Zn(II)-host **2.25I**·2ClO_4, however, ITC experiments indicated a lack of anion binding in pure water. A loss of the host's all-important C_{3v} symmetry was simultaneously observed and reasoned to arise from the water-induced *static* N^2-coordination of (two of) the iodotriazole encompassing '*arms*' to the respective metallo-center, as elucidated from various investigative ^{1}H NMR

spectroscopic studies. Attempting to conduct titrations in CH_3CN/H_2O 6:4 *v/v* (the optimal organic-aqueous solvent ratio in which the N^2-coordination behaviour remained 'dynamic') and utilising an optical sensing strategy with the tris(TEG)-appended XB Cu(II)-analogue **2.26I**·2OTf allowed for the determination of association constants. UV-Vis titration experiments revealed the XB host similarly bound $H_2PO_4^-$ strongly (K_a = 2816 M^{-1}) with an affinity over six times greater than the weakest bound Cl^-, which was again, attributed to the good size match between the tetrahedral anion and the XB tripodal cavity. Furthermore, increasing the solvent water content four-fold had an explicit effect on the binding of Br^- and OAc^-, correlating with their relative energies of hydration. Importantly, the $H_2PO_4^-$ association constant calculated for the XB receptor was approximately thrice as large as that obtained with the HB counterpart **2.26H**·2OTf providing further rare evidence that XB is a more effective *oxo*-anion binding interaction than HB in aqueous media. Similarly augmented binding of the monophosphate-ester PMP^- was evidenced with **2.26I**·2OTf compared to **2.26H**·2OTf thus highlighting the applicability of XB as a worthwhile supramolecular interaction to exploit for the enhanced recognition of toxic G-series substances. In addition, both Cu(II) receptors were also demonstrated to be highly effective electrochemical anion sensors, capable of sensing Br^- *via* magnified cathodic shift perturbations of their respective Cu^I/Cu^{II} redox couples. Finally, a further notable enhancement in the binding of $H_2PO_4^-$ was achieved with the alternative tris(pm*β*CD)-appended XB Cu(II)-receptor **2.36I**·2OTf which displayed almost a three-fold increase in monophosphate anion affinity compared to **2.26I**·2OTf in the same solvent system, bringing to light the synergistic roles of the host's XB donor iodotriazole and HB donor NH amide functionalities in the binding process.

2.9 Future work

Following the above studies, the 'general XB metallo-tripodal motif' could be further exploited to investigate the binding of other, higher-order, polyphosphate-ester nucleotide species (*e.g.* ADP^{3-}, ATP^{4-}, see Figure 1.33B in Chapter One) - by specifically appending its tripodal arm fragments with (i) an additional triad of iodotriazoles (to maximise XB···O^- interactions with the polyphosphate 'tail') and (ii) terminal aromatic groups (capable of forming favourable π-π stacking interactions with the guest's nitrogenous nucleobase), the resultant 'extended' XB metallo-host could facilitate the recognition of polyanionic phosphate nucleotide derivatives (Figure 2.36).

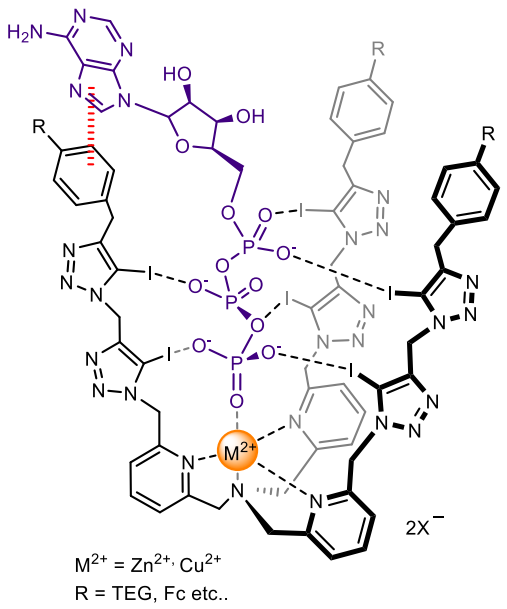


Figure 2.36: *Future work. An 'extended' XB metallo-tripodal host for polyanionic phosphate nucleotide binding. Shown with the proposed binding mode of* ATP^{4-}.

Indeed, the evidenced versatility of the respective XB leitmotif as a synthetic building block makes it an attractive candidate to aid in the construction of more exotic and complex supramolecular host architectures, for example *chiral* XB metallo-tripodal assemblies as well as higher-order, cryptand-like XB host structures capable of complete guest encapsulation. Together, these ideas form the basis of the research undertaken in the forthcoming chapters.

2.10 References

1 D. J. Cram, *Science*, 1988, **240**, 760–767.
2 M. Cametti, K. Raatikainen, P. Metrangolo, T. Pilati, G. Terraneo and G. Resnati, *Org. Biomol. Chem.*, 2012, **10**, 1329–1333.
3 B. Chowdhury, S. Sinha and P. Ghosh, *Chem. – Eur. J.*, 2016, **22**, 18051–18059.
4 F. Zapata, L. González, A. Caballero, A. Bastida, D. Bautista and P. Molina, *J. Am. Chem. Soc.*, 2018, **140**, 2041–2045.
5 F. Zapata, A. Caballero and P. Molina, *Eur. J. Inorg. Chem.*, 2017, **2017**, 237–241.
6 J. Y. C. Lim and P. D. Beer, *New J. Chem.*, 2018, **42**, 10472–10475.
7 S. L. Tobey, B. D. Jones and E. V. Anslyn, *J. Am. Chem. Soc.*, 2003, **125**, 4026–4027.
8 J. Liang, J. Zhang, L. Zhu, A. Duarandin, V. G. Young, N. Geacintov and J. W. Canary, *Inorg. Chem.*, 2009, **48**, 11196–11208.
9 S. Kim, C. Saracini, M. A. Siegler, N. Drichko and K. D. Karlin, *Inorg. Chem.*, 2012, **51**, 12603–12605.
10 X. Zeng, D. Coquière, A. Alenda, E. Garrier, T. Prangé, Y. Li, O. Reinaud and I. Jabin, *Chem. – Eur. J.*, 2006, **12**, 6393–6402.
11 Y. Mikata, Y. Nodomi, R. Ohnishi, A. Kizu and H. Konno, *Dalton Trans.*, 2015, **44**, 8021–8030.
12 W. S. Brotherton, R. J. Clark and L. Zhu, *J. Org. Chem.*, 2012, **77**, 6443–6455.
13 C. Uttamapinant, A. Tangpeerachaikul, S. Grecian, S. Clarke, U. Singh, P. Slade, K. R. Gee and A. Y. Ting, *Angew. Chem. Int. Ed.*, 2012, **51**, 5852–5856.
14 V. Bevilacqua, M. King, M. Chaumontet, M. Nothisen, S. Gabillet, D. Buisson, C. Puente, A. Wagner and F. Taran, *Angew. Chem. Int. Ed.*, 2014, **53**, 5872–5876.
15 Y. Su, L. Li, H. Wang, X. Wang and Z. Zhang, *Chem. Commun.*, 2016, **52**, 2185–2188.
16 D. N. Barsoum, C. J. Brassard, J. H. A. Deeb, N. Okashah, K. Sreenath, J. T. Simmons and L. Zhu, *Synthesis*, 2013, **45**, 2372–2386.
17 T. R. Chan, R. Hilgraf, K. B. Sharpless and V. V. Fokin, *Org. Lett.*, 2004, **6**, 2853–2855.
18 K. Hirose, *J. Inclusion Phenom. Macrocyclic Chem.*, 2001, **39**, 139–209.
19 M. J. Hynes, *J. Chem. Soc. Dalton Trans.*, 1993, **0**, 311–312.
20 M. J. Langton, S. W. Robinson, I. Marques, V. Félix and P. D. Beer, *Nat. Chem.*, 2014, **6**, 1039–1043.
21 M. J. Langton, I. Marques, S. W. Robinson, V. Félix and P. D. Beer, *Chem. – Eur. J.*, 2016, **22**, 185–192.
22 M. B. Smith and J. March, *March's Advanced Organic Chemistry: Reactions, Mechanism, and Structure*, John Wiley & Sons, Ltd, New York, 5th edn., 2001.
23 S. W. Robinson, C. L. Mustoe, N. G. White, A. Brown, A. L. Thompson, P. Kennepohl and P. D. Beer, *J. Am. Chem. Soc.*, 2015, **137**, 499–507.
24 J. Y. C. Lim, M. J. Cunningham, J. J. Davis and P. D. Beer, *Chem. Commun.*, 2015, **51**, 14640–14643.
25 J. Y. C. Lim and P. D. Beer, *Eur. J. Inorg. Chem.*, 2017, **2017**, 220–224.
26 B. R. Mullaney, M. J. Cunningham, J. J. Davis and P. D. Beer, *Polyhedron*, 2016, **116**, 20–25.
27 Byron. Kratochvil, Esther. Lorah and Carl. Garber, *Anal. Chem.*, 1969, **41**, 1793–1796.
28 A. J. Bard and L. R. Faulkner, *Electrochemical Methods: Fundamentals and Applications*, Wiley, New York, 7th edn., 2001.
29 M. J. Langton, C. J. Serpell and P. D. Beer, *Angew. Chem. Int. Ed.*, 2016, **55**, 1974–1987.
30 P. A. Gale, E. N. W. Howe and X. Wu, *Chem*, 2016, **1**, 351–422.
31 J. Y. C. Lim and P. D. Beer, *Chem. Commun.*, 2015, **51**, 3686–3688.
32 A. Borissov, I. Marques, J. Y. C. Lim, V. Félix, M. D. Smith and P. D. Beer, *J. Am. Chem. Soc.*, 2019, **141**, 4119–4129.
33 S. P. Cornes, M. R. Sambrook and P. D. Beer, *Chem. Commun.*, 2017, **53**, 3866–3869.
34 T. Shiraki, A. Dawn, Y. Tsuchiya and S. Shinkai, *J. Am. Chem. Soc.*, 2010, **132**, 13928–13935.

35 A. Trösch and H. Vahrenkamp, *Eur. J. Inorg. Chem.*, 1998, **1998**, 827–832.
36 H. Adams, N. A. Bailey, D. E. Fenton and Q.-Y. He, *J. Chem. Soc. Dalton Trans.*, 1996, **0**, 2857–2865.
37 Y. Marcus, *Biophys. Chem.*, 1994, **51**, 111–127.
38 R. Evans, Z. Deng, A. K. Rogerson, A. S. McLachlan, J. J. Richards, M. Nilsson and G. A. Morris, *Angew. Chem. Int. Ed.*, 2013, **52**, 3199–3202.
39 D. Kurniawan, S. Morita and K. Kitagawa, *Comput. Theor. Chem.*, 2012, **982**, 30–33.
40 S. L. Tobey, PhD thesis, The University of Texas at Austin, 2003.
41 H. Irving and R. J. P. Williams, *J. Chem. Soc.*, 1953, **0**, 3192–3210.
42 M. Sarma, A. Kalita, P. Kumar, A. Singh and B. Mondal, *J. Am. Chem. Soc.*, 2010, **132**, 7846–7847.
43 E. A. Ambundo, M.-V. Deydier, A. J. Grall, N. Aguera-Vega, L. T. Dressel, T. H. Cooper, M. J. Heeg, L. A. Ochrymowycz and D. B. Rorabacher, *Inorg. Chem.*, 1999, **38**, 4233–4242.
44 N. Le Poul, B. Douziech, J. Zeitouny, G. Thiabaud, H. Colas, F. Conan, N. Cosquer, I. Jabin, C. Lagrost, P. Hapiot, O. Reinaud and Y. Le Mest, *J. Am. Chem. Soc.*, 2009, **131**, 17800–17807.
45 G. Izzet, X. Zeng, H. Akdas, J. Marrot and O. Reinaud, *Chem. Commun.*, 2007, 810–812.
46 G. Thiabaud, A. Brugnara, M. Carboni, N. Le Poul, B. Colasson, Y. Le Mest and O. Reinaud, *Org. Lett.*, 2012, **14**, 2500–2503.
47 D. K. Chand and P. K. Bharadwaj, *Inorg. Chem.*, 1996, **35**, 3380–3387.
48 M. M. Roessler and E. Salvadori, *Chem. Soc. Rev.*, 2018, **47**, 2534–2553.
49 P. Thordarson, *Chem. Soc. Rev.*, 2011, **40**, 1305–1323.
50 Y. Marcus, *J. Chem. Soc. Faraday Trans.*, 1991, **87**, 2995–2999.
51 M. E. Colvin, E. Evleth and Y. Akacem, *J. Am. Chem. Soc.*, 1995, **117**, 4357–4362.
52 S. Watchasit, A. Kaowliew, C. Suksai, T. Tuntulani, W. Ngeontae and C. Pakawatchai, *Tetrahedron Lett.*, 2010, **51**, 3398–3402.
53 R. Oliveira, S. Groni, C. Fave, M. Branca, F. Mavré, D. Lorcy, M. Fourmigué and B. Schöllhorn, *Phys. Chem. Chem. Phys.*, 2016, **18**, 15867–15873.
54 P. J. Skinner, A. Beeby, R. S. Dickins, D. Parker, S. Aime and M. Botta, *J. Chem. Soc. Perkin Trans. 2*, 2000, 1329–1338.
55 N. Zhong, H.-S. Byun and R. Bittman, *Tetrahedron Lett.*, 1998, **39**, 2919–2920.
56 J. A. Faiz, N. Spencer and Z. Pikramenou, *Org. Biomol. Chem.*, 2005, **3**, 4239–4245.
57 S. W. Robinson, PhD thesis, The University of Oxford, 2016.

Chapter Three

Chiral halogen bonding metallo-tripodal receptors for enantioselective anion recognition and sensing

3 Chiral halogen bonding metallo-tripodal receptors for enantioselective chiral anion recognition and sensing

3.1 Introduction

Chiral compounds are non-superimposable molecules containing spatially asymmetric arrangements of atoms around one or more chiral centres.[1] Stimulated by the remarkable levels of enantioselectivity found in biological systems, *supramolecular chiral recognition*, *i.e*. the ability of a *chiral host* molecule to selectively bind one enantiomer of a *chiral guest* over the other, has been the subject of much focus over the years, driving advances in areas ranging from analytical chemistry[2–4] to asymmetric synthesis and catalysis.[5,6] In Nature, guest enantiomer selectivity occurs *via* structurally well-defined binding pockets capable of encapsulating the target guest enantiomer in three-dimensional chiral cavities with exquisite complementarity.[7] Indeed, the importance of guest encapsulation in the chiral discrimination process has been demonstrated by the high levels of enantioselectivity attained by abiotic hosts possessing structurally *constrained* three-dimensional chiral cavities (Section 3.1.2).[8–14] In this respect and following on from Chapter Two, the preorganised XB-donor decorated cavity of the 'general XB metallo-tripodal motif' (Figure 2.4) provides a unique potential platform for enantioselective discrimination when appended with appropriate chiral functionalities (*vide infra*). Additionally, the present rarity of chiral XB hosts,[15,16] having exhibited augmented chiral anion discriminatory abilities compared to ubiquitous HB chiral counterparts (Section 3.1.3), provides further motivation for the work undertaken in this chapter which focuses on the construction of *chiral* XB metallo-tripodal receptors for *enantioselective* chiral anion recognition (Section 3.1.4).

3.1.1 Theory of chiral recognition

The basis of any chiral recognition event is the formation of diastereomeric complexes composed of a chiral receptor and substrate possessing different stabilities; the chiral substrate selectively bound is the one capable of forming the energetically most stable diastereomeric host-guest complex.[17] Whilst there has been some debate over the issue, it is usually stated that for chiral

recognition to occur, 'at least *three* simultaneous interactions must be present between a chiral host and its chiral guest, with at least one of these interactions being stereochemically dependent'.[18] The rationalisation of this argument is by consideration of a '*three-point*' model, as illustrated in Figure 3.1: if a chiral receptor (H) has three sites of interaction with a specific enantiomer of a chiral guest (E_1), the other enantiomer of that guest (E_2) will only be able to interact with two of these sites. Notably, this three point rule does not require all three interactions to be attractive (*i.e.* bonding). In many cases *repulsive* interactions (*e.g.* electrostatics, steric hindrance) are invoked, often in concert with one or more attractive interactions (*e.g.* HB, metal-coordination, π-π stacking) to explain chiral recognition.[17] A modified version of this theoretical framework, termed the '*stereocentre-recognition*' model has also been developed to account for tetrahedral substrates containing multiple stereocentres.[19]

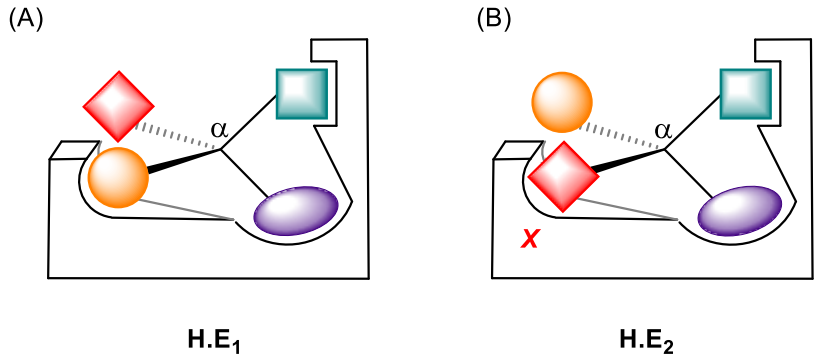


Figure 3.1: *Schematic representation of the classical three-point model for chiral recognition: Guest Enantiomer 1 (E_1) interacts with three sites of the chiral host (H); (b) Enantiomer 2 (E_2) interacts only at two sites of H. Hence Enantiomer 1 will be bound more strongly than Enantiomer 2.The ratio of their respective equilibrium constants is thus a quantitative measure of the intrinsic enantioselectivity of H. (stereocentre labelled with α.).*[17]

3.1.2 Artificial chiral receptors for enantioselective chiral anion recognition

Using the above guiding principles and inspired by the need for *constrained* three-dimensional chiral binding cavities for the effective enantiodiscrimination of chiral anions seen in natural enzymes,[7,20,21] a variety of tripodal receptors,[8,9] macrocycles[10–12] and their strapped counterparts[13,14] have been synthesised by supramolecular chemists which have shown impressive chiral discriminatory abilities. For example, utilising a tripodal host based upon a chiral cholic acid scaffold, Davis and co-workers demonstrated a 7-10 fold selective extraction of *N*-acyl-(*S*)-amino acids from aqueous phosphate buffer (pH = 7.4) into chloroform compared to the (*R*)-enantiomers

(Figure 3.2A).[8] Good selectivity for (*N*Boc-(*S*)-glutamate)$^{2-}$ was also seen with Kilburn's chiral diamine containing bis-guanidinium macrocycle, capable of forming up to eight HB interactions with a single dicarboxylate anion guest (Figure 3.2B).[10] As indicated by ITC experiments in DMSO/H_2O 1:1 *v/v*, (*N*Boc-(*S*)-glutamate)$^{2-}$ was bound strongly in a 1:1 host-guest stoichiometry (K_{11} = 3.8 x 10^4 M^{-1}) whereas (*N*Boc-(*R*)-glutamate)$^{2-}$ was bound strongly in a 1:2 host-guest stoichiometry (K_{12} = 1.4 x 10^4 M^{-1}) with a weaker 1:1 binding event (K_{11} = 2.9 x 10^3 M^{-1}) detected, attributed to the (*R*)-enantiomer not fitting into the chiral cavity of the macrocycle. Comparing only the first binding events, the host's enantioselectivity of K_S/K_R = 13 for the (*S*)-enantiomer is particularly noteworthy.

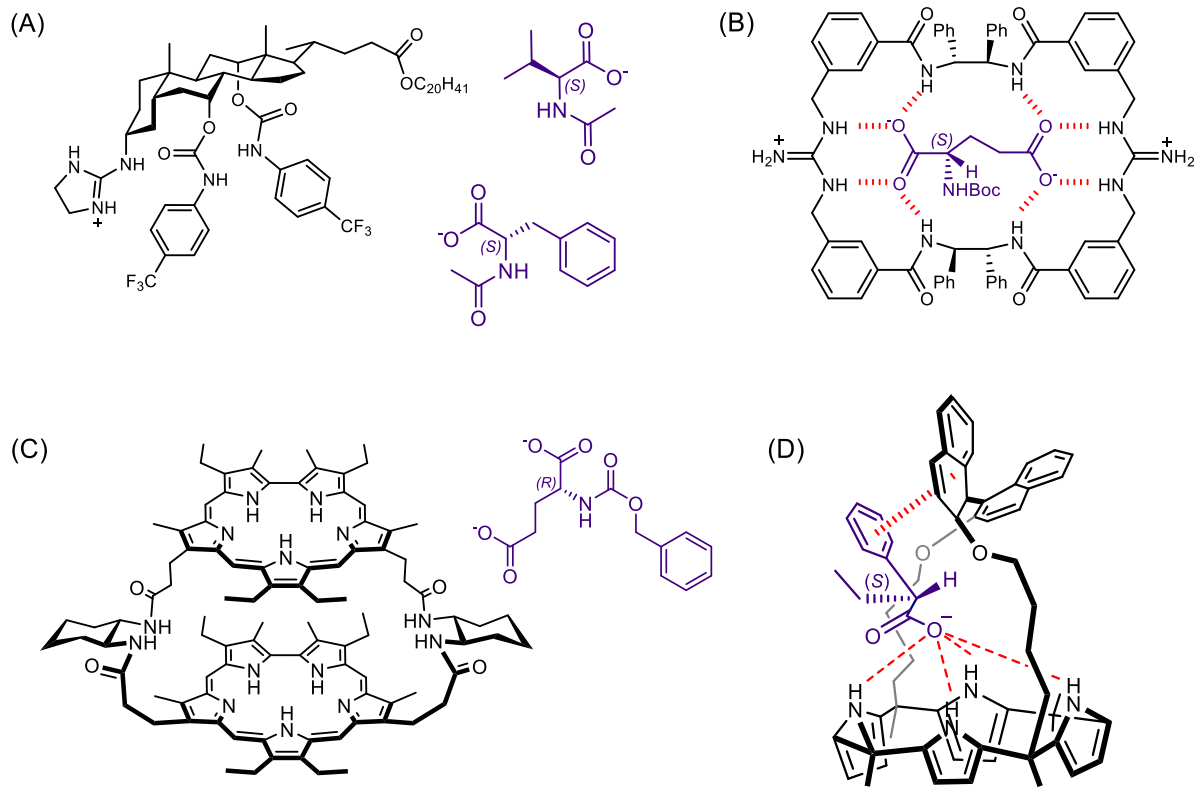


Figure 3.2: *Artificial chiral receptors containing constrained binding cavities. (A) Davis' tripodal steroid receptor;*[8] *(B) Kilburn's bis-guanidinium macrocycle;*[10] *(C) Sessler's chiral sapphyrin-dimer receptor;*[13] *(D) Lee's (S)-BINOL-strapped calix[4]pyrrole host.*[14] *(Guest anion enantiomers preferentially bound are shown in purple next to the chiral host or in the envisioned binding mode).*

To afford even more restricted cavities for enantiodiscrimination, Sessler and co-workers constructed a dimeric receptor derived from a pair of sapphyrin macrocycles linked by chiral 1,2-diamino cyclohexane moieties which exhibited a selectivity of K_R/K_S = 4.3 for (*N*-Cbz-glutamate)$^{2-}$

in CH_2Cl_2/CH_3OH 95:5 *v/v* (Figure 3.2C).[13] Another prominent example is Lee's calix[4]pyrrole host containing a strapped chiral (*S*)-1,1'-Bi-2-naphthol (BINOL) bridge which displayed excellent selectivity of K_S/ K_R = 10 for (*S*)-2-phenylbutyrate$^-$ in CH_3CN (Figure 3.2D).[14] Besides the carboxylate hydrogen bonding to the convergent N-H array from the four pyrroles, the selectivity was attributed to arise from the favourable π-π stacking interaction between one of the naphthyl groups of the chiral host and phenyl ring of the bound substrate, which can occur with the (*S*)-enantiomer guest but not the (*R*)-isomer.

3.1.3 XB-mediated chiral anion recognition

Representing only a very recent addition to the toolkit of supramolecular interactions employed in solution-phase chiral discrimination is XB, whose stringent requirements of linearity coupled with the steric influences of the XB-donor halogen atom constituting the anion binding site have been demonstrated to enhance the enantioselectivity of chiral anion recognition.[15] Indeed Beer and co-workers observed the first indication that XB interactions could significantly influence chiral oxo-anion discrimination by using a XB chiral receptor containing the enantiopure (*S)*-BINOL motif (compound **3a** in Figure 3.3A).[15] From a series of *α*-amino acid derived chiral carboxylates investigated, the largest enantioselectivity of K_S/ K_R = 1.67 was observed for (*N*Boc-tryptophan)$^-$ in CD_3CN/ D_2O 99:1 *v/v*, followed by (*N*Boc-leucine)$^-$ and (*N*Boc-alanine)$^-$ correlating with the steric bulk of the R-group residue. By contrast, the chiral HB host counterpart (compound **3b**) exhibited almost negligible enantioselectivity for all anion enantiomers under similar conditions. DFT calculations also indicated the greater directionality of XB interactions (Figure 3.3B) along with the more localised electrophilic XB-binding site, all contributed to the augmented enantioselectivity of the chiral acyclic XB host.

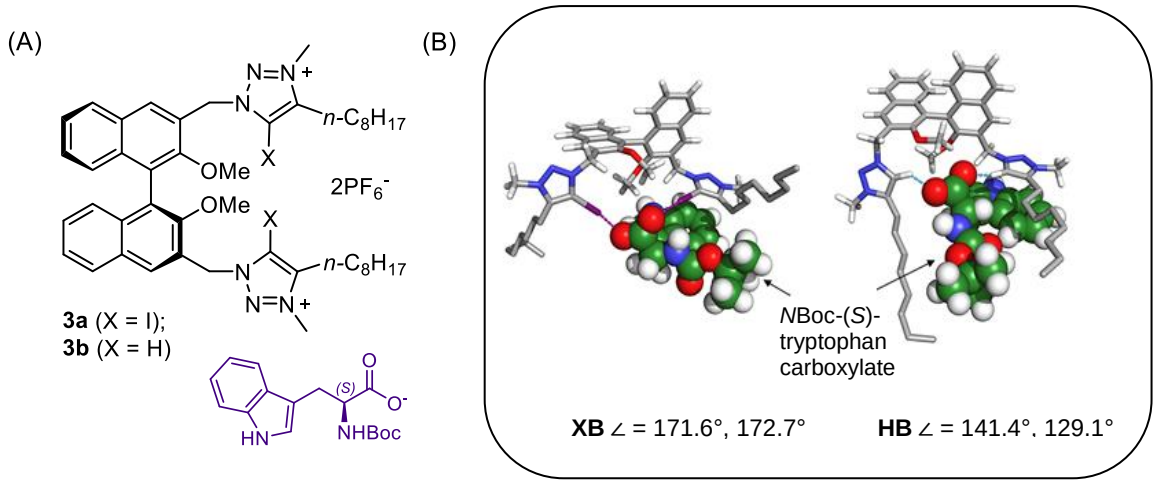


Figure 3.3: *(A)Beer's original chiral XB receptor* ***3a*** *and the preferentially bound oxo-anion guest (NBoc-(S)-tryptophan)- highlighted in purple;*[15] *(B)DFT-optimised structures for host-guest complexes of (left)* ***3a*** *and (right) the HB counterpart* ***3b*** *with NBoc-(S)-tryptophan; the C-X···O- (X = I/H) bond angles are indicated at the side. (DFT structures adapted from Lim et al.*[15] *with permission of the Royal Society of Chemistry).*

In a subsequent study and *via* the incorporation of the respective (*S*)-BINOL motif into a macrocyclic framework, a family of cationic chiral XB [2]rotaxanes (Figure 3.4) were demonstrated to further exhibit an impressive degree of enantiodiscrimination towards various chiral mono oxo-anions (*e.g.* up to K_S/K_R = 2.93 for (*N*Boc-proline)- in acetone-d_6/ D_2O 98:2 *v/v*).[16]

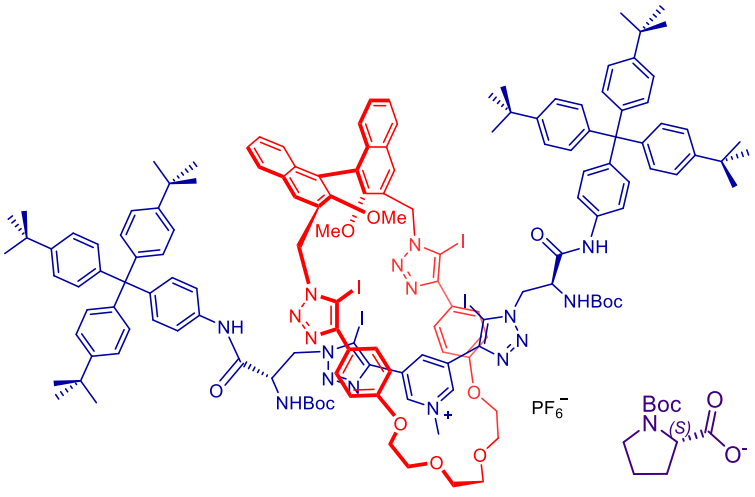


Figure 3.4: *Beer's chiral XB [2]-rotaxane and the preferentially bound oxo-anion guest (NBoc-(S)-proline)- highlighted in purple.*[16]

3.1.4 Chapter aims

Building on the results of Chapter Two, the work in this chapter aims to extend the use of the 'general XB metallo-tripodal motif' for the enantioselective chiral anion recognition of a series of biologically-relevant carboxylate oxo-anions and BINOL phosphate-ester anionic guest species (Figure 3.5). By appropriately extending the tripodal XB leitmotif's '*arm*' fragments with a triad of enantiopure chiral *α*-amino acid derived appendages, specifically *N*Boc-(*S*)-tryptophan and *N*Boc-(*S*)-leucine based functionalities (*vide infra*), a pair of novel *chiral* XB Zn(II)-tripodal receptors are constructed, and their enantio-discriminatory chiral anion recognition properties investigated in competitive organic-aqueous solvent media. For greater insight into the influence of XB on chiral discrimination, the protic HB counterpart of the XB tris(*N*Boc-(*S*)-Tryptophan) host is also prepared and its chiral anion binding properties studied.

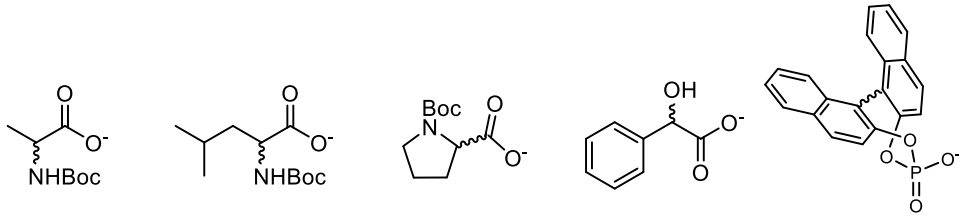


Figure 3.5: *Structures of all the chiral anions studied in this chapter.(Structures shown in the racemic form).*[****]

[****] The TBA salts of the chiral anions were prepared according to a general literature procedure[22] using TBAOH from their commercially-available neutral acids. Further experimental details are mentioned in Chapter Six.

3.2 A tris(*N*Boc-(*S*)-tryptophan)-appended XB Zn(II) chiral tripod

3.2.1 General design

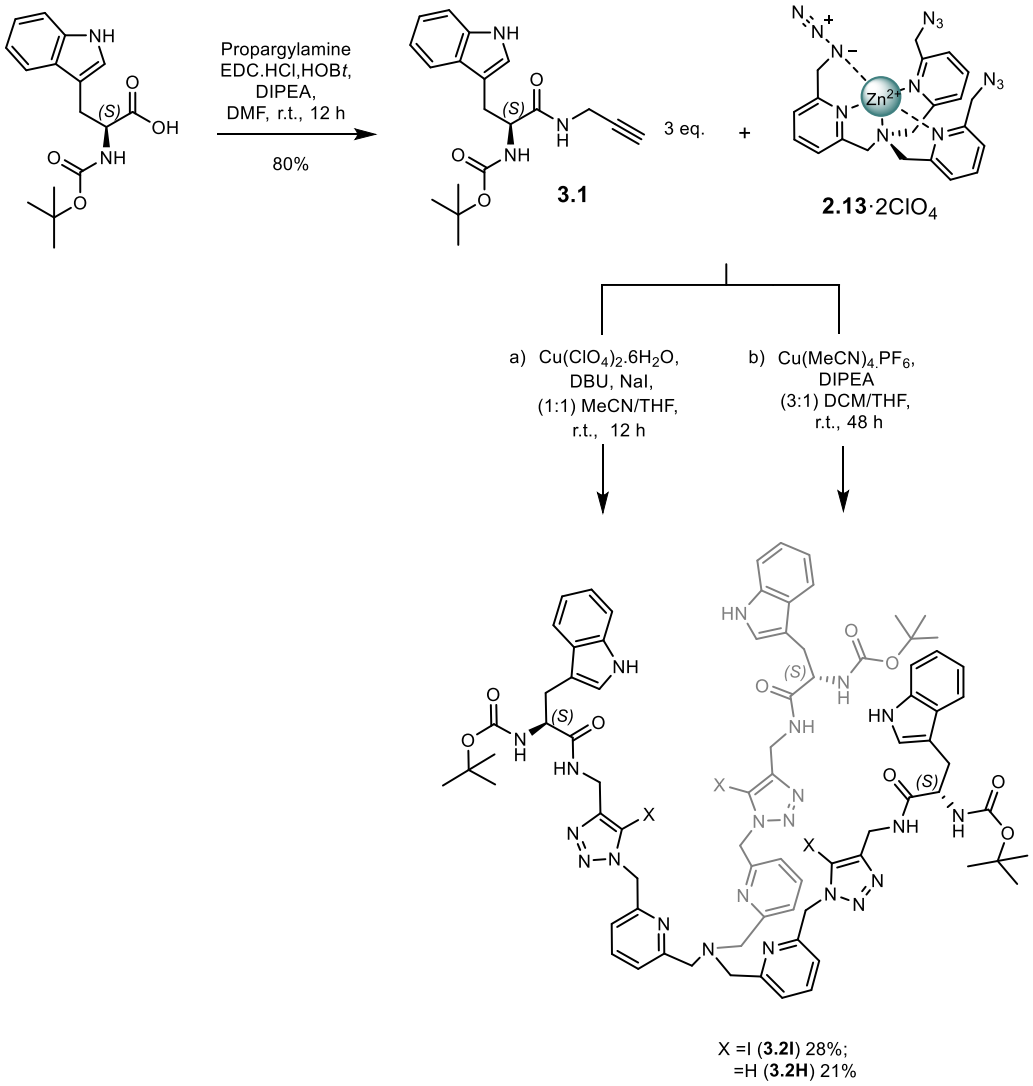
Natural chiral biomolecules such as sugars[23] and amino acids,[24] due to their low-cost and ample availability in enantiopure forms, constitute a popular and important class of building blocks from which artificial chiral host systems are often constructed. *α*-Amino acids in particular, offer an attractive source of chirality to the synthetic supramolecular chemist as their parent (amine and carboxylic acid) functionalities allow for convenient orthogonal chemical manipulation. The design of the initial target chiral XB metallo-receptor **3.3I**·2ClO_4 shown in Scheme 3.2 accordingly features a triad of enantiopure *N*Boc-(*S*)-tryptophan amino acid-derived appendages (highlighted in orange), which along with the pre-organisation by the Zn(II) metal along the C_3 axis, give rise to a *homochiral* tetrahedral binding pocket where the surrounding iodotriazole moieties are positioned for convergent XB interactions with the prospective chiral anion guest. Additionally, the favourable fluorescence properties of the tryptophan residue's indole side chain facilitates the opportunity of chiral anion sensing.

3.2.2 Synthesis and characterisation of **3.3I**·2ClO_4 and **3.3H**·2ClO_4

A 'tris-CuAAC' click reaction strategy between the previously synthesised tris-azide Zn(II)-subunit **2.13**·2ClO_4 and three equivalents of (*S*)-alkyne **3.1** was employed for the synthesis of the tripodal skeleton of the chiral Zn(II)-tripod **3.3I**·2ClO_4 (Scheme 3.1).[††††] Synthesis of the chiral alkyne **3.1** was achieved using commercially available *N*Boc-(*S*)-tryptophan which was coupled with propargylamine under enantio-retentive conditions involving activated ester formation using ethylcarbodiimide hydrochloride (EDC·HCl) and 1-hydroxybenzenetriazole (HOB*t*).[25] Three-equivalents of **3.1** were next reacted with **2.13**·2ClO_4 according to Zhu's one-pot 'iodo-CuAAC'

[††††] *N.B.* It was demonstrated in Chapter Two that the XB '*arm*' formation strategy (Section 2.3.1.2), requiring heavily basic ammonia conditions as part of the tripodal ligand formation step proved to be a succesful route for the synthesis of XB tripodal derivatives. However, in order to supress any base-induced racemisation of the enantiopure *α*-amino acid derived appendages of the chiral tripodal XB ligand **3.2I**, here the alternative 'tris-CuAAC' strategy was adopted instead – importantly omitting the use of any TBTA .

protocol[26] (omitting catalytic TBTA) to afford the chiral tripodal XB derivative **3.2I** in an isolated yield of 28% yield after preparative TLC purification.[‡‡‡‡]



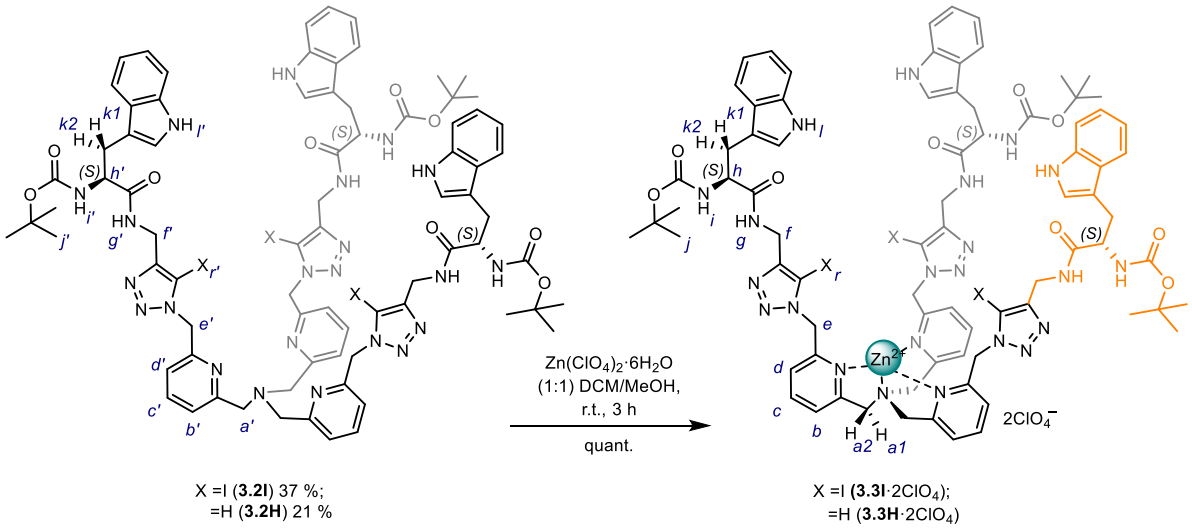
Scheme 3.1: *Synthetic pathway followed to obtain the tris(NBoc(S)-tryptophan)-appended XB tripodal ligand **3.2I**.*

Complexation of **3.2I** with an equimolar quantity of zinc(II) perchlorate hexahydrate produced the enantiomeric (*S*,*S*,*S*)-XB metallo-host **3.3I**·2ClO$_4$ (Scheme 3.2) which was fully characterised by ^{1}H and ^{13}C NMR spectroscopy and high resolution ESI-MS methods, with the assignment of the

[‡‡‡‡] The work-up of this particular synthetic procedure involves the use of basic, aqueous ammonia conditions to remove any Cu(I/II) species present. As a consequence, the Zn(II) cation is also removed from the tripodal cavity of the desired product, affording the *apo*-Zn(II) ligand **3.2I**.

resonances in the ^{1}H spectrum requiring the aid of 2D COSY NMR. The counterpart (*S*,*S*,*S*)-HB zinc metallo-receptor **3.3H**·2ClO$_4$ was prepared *via* an analogous multi-step procedure involving standard 'proto-Click' conditions (Schemes 3.1 and 3.2).

The ^{1}H-NMR spectra of both Zn(II)-receptors **3.3I**·2ClO$_4$ and **3.3H**·2ClO$_4$ compared to their respective zinc-free ligands are displayed in Figure 3.6. Pronounced downfield shifts in the aromatic pyridyl proton $H_{b'-d'}$ signals and proximal aliphatic -CH_2 $H_{a'}$ protons were observed upon coordination to the Zn(II)-centre for both XB and HB systems, whilst the aromatic indole protons (filled blue dots) and methylene $H_{f'}$ and $H_{k'}$ protons of the peripheral homochiral appendages displayed, as expected, comparatively smaller changes in chemical shift. Of particular note with **3.3I**·2ClO$_4$, are the singlet methylene $H_{a'}$ protons of its *apo*-Zn(II) ligand **3.2I** which become diastereotopic in the presence of the metal center and hence appear as two distinct broad multiplet signals H_{a1} and H_{a2}. This diastereotopic splitting of the $H_{a'}$ signal is also presumed to occur with **3.3H**·2ClO$_4$, however due to significant peak overlap with the nearby H_h proton signal producing a multiplet centred at *ca.* 4.67 ppm, the unambiguous assignment of separate H_{a1} and H_{a2} signals was not possible. Nonetheless, the retention of a single set of resonances of both of the ligands' respective core proton $H_{b'-d'}$ and $H_{e'}$ environments upon metal complexation unequivocally affirms the C_{3v} symmetry of the resultant XB and HB metallo-hosts. Indeed, a final further comparison of the key H_e signals reveals the chemical shift to be further downfield in the case of the XB host (5.84 ppm) compared to that of the HB counterpart (5.69 ppm) thus indicating a more electron-deficient homochiral binding pocket of **3.3I**·2ClO$_4$ for chiral anion discrimination.



Scheme 3.2: *Metal complexation of the XB ligand* ***3.2I*** *to afford the pre-organised chiral XB Zn(II)-host* ***3.3I***·*2ClO4.*

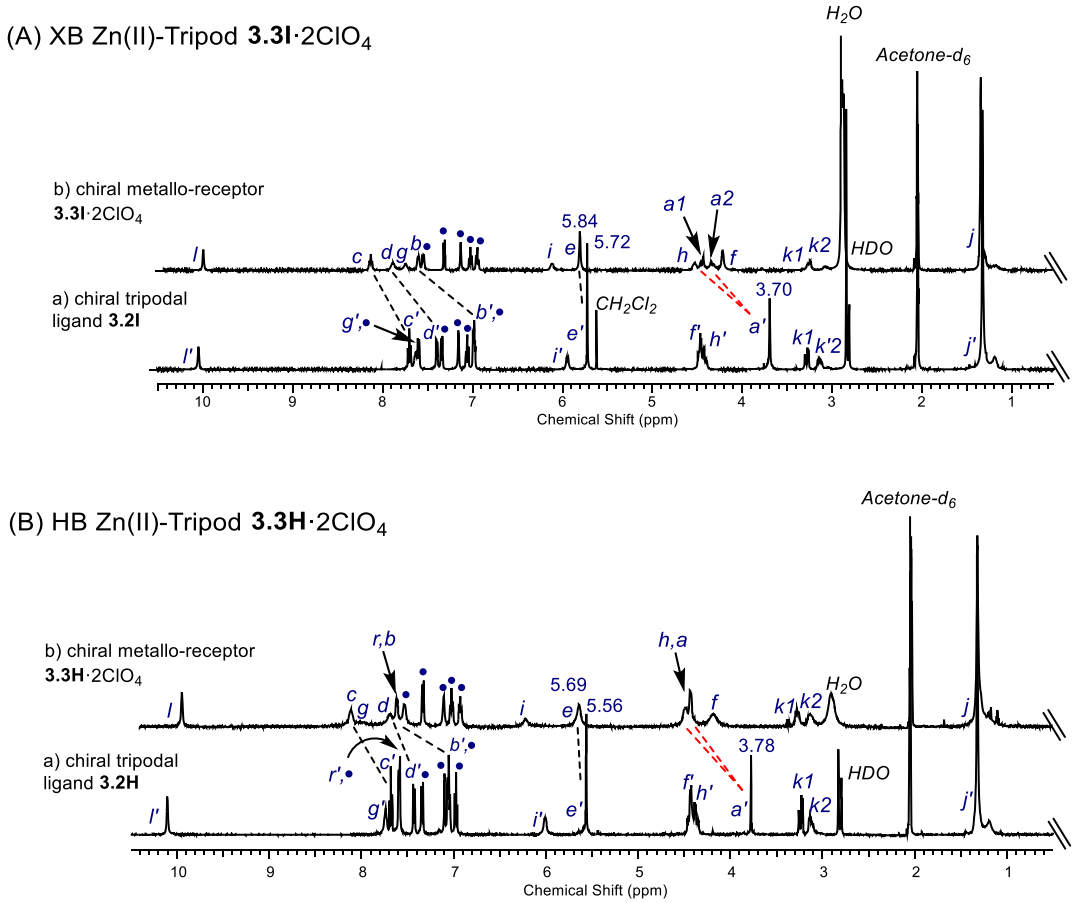


Figure 3.6: *[1]H-NMR characterisation of the chiral Zn(II)-tripodal receptors (A)* ***3.3I***·*2ClO4 and (B)* ***3.3H***.*2ClO4. All spectra were obtained in Acetone-d6 (T = 298 K, 500 MHz). Assignments follow those in Scheme 3.1.(Filled blue dots indicate indole aromatic protons. For clarity only the changes in shifts of the core TPMA protons are highlighted).*

3.2.3 ^{1}H-NMR chiral anion binding studies with **3.3I**·2ClO$_4$

The chiral anion recognition properties of the chiral XB tripod **3.3I**·2ClO$_4$ were initially investigated using ^{1}H-NMR titration experiments in various organic-aqueous solvent media, where increasing quantities of chiral anions (Figure 3.5) as their TBA salt, were added to 1.0 mM solutions of the receptor and the resultant chemical shifts of selected proton signals proximal to the anion binding cavity monitored as a function of anion concentration.

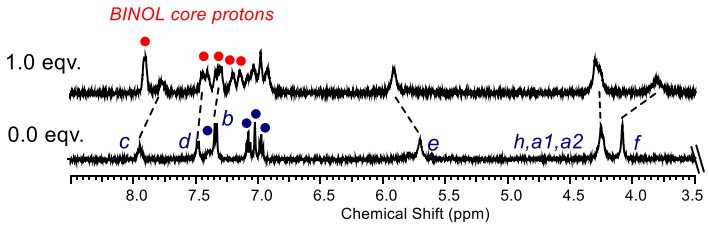
Preliminary ^{1}H NMR titrations with (R)-BINOL-PO$_4^-$

Initial chiral anion titrations with the enantiomers of the target BINOL-PO$_4^-$ species and **3.3I**·2ClO$_4$ were undertaken in CD$_3$CN/ D$_2$O 9:1 *v/v* (Figure 3.7A). Whilst significant downfield perturbations of the iodotriazole adjacent methylene H$_e$ protons and upfield perturbations of the neighbouring H$_f$ and core H$_c$ protons were observed upon initial anion addition ($\Delta\delta$ = 0.22, 0.28 and 0.18 ppm respectively over 1 eqv.) signalling interaction of the phosphate-ester guest within the designated tripodal cavity, subsequent solubility issues unfortunately prevented the determination of quantitative binding data. Similar precipitation problems were encountered when the titrations were repeated in acetone-d_6/ D$_2$O 9:1 *v/v*.

Preliminary ^{1}H NMR titrations with α-amino acid carboxylates

Binding studies with the chiral carboxylate *N*Boc-(*S*)-alanine and **3.3I**·2ClO$_4$ were also performed in CD$_3$CN/ D$_2$O 9:1 *v/v* where the progressive peak broadening of the key H$_e$ signal beyond the addition of 1 equivalent of anion suggested more complex binding (possibly influenced by the additional multiple HB binding sites and/or extended π-surfaces of the host's *N*Boc-(*S*)-tryptophan derived '*arms*'). Additionally, the concomitant splitting of the neighbouring H$_f$ proton signal further increased the complexity of the host's ^{1}H NMR titration spectra negating quantitative binding data being obtained. Similar complex binding was evidenced when the titration was performed with *N*Boc-(*S*)-leucine in the same solvent system. Consequently, further titrations with these carboxylate anions were carried out in the more competitive DMSO-d_6/ D$_2$O 98:2 *v/v* solvent mixture, however no binding was observed in each case (Figure 3.7B).

(A) **3.3I**·2ClO$_4$ + (*R*)-BINOL-PO$_4^-$



(B) **3.3I**·2ClO$_4$ + (*N*Boc-(*S*)-alanine)$^-$

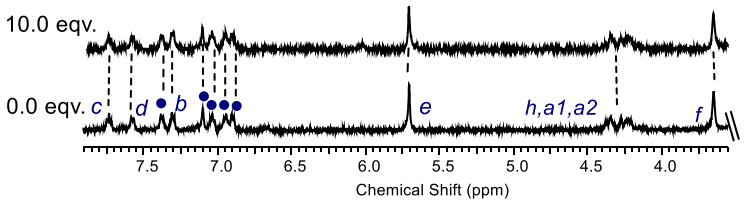


Figure 3.7: *Partial ^{1}H NMR titration spectra of XB chiral Zn(II)-tripod **3.3I**·2ClO$_4$ in the presence of various equivalents of chiral anions: (A) (R)-BINOL-PO$_4^-$ in CD$_3$CN/ D$_2$O 9:1 v/v and (B) (NBoc-(S)-alanine)$^-$ in DMSO-d$_6$/ D$_2$O 98:2 v/v. ([metallo-host] = 1.0 mM, solvent as stated, 500 MHz, T = 298 K). All proton assignments follow those in Scheme 3.2.*

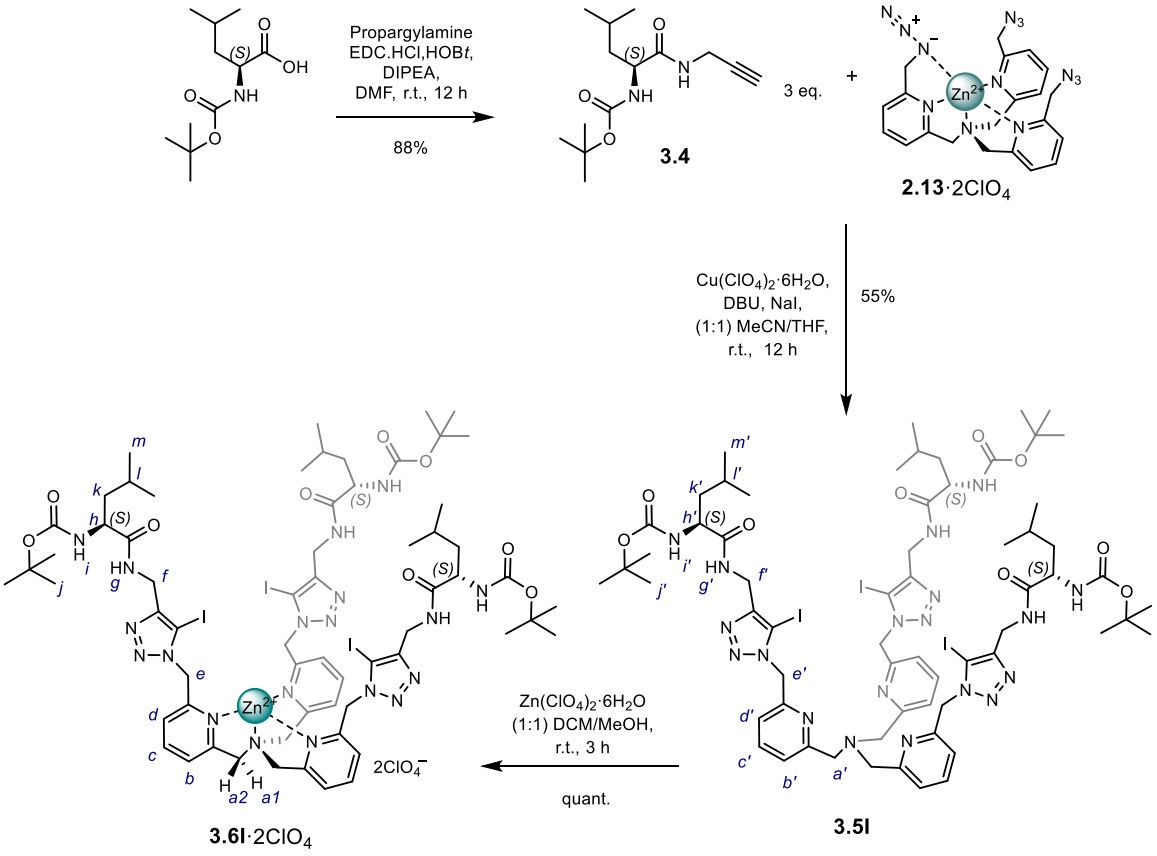
3.3 A tris(*N*Boc-(*S*)-tryptophan)-appended XB Zn(II) chiral tripod

3.3.1 Synthesis and investigation of the chiral anion binding properties of **3.6I**·2ClO$_4$

The complex binding behaviour of **3.3I**·2ClO$_4$ with the chiral carboxylate anions prompted the synthesis of a tris(*N*Boc(*S*)-leucine)-appended XB Zn(II)-host **3.6I**·2ClO$_4$ with alternative aliphatic isobutyl amino acid side groups (Scheme 3.3). An analogous 'tris-CuAAC' reaction between the tris-azide subunit **2.13**·2ClO$_4$ and three equivalents of the appropriate chiral alkyne **3.4** under 'one-pot iodo-Click' conditions[26] afforded the desired chiral XB tripodal framework **3.5I** which was isolated *via* preparative TLC in 55% yield (Scheme 3.4). Complexation with a stoichiometric quantity of zinc(II) perchlorate hexahydrate produced the (*S,S,S*)-XB tripodal receptor **3.6I**·2ClO$_4$, which was fully characterised by ^{1}H and ^{13}C NMR spectroscopy and high resolution ESI-MS methods.

The stacked ^{1}H-NMR spectra of the metallo-host and its zinc-free ligand in acetone-*d*$_6$ are shown in Figure 3.8. Marked downfield shifts of the core aromatic pyridyl proton H$_{b',-d'}$ signals and proximal methylene H$_{a'}$ protons were observed upon complexation to the Zn(II)-centre, whilst the

various $H_{f'\text{-}m'}$ protons of the *N*Boc-(*S*)-leucine based appendages displayed comparatively smaller perturbations. Noteworthy again is the diastereotopic splitting of the *apo*-Zn(II) ligand's singlet $H_{a'}$ proton signal into two separate doublet signals H_{a1} and H_{a2} in the presence of the Zn(II) metal as evidenced previously in the ^{1}H-NMR of **3.3I**·2ClO$_4$ (Figure 3.6A).



Scheme 3.3: *Synthetic pathway followed to obtain the tris(NBoc-(S)-leucine)-appended XB Zn(II)-host* ***3.6I***·2ClO$_4$.

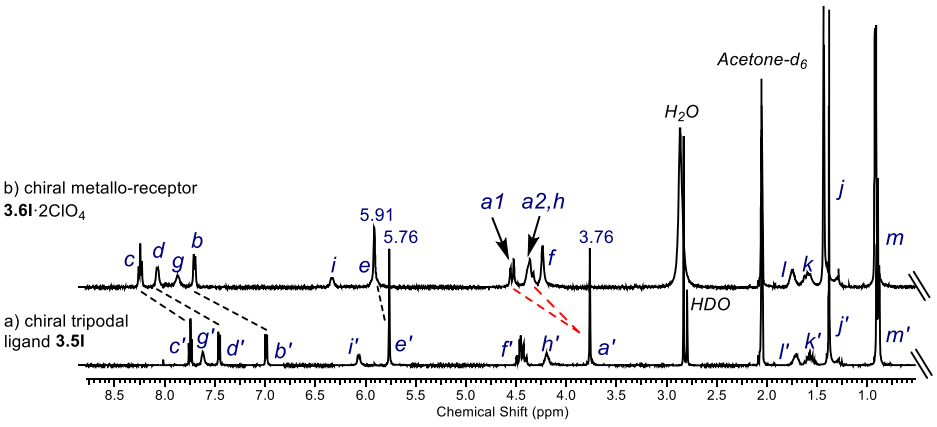


Figure 3.8: *^{1}H-NMR characterisation of the XB chiral Zn(II)-tripodal receptor* ***3.6I***·2ClO$_4$*. All spectra were obtained in Acetone-d$_6$ (T = 298 K, 500 MHz). Assignments follow those in Scheme 3.3. (For clarity only the changes in shifts of the core TPMA protons are highlighted).*

Following the same titration protocol outlined in Section 3.2.3, the chiral anion binding properties of **3.6I**·2ClO_4 were investigated using ^{1}H NMR anion titrations in CD_3CN/D_2O 9:1 *v/v*. Similar guest-induced peak broadening and splittings of the key H_e and H_f signals observed with **3.3I**·2ClO_4 in the presence of (*N*Boc-(*S*)-alanine)$^-$ were seen with **3.6I**·2ClO_4 suggesting the complex binding behaviour of the chiral carboxylate to be unaffected by the nature of the host's chiral appendages. Furthermore, similar solubility problems were encountered when the titration was performed with (*R*)-BINOL-PO_4^-.

In light of the complex ^{1}H NMR spectra and solubility issues encountered in the chiral anion titration experiments with both of the chiral XB tripodal hosts which prevented the derivation of any quantitative binding data, it was decided to probe chiral anion binding alternatively utilising fluorescence spectroscopy *via* the tryptophan residues of the chiral receptors **3.3I**·2ClO_4 and **3.3H**·2ClO_4.

3.4 Optical chiral anion sensing studies with 3.3I·2ClO_4 and 3.3H·2ClO_4

Initially, photophysical studies were performed with **3.3I**·2ClO_4 in CH_3CN/ H_2O 7:3 *v/v*, with the UV-Vis spectrum revealing a broad absorption band at $\lambda_{abs,max}$ (ε/ M^{-1} cm^{-1}) at 280 nm (26 000), corresponding to the indole π-π* transitions of the host's tryptophan residues (Figure 3.9, red line).[27] Photoexcitation of the XB host at 280 nm resulted in a broad fluorescence spectrum with an intense emission maxima at $\lambda_{em,max}$ ~ 335 nm, displaying a Stokes shift of 55 nm, comparable to other tryptophan based complexes reported in the literature (Figure 3.9, blue dashed line).[27] The HB host exhibited a near identical fluorescence emission spectrum with $\lambda_{em,max}$ at 337 nm in the same solvent mixture, suggesting little influence of the iodotriazoles on the electronic levels of the respective tryptophan fluorophores.

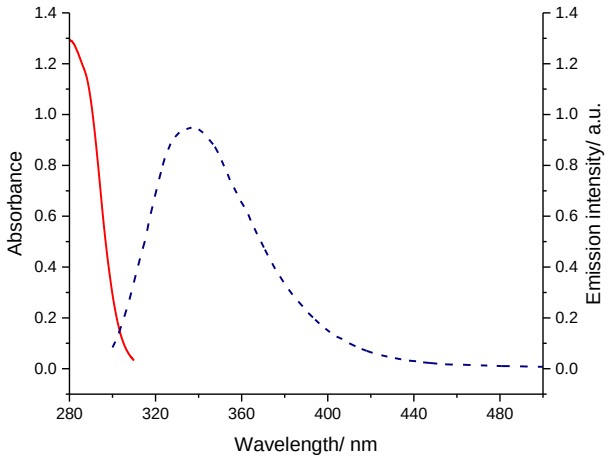


Figure 3.9: *Absorption (red line) and emission (blue dashed line) spectra of receptor* ***3.3I***·*2ClO₄ in CH₃CN/H₂O 7:3 v/v. ($\lambda_{abs,max}$ 280 nm, $\lambda_{em,max}$ 335 nm, [metallo-host] = 50 μM, T = 293 K). (N.B. The difference in excitation- and emission peak intensities are due to the different slitwidths utilised in each experiment.)*

Quantitative fluorescence titration experiments were undertaken by adding increasing quantities of chiral oxo-anions (Figure 3.5) as their TBA salts (up to 600 molar equivalents) to individual 50 μM solutions of **3.3I**·2ClO_4 and **3.3H**·2ClO_4 in CH_3CN/H_2O 7:3 *v/v* and the changes in emission intensity monitored.[§§§§] The responses of the XB and HB hosts to the individual *R*- and *S*-enantiomers of each of the carboxylate anions are displayed in Figures 3.10A and 3.10B respectively, with the horizontal red dashed line in each graph indicating the host's spectrum in the absence of any anion.

From Figure 3.10A (left and middle), detectable changes in the emission intensity of **3.3I**·2ClO_4 were evidenced with the (*N*Boc-(*R/S*)-leucine)$^-$, (*N*Boc-(*R/S*)-proline)$^-$ and (*N*Boc-(*R/S*)-mandelate)$^-$ carboxylates which all induced a general quenching of the tryptophan fluorescence without any changes in wavelength - except for (*N*Boc-(*R*)-leucine)$^-$ with which a slight overall enhancement in emission intensity was observed. Negligible spectral changes were seen during the titrations of (*N*Boc-(*R/S*)-alanine)$^-$, indicating that neither enantiomer of the chiral oxo-anion was interacting appreciably with **3.3I**·2ClO_4. Notably, monitoring the change in emission intensity

[§§§§] In order to prevent co-excitation of both the host and guest species, the binding of the target (*R/S*)-BINOL PO_4^- species was not investigated *via* fluorescence spectroscopy.

during each of the titrations show clear differences in the shape of the resulting binding isotherms for the respective *R*- and *S*- enantiomers of (*N*Boc-leucine)$^-$ and (*N*Boc-mandelate)$^-$ (Figure 3.10A right), indicating appreciable enantio-discrimination by the XB host.

In contrast, much larger luminescence emission spectral perturbations were evidenced when analogous titrations were performed with **3.3H**·2ClO$_4$ as shown in Figure 3.10B (left and middle). Whilst all of the chiral carboxylates brought about initial quenching of the tryptophan fluorescence, a significant overall 'switch on' in receptor emission was observed with each chiral anion guest pair *via* the subsequent, magnified enhancements in emission intensity (arising possibly due to conformational rigidification of the receptor which supresses non-radiative decay pathways) and further indicating greater sensitivity of **3.3H**·2ClO$_4$ to chiral anion sensing. Yet again, confirmation of the chiral discriminatory ability of the HB host can be seen from the corresponding binding isotherms (Figure 3.10B right), where the different guest enantiomers elicit varying magnitudes and steepness of emission intensities.

Anion association constants were determined by global spectral fitting of the titration data using the BindFit[28,29] software for all receptor-anion enantiomer combinations and the binding data for **3.3I**·2ClO$_4$ and **3.3H**·2ClO$_4$ are summarised in Table 3.1. Both receptors were found to bind the anion enantiomers in a 1:2 host-guest stoichiometry, however the magnitude of the second binding constant (K_{12}) was much smaller than the first (K_{11}) in all cases, suggesting weak peripheral association of the second anion with the bound complex likely driven by the electrostatic attraction of the host's divalent Zn(II)-metallocentre. Accordingly, only the values of K_{11} were used for determining the host's chiral selectivity (ξ) by taking the ratios of the association constants from each individual anion enantiomer (*i.e.* $\xi = K_S/ K_R$). For greater ease of comparison, Figure 3.11 further summarises the guest enantiomer preferences and magnitudes of enantioselectivity of both **3.3I**·2ClO$_4$ and **3.3H**·2ClO$_4$ collected in Table 3.1 visually.

(A) XB Zn(II)-Tripod **3.3I**·2ClO_4 + (*R/S*) oxo-anion$^-$

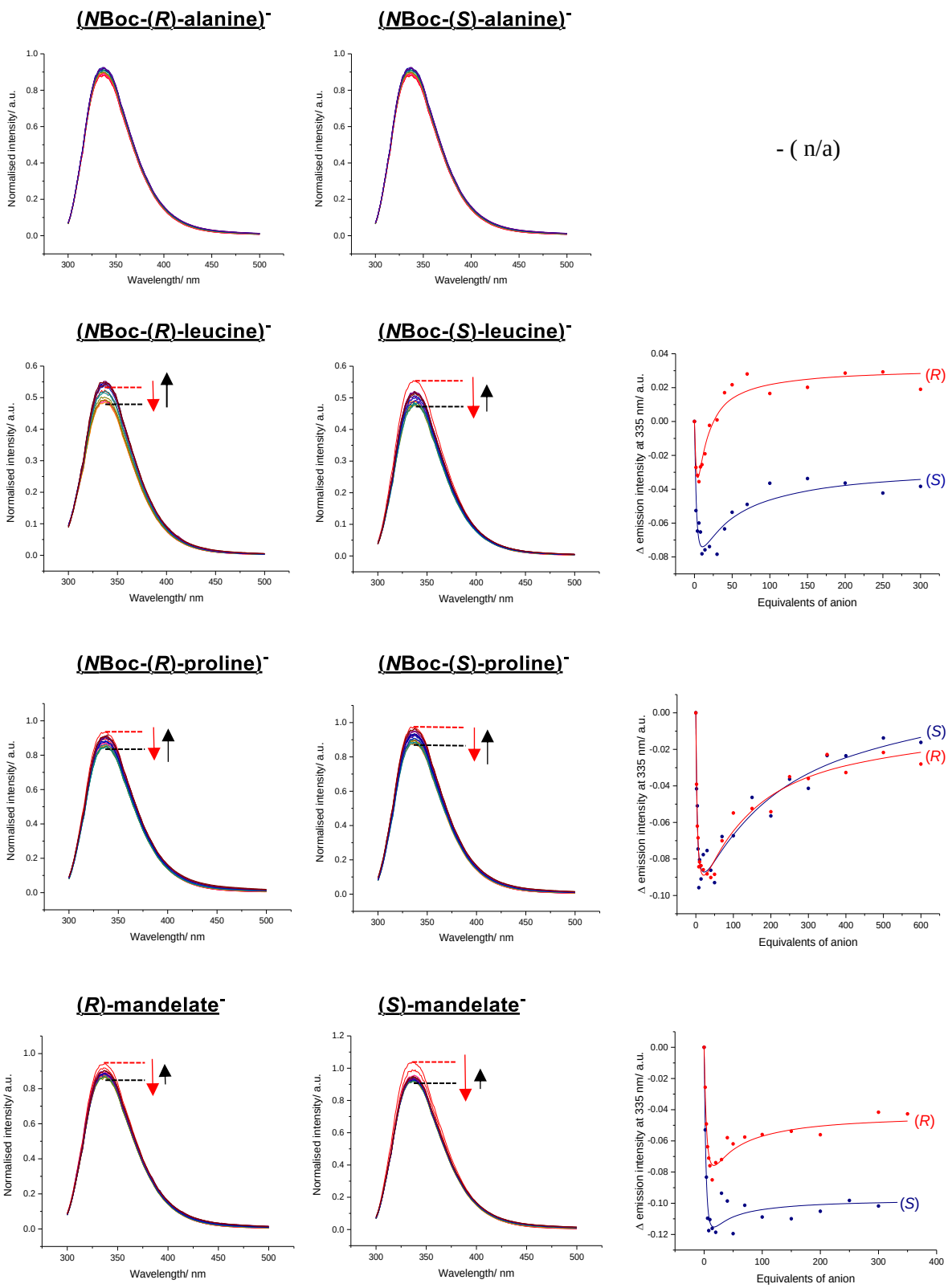


Figure 3.10A: *(Left and middle) changes in the fluorescence intensities of* ***3.3I***·2ClO_4*.in the presence of increasing quantities of chiral oxo-anion enantiomers added as their TBA salts.(*[*metallo-host] = 50 μM,* λ_{ex} *280 nm ,* CH_3CN*/* H_2O *7:3 v/v, T = 293 K). (Right) Corresponding binding isotherms monitoring changes in emission intensity as a function of R-/ S- enantiomer concentration.*

(B) HB Zn(II)-Tripod **3.3H**·2ClO_4 + (*R/S*) oxo-anion$^-$

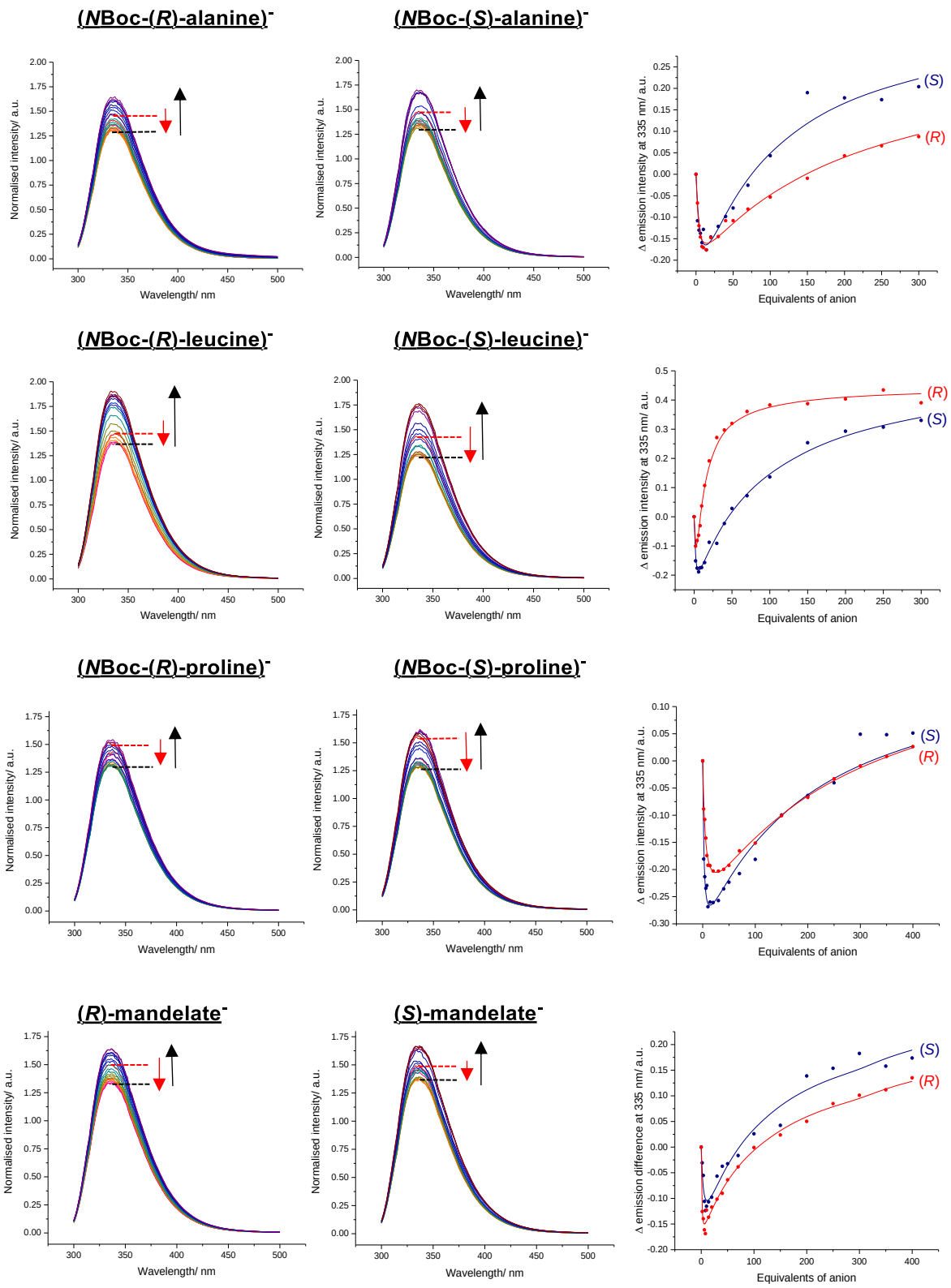


Figure 3.10B: *(Left and middle) changes in the fluorescence intensities of* ***3.3H***·*2ClO₄.in the presence of increasing quantities of chiral oxo-anion enantiomers added as their TBA salts.(*[metallo-host] = 50 μM, λ_{ex} 280 nm , CH_3CN/ H_2O 7:3 v/v, T = 293 K). (Right) Corresponding binding isotherms monitoring changes in emission intensity as a function of R-/ S- enantiomer concentration.*

Table 3.1: Anion association constants (K_a/ M^{-1}) for chiral anion pairs and the magnitudes of chiral selectivity ($\xi = K_S/K_R$) by the chiral Zn(II)-tripodal receptors **3.3I**·2ClO4 and **3.3H**·2ClO4 from fluorescence binding studies.[a]

Anion[b,c]	CH_3CN/ H_2O 7:3 *v/v*			
	3.3I·2ClO4 **XB**		**3.3H**·2ClO4 **HB**	
	K_a/ M^{-1}	ξ	K_a/ M^{-1}	ξ
(*N*Boc-(*S*)-alanine)$^-$	-[d]	-[e]	K_{11} = 3329 (199) K_{12} = 234 (5)	0.44 (0.03)
(*N*Boc-(*R*)-alanine)$^-$	-[d]		K_{11} = 7481 (299) K_{12} = 99 (1)	
(*N*Boc-(*S*)-leucine)$^-$	K_{11} = 12 044 (120) K_{12} = 594 (23)	1.33 (0.03)	K_{11} = 21 616 (1296) K_{12} = 222 (2)	2.39 (0.15)
(*N*Boc-(*R*)-leucine)$^-$	K_{11} = 9004 (180) K_{12} = 2251 (45)		K_{11} = 9025 (180) K_{12} = 2256 (40)	
(*N*Boc-(*S*)-proline)$^-$	K_{11} = 7762 (388) K_{12} = 90 (3)	1.31 (0.08)	K_{11} = 12 950 (907) K_{12} = 96 (2)	2.97 (0.23)
(*N*Boc-(*R*)-proline)$^-$	K_{11} = 5887 (235) K_{12} = 171 (3)		K_{11} = 4350 (130) K_{12} = 68 (1)	
(*S*)-Mandelate$^-$	K_{11} = 6766 (271) K_{12} = 1692 (67)	1.71 (0.09)	K_{11} = 5204 (416) K_{12} = 190 (4)	0.11 (0.01)
(*R*)-Mandelate$^-$	K_{11} = 3948 (158) K_{12} = 987 (69)		K_{11} = 47 927 (3834) K_{12} =167 (2)	

[a] A 1:2 host-guest binding model was used, unless otherwise stated, to determine the values of K_a from global fitting of the fluorescence titration spectra (monitoring the change in emission from 320-360 nm) using BindFit[28,29], errors (±) in parenthesis (<10%); $\xi = K_S/K_R$ only for the first binding event; [metallo-host] = 50 μM, λ_{ex} = 280 nm, T = 293 K. [b]Anions added as their TBA salt. [c]The binding of the fluorescent (*R/S*)-BINOL-PO_4^- enantiomers was not investigated to prevent co-excitation of both of the host and guest species. [d]Fluorescence changes too small to accurately determine K_a values. [e]Undetermined.

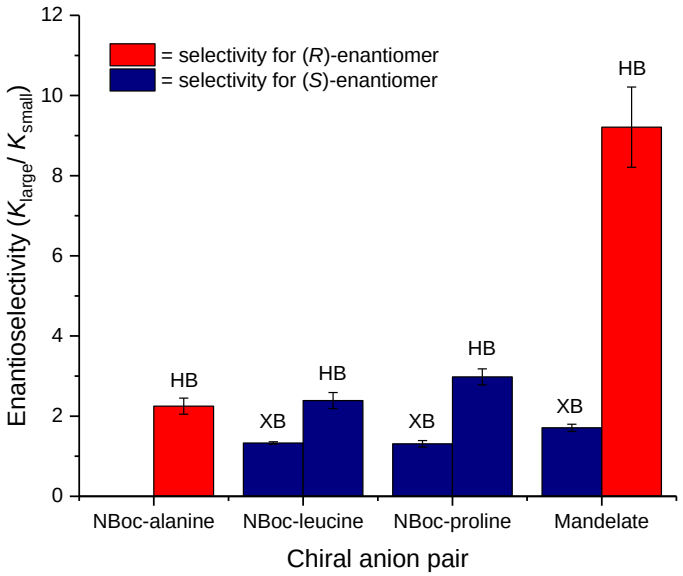


Figure 3.11: *Bar chart summarising the magnitudes of chiral selectivity and enantiomer binding preference by the tripodal receptors **3.3I**·2ClO4 and **3.3H**·2ClO4. (N.B. the enantioselectivity of NBoc-alanine with the XB host was undetermined and hence is not displayed in the bar chart).*

From inspection of the binding data in Table 3.1, receptors **3.3I**·2ClO_4 and **3.3H**·2ClO_4 show numerous differences which highlight the influences of XB on chiral discrimination. Firstly, all chiral anions, with the exception of (*N*Boc-(*R*)-proline)$^-$ and (*S*)-mandelate$^-$, exhibited superior binding strength with **3.3H**·2ClO_4 than with **3.3I**·2ClO_4, implying that the voluminous XB donor iodine atoms of **3.3I**·2ClO_4 impart a degree of steric hindrance to the overall anion recognition process. Notably, this was found to detrimentally impact on chiral discrimination, as **3.3I**·2ClO_4 displayed much lower chiral selectivity when compared to **3.3H**·2ClO_4 in all cases (Figure 3.11). For example, whilst the XB host **3.3I**·2ClO_4, showed the best enantio-selectivity of K_S/K_R = 1.7 for (*S*)-mandelate$^-$ over its (*R*)-isomer, it was outperformed by the HB host which gave an impressive selectivity of K_R/K_S = 9.2 for (*R*)-mandelate$^-$ over its (*S*)-isomer – with both receptors also curiously displaying opposite stereo-preferences. For the amino acid derivatives, reduced chiral discrimination of (*N*Boc-leucine)$^-$ and (*N*Boc-proline)$^-$ was exhibited by both XB and HB hosts, with **3.3H**·2ClO_4 showing greater variation in selectivity (ξ) between these respective oxo-anions whereas **3.3I**·2ClO_4 showed surprisingly uniform magnitudes of selectivity, independent of the steric bulk of the guest anion's R-group residue. Together the above observations seem to suggest that the XB tetrahedral chiral cavity of **3.3I**·2ClO_4 is too sterically congested and constrained for effective chiral discrimination, with the strict directionality requirements of XB imposing further restriction on the binding geometry of the chiral anions. On the other hand, substitution of the large XB donor iodines with much smaller hydrogen atoms results in a more open three-dimensional homochiral binding pocket of **3.3H**·2ClO_4, which is of sufficient size to enable better host-guest contact for chiral discrimination. This is most evident with the anion enantiomers of (*N*Boc-alanine)$^-$ which exhibited no binding with **3.3I**·2ClO_4 whereas **3.3H**·2ClO_4 afforded stereo-selectivity of K_R/K_S = 2.2 for (*N*Boc-(*R*)-alanine)$^-$ over the (*S*)-isomer – in particular, the reversal of enantiomer preference (*R*-selectivity) compared with the other two amino acids (*S*-selectivity) yet again serving to highlight the difficulty associated with the *a priori* prediction of enantioselectivity resultant from the chiral discrimination process.

3.5 Conclusions

To summarise, the research discussed in this chapter has demonstrated how substitution of HB donor prototriazoles with XB donor iodotriazoles in amino-acid derived, chiral metallo-tripodal host molecules can have significant impact on their stereoselective chiral anion recognition properties - for optimal XB-mediated chiral discrimination, additional considerations of the steric bulk of the XB-donor iodine atoms decorating the receptor's binding pocket should importantly be kept in mind in the design of potential 'constrained cavity' containing chiral XB host systems.

Initially, a novel chiral tris(*N*Boc-(*S*)-tryptophan)-appended XB Zn(II)-receptor **3.3I**·2ClO_4 was synthesised alongside the HB analogue **3.3H**·2ClO_4 and the enantio-discriminatory properties of the former host investigated *via* ^{1}H NMR titrations. Experiments in a range of competitive organic-aqueous solvent media revealed complex binding behaviour of various chiral oxoanions as well as solubility issues with the target axial chiral BINOL-PO_4^- species, which prevented the determination of quantitative binding data. Similar issues were encountered when analogous titrations were performed with an alternative novel tris(*N*Boc-(*S*)-leucine)-appended XB Zn(II)-host **3.6I**·2ClO_4. Utilisation of an optical sensing strategy, exploiting the tryptophan fluorescence of **3.3I**·2ClO_4 and **3.3H**·2ClO_4 enabled the derivation of association constants for the carboxylate oxo-anion enantiomers in the competitive aqueous-acetonitrile CH_3CN/ H_2O 7:3 *v/v* solvent mixture. Spectrofluorometric titrations revealed an overall quenching effect on the fluorescence response of **3.3I**·2ClO_4 with all chiral carboxylates whereas an overall 'switch-on' response was observed with **3.3H**·2ClO_4. More importantly, the presence of convergent iodotriazoles in the constrained chiral cavity of **3.3I**·2ClO_4 was found to have a detrimental influence on enantio-discrimination as the XB host displayed generally reduced chiral anion affinities and diminished stereo-selectivity compared to HB **3.3H**·2ClO_4, which was presumed to arise from the steric bulk of the XB donor iodine atoms preventing optimal host-guest contact for chiral discrimination.

3.6 Future work

As previously mentioned, all instances of chiral discrimination tend to obey the '*three-point'* model expounded in Section 3.1.1; thus for greater insight into the specific stereoselective interactions governing the experimentally observed enantioselectivity of **3.3I**·2ClO_4 and **3.3H**·2ClO_4 towards the various carboxylate enantiomers, computational modelling experiments such as molecular dynamics (MD) simulations and DFT calculations should be undertaken. Additionally, given the well-defined tetrahedral geometry of the XB receptor's homochiral binding pocket, the enantioselective recognition of a greater diversity of chiral phosphate-ester and phosphonate-ester anions which offer better size- and shape complementarity (in comparison to the amino-acid carboxylates previously studied) to **3.3I**·2ClO_4 should be investigated. Interesting potential candidates in this regard include the enantiomers of (i) the nerve-agent simulant pinacolyl methyl phosphonate $(PMP)^-$ (Figure 3.12A), which in its racemic form demonstrated augmented binding with the achiral XB Cu(II)-tripodal receptor **2.26I**·2OTf than the HB analogue **2.26I**·2OTf in the previous chapter (see Section 2.6.2.1 of Chapter Two), as well as (ii) 3-phenyl-2-((phosphonomethyl)amino)propanoate ($ppapH_3$) (Figure 3.12B) – a biologically relevant chiral phosphonate whose derivatives give rise to antibacterial and antifungal agents, a wide range of proteolytic enzyme inhibitors and haptens for catalytic antibodies.[30–32]

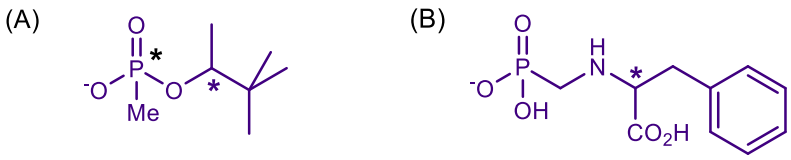


Figure 3.12: *Potential chiral phosphate-ester anionic species (A) PMP and (B) $ppapH_3$ for future XB-mediated chiral discrimination studies with* ***3.3I***·*2ClO_4. (Structures shown in the racemic form, stereocentres marked with an asterisk).*

3.7 References

1 F. R. Keene, Ed., *Chirality in Supramolecular Assemblies: Causes and Consequences*, John Wiley & Sons, Ltd, 2016.
2 H. H. Jo, C.-Y. Lin and E. V. Anslyn, *Acc. Chem. Res.*, 2014, **47**, 2212–2221.
3 G. A. Hembury, V. V. Borovkov and Y. Inoue, *Chem. Rev.*, 2008, **108**, 1–73.
4 M. G. Finn, *Chirality*, 2002, **14**, 534–540.
5 R. J. Phipps, G. L. Hamilton and F. D. Toste, *Nat. Chem.*, 2012, **4**, 603–614.
6 M. Mahlau and B. List, *Angew. Chem. Int. Ed.*, 2013, **52**, 518–533.
7 A. Mezzetti, J. D. Schrag, C. S. Cheong and R. J. Kazlauskas, *Chem. Biol.*, 2005, **12**, 427–437.
8 B. Baragaña, A. G. Blackburn, P. Breccia, A. P. Davis, J. de Mendoza, J. M. Padrón-Carrillo, P. Prados, J. Riedner and J. G. de Vries, *Chem. – Eur. J.*, 2002, **8**, 2931–2936.
9 A. Barnard, S. J. Dickson, M. J. Paterson, A. M. Todd and J. W. Steed, *Org. Biomol. Chem.*, 2009, **7**, 1554.
10 S. Bartoli, T. Mahmood, A. Malik, S. Dixon and J. D. Kilburn, *Org. Biomol. Chem.*, 2008, **6**, 2340–2345.
11 A. Akdeniz, T. Minami, S. Watanabe, M. Yokoyama, T. Ema and P. Anzenbacher, *Chem. Sci.*, 2016, **7**, 2016–2022.
12 H.-T. Feng, X. Zhang and Y.-S. Zheng, *J. Org. Chem.*, 2015, **80**, 8096–8101.
13 J. L. Sessler, A. Andrievsky, V. Král and V. Lynch, *J. Am. Chem. Soc.*, 1997, **119**, 9385–9392.
14 H. Miyaji, S.-J. Hong, S.-D. Jeong, D.-W. Yoon, H.-K. Na, J. Hong, S. Ham, J. L. Sessler and C.-H. Lee, *Angew. Chem. Int. Ed.*, 2007, **46**, 2508–2511.
15 J. Y. C. Lim, I. Marques, L. Ferreira, V. Félix and P. D. Beer, *Chem. Commun.*, 2016, **52**, 5527–5530.
16 J. Y. C. Lim, I. Marques, V. Félix and P. D. Beer, *J. Am. Chem. Soc.*, 2017, **139**, 12228–12239.
17 N. H. Evans and P. D. Beer, in *Chirality in Supramolecular Assemblies: Causes and Consequences*, ed. F. R. Keene, John Wiley & Sons, Ltd, 2016, pp. 142–158.
18 A. Berthod, *Anal. Chem.*, 2006, **78**, 2093–2099.
19 V. Sundaresan and R. Abrol, *Protein Sci.*, 2002, **11**, 1330–1339.
20 D. A. Lang, M. L. M. Mannesse, G. H. D. Haas, H. M. Verheij and B. W. Dijkstra, *Eur. J. Biochem.*, 1998, **254**, 333–340.
21 T. A. Müller, M. I. Zavodszky, M. Feig, L. A. Kuhn and R. P. Hausinger, *Protein Sci.*, 2006, **15**, 1356–1368.
22 E. Zhou, J. Zhang, Y. Lu and C. Dong, *ARKIVOC*, 2014, **v**, 351–364.
23 J. M. Granda and J. Jurczak, *Chem. – Eur. J.*, 2015, **21**, 16585–16592.
24 S. Kubik, *Chem. Soc. Rev.*, 2009, **38**, 585–605.
25 E. Valeur and M. Bradley, *Chem. Soc. Rev.*, 2009, **38**, 606–631.
26 W. S. Brotherton, R. J. Clark and L. Zhu, *J. Org. Chem.*, 2012, **77**, 6443–6455.
27 A. B. T. Ghisaidoobe and S. J. Chung, *Int. J. Mol. Sci.*, 2014, **15**, 22518–22538.
28 P. Thordarson, *Chem. Soc. Rev.*, 2011, **40**, 1305–1323.
29 D. B. Hibbert and P. Thordarson, *Chem. Commun.*, 2016, **52**, 12792–12805.
30 J.-S. Feng, M. Ren, Z.-S. Cai, K. Fan, S.-S. Bao and L.-M. Zheng, *Chem. Commun.*, 2016, **52**, 6877–6880.
31 J.-A. Ma, *Chem. Soc. Rev.*, 2006, **35**, 630–636.
32 D. Guest and B. Grant, *Biol. Rev.*, 1991, **66**, 159–187.

Chapter Four

A dimetallic halogen bonding cryptate for the recognition of inorganic polyphosphate anionic species

4 A dimetallic halogen bonding cryptate for the recognition of inorganic polyphosphate anionic species

4.1 Introduction

Derived from the Greek term '*kruptos*' meaning 'hidden', a *cryptand* refers to any bicyclic (or polycyclic) host molecule capable of binding guests within a crypt-like structure, interring them as in a burial. The term was first introduced by Lehn, Dietrich and Sauvage in the 1968 publication 'Les Cryptates',[1] in reference to these macrobicyclic hosts, as three-dimensional analogues of crown ethers, with superior strength and selectivity when complexing Group 1 metal cations (see Figure 1.1B of Chapter One). Since their pioneering work, a vast arena of cryptand and cryptand-type hosts has appeared establishing an independent field of supramolecular host-guest chemistry, in particular for anion receptor design.[2] This final R&D chapter introduces enclosed, primarily bicyclic cryptand anion hosts (Sections 4.1.1 and 4.1.2) and focuses on the construction of a novel ditopic XB metallo-cage envisaged for the encapsulation of *poly*phosphate anionic species such as inorganic triphosphate (see Figure 1.33A of Chapter one). Indeed in spite of the many well-known HB cryptand anion host systems, XB cryptands for anion recognition remain unprecedented with no examples reported in the literature. By virtue of its tripodal framework, the 'general XB metallo-tripodal motif' recurrent in Chapters Two and Three yet again presents itself as an ideal synthon, particularly for the assembly of a dimetallic XB cryptate host when appended with appropriate reactive functionalities (*vide infra*) and hence further features prominently herein.

4.1.1 Cryptands for anion recognition

Of the many classes of bicyclic anion receptors, most studied are those in which tertiary amines form the bridgeheads and as previously mentioned in Section 1.1.1 of Chapter One, these were historically also the first to be employed as anion hosts: Park and Simmons' original, di-aza aliphatic cryptands, known as '*katapinands*', in their protonated form, displayed internal binding of the halides (Cl^-, Br^- and I^-) in 50% deuterotrifluoroacetic acid aqueous solvent (Figure 1.1D).[3,4] After this seminal discovery, a variety of bis-tris(2-aminoethyl)amine (bistren) polyammonium

cryptands for the selective encapsulation of linear multi-atomic anions such as azide,[5] as well as the halides[6] were developed by Lehn and co-workers. For example, the 'tiny' hexaprotonated octa-aza polyammonium macrobicyclic host in Figure 4.1A exhibited selective recognition of fluoride in acidic aqueous media *via* two pyramidal arrays of three charge-assisted hydrogen bonds – the obtained association constant value of log K_a = 10.6 being the largest observed for fluoride at that time.[6] Another prominent example is Nelson's octa-aza cryptand containing heterocyclic furan bridges (Figure 4.1B), which similarly in the hexaprotonated state, was found to wholly encapsulate sulfate in tosylate media (log K_a = 7.21 in 0.1 M NaOTs).[7]

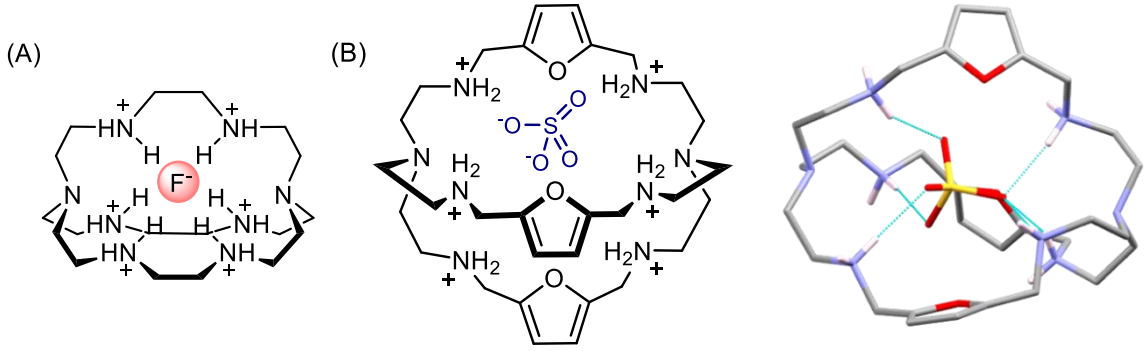


Figure 4.1: *Polyammonium cryptands for anion recognition. (A) Lehn's hexaprotonated 'C2-bistren' cryptand capable of F^- encapsulation.[6] (B) Nelson's furan-containing aza-cryptand and the crystal structure of its sulfate adduct (right).[7](HB interactions shown as blue dashed lines, counter-anions and most H-atoms have been omitted for clarity).*

Beyond these essentially pH-dependent secondary ammonium aza-hosts, bicyclic anion receptors have evolved over the years with various other HB-donating functionalities such as amides, thioamides, sulphonamides, ureas, thioureas and pyrroles, among a number of others, incorporated into their design.[2] For example, Bowman-James and co-workers prepared a cryptand incorporating six amide linker units (Figure 4.2A) which exhibited the greatest affinity for fluoride over the other halides (Br^- and Cl^-) and oxo-anions (OAc^-, $H_2PO_4^-$, NO_3^- and HSO_4^-) in d_6-DMSO.[8] As evidenced in the solid-state crystal structure of the fluoride adduct, the spherical anion is neatly centered within the cryptand's 'pinwheel-like' cavity and bound *via* a symmetric array of six convergent amide NH···F^- hydrogen bonds (Figure 4.2A right). Furthermore, other bridgeheads, most notably carbon and cyclophane have also been utilised. For example, Sessler and co-workers very recently reported a naphthobipyrrole-strapped calix[4]pyrrole (Figure 4.2B)[9] which vertically

bound azide (K_a = 6.35 x 10^5 M^{-1}) in CH_3CN, whilst Anslyn's bicyclic cyclophane (Figure 4.2C)[10] formed an inclusion complex with acetate (K_a = 770 M^{-1}) in CD_3CN/ $CDCl_3$ 3:1 *v/v*. The acetate-complexed solid state structure shows the planar acetate horizontally bound by a total of four HB interactions, with each acetate oxygen atom hydrogen bonded to two amide hydrogen atoms of the 2,6-pyridine diamide spacer units (Figure 4.2C right).

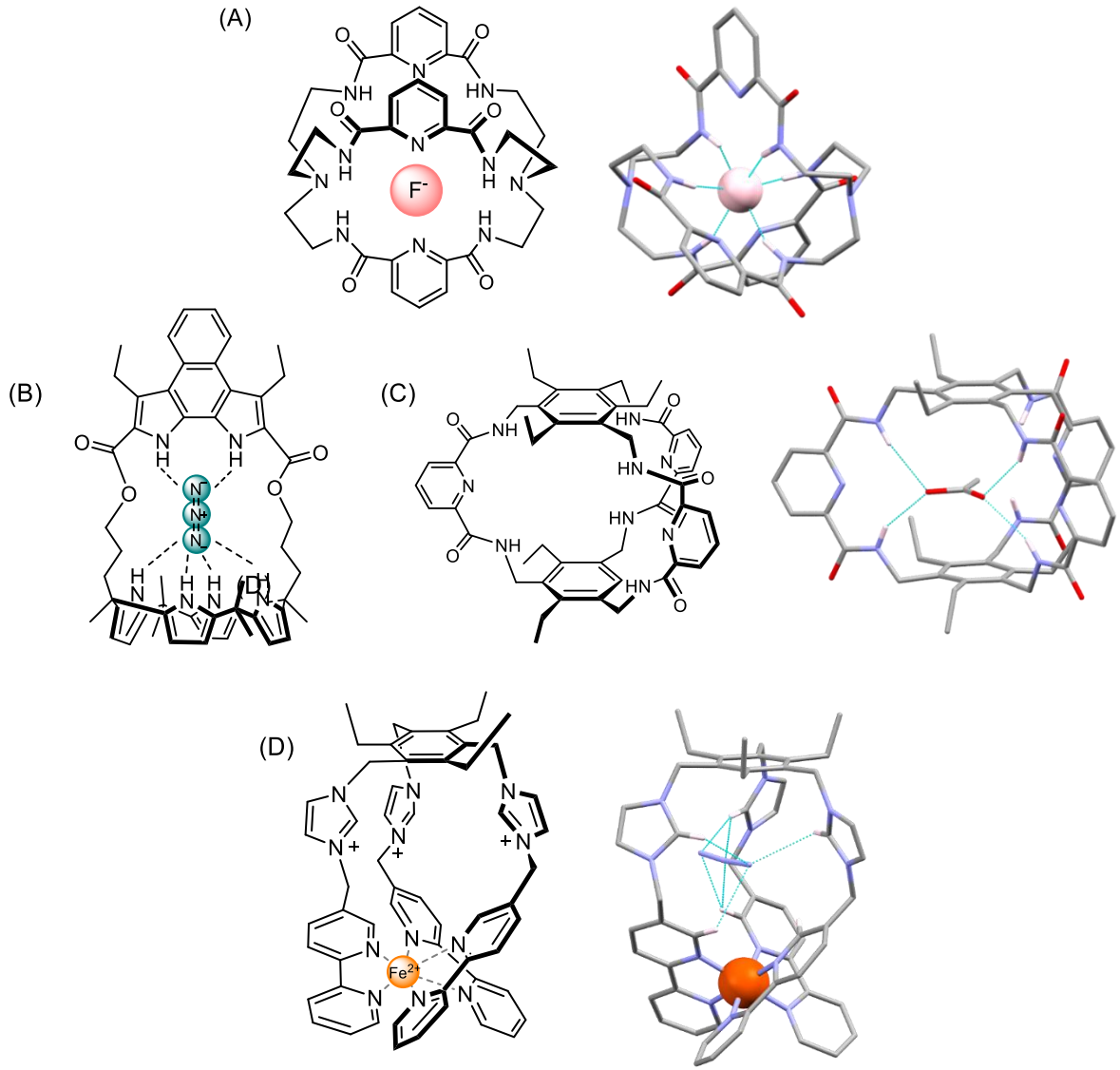


Figure 4.2: *(A)Bowman-James' hexa-amide cryptand and the crystal structure of its fluoride adduct (right);[8] (B) Sessler's azide-complexed strapped calix[4]pyrrole;[9] (C) Anslyn's bicyclic cyclophane and the crystal structure of its acetate adduct (right);[10] (D) Fabrizzi's cyclophane-derived Fe(II)-BIPY cryptand and the crystal structure of its azide adduct (right);[11] (HB interactions shown as blue dashed lines, counter-anions and most H-atoms have been omitted for clarity).*

Fabrizzi has also reported a more exotic cyclophane-derived tris-imidazolium cage where an Fe(II) cation serves to 'zip up' the cryptand by coordinating to the three pairs of bipyridine (BIPY)

nitrogen atoms of the tripodal ligand (Figure 4.2D).[11] The host exhibited a distinct selectivity for azide (log K_a = 5.7) in CH_3CN/ H_2O 4:1 *v/v*, which was ascribed to the multi-point hydrogen bonds established by its multiple imidazolium C-H^+, as well as BIPY C-H fragments with all of the nitrogen atoms of the anion - as evidenced in the solid state crystal structure of the corresponding azide adduct (Figure 4.2D right).

4.1.2 Ditopic cryptands for anion recognition

In addition to the above examples, a variety of ditopic cryptand hosts designed to profit from the metal-ligand interaction for anion binding have also been synthesised, bearing both cation and anion binding sites where the coordinated transition metal cations serve to 'tie-down' additionally bound anions.[12–14] These rather iconic enclosed molecules are known as dinuclear 'cascade complexes', termed after the two-step *cascade* mechanism by which the bistren derived cryptand sequentially includes first two equivalent metal centres (affording a 'cryptate') and then an ambidentate anion, as shown in Figure 4.3. In such complexes, the inclusion selectivity largely derives from the matching of the ambidentate anion's 'bite length' (*i.e.* the distance between two terminal donor atoms) and the distance between the axial positions of the two coordinatively unsaturated metal centres, which is ultimately related to the length of the spacer units (highlighted in green, Figure 4.3).[13]

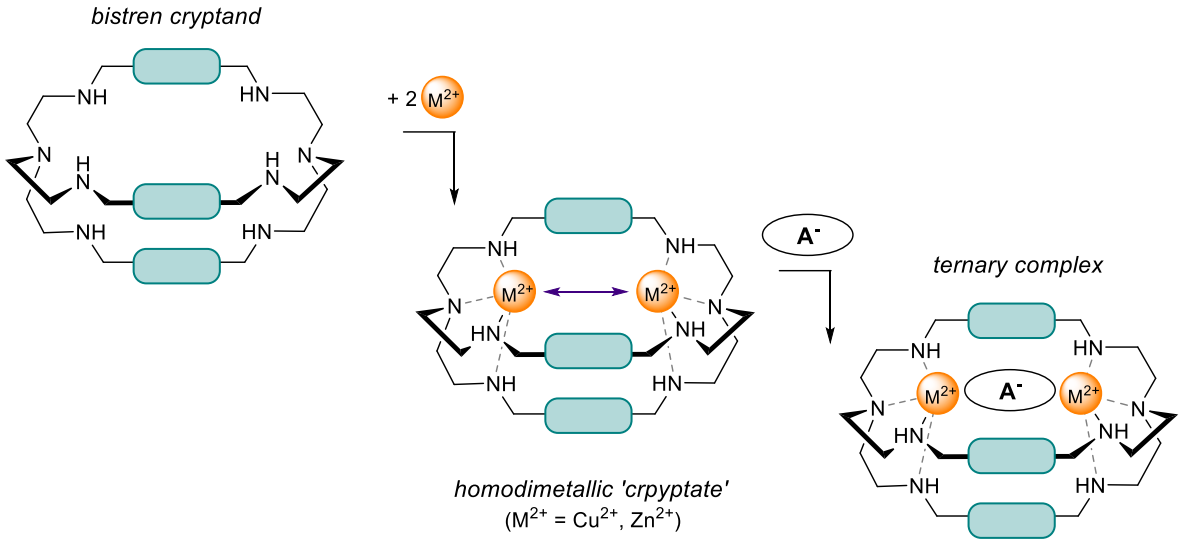


Figure 4.3: *The 'cascade' process for the inclusion of an Anion (A^-)into a bistren homodimetallic cage. (The ambidentate anion establishes a coordinative interaction with a coordinatively unsaturated M(II) centre ligated to each tren subunit).*[13]

The first example of a ditopic cryptate anion host was Lehn's diCu(II) cascade complex of an 'O-bistren' cage capable of recognising the polyatomic azide and cyanide anions in CH_3CN.[15] Since then, and exploiting the simple and high yielding synthetic procedure based on the Schiff base condensation of two molecules of tren with 3 molecules of dialdehyde, a variety of dimetallic bistren cryptates with different aromatic and heterocyclic spacer units have been constructed (Figure 4.4).

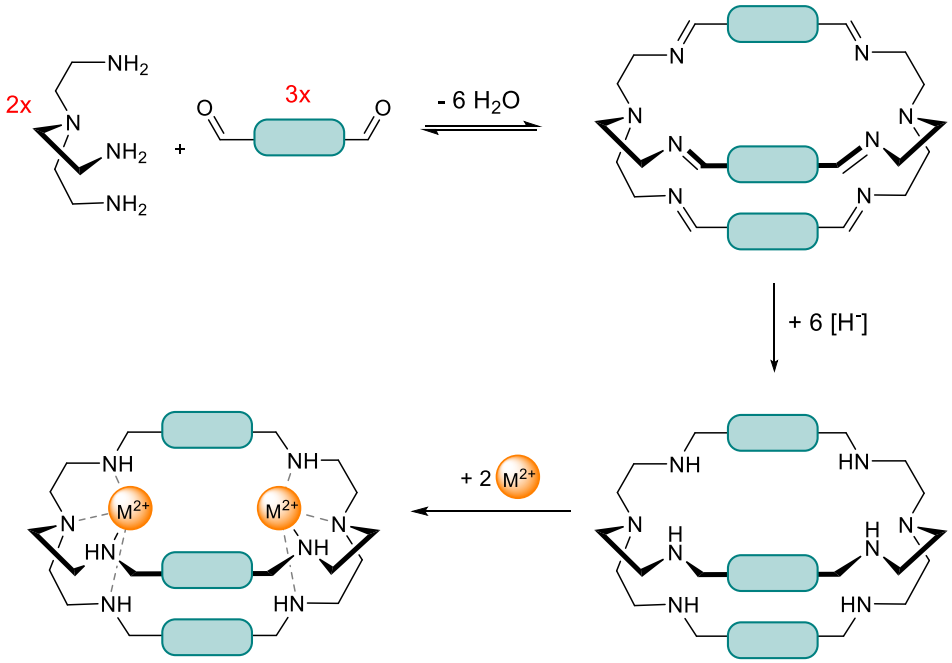


Figure 4.4: *Schematic representation of the three-step synthesis of a traditional dimetallic bistren cryptate. The first step involves the Schiff base condensation of 2 molecules of tren with 3 molecules of dialdehyde, followed by hydrogenation of the six imine bonds to yield a robust cage. In the final step, the complexation of 2 equivalent transition metals affords the dimetallic cryptate.*

For example, Fabrizzi and co-workers prepared a diCu(II) bistren cryptate containing *m*-xylyl spacer units (Figure 4.5A), which exhibited selectivity for azide (log K_a = 4.78) over other polyatomic anions (OAc^-, NO_3^-, NCS^-, SO_4^{2-}) in aqueous solution (buffered at pH 8).[16] As evidenced in the solid-state crystal structure of the azide adduct, the rod-like anion is collinearly bound within the cryptate's ellipsoidal cavity with the two terminal nitrogen atoms of the anion coordinated to the two Cu(II) centres (Figure 4.5A right).[17] Notably, the cryptate displayed no internal binding of the monoatomic halides which was ascribed to their inability to effectively bridge the two metal centres, as well as the rigidity of the *m*-xylyl spacer units preventing any endoergonic contraction

of the bistren framework. In contrast, when alternative 2,5-dimethylfuran spacers were utilised, the resultant smaller diCu(II) cryptate was able to encapsulate the Cl^- and Br^- anions, forming stable complexes in water (Figure 4.5B).[18]

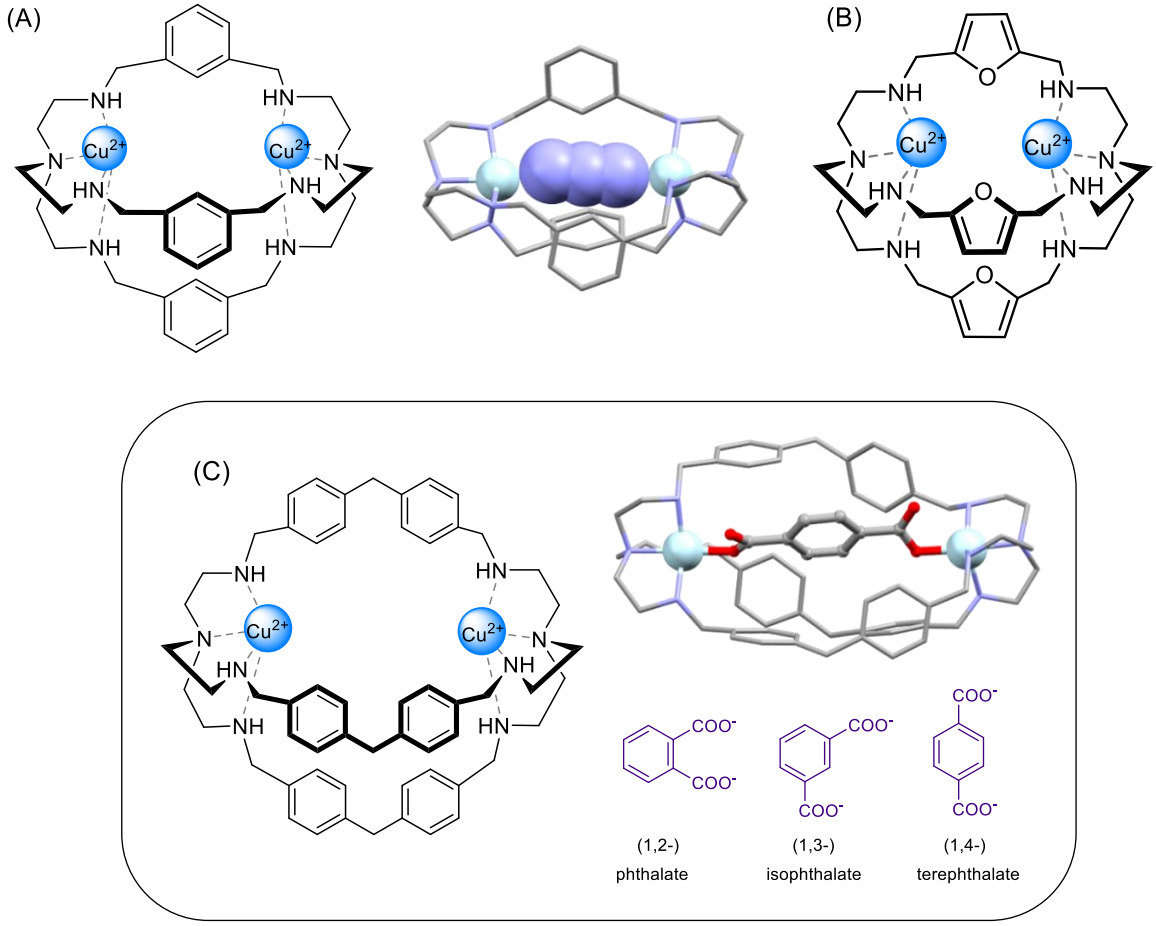


Figure 4.5: *(A) Fabrizzi's diCi(II)bistren cryptate with m-xylyl spacers*[16] *(left) and the crystal structure of the azide adduct (right);*[17] *(B) Fabrizzi's diCi(II)bistren cryptate with 2.5-dimethylfurane spacers, capable of halide encapsulation;*[18] *(C) Delgado's 'elongated' diCi(II)bistren cryptate (left) capable of discriminating between the positional isomers of phthalate (highlighted in purple) and the crystal structure of its inclusion complex with terephthalate (right).*[19] *(In all of the structures, counter-anions and most H-atoms have been omitted for clarity).*

By expanding the spacers with biphenylmethane functionalities, Delgado and co-workers also synthesised a more elongated and 'flexible' diCu(II) bistren cryptate for the inclusion of benzene dicarboxylate oxoanions (Figure 4.5C).[19] Out of the three positional isomers of phthalate studied, the host exhibited the highest affinity for terephthalate (log K_a = 9.79) in a EtOH/ H_2O 1:1 *v/v* mixture, which was attributed to the optimal 'O-O bite' of the latter 1,4-isomer. As shown in the solid state crystal structure of the cascade complex with terephthalate (Figure 4.5C top right), the

oxoanion encompasses beautifully the length of the main axis of the ellipsoid, with the terminal carboxylate atoms coordinated to the apical positions of the two trigonal bipyramidal Cu(II) centres.

Most recently and conversely employing ethylene di*amines* as bridges, Zonta has reported a novel dimetallic polyimine supramolecular cage constructed from the self-assembly of two tris(2-pyridylmethyl)amine (TPMA) derived Zn(II) tripodal trialdehyde subunits also *via* Schiff base chemistry (Figure 4.6).[20] The host was able to perform linear recognition of a series of aliphatic dicarboxylates of varying chain length (C_n where n = 4 to 14) in CH_3CN.

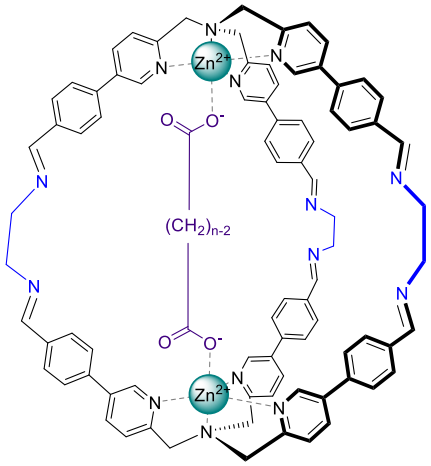


Figure 4.6: *Zonta's diZn(II) polyimine cage capable of recognising linear aliphatic dicarboxylates (trialdehyde derived subunits are highlighted in black and ethylene diamine linkers highlighted in blue, counter-anions not shown).*[20]

4.1.3 Chapter aims

Further building on the work in Chapter Two, and in keeping with the overall XB-mediated, phosphate-oriented molecular recognition goals of the thesis, this chapter aims to expand the use of the 'general XB metallo-tripodal motif' (Figure 2.4) for the construction of a novel, higher-order dimetallic XB cryptate host, envisaging its unique enclosed cavity to facilitate the multi-point binding of higher-order, inorganic *poly*phosphate anionic species (*vide infra*). By appending the tripodal XB leitmotif's '*arm*' fragments with a triad of reactive aldehyde functionalities, cage formation is investigated specifically using a di-amine based [2+3] imine condensation synthetic strategy.

4.2 Towards a dimetallic Zn(II) XB cryptate host

4.2.1 General design

The design of the target dimetallic XB cryptate **4.9I**·4ClO$_4$ shown in Figure 4.7 is based upon two individual derivatives of the 'general XB metallo-tripodal motif' (highlighted in black) covalently linked together by three aliphatic ethylene diamine linkers (highlighted in blue). The enclosed cavity thus features two distinct tetrahedral binding pockets, with two diametrically opposed Zn(II) metal apices and a total of six convergent XB-donor iodotriazoles, which are positioned ideally for XB interactions with a prospective bridging guest that contains two tetrahedral anionic 'heads' – such as an inorganic *poly*phosphate, for example, inorganic triphosphate (PPPi) (see Figure 1.33A of Chapter One).

.

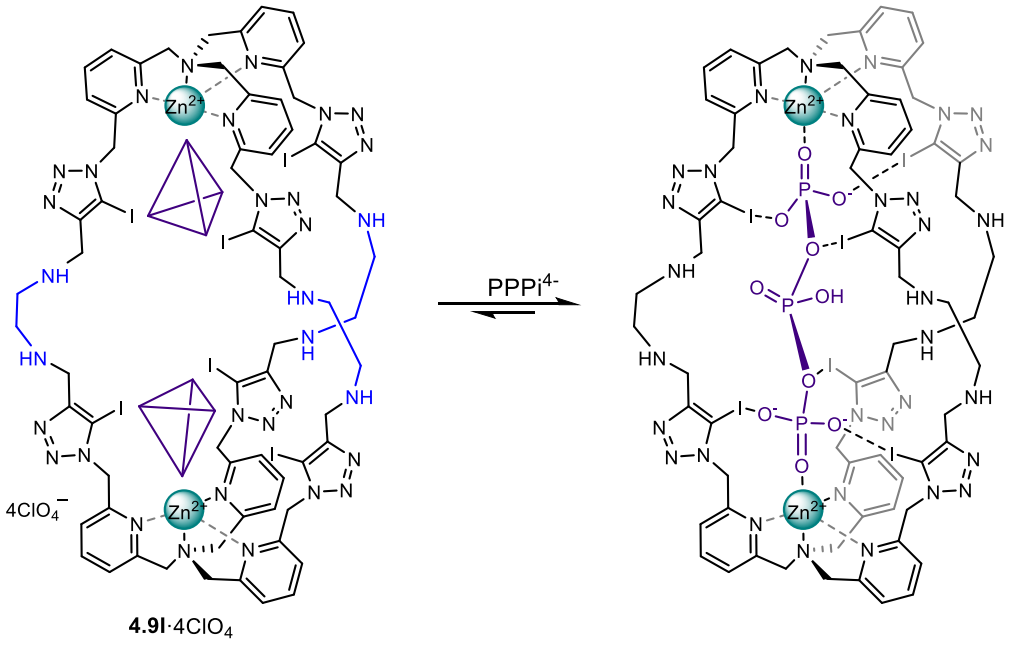
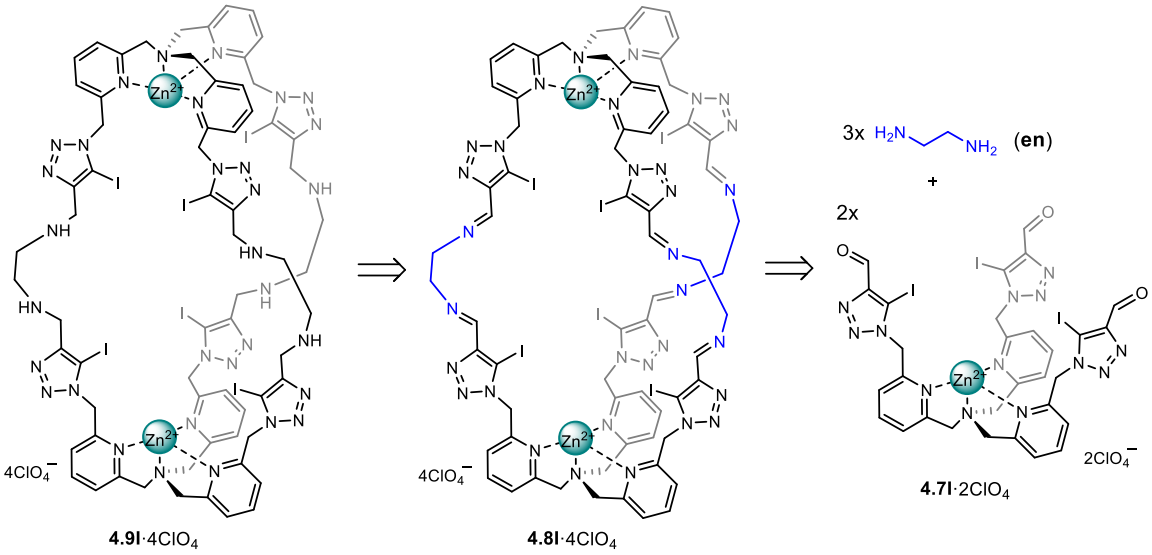


Figure 4.7: *The design of the target diZn(II) XB cryptate* ***4.9I***·*4ClO$_4$ (left) and also shown with the proposed binding mode of the inorganic polyphosphate anion PPPi^{4-} (right) .*

4.2.2 Synthetic attempts towards **4.9I**·4ClO$_4$

Derived from the retrosynthetic analysis of the target XB cryptate **4.9I**·4ClO$_4$, a Schiff-base synthetic strategy involving the '[2+3]' imine condensation of two 'facially coordinating' molecules of the pre-organised tris-aldehyde appended XB Zn(II)-tripod **4.7I**·2ClO$_4$ with three

molecules of commercially available ethylene diamine (**en**), was envisaged as a convenient route for the formation of the initial enclosed polyimine cryptate framework **4.8I**·4ClO$_4$ (Scheme 4.1) – with the direct conjugation of the opportunely positioned aldehyde appendages to the electron-withdrawing iodotriazoles in particular expected to increase their electrophilicity and hence favour imine formation with the **en** linkers. Subsequent reduction of the six C=N imine bonds would afford the desired robust diZn(II) XB cryptate host **4.9I**·4ClO$_4$.

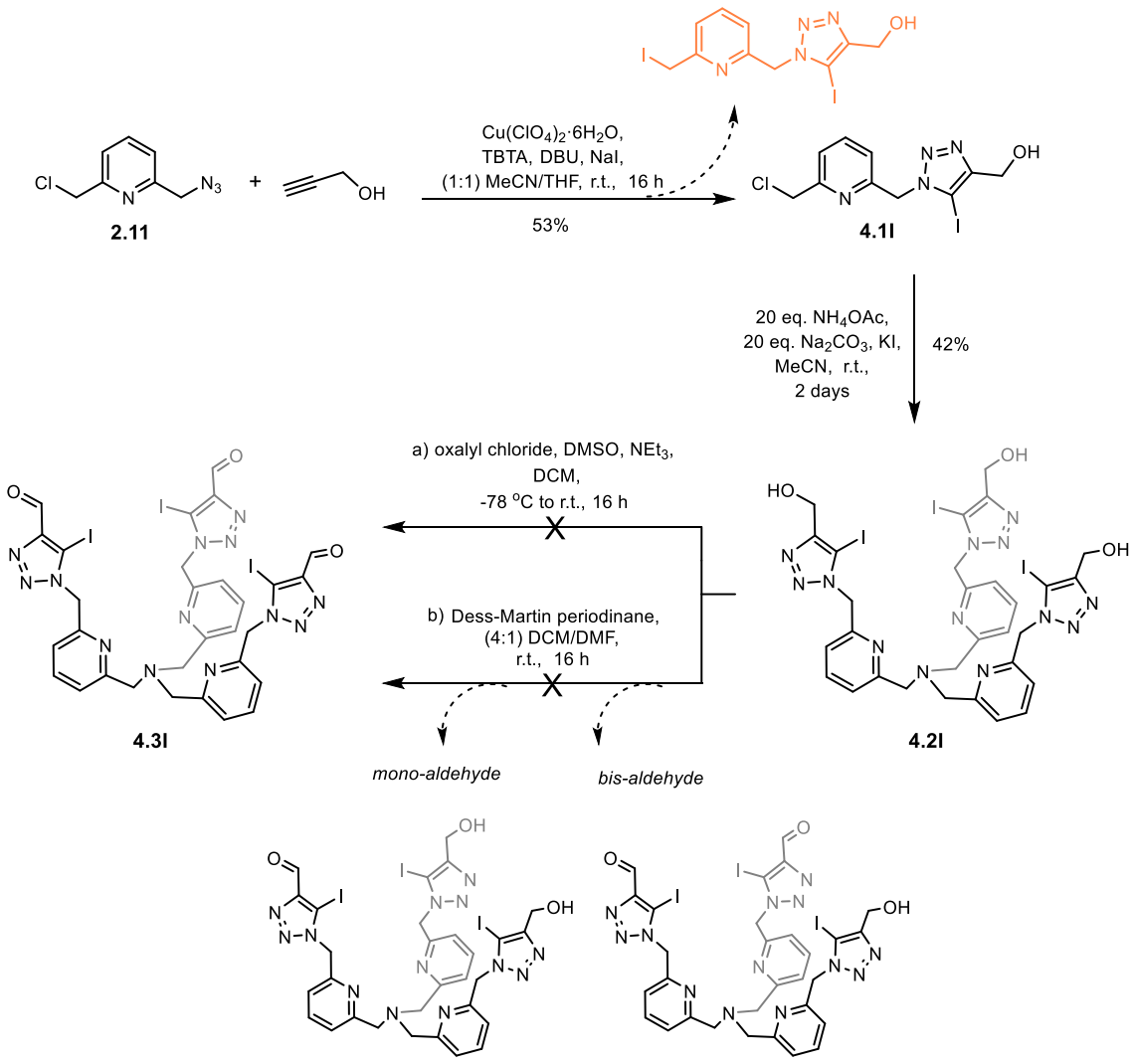


Scheme 4.1: *Retrosynthetic analysis of* ***4.9I***·*4ClO$_4$.*

Accordingly initial synthetic efforts were targeted towards the preparation of the key XB Zn(II)-tripodal synthon **4.7I**·2ClO$_4$, derived from the *apo*-Zn(II) precursor ligand **4.3I** (Scheme 4.2). Commercially available propargyl alcohol was first reacted with the chlorinated azide **2.11** under one-pot 'iodo-Click' conditions to afford the primary alcohol-appended XB '*arm*' **4.1I** in 53% yield.[*****] Reaction of **4.1I** with excess NH_4OAc and Na_2CO_3 (20 equivalents of each) in MeCN at room temperature afforded the corresponding tris-alcohol XB tripodal ligand **4.2I** in 42% yield after

[*****] During the purification process, a second compound was found to partially co-elute with **4.1I**. This was identified by ESI-MS analysis (peak at *m/z* = 456.9 $[M + H]^+$) as the corresponding '6-(iodomethyl)pyridine-*arm*' (highlighted in orange, Scheme 4.2). This was presumed to have formed due to the use of excess NaI in the respective iodo-CuAAC and re-combined with the chlorinated analogue **4.1I** for further use in the tripodal ligand formation step.

purification *via* repeated recrystallisations from a hot MeOH solution. Subsequently, oxidation to form the corresponding tris-aldehyde XB tripodal derivative **4.3I** was attempted, first through a 'Swern' oxidation of **4.2I** (by dissolving an excess of oxalyl chloride and DMSO in DCM at -78°C after which the tris-alcohol and NEt_3 were added), and also by alternatively utilising an excess of the 'milder' Dess-Martin periodinane oxidant in DCM at room temperature.



Scheme 4.2: *Initially attempted synthesis of the tris-aldehyde appended XB ligand* ***4.3I****.*

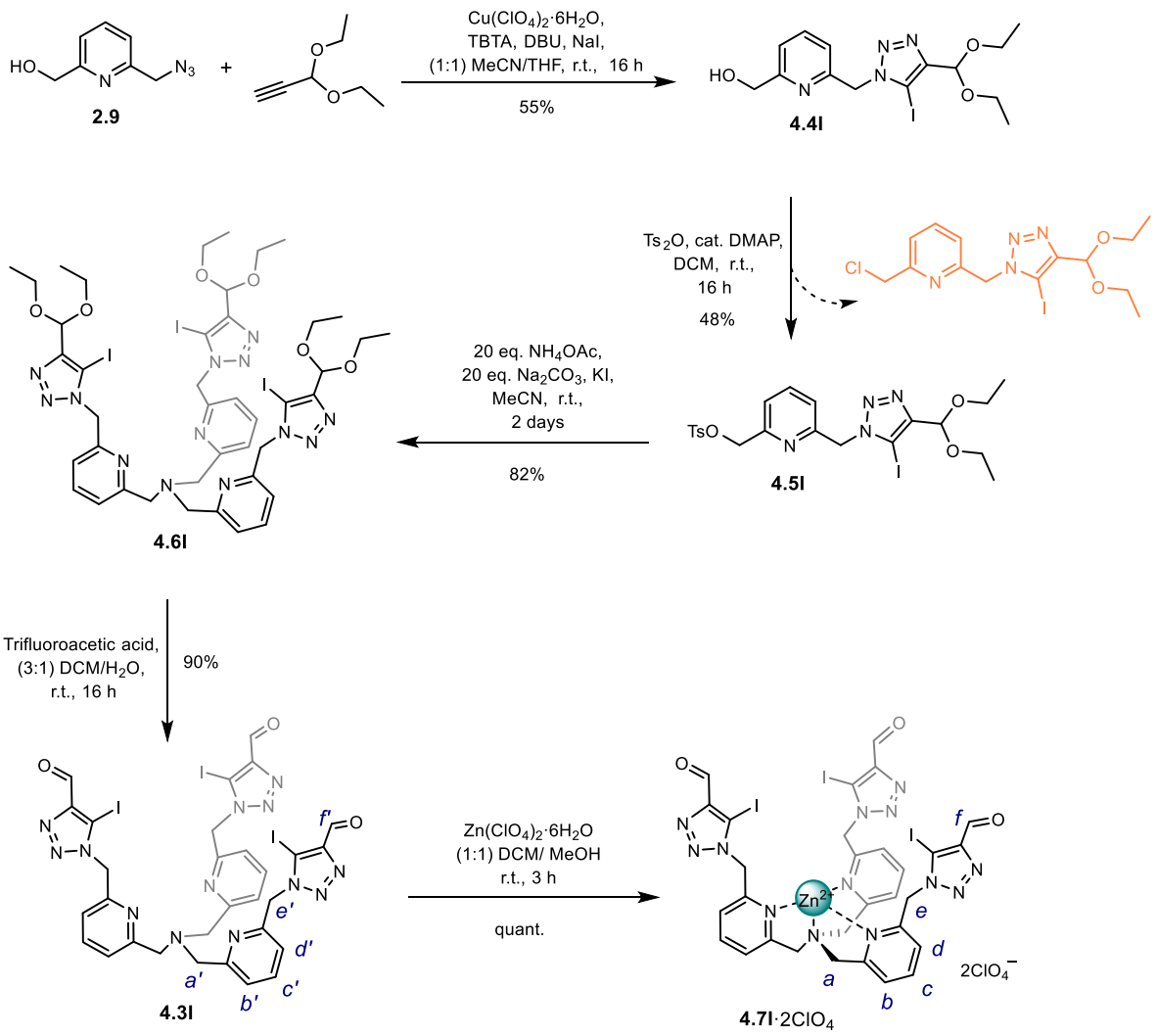
However, ESI-MS analysis of the crude reaction mixtures in each attempt revealed distinct peaks at *m/z* = 1000.0 $[M + H]^+$, 997.9 $[M + H]^+$ and 995.9 $[M + H]^+$ corresponding to the formation of the mono, bis- and tris-aldehyde derivatives respectively – which was attributed to the poor

solubility of **4.2I** in chlorinated solvents. Subsequent purification efforts *via* preparative TLC unfortunately failed to separate the components.

The alternate 'acetal deprotection' strategy using the diethyl acetal-appended XB tripodal precursor **4.6I** proved to be much more successful (Scheme 4.3). Following Zhu's one-pot iodo-CuAAC protocol, the reaction between azide **2.9** and commercially available 3,3-diethoxy-1-propyne produced the XB-donor containing synthon **4.4I** in 55% yield after chromatographic purification. Through treatment with *p*-toluenesulfonic anhydride, the corresponding tosylated '*arm*' derivative **4.5I** was produced[†††††] and reacted with excess portions of NH_4OAc and Na_2CO_3 (20 equivalents of each) in MeCN at room temperature over two days. Pleasingly, after trituration with a cold Et_2O solution, the ^{1}H-NMR of the crude product indicated no further purification was necessary and thus the diethyl acetal-appended tripodal ligand **4.6I** was isolated in an impressive 82% yield. Deprotection of the acetal protecting groups proceeded *via* reaction with trifluoroacetic acid in DCM/H_2O (3:1) and afforded the tris-aldehyde XB ligand **4.3I** in 90% yield. Subsequent complexation with a stoichiometric quantity of zinc(II) perchlorate hexahydrate produced the desired metallo-aldehyde XB tripodal subunit **4.7I**·$2ClO_4$.

The ^{1}H-NMR spectrum of **4.7I**·$2ClO_4$ compared to the *apo*-Zn(II) precursor ligand **4.3I** (in CD_3CN) is displayed in Figure 4.8. **4.7I**·$2ClO_4$ displayed pronounced downfield shifts of its core pyridyl proton $H_{b\text{-}d}$ and methylene proton H_a signals which confirmed ligation of the TPMA cavity to the Zn(II) center, while the distal aldehyde proton H_f signal of the aldehyde appendages experienced a comparatively minor upfield shift.

[†††††]During the chromatographic purification process, a second compound was also isolated in an appreciable quantity and later identified by ESI-MS analysis (peak at *m/z* = 437.0 $[M + H]^+$) as the corresponding '6-(chloromethyl)pyridine-*arm*' (highlighted in orange, Scheme 4.3). This was presumed to have formed due to the use of chlorinated DCM solvent in the respective tosylation step and as a consequence of the increased lability of the C-OTs bond, which is typical of 2-pyridinemethyl tosylated systems.[21]
The alternate '*arm*' was simply re-combined with the tosylated analogue **4.5I** for further use in the tripodal ligand formation step.



Scheme 4.3: *Synthetic pathway for* ***4.7I***·$4ClO_4$ *following the 'acetal deprotection' strategy.*

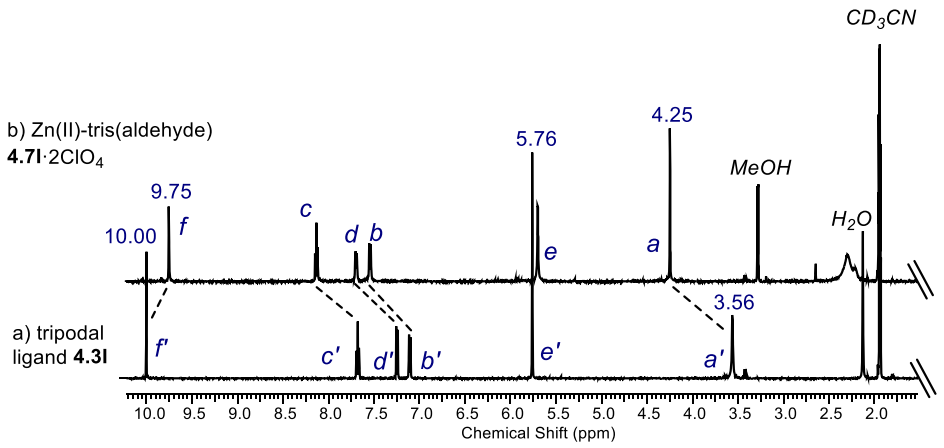
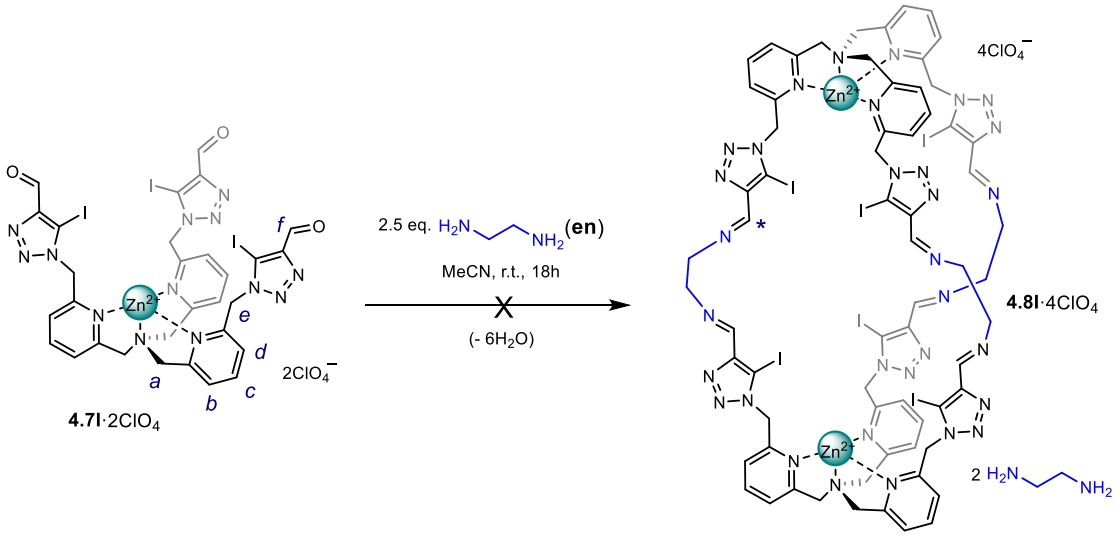


Figure 4.8: *^1H NMR spectra of (a) the tripodal ligand* ***4.3I*** *and (b) XB Zn(II)-tripod* ***4.7I***·$2ClO_4$ *(in CD_3CN, 500 MHz, T = 298 K) Assignments follow those in Scheme 4.3.*

With the key tris-aldehyde in hand, synthesis of the target dimetallic XB cryptate **4.8I**·4ClO_4 was attempted following the literature protocol reported by Zonta and co-workers[20]: the appropriate Schiff base condensation was carried out by treating a solution of **4.7I**·2ClO_4 in MeCN under strict dilution conditions with 2.5 equivalents of **en** per equivalent of **4.7I**·2ClO_4 (Scheme 4.4). The **en** solution was slowly added portion-wise over a period of 6 hours and the reaction mixture was left to stir for a further 6 hours at room temperature, during which a white precipitate was formed.



Scheme 4.4: *Initially attempted Schiff base reaction towards XB cage* ***4.8I***·4ClO_4 *according to Zonta's protocol.*[20]

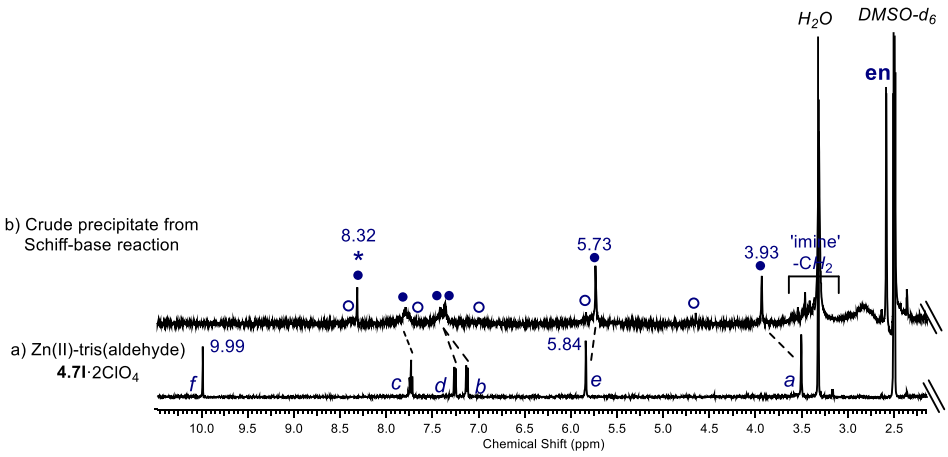


Figure 4.9: *^{1}H NMR spectra of (a)* ***4.7I***·2ClO_4 *and (b) the precipitate from the crude Schiff base reaction mixture. (in DMSO-d_6, 500 MHz, T = 298 K) Assignments follow those in Scheme 4.4. (Filled and hollow dots indicate major and minor species, respectively).*

After filtration and despite its poor solubility in a variety of organic solvents, the ^{1}H-NMR spectrum of the resultant crude precipitate was obtained in DMSO-d_6 which, along with the comparative ^{1}H-NMR of the precursor XB tripodal subunit **4.7I**·2ClO$_4$, is displayed in Figure 4.9. Pleasingly, the complete disappearance of the key aldehyde proton H$_f$ signal at 9.99 ppm and the appearance of a singlet peak further upfield in the diagnostic imine-N*H* region *ca*. 8.32 ppm indicated the complete consumption of the tris-aldehyde precursor and hence successful imine condensation. Indeed, whilst a single set of signals (highlighted by the filled blue dots) corresponding to the core H$_{a-e}$ protons of the precursor **4.7I**·2ClO$_4$ were retained (as expected) in the ^{1}H-NMR of the crude product, the critical presence of *multiple* imine-C*H*$_2$ resonances (largely buried under the water peak) implied the inequivalence of the imine methylene protons and was thus suggestive of the formation of a non-enclosed XB polyimine species. Furthermore, the presence of a duplicate set of H$_{a-e}$ proton signals of lower intensity, (highlighted by the hollow blue dots in Figure 4.9) indicated the presence of an additional, very minor, polyimine XB species.

To shed light on the identity of the obtained products, ESI-MS analysis was further performed where distinct peaks at *m/z* = 1218.2, 1241.1 and 1284.1 were evidenced in the mass spectrum of the crude precipitate. Although the identity of the first peak at *m/z* = 1218.2 could not be definitively ascertained, the peak at *m/z* = 1284.1 corresponds to the monoperchlorate adduct of the 1+3 imine condensation product of one molecule of **4.7I**·2ClO$_4$ with three molecules of **en**, while the peak at *m/z* = 1241.1 corresponds to the monoperchlorate adduct of the analogous 1+2 imine condensation product (Figure 4.10). Given the total absence of the aldehyde H$_f$ proton signal in the ^{1}H NMR spectrum of the crude precipitate however (Figure 4.9), it is reasonably assumed that the latter peak arises due to partial hydrolysis of the 1+3 condensation product in the mass spectrometer. Notably, the single set of the H$_{a-e}$ proton signals of the 'major' product observed in the respective ^{1}H NMR (Figure 4.9) correspond very well with the C_{3v} symmetric structure of the 1+3 imine condensation product, which was hence confirmed as the major product produced from the Schiff base cryptate formation attempt. Presumably, its poor solubility prevented the effective completion of the '2+3'

imine condensation reaction and as a consequence the desired XB cryptate framework **4.8I**·2ClO_4 was unfortunately unable to be obtained.

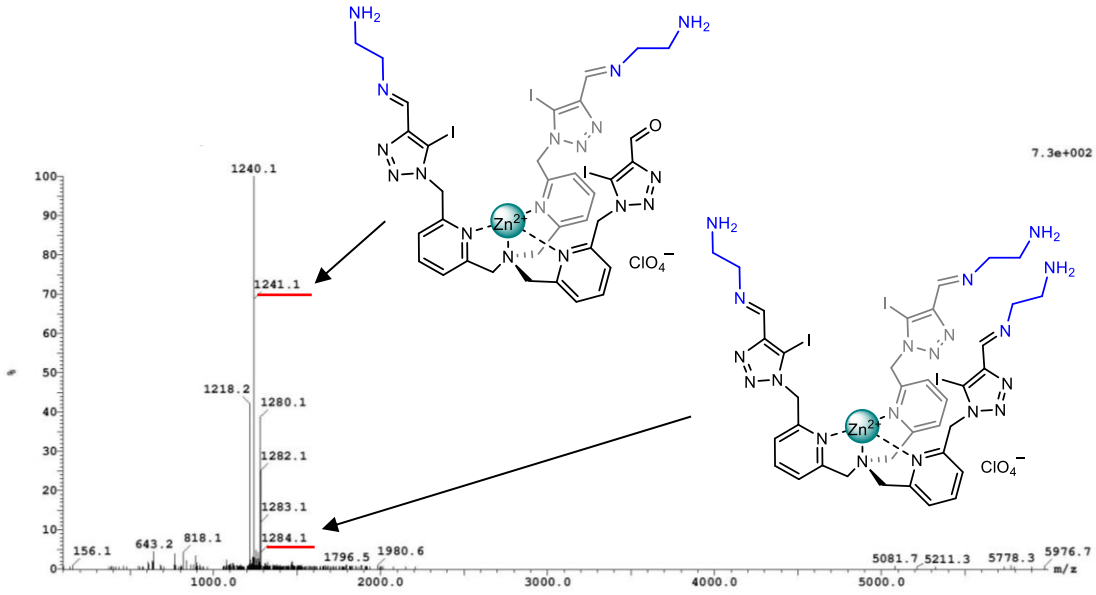


Figure 4.10: *ESI-MS of the precipitate formed from the Schiff base reaction of* ***4.7I***·2ClO_4 *with* ***en****.*

4.3 Conclusions and future work

To conclude, the work presented in this chapter has explored, for the first time, the use of a di-amine based [2+3] Schiff base condensation synthetic strategy towards the construction of an unprecedented dimetallic XB cryptate anion host **4.9I**·4ClO_4. A novel tris-aldehyde appended XB metallo-tripodal subunit **4.71**·2ClO_4 was initially prepared *via* an acetal deprotection strategy and subsequently employed with a stoichiometric quantity of **en** linkers in the polyimine cage formation reaction in MeCN. Whilst imine formation was clearly evidenced *via* ^{1}H NMR spectroscopy, solubility issues of the resultant '1+3' intermediate product unfortunately prevented the formation of the desired '2+3' polyimine XB cryptate framework **4.8I**·2ClO_4.

Future work with **4.71**·2ClO_4 should thus involve attempting Schiff base XB cryptate formation in alternative solubilising solvents, and, perhaps also utilising anion templation methods to aid the self-assembly of the cage framework. For example, by using the target $PPPi^{4-}$ guest as a templating anion to bridge two subunits of **4.71**·2ClO_4, successful '2+3' imine formation may be achieved.

4.4 References

1 B. Dietrich, J. M. Lehn and J. P. Sauvage, *Tetrahedron Lett.*, 1969, **10**, 2889–2892.
2 S. O. Kang, J. M. Llinares, V. W. Day and K. Bowman-James, *Chem. Soc. Rev.*, 2010, **39**, 3980–4003.
3 C. H. Park and H. E. Simmons, *J. Am. Chem. Soc.*, 1968, **90**, 2429–2431.
4 C. H. Park and H. E. Simmons, *J. Am. Chem. Soc.*, 1968, **90**, 2431–2432.
5 J. M. Lehn, E. Sonveaux and A. K. Willard, *J. Am. Chem. Soc.*, 1978, **100**, 4914–4916.
6 B. Dietrich, J.-M. Lehn, J. Guilhem and C. Pascard, *Tetrahedron Lett.*, 1989, **30**, 4125–4128.
7 J. Nelson, M. Nieuwenhuyzen, I. Pál and R. M. Town, *Dalton Trans.*, 2004, 2303–2308.
8 S. O. Kang, J. M. Llinares, D. Powell, D. VanderVelde and K. Bowman-James, *J. Am. Chem. Soc.*, 2003, **125**, 10152–10153.
9 S. H. Kim, J. Lee, G. I. Vargas-Zúñiga, V. M. Lynch, B. P. Hay, J. L. Sessler and S. K. Kim, *J. Org. Chem.*, 2018, **83**, 2686–2693.
10 A. P. Bisson, V. M. Lynch, M.-K. C. Monahan and E. V. Anslyn, *Angew. Chem. Int. Ed. Engl.*, 1997, **36**, 2340–2342.
11 V. Amendola, M. Boiocchi, B. Colasson, L. Fabbrizzi, M.-J. R. Douton and F. Ugozzoli, *Angew. Chem. Int. Ed.*, 2006, **45**, 6920–6924.
12 V. Amendola, L. Fabbrizzi, C. Mangano, P. Pallavicini, A. Poggi and A. Taglietti, *Coord. Chem. Rev.*, 2001, **219–221**, 821–837.
13 V. Amendola, M. Bonizzoni, D. Esteban-Gómez, L. Fabbrizzi, M. Licchelli, F. Sancenón and A. Taglietti, *Coord. Chem. Rev.*, 2006, **250**, 1451–1470.
14 G. Alibrandi, V. Amendola, G. Bergamaschi, L. Fabbrizzi and M. Licchelli, *Org. Biomol. Chem.*, 2015, **13**, 3510–3524.
15 J. M. Lehn, S. H. Pine, E. Watanabe and A. K. Willard, *J. Am. Chem. Soc.*, 1977, **99**, 6766–6768.
16 L. Fabbrizzi, P. Pallavicini, L. Parodi and A. Taglietti, *Inorganica Chim. Acta*, 1995, **238**, 5–8.
17 C. J. Harding, F. E. Mabbs, E. J. L. MacInnes, V. McKee and J. Nelson, *J. Chem. Soc. Dalton Trans.*, 1996, 3227–3230.
18 V. Amendola, E. Bastianello, L. Fabbrizzi, C. Mangano, P. Pallavicini, A. Perotti, A. M. Lanfredi and F. Ugozzoli, *Angew. Chem. Int. Ed.*, 2000, **39**, 2917–2920.
19 P. Mateus, R. Delgado, V. André and M. T. Duarte, *Inorg. Chem.*, 2015, **54**, 229–240.
20 C. Bravin, E. Badetti, F. A. Scaramuzzo, G. Licini and C. Zonta, *J. Am. Chem. Soc.*, 2017, **139**, 6456–6460.
21 R. Ding, Y. He, X. Wang, J. Xu, Y. Chen, M. Feng and C. Qi, *Molecules*, 2011, **16**, 5665–5673.

Chapter Five

Conclusions

5 Conclusions

The work described in this thesis was focused on the incorporation of halogen bond (XB) donor groups into C_{3v} symmetric metallo-tripodal host frameworks, strategically designed utilising the 'lock and key' principle, for the selective recognition and sensing of phosphate anionic species.

Chapter Two introduced the novel, tris(iodotriazole) encompassing 'general XB metallo-tripodal motif' which was demonstrated to be an effective structure for tetrahedral anion guest binding. Through modification of its XB '*arm*' fragments with a triad of various octyl chain, ferrocene, TEG and pm*β*CD appendages, a family of Zn(II)- and Cu(II)-based XB redox-active, optical and water-soluble tripodal sensory hosts were constructed which exhibited potent inorganic monophosphate and simple phosphate-ester recognition capabilities, impressively in competitive aqueous-organic solvent mixtures containing up to 40% water. Extensive ^{1}H NMR, voltammetric and UV-Vis anion binding studies revealed each of the XB hosts as superior anion complexants when compared to their tris(prototriazole) containing HB metallo-tripodal host counterparts, not only exemplifying the halogen bonding interaction as a strong alternative to the ubiquitous hydrogen bond for molecular recognition but also providing further *rare* evidence of the ability of XB receptors to preferentially bind 'harder' *oxo*anions over the 'softer' and less strongly solvated halides, as well as augment their recognition in aqueous environments.

Building on these findings and with the aim of further exploiting its unique 'constrained cavity', **Chapter Three** expanded the use of the 'general XB metallo-tripodal motif' for the enantioselective chiral anion recognition of a series of biologically-relevant carboxylate oxoanions and BINOL phosphate-ester anion enantiomers. By extending its arm fragments specifically with a triad of enantiopure *N*Boc-(*S*)-tryptophan and *N*Boc-(*S*)-leucine based functionalities, the first examples of amino acid-derived *homochiral* XB Zn(II)-tripodal receptors were prepared. Whilst ^{1}H NMR titrations with both XB systems in a range of organic-aqueous solvent media revealed complex binding behaviour of various chiral *α*-amino acid carboxylates as well as solubility issues with the target axial chiral BINOL-PO_4^- species which prevented the determination of quantitative

binding data, the chiral discrimination properties of the tris(*N*Boc-(*S*)-tryptophan) XB host were determined by means of fluorescence anion binding experiments in the competitive CH_3CN/H_2O 7:3 *v/v* solvent mixture. Surprisingly, the presence of convergent iodotriazoles was found to have a detrimental influence on enantio-discrimination as the XB host elicited generally reduced chiral anion affinities and diminished stereo-selectivity compared to the chiral HB host analogue., This was presumed to arise from the steric bulk of the XB donor iodine atoms stymieing optimal host-guest contact for chiral discrimination, thus underscoring the importance of steric considerations in the design of potential 'constrained cavity' containing XB host systems.

Continuing with the theme of XB-mediated phosphate recognition, **Chapter Four** presented synthetic efforts to incorporate the 'general XB metallo-tripodal motif' into a more complex, unprecedented dimetallic XB cryptate host architecture envisioned for the encapsulation of higher-order inorganic *poly*phosphate anionic species. Specifically, self-assembly of the target diZn(II) XB cage was explored utilising dynamic imine chemistry, *via* a [2+3] Schiff base condensation reaction between two molecules of a novel XB Zn(II)-tripodal subunit appended with a triad of reactive aldehyde functionalities with three molecules of ethylene diamine linkers. Whilst the complete consumption of the XB tris(aldehyde) substrate and successful polyimine formation was observed in the ^{1}H NMR spectrum of the crude precipitate, ESI-MS analysis revealed largely the presence of the intermediate '1+3' condensation product – presumably its poor solubility hampered the effective completion of the '2+3' imine condensation reaction and as a consequence the desired initial XB cryptate framework was unable to be obtained.

To summarise, the results described herein have demonstrated the efficacy of preorganised metallo-tripodal halogen bonding host systems in overcoming the formidable challenges of phosphate anion recognition, even in highly competitive aqueous solvent mixtures. The 'general XB metallo-tripodal motif' in particular, has been further shown to be an indispensable synthetic building block, allowing for the construction of exotic chiral C_{3v} symmetric XB metallo-hosts, as well as key synthons capable of enabling access ultimately to more complex, phosphate-selective

supramolecular XB host systems. The latter in particular provides an exiting avenue of exploration for future synthetic endeavours.

Chapter Six

Experimental

6 Experimental

6.1 General considerations

6.1.1 Solvents and reagents

All solvents, deuterated solvents and reagents were purchased from commercial sources and used as received unless otherwise stated. Anhydrous organic solvents were obtained by purging with N_2 and then dehydrated by passing through an MBraun MPSP-800 column. Water was de-ionised and micro filtered using a Milli-Q® Millipore machine. Where mixtures of solvents were used, ratios reported are by volume. Brine refers to a saturated aqueous solution of NaCl and $NH_4OH_{(aq)}$ refers to an approximately 28-30% solution of NH_3 in water. All tetrabutylammonium (TBA) salts (apart from the TBA chiral anion salts) as well as $[Cu(MeCN)_4][PF_6]$, $Zn(ClO_4)_2 \cdot 6H_2O$, $Zn(OTf)_2$ and $Cu(OTf)_2$ were stored in a vacuum desiccator at room temperature with P_2O_5 desiccant prior to use. All TBA chiral anion salts were stored in a vacuum desiccator with P_2O_5 desiccant at -20 °C in order to prevent racemisation. Triethylamine was distilled from and stored over KOH pellets. Thin layer chromatography (TLC) analysis was performed using Merck aluminium-backed DC 60 F_{254} 0.2 mm silica precoated plates, with spots visualised under UV light (254 nm) and/ or staining with basified aqueous $KMnO_4$ solution followed by gentle heating. Column chromatography was undertaken using silica gel (particle size: 40-63 μm) under a positive pressure of nitrogen. Preparative TLC was performed using Analtech glass-backed pre-coated plates (20 × 20 cm, 0.1 cm silica thickness). Literature procedures were used to prepare known compounds as referenced in the text. TBTA was synthesised as described[1] and stored under ambient conditions.

Safety note: Organic azides, NaN_3, 1,2,3-triazoles and the amide coupling agent HOBt used throughout this thesis are potentially explosive. While no problems were encountered in the course of this work, they should be handled with care and in small quantities. In particular, direct heating under reduced pressure should, wherever possible, be avoided. Especially for reactions with NaN_3, chlorinated solvents (i.e. CH_2Cl_2, $CHCl_3$ and CCl_4) should be strictly avoided even for reaction

work-ups due to their potential for forming highly explosive poly-azidomethanes.[2,3] In addition, NaN_3 should not be used in the presence of acids due to formation of highly toxic $HN_{3(g)}$.[4] If this is unavoidable, the reaction should be performed strictly in the fume hood.

6.1.2 Instrumentation

^{1}H and ^{13}C NMR spectra were recorded using Bruker Avance III 400 HD nanobay NMR spectrometers (Hg400 or Venus400) each equipped with a 9.4 T magnet, or a Bruker Avance III 500 machine (AVD500) equipped with a 11.75 T magnet (and cryoprobe) at T = 298 K. Chemical shifts are quoted in parts per million (ppm) with signal splittings denoted using standard abbreviations: singlet (s), doublet (d), doublet of doublets (dd), triplet (t), quartet (quart.), quintet (quint.), multiplet (m) and broad (br). ^{1}H-^{1}H coupling constants are reported as 3-bond (^{3}J) unless otherwise indicated, in Hertz (Hz) and to the nearest 0.1 ppm. Spectra were recorded relative to the residual solvent peak and assigned with the aid of 2D COSY NMR spectroscopy. Low and high resolution ESI mass spectra were recorded on a Waters LCT premier spectrometer and a Bruker microTOF spectrometer respectively. pH measurements of solutions of complexes in aqueous and aqueous-organic media were performed using a Hanna pH meter. Isothermal titration calorimetry experiments were performed on a Microcal PEAQ-ITC automated system and an iTC MicroCalorimeter. EPR spectra were recorded using a Bruker EMXmicro continuous wave (CW) spectrometer (X-band) at T = 95 K. UV-Vis and Fluorescence spectra were recorded on a T60U (PG Instruments Ltd) spectrophotometer and a Jobin Yvon Horiba FluoroLog 3 respectively at T = 293 K, using a Hellma quartz cuvette with path length of 1 cm. Optical rotation data were measured on a Perkin-Elmer 241 polarimeter with a path length of 1 dm (using the 589 nm sodium D), with concentrations (c) reported in g/100 mL and temperatures reported in °C.

6.1.3 ^{1}H-NMR titration protocols

Spectra for all ^{1}H-NMR titrations were performed on the Bruker Avance III 500 spectrometer (AVD 500) operating at 500 MHz and at T = 298 K.

- **Aqueous-organic and Organic solvent mixtures**

In a typical titration experiment, a 0.5 mL initial volume of the host (**2.16I/H**·$2ClO_4$, **2.20I/H**·$2ClO_4$, **3.3I**·$2ClO_4$, **3.6I**·$2ClO_4$) was used at a concentration of either 1.0 mM or 1.5 mM. Solutions of anions (50 mM and 75 mM, respectively) as their tetrabutylammonium salts were added in aliquots, the samples thoroughly shaken and spectra recorded at 0, 0.2, 0.4, 0.6, 0.8, 1.0, 1.2, 1.4, 1.6, 1.8, 2.0, 2.5, 3.0, 4.0, 5.0, 7.0 and 10.0 equivalents of anion (0.2 eq = 2 μL). The chemical shift of the appropriate proton environments was monitored over the course of the titration. Where titrations were performed in aqueous-organic mixtures, the spectra were referenced to the residual organic solvent peak and where titrations were performed in organic mixtures, the spectra were referenced to the solvent with the greatest number of deuterium atoms. In all cases where association constants were calculated, bound and unbound species were found to be in fast-exchange on the NMR timescale, except for the titrations with $TBAH_2PO_4$.

The chemical shift at each guest concentration were entered into the WINEQNMR2[5] software package for every titration point and estimates for the binding constant and limiting shifts were made. The parameters were refined by non-linear least-squares regression analysis using either a host-guest 1:1 or 1:2 stoichiometric binding model (as appropriate) to obtain the best-fit between the observed and calculated chemical shifts, until convergence was reached. Estimates for the standard error of the association constant calculated were provided by the program, as a standard deviation. However, these errors only account for the fitting of the binding isotherm to the titration data and do not account for the any systematic errors associated with the experimental procedure *e.g.* the incorrect addition of titrant solution.

- **Aqueous titration of 2.25I**·$2ClO_4$ **with NaI**

A 0.5 mL initial volume of the host was used at a concentration of 1.0 mM in unbuffered D_2O. A 200 mM solution of sodium iodide was added in aliquots, the samples thoroughly shaken and the spectra recorded at 0, 1.0, 2.0, 5.0, 10.0, 20.0, 40.0, 60.0, 80.0 and 100.0 equivalents of anion (1.0 eq = 2.5 μL). A trace amount of acetone was added as an internal reference, such that it made up

less than 0.05% of the total volume, and all spectra referenced to its resonance at 2.10 ppm. No changes in chemical shift of any of the host's proton resonances were observed upon anion addition and hence no further data manipulation was undertaken.

6.1.4 Electrochemical titration protocols

All Cyclic voltammetry (CV), differential pulse voltammetry (DPV) and square wave voltammetry (SWV) voltammetric measurements discussed in Chapter Two were performed using an Autolab Potentiostat/Galvanostat model PG-STAT 12 (Metrohm Autolab, Netherlands), using a standard single compartment three-electrode electrochemical cell placed inside a Faraday cage and the data processed using the OriginPro 2015 software package. In each case, titrations were performed in the stated solvent systems at T = 293 K.

- **Anion titrations of 2.20I/H**·$2ClO_4$ **in CH_3CN/ H_2O 9:1 *v/v***

A glassy carbon solid disc working electrode (3 mM diameter, BASi), platinum wire counter electrode and a non-aqueous Ag/ $AgNO_3$ reference electrode (prepared as described[]) was used, in a 0.1 M $TBAClO_4$ electrolyte solution. Prior to performing redox titration experiments, the redox reversibility of each receptor was first studied by recording successive CV scans at scan rates of 25, 50, 75, 100, 250 and 300 mV s^{-1} (see Appendix B for more details). After establishing receptor redox quasi-reversibility and reproducibility of each receptor's Fc/ Fc^+ $E_{1/2}$ value, electrochemical DPV titrations were carried out using a 2 mL initial volume of the host at a concentration of 0.5 mM and the measurements typically performed with 1 s equilibration time, a step potential of 1 mV and a scan rate of 100 mV s^{-1}. Solutions of anions (200 mM) as their tetrabutylammonium salts were added in aliquots, the samples thoroughly mixed by mechanical agitation and the voltammograms recorded at 0, 0.5, 1.0, 3.0, 5.0, 7.0 and 10.0 equivalents of anion (1.0 eq = 5 μL). The delta $E_{1/2}$ value from 0 to 10.0 equivalents anion were recorded in each case.

- **Titrations of 2.26I/H**·2OTf **with TBABr in CH_3CN**

The same three-electrode cell was used with the same working and counter electrodes as stated above except using a Ag/ AgCl (3.4 M KCl) leak-free reference electrode (Innovative Instruments)

in a 0.1 M $TBAClO_4$ supporting electrolyte solution. All experiments were conducted in Argon purged solutions under an Argon blanket. The working electrode was polished with alumina slurry (0.05 μm) before each experiment. (In order to circumvent the development of junction potentials of the latter reference electrode in the presence of various ions a Ag/ AgCl reference electrode with a Pt wire frit was utilized for titration experiments). Prior to performing redox titration experiments, the redox reversibility of each receptor was first studied by recording successive CV scans at scan rates of 25, 50, 75, 100, 200, 400, 600 and 800 mV s^{-1} (see Appendix C for more details). After establishing receptor redox quasi-reversibility and reproducibility of each receptor's Cu^{I}/Cu^{II} $E_{1/2}$ value, electrochemical SWV titrations were carried out using a 0.9 mL initial volume of the host at a concentration of 0.5 mM and the measurements recorded with 1 s equilibration time, utilising a frequency of 25 Hz, an amplitude of 20 mV and a step potential of 2 mV. A 100 mM solution of TBABr was added in aliquots, the samples thoroughly mixed by mechanical agitation and the voltammograms recorded at 0, 1.0, 2.0, 10.0, 20.0, 35.0, 60.0 and 100.0 equivalents of anion (1.0 eq = 4.5 μL). The delta $E_{1/2}$ values were recorded and plotted against the concentration of anion. The resulting binding isotherms were curve fit as described by Schöllhorn.[6]

Electrochemical reversibility studies of **2.26I/H**·2OTf in water were also performed by recording CV scans (at the same scan rates as above) and a SWV voltammogram (using the same parameters as above). The same three-electrode cell was used as above, with the same working, counter and reference electrodes instead in a 0.05 M KPF_6 supporting electrolyte solution. A host solution of 0.25 mM was used for all measurements.

6.1.5 Isothermal Calorimetry (ITC) titration protocols

All isothermal titration calorimetry experiments discussed in Chapter Two, were performed on a Microcal PEAQ-ITC automated system and an iTC MicroCalorimeter in distilled water at T = 298 K.

- **Anion titrations of 2.25I·$2ClO_4$ in water (buffered at pH 7.4 with 10 mM HEPES)**

An initial concentration of the host of 0.2 mM was used, with individual 20 mM solutions of Na_2HPO_4, NaBr and NaI added in 35 aliquots. The data from the first addition of 0.5 μL was discarded, with the data collected for the subsequent 34 additions of 1 μL. Heats of dilution were measured by a preliminary titration of each anion solution as their sodium salts into buffered water (pH 7.4 with 10 mM HEPES). Subtraction of this control data from the anion titration data indicated negligible heat changes evolved in each case and hence no further data manipulation was undertaken.

- **Cu(II) titrations of 2.24I and 2.35I in unbuffered water**

An initial concentration of the host of 0.5 mM was used, with a 4 mM solution of $CuOTf_2$ added in 35 aliquots. The data from the first addition of 0.5 μL was discarded, with data collected for the subsequent 34 additions of 1 μL. Heats of dilution were measured by a preliminary titration of $CuOTf_2$ into unbuffered water. Values of K_a and ΔH were calculated using the MicroCal PEAQ-ITC Analysis Software, *via* a non-linear least squares regression fit of the experimental data to the one-set-of-sites model. These values were then used to determine the ΔG and ΔS values.

6.1.6 UV-Vis titration protocols

All UV-Vis spectroscopy titrations were performed on a T60U (PG Instruments Ltd) spectrophotometer and the data processed using the OriginPro 2015 software package. In each case, titrations were performed in the stated solvent systems at T = 293 K, using a standard 1 mL Hellma quartz cuvette with path length of 1 cm.

- **Anion titrations of 2.26I/H**·2OTf **and 2.36I**·2OTf **in CH_3CN/ H_2O 6:4 *v/v* (buffered at pH 6.3 with 10 mM HEPES)**

In a typical titration experiment, a 0.75 mL initial volume of the host was used at a concentration of 2 mM, with 600 mM solutions of anion guests. Specifically, each of the anion solutions were prepared by dissolving the tetrabutylammonium salt of the desired anion in a solution containing the same concentration of the host (*i.e.* 2 mM), to ensure that the total host concentration remained constant throughout the titration - thus any absorption changes could be reasonably attributed to anion complexation and not dilution effects upon anion addition. Aliquots of anion solutions (1.0 eq = 2.5 μL) were added to the UV-Vis cuvette, the samples thoroughly mixed using a syringe needle and the changes in the absorption spectra recorded from 0 equivalents to up to 100 equivalents of anion, with at least 15 data sets collected, until saturation of the binding curve was seen. After each aliquot addition, the spectra were recorded at least twice till consistent spectra were obtained. Association constants were calculated from the UV-Vis titration data by non-linear global fitting analysis to a host-guest 1:1 or 1:2 stoichiometric binding model (as appropriate) using the Bindfit[7,8] software, monitoring the change in absorbance in the range 800–850 nm.

NB. The interaction of Cu(II) with the zwitterionic HEPES buffer has previously been shown to be negligible[9] and hence the observed changes in the UV-Vis titration spectra were attributed to arise invariably from the interactions of the guest anions with the respective Cu(II)- host.

- **Cu(II) titration of 2.24I in CH_3CN**

A 0.75 mL initial volume of the host was used at a concentration of 2 mM. A 15 mM solution of the cationic Cu(II) guest was prepared by dissolving copper triflate salt in a solution containing the

same concentration of the host (*i.e.* 2 mM). Aliquots of the Cu(II) solution were added to the UV-Vis cuvette, the samples thoroughly mixed using a syringe needle and the absorption spectra recorded at 0, 0.1, 0.2, 0.3, 0.4, 0.5, 0.6, 0.7, 0.8, 0.9, 1.0, 1.2, 1.4, 1.6, 1.8 and 2.0 equivalents of cation (0.1 eq = 10 μL). The absorbances for each addition, at a chosen wavelength (640 nm), were used to calculate the delta absorbances relative to the first absorbance reading. These values were then plotted versus the equivalents of the added Cu(II) guest for each aliquot, to obtain a qualitative isotherm which affirmed the expected 1:1 stoichiometry of ligand to metal binding.

6.1.7 Fluorescence titration protocols

All fluorescence spectroscopy chiral anion titrations with **3.3I**·2ClO_4 and **3.3H**·2ClO_4 were performed on a Jobin Yvon Horiba FluoroLog 3 spectrophotometer and the data processed using the OriginPro 2015 software package. All titrations were performed in CH_3CN/ H_2O 7:3 *v/v* at T = 293 K, using a standard 1 mL Hellma quartz cuvette with path length of 1 cm. In a typical titration experiment, a 0.75 mL initial volume of the host was used at a concentration of 50 μM, with 150 mM solutions of chiral anion guests. Specifically, each of the anion solutions were prepared by dissolving the tetrabutylammonium salt of the desired chiral anion in a solution containing the same concentration of the host (*i.e.* 50 μM), to ensure that the total host concentration remained constant throughout the titration. Aliquots of anion solutions (4.0 eq = 1 μL) were added to the fluorescence cuvette, the samples thoroughly mixed using a syringe needle and the changes in the absorption spectra recorded from 0 equivalents to up to 600 equivalents of anion, with at least 15 data sets collected, until saturation of the binding curve was seen. After each aliquot addition, the spectra were recorded at least twice till consistent spectra were obtained. Association constants were calculated from the fluorescence titration data by non-linear global fitting analysis to a host-guest 1:2 stoichiometric binding model using the Bindfit[7,8] software, monitoring the change in emission in the range 320–360 nm.

6.1.8 2D DOSY experiments

All DOSY experiments discussed in Chapter Two were conducted using a Bruker Avance III 500 MHz spectrometer at T = 298 K, and in triplicate. Data were collected with the BPP-LED sequence with convection compensation (dstebpgp3s), using diffusion times (Δ) in the range 13.8 -29.9 ms, encoding gradient pulses of total duration (δ) of 4.2-5.0 ms (applied as half-sine shaped bipolar pairs) and an LED period of 4.4 ms. 16 data sets were collected per experiment with gradient strengths up to 30.3 G cm^{-1}. The temperature was set and controlled at 298 K with an air flow of 400 l h^{-1} in order to avoid any temperature fluctuations due to sample heating during the magnetic field pulse gradient. After Fourier transformation and baseline correction, the diffusion dimension was processed with the TopSpin 3.5 software. Diffusion coefficients, processed with a line broadening of 0.3 -1 Hz, were calculated by Gaussian fits with the T1/T2 software of TopSpin. Individual 2 mM samples of **2.24I** and **2.25I**·$2ClO_4$ were prepared in both $CDCl_3$ and D_2O solvents, and measurements performed using 0.5 mL of each sample.

Diffusion coefficients and hydrodynamic radii are correlated theoretically by the Stokes-Einstein relation[] (eqn. 1):

$$D = \frac{kT}{6\mu\eta r_H} \quad \Rightarrow \quad r_H = \frac{kT}{6\pi\eta D} \qquad \text{Eqn. 1}$$

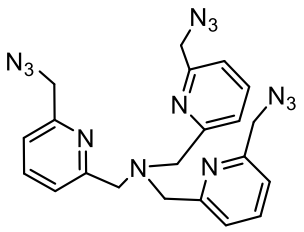
where D is the diffusion coefficient, k is the Boltzmann constant (1.3807 x 10^{-23} m^2 Kg s^{-2} K^{-1}), T is the temperature in Kelvin (298 K), η is the viscosity of the solution ($CDCl_3$ = 5.28 x 10^{-4} Kg m^{-1} s^{-1}, D_2O = 1.10 x 10^{-3} Kg m^{-1} s^{-1}), and r_H is the hydrodynamic radius of the molecular sphere.

The calculated D and values of **2.24I** and **2.25I**·$2ClO_4$ in both $CDCl_3$ and D_2O are stated in Table 2.4 in the main body of the text (see Chapter Two).

6.2 Synthetic Procedures

6.2.1 Synthesis of key and novel compounds from Chapter Two

Tris((6-azidomethyl)pyridine-2-yl)methyl)amine (2.5)[9]



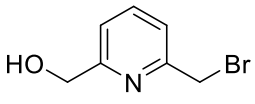
Method 1: (using a modified reported synthetic procedure)[10]. To a solution of tosylate **2.10** (250 mg, 0.79 mmol) in acetonitrile (6 mL) was added acetaldehyde ammonia trimer trihydrate (32.2 mg, 0.175 mmol), Na_2CO_3 (84 mg, 0.79 mmol), KI (131 mg, 0.79 mmol) and the reaction flask sealed. The suspension was stirred at room temperature for 7 days, after which no evidence of **2.10** was observed by TLC or ESI-MS analyses. The solvent was removed *in vacuo* and the residue partitioned between chloroform and water. After separating the layers, the aqueous phase was extracted with chloroform (2 x 10 mL). The organic layers were then combined, washed with H_2O (3 x 10 mL) and dried over $MgSO_4$. After removal of the solvent *in vacuo*, purification by preparative silica gel thin-layer chromatography (3% MeOH in CH_2Cl_2) afforded **2.5** as a pale yellow oil (56.5 mg, 71% yield).

Method 2: To a solution of 2-(azidomethyl)-6-(chloromethyl)-pyridine **2.11** (2 g, 10.9 mmol) in dry CH_3CN (50 mL) was added NH_4OAc (8.44 g, 109 mmol), Na_2CO_3 (11.6 g, 109 mmol) and KI (1.16 g, 10.9 mmol) as solid portions. The reaction flask was sealed, and the mixture vigorously stirred for two days at room temperature after which no evidence of **2.11** was observed by TLC or ESI-MS analyses. Thereafter, the creamy white suspension was directly transferred to a separating funnel and *ca.* 50 ml H_2O very gently pipetted into the vessel. The cloudy, lower aqueous layer was separated, and the remaining pale yellow organic layer concentrated *in vacuo*. The resultant crude residue was redissolved in $CHCl_3$ (50 mL) and washed with water (2 x 25 mL) and the organics dried over $MgSO_4$. Solvent removal and purification by silica gel column chromatography (gradient

from neat EtOAc to 1% MeOH in EtOAc) afforded the tris-azide subunit **2.4** as a pale yellow oil (1.19 g, 72% yield).

^{1}H NMR (400 MHz, CD_3OD) δ (ppm): 7.75 (3H, t, ^3J = 7.6 Hz, pyridine Ar*H*), 7.59 (3H, d, ^3J = 7.6 Hz, pyridine Ar*H*), 7.26 (3H, d, ^3J = 7.6 Hz, pyridine Ar*H*), 4.42 (6H, s, pyridine C*H*$_2$), 3.89 (6H, s, C*H*$_2$-N tertiary amine); **^{13}C NMR** (100 MHz, CD_3OD) δ (ppm): 160.9, 156.8, 139.5, 124.3, 122.4, 61.6, 56.5; **LRMS** (ESI +ve) *m/z*: 456.2 ($[M+H]^+$, $C_{21}H_{22}N_{13}$ calc. 456.2)

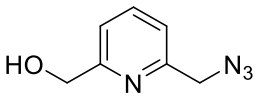
(6-(bromomethyl)pyridine-2-yl)methanol (**2.8**)[11]



A mixture of 2,6-pyridinedimethanol (5 g, 7.18 mmol) and HBr (48%, 50 mL) was heated at reflux with stirring under a N_2 atmosphere for 2-3 hours. The crude amber mixture was cooled down to 0 °C and carefully neutralized (pH 6.9) with a 6M $NaOH_{(aq)}$ solution producing a cloudy white suspension. Thereafter, H_2O (200 mL) was added and the white precipitate extracted with CH_2Cl_2 (5 x 100 mL). The combined organic layers were dried over $MgSO_4$ and the solvent removed *in vacuo.* Purification of the crude pink solid by silica gel column chromatography using neat CH_2Cl_2 to separate the first dibromo adduct, followed by elution with Et_2O afforded the monobromo adduct **2.8** as a pale pink powder (3.15 g, 44% yield).

^{1}H NMR (400 MHz, $CDCl_3$) δ (ppm): 7.73 (1H, t, ^3J = 7.7 Hz, pyridine Ar*H*), 7.39 (1H, d, ^3J = 7.8 Hz, pyridine Ar*H*), 7.20 (1H, d, ^3J = 7.8 Hz, pyridine Ar*H*), 4.79 (2H, d, pyridine C*H*$_2$), 4.58 (2H, s, pyridine C*H*$_2$); **LRMS** (ESI +ve) *m/z*: 202.0 ($[M+H]^+$, C_7H_9BrNO calc. 202.0).

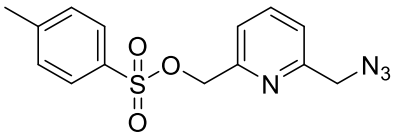
(6-(azidomethyl)pyridine-2-yl)methanol (2.9)[12]



This literature compound was prepared using modified synthetic procedures: to a solution of **2.8** (1.58 g, 7.82 mmol) in dry, degassed DMF (40 mL) was added NaN_3 (1.02 g, 15.6 mmol) and the reaction stirred under a N_2 atmosphere at 80 °C overnight. Thereafter, azeotropic removal of the solvent *in vacuo* with toluene produced a dark yellow residue which was redissolved in ethyl acetate (20 mL). The resultant precipitate was removed *via* filtration through a pad of celite and the celite thoroughly washed with ethyl acetate. Removal of the solvent *in vacuo* afforded the target compound **2.9** in excellent purity as a deep yellow oil which was dried *in vacuo* at less than 7 mbar for 2 days (1.13 g, 88% yield).

^{1}H NMR (400 MHz, $CDCl_3$) δ (ppm): 7.73 (1H, t, ^3J = 8.0 Hz, pyridine Ar*H*), 7.26 (1H, d, ^3J = 8.0 Hz, pyridine Ar*H*), 7.22 (1H, d, ^3J = 8.0 Hz, pyridine Ar*H*), 4.78 (2H, s, pyridine CH_2), 4.49 (2H, s, pyridine CH_2), 3.70 (1H, br. s, CH_2-O*H*); **LRMS** (ESI +ve) *m/z*: 165.1 ($[M+H]^+$, $C_7H_9N_4O$ calc. 165.1)

(6-(azidomethyl)pyridine-2-yl)methyl-4-methylbenzenesulfonate (2.10)[12]

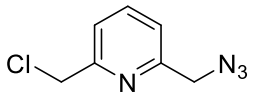


To a fully dissolved solution of **2.9** (0.54 g, 3.29 mmol) in a 1:1 mixture of THF/H_2O (10 mL) at 0 °C was added NaOH (0.39 g, 9.87 mmol) in small, portions. Separately, *p*-toluenesulfonyl chloride (0.69 g, 3.62 mmol) was dissolved in THF (5 mL) and slowly added to the stirring reaction. The reaction was allowed to warm to room temperature and the mixture stirred for 6 hours. H_2O was added (20 mL) and the aqueous layer extracted with CH_2Cl_2 (2 x 50 ml). The organic fractions

were combined dried over $MgSO_4$. Removal of the solvent *in vacuo* afforded **2.10** as a light brown oil which solidified to a light yellow crystalline solid upon standing overnight (723 mg, 69% yield).

^{1}H NMR (400 MHz, $CDCl_3$) δ (ppm): 7.82 (2H, d, ^3J = 8.3 Hz, tosyl Ar*H*), 7.73 (1H, t, ^3J = 7.8 Hz, pyridine Ar*H*), 7.38 (1H, d, ^3J = 7.8 Hz, pyridine Ar*H*), 7.34 (2H, d, ^3J = 7.8 Hz, tosyl Ar*H*), 7.27 (1H, d, ^3J = 7.8 Hz, pyridine Ar*H*), 5.13 (2H, s, pyridine CH_2), 4.40 (2H, s, pyridine CH_2), 2.45 (3H, s, tosyl CH_3); **LRMS** (ESI +ve) *m/z*: 319.1 ([M+H]$^+$, $C_{14}H_{15}O_3N_4S$ calc. 319.1).

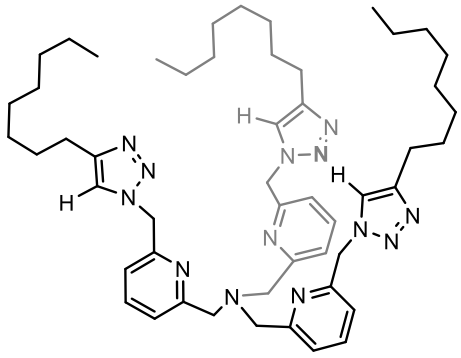
2-(azidomethyl)-6-(chloromethyl)pyridine (2.11)[13]



This literature compound was prepared using modified synthetic procedures: to a solution of 2-(azidomethyl)-6-(hydroxymethyl)-pyridine **2.9** (1.4 g, 8.52 mmol) in dry CH_2Cl_2 (15 ml) at 0 °C, was slowly added $SOCl_2$ (1.24 ml) and the reaction stirred at rt under a N_2 atmosphere for 6 hrs. The stirring mixture was carefully quenched and neutralised by the slow addition of a saturated $Na_2CO_{3(aq)}$ solution at 0 °C resulting in vigorous gas evolution. Thereafter, the biphasic mixture was further diluted with CH_2Cl_2 (20 ml) and washed with H_2O (2 x 25 ml). The organic layer was dried over $MgSO_4$ and the solvent removed *in vacuo*. Purification using silica gel column chromatography (0.5% MeOH in CH_2Cl_2) afforded **2.11** as a pale yellow oil (1.24 g, 80% yield).

^{1}H NMR (500 MHz, $CDCl_3$) δ (ppm): 7.77 (1H, t, ^3J = 7.71 Hz, pyridine Ar*H*), 7.45 (1H, d, ^3J = 7.8 Hz, pyridine Ar*H*), 7.30 (1H, d, ^3J = 7.8 Hz, pyridine Ar*H*), 4.67 (2H, s, pyridine CH_2), 4.49 (2H, s, pyridine CH_2); **^{13}C NMR** (125 MHz, $CDCl_3$) δ (ppm): 156.7, 155.6, 138.1, 122.0, 121.2, 55.4, 46.5; **LRMS** (ESI +ve) *m/z*: 183.0 ([M+H]$^+$, $C_7H_8ClN_4$ calc. 183.0)

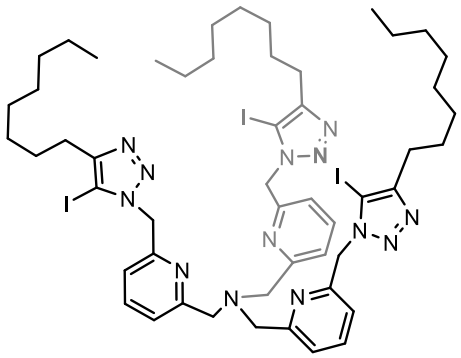
Tris(octyl chain)-appended HB tripodal ligand (**2.12H)**



To a solution of **2.15H** (540 mg, 1.68 mmol) fully dissolved in dry CH_3CN (30 mL) was added NH_4OAc (2.58 g, 33.6 mmol), Na_2CO_3 (3.56 g, 33.6 mmol) and KI (278 mg, 1.68 mmol) as solid portions. The reaction flask was completely sealed, and the mixture vigorously stirred for two days at room temperature after which no evidence of **2.15H** was observed by TLC or ESI-MS analyses.. Thereafter, the creamy off-white suspension was directly transferred to a separating funnel and *ca.* 20 ml H_2O very gently pipetted into the vessel. The cloudy, lower aqueous layer was separated, and the remaining clear pale yellow organic layer concentrated *in vacuo*. The resultant crude residue was redissolved in $CHCl_3$ (30 mL) and washed with water (2 x 20 mL) and the organics dried over $MgSO_4$. Solvent removal and purification by preparative thin layer chromatography (5% MeOH in CH_2Cl_2) afforded the tripodal ligand **2.12H** as a cream coloured solid (371 mg, 76% yield).

^{1}H NMR (500 MHz, $CDCl_3$) δ (ppm): 7.62 (3H, t, ^3J = 7.7 Hz, pyridine Ar*H*), 7.45 (3H, d, ^3J = 7.8 Hz, pyridine Ar*H*), 7.41 (3H, s, triazole C*H*), 6.95 (3H, d, ^3J = 7.6 Hz, pyridine Ar*H*), 5.59 (6H, s, CH_2-N triazole), 3.86 (6H, s, CH_2-N tertiary amine), 2.70 (6H, t, ^3J = 7.8 Hz, CH_2-C triazole), 1.65 (6H, quint., ^3J = 7.6 Hz, CH_2CH_2-C triazole), 1.25–1.35 (30H, m, alkyl-CH_2), 0.87 (9H, t, ^3J = 6.9 Hz, alkyl-CH_3); **^{13}C NMR** (125 MHz, $CDCl_3$) δ (ppm): 159.3, 154.3, 148.9, 137.6, 122.3, 121.2, 120.3, 59.9, 55.4, 31.8, 29.4, 29.3, 29.2, 29.1, 25.7, 22.6, 14.0; **HRMS** (ESI +ve) *m/z*: 870.6331 ($[M + H]^+$, $C_{51}H_{76}N_{13}$, calc. 870.6341).

Tris(octyl chain)-appended XB tripodal ligand (**2.12I)**



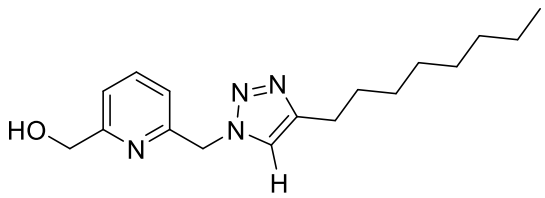
Method 1: (using a modified reported synthetic procedure)[10]. To a solution of **2.15I** (350 mg, 0.783 mmol) in acetonitrile (10 mL) was added acetaldehyde ammonia trimer trihydrate (31.9 mg, 0.174 mmol), Na_2CO_3 (83 mg, 0.783 mmol), KI (130 mg, 0.783 mmol) and the reaction flask sealed. The suspension was stirred at room temperature for 7 days, after which no evidence of **2.10** was observed by TLC or ESI-MS analyses. The solvent was removed *in vacuo* and the residue partitioned between chloroform and water. After separating the layers, the aqueous phase was extracted with chloroform (2 x 10 mL). The organic layers were then combined, washed with H_2O (3 x 10 mL) and dried over $MgSO_4$. After removal of the solvent *in vacuo*, purification by preparative silica gel thin-layer chromatography (5% MeOH in CH_2Cl_2) afforded **2.12I** as an off-white solid (135 mg, 62%).

Method 2: To a solution of **2.15I** (500 mg, 1.12 mmol) fully dissolved in dry CH_3CN (30 mL) was added NH_4OAc (1.73 g, 22.4 mmol), Na_2CO_3 (2.37 g, 22.4 mmol) and KI (186 mg, 1.12 mmol) as solid portions. The reaction flask was completely sealed, and the mixture vigorously stirred for two days at room temperature after which no evidence of **2.15H** was observed by TLC or ESI-MS analyses.. Thereafter, the creamy off-white suspension was directly transferred to a separating funnel and *ca.* 20 ml H_2O very gently pipetted into the vessel. The cloudy, lower aqueous layer was separated, and the remaining clear pale yellow organic layer concentrated *in vacuo*. The resultant crude residue was redissolved in $CHCl_3$ (30 mL) and washed with water (2 x 20 mL) and the organics dried over $MgSO_4$. Solvent removal and purification by preparative thin layer

chromatography (5% MeOH in CH_2Cl_2) afforded the tripodal ligand **2.12H** as an off-white solid (372 mg, 80% yield).

^{1}H NMR (500 MHz, $CDCl_3$) δ (ppm): 7.61 (3H, t, ^3J = 7.7 Hz, pyridine Ar*H*), 7.43 (3H, d, ^3J = 7.6 Hz, pyridine Ar*H*), 6.71 (3H, d, ^3J = 7.6 Hz, pyridine Ar*H*), 5.70 (6H, s, C*H*$_2$-N iodotriazole), 3.86 (3H, s, C*H*$_2$-N tertiary amine), 2.66 (6H, t, ^3J = 7.7 Hz, C*H*$_2$-C iodotriazole), 1.70 (6H, quin., ^3J = 7.4 Hz, C*H*$_2$CH$_2$-C iodotriazole), 1.25–1.35 (30H, m, alkyl-C*H*$_2$), 0.88 (9H, t, ^3J = 6.9 Hz, alkyl-C*H*$_3$); **^{13}C NMR** (125 MHz, $CDCl_3$) δ (ppm): 159.3, 153.8, 152.6, 137.5, 122.3, 119.5, 79.1, 59.6, 55.5, 31.8, 29.2, 29.1, 28.9, 26.2, 22.6, 14.1, one peak missing, presumed overlapped; **HRMS** (ESI +ve) *m/z*: 1248.3254 ($[M + H]^+$, $C_{51}H_{73}N_{13}I_3$ calc. 1248.3240).

Octyl chain-appended HB 'arm' precursor (**2.14H)**

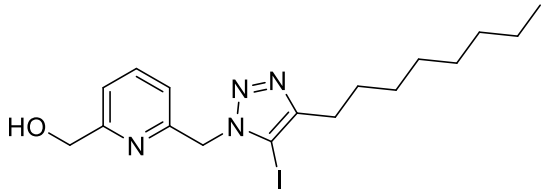


To a solution of (6-(azidomethyl)pyridine-2-yl)methanol **2.9** (250 mg, 1.52 mmol) and 1-decyne (0.28 mL, 1.52 mmol) in dry degassed CH_2Cl_2 (5 mL) was added $[Cu(MeCN)_4][PF_6]$ (284 mg, 0.76 mmol) and diisopropylethylamine (DIPEA) (0.13 mL, 0.76 mmol) and the mixture stirred at room temperature under a N_2 atmosphere for 2 days. The reaction mixture was diluted with CH_2Cl_2 (25 mL) and washed with $NH_4OH_{(aq)}$ (3 x 20 mL), brine (2 x 20 mL) and dried over $MgSO_4$. After removal of the solvent *in vacuo*, purification by silica gel column chromatography (gradient from pure CH_2Cl_2 to 1.5% MeOH in CH_2Cl_2) followed importantly by trituration with Et_2O afforded **2.14H** as a pure white solid (202 mg, 44%).

^{1}H NMR (500 MHz, $CDCl_3$) δ (ppm): 7.68 (1H, t, ^3J = 7.7 Hz, pyridine Ar*H*), 7.39 (1H, s, triazole C*H*), 7.22 (1H, d, ^3J = 7.8 Hz, pyridine Ar*H*), 7.04 (1H, d, ^3J = 7.6 Hz, pyridine Ar*H*), 5.64 (2H, s, C*H*$_2$-N triazole), 4.78 (2H, d, ^3J = 4.9 Hz, C*H*$_2$OH), 3.63 (1H, t, ^3J = 5 Hz, O*H*), 2.72 (2H, t, ^3J = 7.8 Hz, C*H*$_2$-C triazole), 1.67 (2H, quin., ^3J = 7.4 Hz, C*H*$_2$CH$_2$-C triazole), 1.26–1.38 (10H, m,

alkyl-CH_2), 0.88 (3H, t, ^3J = 6.9 Hz, alkyl-CH_3); **^{13}C NMR** (125 MHz, $CDCl_3$) δ (ppm): 159.3, 153.8, 149.0, 137.9, 121.1, 120.6, 120.0, 63.9, 55.2, 31.8, 29.4, 29.3, 29.2, 29.1, 25.7, 22.6, 14.0; **HRMS** (ESI +ve) *m/z*: 303.2176 ([M + H]$^+$, $C_{17}H_{27}ON_4$ calc. 303.2179).

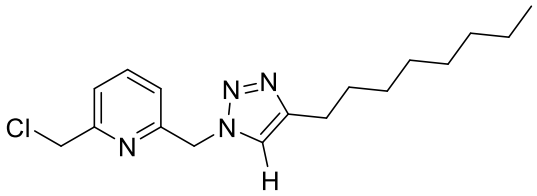
Octyl chain-appended XB 'arm' precursor (2.14I)



(6-(azidomethyl)pyridine-2-yl)methanol **2.9** (250 mg, 1.52 mmol) was dissolved in a 1:1 mixture of dry, degassed THF/CH_3CN (6 mL) and the reaction vessel covered in foil. Sodium iodide (911 mg, 6.08 mmol) and copper(II) perchlorate hexahydrate (1.13 g, 3.04 mmol) were added and the solution stirred for 5 minutes. Further added were TBTA (16.1 mg, 0.03 mmol), 1,8-Diazabicyclo[5.4.0]undec-7-ene (DBU) (231 mg, 1.52 mmol, in 0.5 mL 1:1 THF/CH_3CN) and 1-decyne (0.28 mL, 1.52 mmol) and the mixture stirred at room temperature under a N_2 atmosphere overnight. The reaction mixture was diluted with CH_2Cl_2 (25 mL) and washed with $NH_4OH_{(aq)}$ (3 x 20 mL), brine (2 x 20 mL) and dried over $MgSO_4$. After removal of the solvent *in vacuo*, purification by silica gel column chromatography (gradient from pure CH_2Cl_2 to 2% MeOH in CH_2Cl_2) followed importantly by trituration with Et_2O afforded **2.14I** as an off-white solid (462 mg, 71%).

^{1}H NMR (500 MHz, $CDCl_3$) δ (ppm): 7.66 (1H, t, ^3J = 7.8 Hz, pyridine Ar*H*), 7.18 (1H, d, ^3J = 7.6 Hz, pyridine Ar*H*), 6.85 (1H, d, ^3J = 7.6 Hz, pyridine Ar*H*), 5.73 (2H, s, CH_2-N iodotriazole), 4.76 (2H, d, ^3J = 4.9 Hz, CH_2OH), 3.69 (1H, t, ^3J = 5.0 Hz, O*H*), 2.69 (2H, t, ^3J = 7.5 Hz, CH_2-C iodotriazole), 1.72 (2H, quin., ^3J = 7.4 Hz, CH_2CH$_2$-C iodotriazole), 1.27–1.38 (10H, m, alkyl-CH_2), 0.88 (3H, t, ^3J = 6.8 Hz, alkyl-CH_3); **^{13}C NMR** (125 MHz, $CDCl_3$) δ (ppm): 159.0, 153.3, 152.7, 137.8, 120.0, 119.8, 79.1, 63.7, 55.1, 31.8, 29.3, 29.2, 29.1, 28.9, 26.1, 22.6, 14.1; **HRMS** (ESI +ve) *m/z*: 429.1147 ([M + H]$^+$, $C_{17}H_{26}ON_4I$ calc. 429.1145).

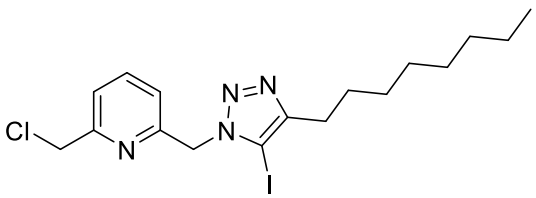
Octyl chain-appended HB 'chloro-arm' (2.15H)



To a solution of **2.14H** (930 mg, 3.08 mmol) in dry CH_2Cl_2 (20 ml) at 0 °C, was slowly added $SOCl_2$ (0.34 ml, 4.62 mmol) and the reaction stirred at rt under a N_2 atmosphere for 6 hrs. The stirring mixture was carefully quenched and neutralised by the slow addition of a saturated $Na_2CO_{3(aq)}$ solution at 0 °C resulting in vigorous gas evolution. Thereafter, the biphasic mixture was further diluted with CH_2Cl_2 (25 ml) and washed with H_2O (2 x 25 ml). The organic layer was dried over $MgSO_4$ and the solvent removed *in vacuo*. Purification using silica gel column chromatography (2% MeOH in CH_2Cl_2) afforded the chloro-arm **2.15H** as a white powder (799 mg, 81%).

^{1}H NMR (500 MHz, $CDCl_3$) δ (ppm): 7.71 (1H, t, ^3J = 7.8 Hz, pyridine Ar*H*), 7.45 (1H, d, ^3J = 8.0 Hz, pyridine Ar*H*), 7.43 (1H, s, triazole C*H*), 7.06 (1H, d, ^3J = 7.8 Hz, pyridine Ar*H*), 5.63 (2H, s, C*H*$_2$-N triazole), 4.67 (2H, s, C*H*$_2$Cl), 2.72 (2H, t, 7.7 Hz, C*H*$_2$-C triazole), 1.67 (2H, quin., ^3J = 7.5 Hz, C*H*$_2$CH$_2$-C triazole), 1.26–1.37 (10H, m, alkyl-C*H*$_2$), 0.88 (3H, t, ^3J = 6.9 Hz, alkyl-C*H*$_3$); **^{13}C NMR** (125 MHz, $CDCl_3$) δ (ppm): 156.6, 154.7, 149.0, 138.3, 122.3, 121.4, 121.2, 55.2, 46.3, 31.8, 29.4, 29.3, 29.2, 29.1, 25.7, 22.6, 14.1; **HRMS** (ESI +ve) *m/z*: 321.1837 ($[M + H]^+$, $C_{17}H_{26}N_4Cl$ calc. 321.1840).

Octyl chain-appended XB 'chloro-arm' (2.15I)

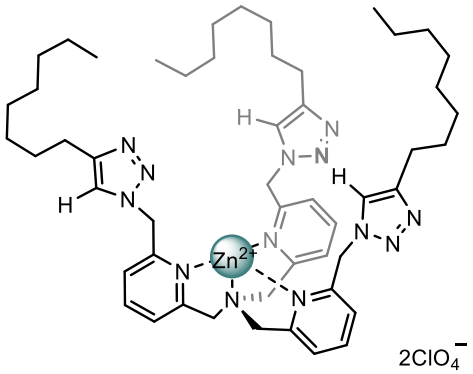


To a solution of **2.14I** (1.3 g, 3.04 mmol) in dry CH_2Cl_2 (20 ml) at 0 °C, was slowly added $SOCl_2$ (0.33 ml, 4.56 mmol) and the reaction stirred at rt under a N_2 atmosphere for 6 hrs. The stirring

mixture was carefully quenched and neutralised by the slow addition of a saturated $Na_2CO_{3(aq)}$ solution at 0 °C resulting in vigorous gas evolution. Thereafter, the biphasic mixture was further diluted with CH_2Cl_2 (25 ml) and washed with H_2O (2 x 25 ml). The organic layer was dried over $MgSO_4$ and the solvent removed *in vacuo*. Purification using silica gel column chromatography (2% MeOH in CH_2Cl_2) afforded the chloro-arm **2.15I** as a white powder (1.11 g, 82%).

^{1}H NMR (500 MHz, $CDCl_3$) δ (ppm): 7.68 (1H, t, ^3J = 7.8 Hz, pyridine Ar*H*), 7.43 (1H, d, ^3J = 7.8 Hz, pyridine Ar*H*), 6.76 (1H, d, ^3J = 7.8 Hz, pyridine Ar*H*), 5.72 (2H, s, C*H*$_2$-N iodotriazole), 4.67 (2H, s, C*H*$_2$Cl), 2.69 (2H, t, ^3J = 7.9 Hz, C*H*$_2$-C iodotriazole), 1.72 (2H, quin., ^3J = 7.4 Hz, C*H*$_2$CH$_2$-C iodotriazole), 1.27–1.36 (10H, m, alkyl -C*H*$_2$), 0.88 (3H, t, ^3J = 6.9 Hz, alkyl-C*H*$_3$); **^{13}C NMR** (125 MHz, $CDCl_3$) δ (ppm): 156.6, 154.4, 152.8, 138.2, 122.0, 120.4, 79.0, 55.3, 46.4, 31.8, 29.3, 29.2, 29.1, 28.9, 26.2, 22.6, 14.1; **HRMS** (ESI +ve) *m/z*: 447.0803 ([M + H]$^+$, $C_{17}H_{25}N_4ClI$ calc. 447.0806).

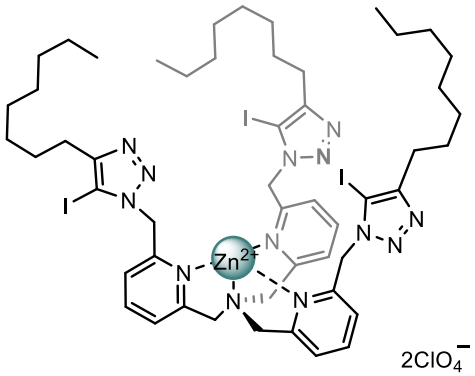
Tris(octyl chain)-appended HB Zn(II)-tripod (2.16H·2ClO$_4$)



To tripodal ligand **2.12H** (75 mg, 0.087 mmol) in a 1:1 mixture of CH_2Cl_2/MeOH (10 mL) was added zinc(II) perchlorate hexahydrate (32.4 mg, 0.087 mmol) and the solution stirred at room temperature under a N_2 atmosphere for 3 hours. After removal of the solvent *in vacuo*, the resultant residue was triturated with ice cold Et_2O (*ca*. 5 mL). The ethereal layer was carefully decanted with a pipette and the contents of the flask dried under high vacuum to afford metallo-tripodal receptor **2.16H**·2ClO_4 as a fine, cream coloured powder (97 mg, quantitative).

^{1}H NMR (500 MHz, CD_3CN) δ (ppm): 8.07 (3H, t, ^{3}J = 7.8 Hz, pyridine Ar*H*), 7.59 (3H, s, triazole C*H*), 7.55 (3H, d, ^{3}J = 7.6 Hz, pyridine Ar*H*), 7.50 (3H, d, ^{3}J = 7.9 Hz, pyridine Ar*H*), 5.47 (6H, s, CH_2-N triazole), 4.20 (6H, s, CH_2-N tertiary amine), 2.44 (6H, t, ^{3}J = 7.6 Hz, CH_2-C triazole), 1.43 (6H, quin., ^{3}J = 7.3 Hz, CH_2CH$_2$-C triazole), 1.19–1.31 (30H, m, alkyl-CH_2), 0.88 (9H, t, ^{3}J = 6.9 Hz, alkyl-CH_3); **^{13}C NMR** (125 MHz, CD_3CN) δ (ppm): 156.5, 154.3, 149.5, 142.7, 125.9, 125.8, 125.6, 56.7, 54.1, 32.7, 30.1, 30.0, 29.8, 29.7, 25.9, 23.5, 14.5; **HRMS** (ESI +ve) *m/z*: 1032.5015 ($[M - ClO_4]^+$, $C_{51}H_{75}N_{13}O_4Cl^{64}Zn$ calc. 1032.5039).

Tris(octyl chain)-appended XB Zn(II)-tripod (2.16I·2ClO$_4$)

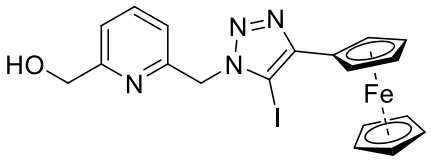


To tripodal ligand **2.12I** (85 mg, 0.069 mmol) in a 1:1 mixture of CH_2Cl_2/MeOH (10 mL) was added zinc(II) perchlorate hexahydrate (25.7 mg, 0.069 mmol) and the solution stirred at room temperature under a N_2 atmosphere for 3 hours. After removal of the solvent *in vacuo*, the resultant residue was triturated with ice cold Et_2O (*ca*. 5 mL). The ethereal layer was carefully decanted with a pipette and the contents of the flask dried under high vacuum to afford metallo-tripodal receptor **2.16I**·2ClO_4 as a fine, off-white powder (103 mg, quantitative).

^{1}H NMR (500 MHz, $CDCl_3$) δ (ppm): 8.03 (3H, t, ^{3}J = 7.7 Hz, pyridine Ar*H*), 7.60 (3H, d, ^{3}J = 7.6 Hz, pyridine Ar*H*), 7.57 (3H, d, ^{3}J = 7.8 Hz, pyridine Ar*H*), 5.70 (6H, s, CH_2-N iodotriazole), 4.39 (6H, s, CH_2-N tertiary amine), 2.42 (6H, t, ^{3}J = 7.6 Hz, CH_2-C iodotriazole), 1.39 (6H, quin., ^{3}J = 7.1 Hz, CH_2CH$_2$-C triazole), 1.20–1.31 (30H, m, alkyl-CH_2), 0.89 (9H, t, ^{3}J =6.9 Hz, alkyl-CH_3); **^{13}C NMR** (125 MHz, $CDCl_3$) δ (ppm): 155.4, 152.8, 152.3, 141.7, 125.6, 125.2, 55.7, 54.3, 31.9,

29.3, 29.2, 29.0, 28.2, 26.0, 22.7, 14.1, one peak missing, presumed overlapped; **HRMS** (ESI +ve) *m/z*: 1410.1922 ($[M - ClO_4]^+$, $C_{51}H_{72}N_{13}O_4ClI_3{}^{64}Zn$ calc. 1410.1938).

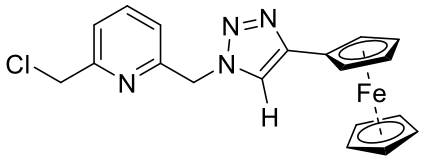
Ferrocene-appended XB 'arm' precursor (2.17I)



(6-(azidomethyl)pyridine-2-yl)methanol **2.9** (250 mg, 1.52 mmol) was dissolved in a 1:1 mixture of dry, degassed THF/CH_3CN (6 mL) and the reaction vessel covered in foil. Sodium iodide (911 mg, 6.08 mmol) and copper(II) perchlorate hexahydrate (1.13 g, 3.04 mmol) were added and the solution stirred for 5 minutes. Further added were TBTA (16.1 mg, 0.03 mmol), DBU (231 mg, 1.52 mmol, in 0.5 mL 1:1 THF/CH_3CN) and ethynylferrocene (320 mg, 1.52 mmol) and the mixture stirred at room temperature under a N_2 atmosphere overnight. The reaction mixture was diluted with CH_2Cl_2 (25 mL) and washed with $NH_4OH_{(aq)}$ (3 x 20 mL), brine (2 x 20 mL) and dried over $MgSO_4$. After removal of the solvent *in vacuo*, purification by silica gel column chromatography (gradient from pure CH_2Cl_2 to 3% MeOH in CH_2Cl_2) afforded **2.17I** as dark orange solid (503 mg, 66%).

^{1}H NMR (500 MHz, $CDCl_3$) δ (ppm): 7.68 (1H, t, ^3J = 7.8 Hz, pyridine Ar*H*), 7.20 (1H, d, ^3J = 7.6 Hz, pyridine Ar*H*), 6.88 (1H, d, ^3J = 7.6 Hz, pyridine Ar*H*), 5.79 (2H, s, C*H*$_2$-N iodotriazole), 5.08 (2H, m, Fc*H*), 4.78 (2H, d, ^3J = 4.7 Hz, C*H*$_2$OH), 4.36 (2H, m, Fc*H*), 4.14 (5H, s, Fc*H*), 3.67 (1H, t, ^3J = 4.9 Hz, O*H*); **^{13}C NMR** (125 MHz, $CDCl_3$) δ (ppm): 159.0, 153.4, 150.2, 137.9, 119.9, 119.8, 75.3, 74.5, 69.5, 68.9, 67.0, 63.8, 55.1; **HRMS** (ESI +ve) *m/z*: 500.9865 ($[M + H]^+$, $C_{19}H_{18}ON_4{}^{54}FeI$ calc. 500.9869).

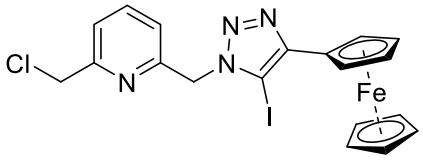
Ferrocene-appended HB 'chloro-arm' (2.18H)



To a solution of 2-(azidomethyl)-6-(chloromethyl)pyridine **2.11** (350 mg, 1.91 mmol) and ethynylferrocene (402 mg, 1.91 mmol) in dry degassed CH_2Cl_2 (10 mL) was added $[Cu(MeCN)_4][PF_6]$ (357 mg, 0.95 mmol) and diisopropylethylamine (DIPEA) (0.17 mL, 0.95 mmol) and the mixture stirred at room temperature under a N_2 atmosphere for 2 days. The reaction mixture was diluted with CH_2Cl_2 (25 mL) and washed with $NH_4OH_{(aq)}$ (3 x 20 mL), brine (2 x 20 mL) and dried over $MgSO_4$. After removal of the solvent *in vacuo*, purification by silica gel column chromatography (1.5% MeOH in CH_2Cl_2) afforded the chloro-arm **2.18H** as a pale orange oil which solidified to a dark orange crystalline solid upon standing overnight (323 mg, 43%).

^{1}H NMR (500 MHz, Acetone-d_6) δ (ppm): 8.11 (1H, s, triazole C*H*), 7.88 (1H, t, ^3J = 7.8 Hz, pyridine Ar*H*), 7.54 (1H, d, ^3J = 7.8 Hz, pyridine Ar*H*), 7.21 (1H, d, ^3J = 7.8 Hz, pyridine Ar*H*), 5.73 (2H, s, CH_2-N triazole), 4.75 (2H, m, Fc*H*), 4.74 (2H, s, CH_2Cl), 4.28 (2H, m, Fc*H*), 4.03 (5H, s, Fc*H*); **^{13}C NMR** (125 MHz, Acetone-d_6) δ (ppm): 157.8, 156.4, 147.2, 139.4, 123.3, 122.2, 121.5, 77.3, 70.3, 69.2, 67.4, 55.6, 47.4; **HRMS** (ESI +ve) *m/z*: 393.0552 ($[M + H]^+$, $C_{19}H_{18}N_4Cl^{54}Fe$ calc. 393.0564).

Ferrocene-appended XB 'chloro-arm' (2.18I)

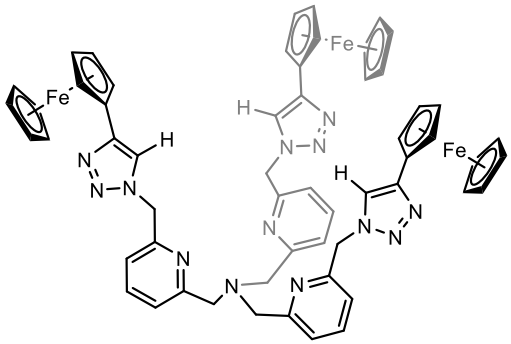


2-(azidomethyl)-6-(chloromethyl)pyridine **2.11** (330 mg, 1.81 mmol) was dissolved in a 1:1 mixture of dry, degassed THF/CH_3CN (6 mL) and the reaction vessel covered in foil. Sodium iodide

(1.09 g, 7.24 mmol) and copper(II) perchlorate hexahydrate (1.34 g, 3.62 mmol) were added and the solution stirred for 5 minutes. Further added were DBU (275 mg, 1.81 mmol, in 0.5 mL 1:1 THF/CH_3CN) and ethynylferrocene (380 mg, 1.81 mmol) and the mixture stirred at room temperature under a N_2 atmosphere overnight. The reaction mixture was diluted with CH_2Cl_2 (25 mL) and washed with $NH_4OH_{(aq)}$ (3 x 20 mL), brine (2 x 20 mL) and dried over $MgSO_4$. After removal of the solvent *in vacuo*, purification by silica gel column chromatography (30% EtOAc in hexane followed by 50% EtOAc in hexane) afforded the chloro-arm **2.18I** as dark orange solid (601 mg, 64%).

^{1}H NMR (500 MHz, $CDCl_3$) δ (ppm): 7.71 (1H, t, ^3J = 7.8 Hz, pyridine Ar*H*), 7.45 (1H, d, ^3J = 7.6 Hz, pyridine Ar*H*), 6.81 (1H, d, ^3J = 7.8 Hz, pyridine Ar*H*), 5.79 (2H, s, C*H*$_2$-N iodotriazole), 5.09 (2H, m, Fc*H*), 4.67 (2H, s, C*H*$_2$Cl), 4.37 (2H, m, Fc*H*), 4.14 (5H, s, Fc*H*); **^{13}C NMR** (125 MHz, $CDCl_3$) δ (ppm): 156.7, 154.3, 150.3, 138.2, 122.1, 120.3, 75.3, 74.5, 69.5, 68.9, 67.0, 55.2, 46.4; **HRMS** (ESI +ve) *m/z*: 518.9519 ([M + H]$^+$, $C_{19}H_{17}N_4Cl^{54}FeI$ calc. 518.9530).

Tris(ferrocene)-appended HB tripodal ligand (2.19H)

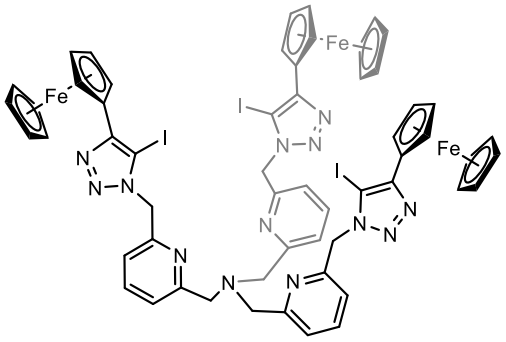


To a solution of **2.18H** (478 mg, 1.22 mmol) fully dissolved in dry CH_3CN (30 mL) was added NH_4OAc (1.88 g, 24.4 mmol), Na_2CO_3 (2.59 g, 24.4 mmol) and KI (202.5 mg, 1.22 mmol) as solid portions. The reaction flask was completely sealed, and the mixture vigorously stirred for two days at room temperature after which no evidence of **2.18H** was observed by TLC or ESI-MS analyses.. Thereafter, the creamy light orange suspension was directly transferred to a separating funnel and *ca.* 20 ml H_2O very gently pipetted into the vessel. The cloudy, lower aqueous layer was separated,

and the remaining clear bright orange organic layer concentrated *in vacuo*. The resultant crude residue was redissolved in CH_2Cl_2 (50 mL) and washed with water (2 x 20 mL) and the organics dried over $MgSO_4$. Solvent removal and purification by preparative thin layer chromatography (5% MeOH in CH_2Cl_2) afforded the tripodal ligand **2.19H** as a pale orange oil which solidified upon standing overnight (277 mg, 63% yield).

^{1}H NMR (500 MHz, $CDCl_3$) δ (ppm): 7.61 (3H, s, triazole C*H*), 7.60 (3H, t, ^3J = 7.8 Hz, pyridine Ar*H*), 7.42 (3H, d, ^3J = 7.8 Hz, pyridine Ar*H*), 7.00 (3H, d, ^3J = 7.6 Hz, pyridine Ar*H*), 5.60 (6H, s, C*H*$_2$-N triazole), 4.70 (6H, m, Fc*H*), 4.28 (6H, m, Fc*H*), 4.05 (15H, s, Fc*H*), 3.87 (6H, s, C*H*$_2$-N tertiary amine); **^{13}C NMR** (125 MHz, $CDCl_3$) δ (ppm): 159.3, 154.0, 147.1, 137.7, 122.5, 120.4, 119.6, 75.3, 69.5, 68.6, 66.6, 59.8, 55.3; **HRMS** (ESI +ve) *m/z*: 1086.2486 ($[M + H]^+$, $C_{57}H_{52}N_{13}{}^{54}Fe_3$ calc. 1086.2511).

Tris(ferrocene)-appended XB tripodal ligand (2.19I)

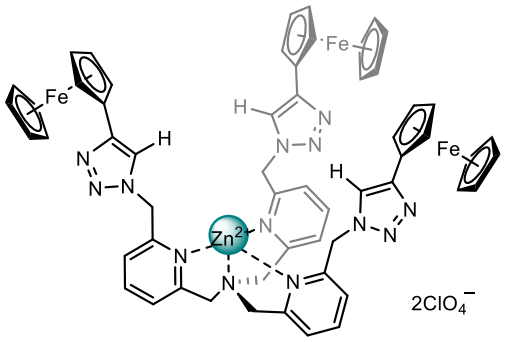


To a solution of **2.18I** (516 mg, 0.995 mmol) fully dissolved in dry CH_3CN (30 mL) was added NH_4OAc (1.53 g, 19.9 mmol), Na_2CO_3 (2.11 g, 19.9 mmol) and KI (165 mg, 0.995 mmol) as solid portions. The reaction flask was completely sealed, and the mixture vigorously stirred for two days at room temperature after which no evidence of **2.18I** was observed by TLC or ESI-MS analyses.. Thereafter, the creamy light orange suspension was directly transferred to a separating funnel and *ca.* 20 ml H_2O very gently pipetted into the vessel. The cloudy, lower aqueous layer was separated, and the remaining clear bright orange organic layer concentrated *in vacuo*. The resultant crude

residue was redissolved in CH_2Cl_2 (50 mL) and washed with water (2 x 20 mL) and the organics dried over $MgSO_4$. Solvent removal and purification by preparative thin layer chromatography (5% MeOH in CH_2Cl_2) afforded the tripodal ligand **2.19I** as a dark orange oil which solidified upon standing overnight (330 mg, 68% yield).

^{1}H NMR (500 MHz, $CDCl_3$) δ (ppm): 7.61 (3H, t, ^3J = 7.7 Hz, pyridine Ar*H*), 7.41 (3H, d, ^3J = 7.8 Hz, pyridine Ar*H*), 6.77 (3H, d, ^3J = 7.8 Hz, pyridine Ar*H*), 5.75 (6H, s, C*H*$_2$-N iodotriazole), 5.06 (6H, m, Fc*H*), 4.35 (6H, m, Fc*H*), 4.11 (15H, s, Fc*H*), 3.85 (6H, s, C*H*$_2$-N tertiary amine); **^{13}C NMR** (125 MHz, $CDCl_3$) δ (ppm): 159.3, 153.7, 150.1, 137.6, 122.4, 119.4, 75.5, 74.6, 69.5, 68.9, 67.0, 59.6, 55.4; **HRMS** (ESI +ve) *m/z*: 1463.9371 ($[M + H]^+$, $C_{57}H_{49}N_{13}{}^{54}Fe_3I_3$ calc. 1463.9411).

Tris(ferrocene)-appended HB Zn(II)-tripod (2.20H·2ClO$_4$)

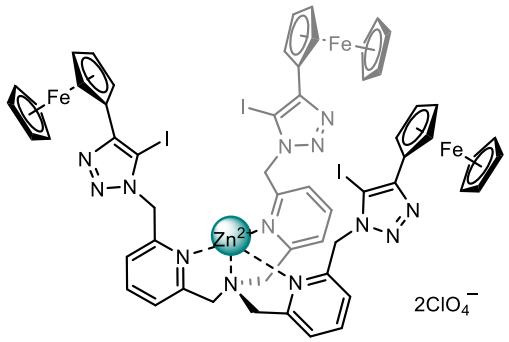


To tripodal ligand **2.19H** (100 mg, 0.093 mmol) in a 1:1 mixture of CH_2Cl_2/MeOH (10 mL) was added zinc(II) perchlorate hexahydrate (34.6 mg, 0.093 mmol) and the solution stirred at room temperature under a N_2 atmosphere for 3 hours. After removal of the solvent *in vacuo*, the resultant orange residue was triturated with ice cold Et_2O (*ca*. 5 mL). The ethereal layer was carefully decanted with a pipette and the contents of the flask dried flask dried under high vacuum to afford metallo-tripodal receptor **2.20H**·2ClO_4 as a fine, deep orange crystalline powder (121 mg, quantitative).

^{1}H NMR (500 MHz, CD_3CN) δ (ppm): 8.09 (3H, t, ^3J = 7.8 Hz, pyridine Ar*H*), 7.87 (3H, s, triazole C*H*), 7.67 (3H, d, ^3J = 7.6 Hz, pyridine Ar*H*), 7.48 (3H, d, ^3J = 7.9 Hz, pyridine Ar*H*), 5.63 (6H, s,

CH_2-N triazole), 4.54 (6H, s, Fc*H*), 4.29 (6H, s, Fc*H*), 4.22 (6H, s, CH_2-N tertiary amine), 3.98 (15H, s, Fc*H*); **^{13}C NMR** (125 MHz, CD_3CN) δ (ppm): 156.6, 154.2, 148.2, 142.9, 126.1, 125.7, 123.9, 70.7, 70.1, 67.8, 56.7, 54.2, one peak missing, presumed overlapped; **HRMS** (ESI +ve) *m/z*: 574.5850 ($[M - 2ClO_4]^{2+}$, $C_{57}H_{51}N_{13}{}^{54}Fe_3{}^{64}Zn$ calc. 574.5859).

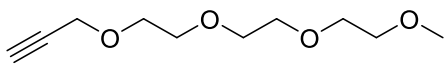
Tris(ferrocene)-appended XB Zn(II)-tripod (2.20I·2ClO$_4$)



To tripodal ligand **2.19I** (100 mg, 0.069 mmol) in a 1:1 mixture of CH_2Cl_2/MeOH (10 mL) was added zinc(II) perchlorate hexahydrate (25.7 mg, 0.069 mmol) and the solution stirred at room temperature under a N_2 atmosphere for 3 hours. After removal of the solvent *in vacuo*, the resultant orange residue was triturated with ice cold Et_2O (*ca*. 5 mL). The ethereal layer was carefully decanted with a pipette and the contents of the flask dried flask dried under high vacuum to afford metallo-tripodal receptor **2.20I**·2ClO_4 as a fine, dark orange crystalline powder (116 mg, quantitative).

^{1}H NMR (500 MHz, CD_3CN) δ (ppm): 8.16 (3H, t, ^3J = 7.8 Hz, pyridine Ar*H*), 7.77 (3H, d, ^3J = 7.6 Hz, pyridine Ar*H*), 7.55 (3H, d, ^3J = 7.8 Hz, pyridine Ar*H*), 5.72 (6H, s, CH_2-N iodotriazole), 4.76 (6H, s, Fc*H*), 4.34 (6H, s, Fc*H*), 4.24 (6H, s, CH_2-N tertiary amine), 4.01 (15H, s, Fc*H*); **^{13}C NMR** (125 MHz, CD_3CN) δ (ppm): 156.8, 153.5, 151.6, 143.0, 126.6, 126.0, 70.6, 70.3, 68.1, 56.7, 54.8, two peaks missing, presumed overlapped; **HRMS** (ESI +ve) *m/z*: 1625.8108 ($[M - ClO_4]^+$, $C_{57}H_{48}N_{13}O_4Cl^{54}Fe_3I_3{}^{64}Zn$ calc. 1625.8109).

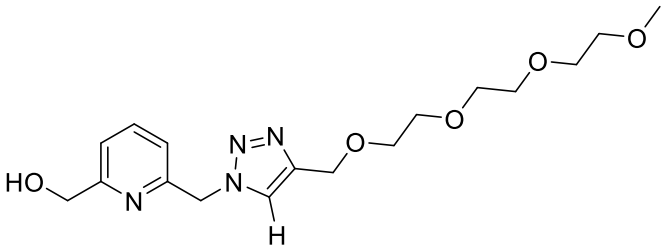
TEG alkyne (2.21)[14]



To a stirring solution of triethylene glycol monomethyl ether (2.0 g, 12.2 mmol) in dry degassed THF (3 mL) at 0 °C, was added a suspension of potassium *tert*-butoxide (1.56 g, 13.9 mmol) in 25 mL THF. Separately 1.82 mL of propargyl bromide (24.2 mmol) was dissolved in THF (50 mL) and then added dropwise to the solution. The reaction mixture was stirred at room temperature under a N_2 atmosphere for 24 h. Thereafter, ethyl acetate (200 mL) was added and the organics washed with brine (3 x 75 mL). The separated organic layer was dried over $MgSO_4$ and filtered. Removal of the solvent *in vacuo* afforded **2.21** in good purity as a pale yellow oil (1.69 g, 69%).

^{1}H NMR (500 MHz, $CDCl_3$) δ (ppm): 4.21 (2H, d, ^4J = 2.4 Hz, CH_2C≡C), 3.55 – 3.71 (12H, m, TEG alkyl-CH_2), 3.38 (3H, s, TEG alkyl-CH_3), 2.43 (1H, t, ^4J = 2.4 Hz, C≡C*H*); **^{13}C NMR** (125 MHz, $CDCl_3$) δ (ppm): 79.6, 74.4, 71.9, 70.6, 70.5, 70.4, 69.0, 59.0, 58.3, one peak missing, presumed overlapped; **HRMS** (ESI +ve) *m/z*: 203.1277 ([M + H]$^+$, $C_{10}H_{19}O_4$ calc. 203.1277).

TEG-appended HB 'arm' precursor (2.22H)

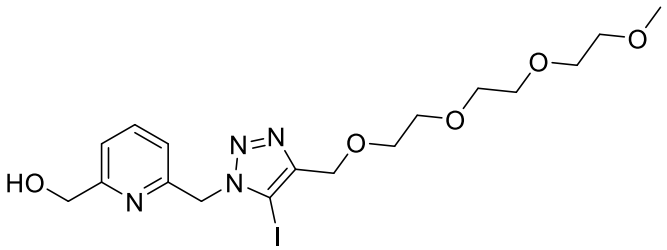


To a solution of (6-(azidomethyl)pyridine-2-yl)methanol **2.9** (350 mg, 2.13 mmol) and TEG alkyne **2.21** (431 mg, 2.13 mmol) in dry degassed THF (5 mL) was added $[Cu(MeCN)_4][PF_6]$ (397 mg, 1.07 mmol) and diisopropylethylamine (DIPEA) (0.18 mL, 1.07 mmol) and the mixture stirred at room temperature under a N_2 atmosphere for 2 days. The reaction mixture was diluted with CH_2Cl_2 (25 mL) and washed with $NH_4OH_{(aq)}$ (3 x 20 mL), brine (2 x 20 mL) and dried over $MgSO_4$. After

removal of the solvent *in vacuo*, purification by silica gel column chromatography (gradient from pure CH_2Cl_2 to 4% MeOH in CH_2Cl_2) afforded **2.22H** as a pale yellow oil (312 mg, 40%).

^{1}H NMR (500 MHz, $CDCl_3$) δ (ppm): 7.73 (1H, s, triazole C*H*), 7.69 (1H, t, ^3J = 7.7 Hz, pyridine Ar*H*), 7.24 (1H, d, ^3J = 7.8 Hz, pyridine Ar*H*), 7.09 (1H, d, ^3J = 7.6 Hz, pyridine Ar*H*), 5.66 (2H, s, C*H*$_2$-N triazole), 4.77 (2H, d, ^3J = 5.2 Hz, C*H*$_2$OH), 4.70 (2H, s, C*H*$_2$-C triazole), 3.53–3.71 (13H, m, TEG alkyl-*CH*$_2$ + O*H*), 3.36 (3H, s, TEG alkyl-*CH*$_3$); **^{13}C NMR** (125 MHz, $CDCl_3$) δ (ppm): 159.9, 153.2, 145.3, 137.8, 123.2, 120.6, 120.0, 71.6, 70.3, 70.3, 70.3, 70.2, 69.5, 64.4, 64.0, 58.7, 55.1; **HRMS** (ESI +ve) *m/z*: 367.1969 ($[M + H]^+$, $C_{17}H_{27}O_5N_4$ calc. 367.1976).

TEG-appended XB 'arm' precursor (2.22I)

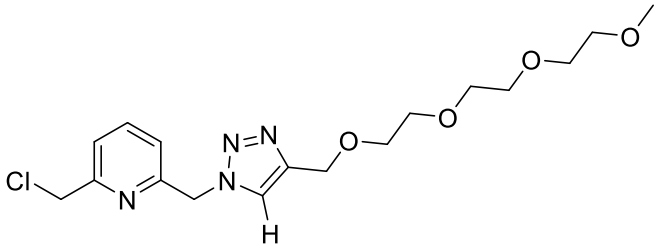


(6-(azidomethyl)pyridine-2-yl)methanol **2.9** (272 mg, 1.66 mmol) was dissolved in a 1:1 mixture of dry, degassed THF/CH_3CN (5 mL) and the reaction vessel covered in foil. Sodium iodide (995 mg, 6.64 mmol) and copper(II) perchlorate hexahydrate (1.23 g, 3.32 mmol) were added and the solution stirred for 5 minutes. Further added were TBTA (17.6 mg, 0.033 mmol), DBU (252 mg, 1.66 mmol, in 0.5 mL 1:1 THF/CH_3CN) and TEG alkyne **2.21** (335 mg, 1.66 mmol, in 0.5 ml 1:1 THF/CH_3CN) and the mixture stirred at room temperature under a N_2 atmosphere overnight. The reaction mixture was diluted with CH_2Cl_2 (25 mL) and washed with $NH_4OH_{(aq)}$ (3 x 20 mL), brine (2 x 20 mL) and dried over $MgSO_4$. After removal of the solvent *in vacuo*, purification by silica gel column chromatography (gradient from pure CH_2Cl_2 to 3% MeOH in CH_2Cl_2) afforded **2.22I** as a pale orange oil which solidified to an off-white solid upon standing overnight (522 mg, 64%).

^{1}H NMR (500 MHz, $CDCl_3$) δ (ppm): 7.68 (1H, t, ^3J = 7.8 Hz, pyridine Ar*H*), 7.20 (1H, d, ^3J = 7.6 Hz, pyridine Ar*H*), 6.93 (1H, d, ^3J = 7.6 Hz, pyridine Ar*H*), 5.75 (2H, s, C*H*$_2$-N iodotriazole), 4.75

(2H, d, ^{3}J = 5.0 Hz, CH_2OH), 4.66 (2H, s, CH_2-C iodotriazole), 3.54–3.71 (13H, m, TEG alkyl-CH_2 + O*H*), 3.37 (3H, s, TEG alkyl-CH_3); **^{13}C NMR** (125 MHz, $CDCl_3$) δ (ppm): 159.2, 152.9, 148.9, 137.8, 120.2, 119.9, 81.4, 71.9, 70.6, 70.5, 70.4, 69.7, 64.3, 63.8, 59.0, 55.2; one peak missing, presumed overlapped; **HRMS** (ESI +ve) *m/z*: 493.0945 ($[M + H]^+$, $C_{17}H_{26}O_5N_4I$ calc. 493.0942).

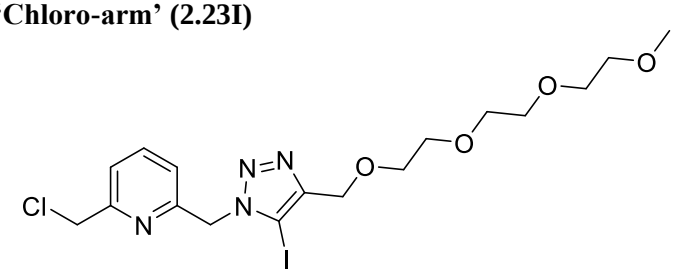
TEG-appended HB 'chloro-arm' (2.23H)



To a solution of **2.22H** (974 mg, 2.66 mmol) in dry CH_2Cl_2 (20 ml) at 0 °C, was slowly added $SOCl_2$ (0.29 ml, 3.99 mmol) and the reaction stirred at room temperature under a N_2 atmosphere for 6 hrs. The stirring mixture was carefully quenched and neutralised by the slow addition of a saturated $Na_2CO_{3(aq)}$ solution at 0 °C resulting in vigorous gas evolution. Thereafter, the biphasic mixture was further diluted with CH_2Cl_2 (25 ml) and washed with H_2O (2 x 25 ml). The organic layer was dried over $MgSO_4$ and the solvent removed *in vacuo*. Purification using silica gel column chromatography (gradient from pure CH_2Cl_2 to 3% MeOH in CH_2Cl_2) afforded the chloro-arm **2.23H** as a clear, light orange oil (879 mg, 86%).

^{1}H NMR (500 MHz, $CDCl_3$) δ (ppm): 7.74 (1H, s, triazole C*H*), 7.72 (1H, t, ^{3}J = 7.78 Hz, pyridine Ar*H*), 7.45 (1H, d, ^{3}J = 7.78 Hz, pyridine Ar*H*), 7.11 (1H, d, ^{3}J = 7.76 Hz, pyridine Ar*H*), 5.65 (2H, s, CH_2-N triazole), 4.70 (2H, s, CH_2-C triazole), 4.66 (2H, s, CH_2Cl), 3.53–3.71 (12H, m, TEG alkyl-CH_2), 3.37 (3H, s, TEG alkyl-CH_3); **^{13}C NMR** (125 MHz, $CDCl_3$) δ (ppm): 156.7, 154.1, 145.6, 138.3, 123.2, 122.3, 121.4, 71.8, 70.5, 70.4, 70.4, 70.4, 69.6, 64.6, 58.9, 55.2, 46.2; **HRMS** (ESI +ve) *m/z*: 385.1636 ($[M + H]^+$, $C_{17}H_{26}N_4O_4Cl$ calc. 385.1637).

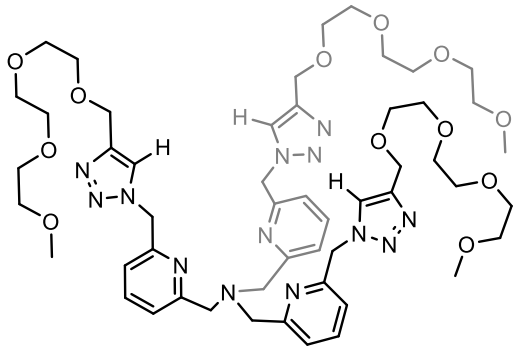
TEG-appended XB 'Chloro-arm' (2.23I)



To a solution of **2.22I** (1.42 g, 2.88 mmol) in dry CH_2Cl_2 (25 ml) at 0 °C, was slowly added $SOCl_2$ (0.32 ml, 4.32 mmol) and the reaction stirred at room temperature under a N_2 atmosphere for 6 hrs. The stirring mixture was carefully quenched and neutralised by the slow addition of a saturated $Na_2CO_{3(aq)}$ solution at 0 °C resulting in vigorous gas evolution. Thereafter, the biphasic mixture was further diluted with CH_2Cl_2 (25 ml) and washed with H_2O (2 x 25 ml). The organic layer was dried over $MgSO_4$ and the solvent removed *in vacuo*. Purification using silica gel column chromatography (gradient from pure CH_2Cl_2 to 3% MeOH in CH_2Cl_2) afforded the chloro-arm **2.23I** as a clear, amber oil (1.19 g, 81%).

^{1}H NMR (500 MHz, $CDCl_3$) δ (ppm): 7.70 (1H, t, ^3J = 7.8 Hz, pyridine Ar*H*), 7.44 (1H, d, ^3J = 7.8 Hz, pyridine Ar*H*), 6.85 (1H, d, ^3J = 7.8 Hz, pyridine Ar*H*), 5.74 (2H, s, C*H*$_2$-N iodotriazole), 4.67 (2H, s, C*H*$_2$-C iodotriazole), 4.66 (2H, s, C*H*$_2$Cl), 3.55–3.71 (12H, m, TEG alkyl-*CH*$_2$), 3.38 (3H, s, TEG alkyl-*CH*$_3$); **^{13}C NMR** (125 MHz, $CDCl_3$) δ (ppm): 156.6, 153.8, 148.9, 138.2, 122.1, 120.6, 81.4, 71.9, 70.5, 70.5, 70.4, 69.7, 64.2, 59.0, 55.3, 46.3, one peak missing, presumed overlapped; **HRMS** (ESI +ve) *m/z*: 533.0428 ($[M + Na]^+$, $C_{17}H_{24}N_4O_4ClINa$ calc. 533.0423).

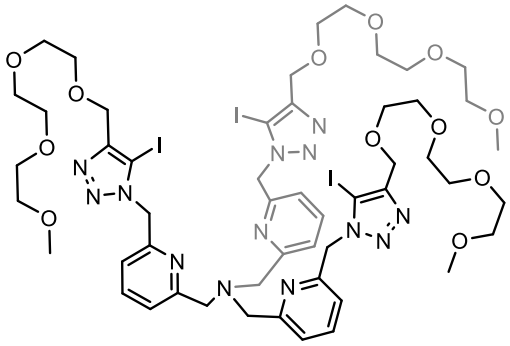
Tris(TEG)-appended HB tripodal ligand (2.24H)



To a solution of **2.23H** (825 mg, 2.14 mmol) fully dissolved in dry CH_3CN (30 mL) was added NH_4OAc (3.30 g, 42.8 mmol), Na_2CO_3 (4.54 g, 42.8 mmol) and KI (356 mg, 2.14 mmol) as solid portions. The reaction flask was completely sealed, and the mixture vigorously stirred for two days at room temperature after which no evidence of **2.23H** was observed by TLC or ESI-MS analyses. Thereafter, the creamy off-white suspension was directly transferred to a separating funnel and *ca.* 20 ml H_2O very gently pipetted into the vessel. The cloudy, lower aqueous layer was separated, and the remaining clear pale yellow organic layer concentrated *in vacuo*. The resultant crude residue was redissolved in $CHCl_3$ (50 mL) and washed with water (2 x 20 mL) and the organics dried over $MgSO_4$. Solvent removal and purification by preparative thin layer chromatography (5% MeOH in $CHCl_3$) afforded the tripodal ligand **2.24H** as a deep yellow oil (501 mg, 66% yield).

^{1}H NMR (500 MHz, $CDCl_3$) δ (ppm): 7.73 (3H, s, triazole C*H*), 7.64 (3H, t, ^3J = 7.7 Hz, pyridine Ar*H*), 7.46 (3H, d, ^3J = 7.6 Hz, pyridine Ar*H*), 7.01 (3H, d, ^3J = 7.6 Hz, pyridine Ar*H*), 5.62 (6H, s, CH_2-N triazole), 4.68 (6H, s, CH_2-C triazole), 3.86 (6H, s, CH_2-N tertiary amine), 3.53–3.70 (36 H, m, TEG alkyl-CH_2), 3.36 (9H, s, TEG alkyl-CH_3); **^{13}C NMR** (125 MHz, $CDCl_3$) δ (ppm): 159.4, 153.8, 145.5, 137.7, 123.2, 122.4, 120.5, 71.9, 70.5, 70.5, 70.4, 69.7, 64.6, 59.9, 59.0, 55.5, one peak missing, presumed overlapped. **HRMS** (ESI +ve) *m/z*: 1062.5746 ($[M + H]^+$, $C_{51}H_{76}N_{13}O_{12}$ calc.1062.5736).

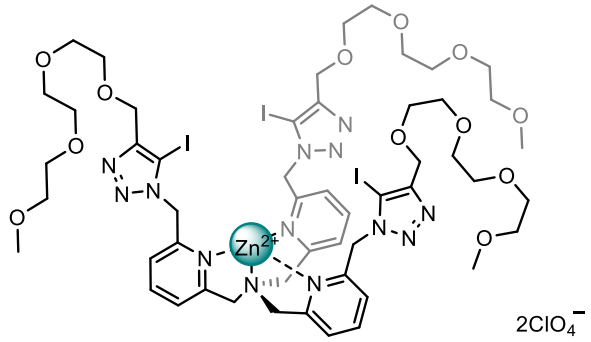
Tris(TEG)-appended XB tripodal ligand (2.24I)



To a solution of **2.23I** (882 mg, 1.73 mmol) fully dissolved in dry CH_3CN (30 mL) was added NH_4OAc (2.67 g, 34.6 mmol), Na_2CO_3 (3.67 g, 34.6 mmol) and KI (287 mg, 1.73 mmol) as solid portions. The reaction flask was completely sealed, and the mixture vigorously stirred for two days at room temperature after which no evidence of **2.23I** was observed by TLC or ESI-MS analyses.. Thereafter, the creamy off-white suspension was directly transferred to a separating funnel and *ca.* 20 ml H_2O very gently pipetted into the vessel. The cloudy, lower aqueous layer was separated, and the remaining clear light yellow organic layer concentrated *in vacuo*. The resultant crude residue was redissolved in $CHCl_3$ (50 mL) and washed with water (2 x 20 mL) and the organics dried over $MgSO_4$. Solvent removal and purification by preparative thin layer chromatography (6% MeOH in CH_2Cl_2) afforded the tripodal ligand **2.24I** as a dark yellow oil (497 mg, 60% yield).

^{1}H NMR (500 MHz, $CDCl_3$) δ (ppm): 7.63 (3H, t, ^3J = 7.7 Hz, pyridine Ar*H*), 7.43 (3H, d, ^3J = 7.6 Hz, pyridine Ar*H*), 6.79 (3H, d, ^3J = 7.0 Hz, pyridine Ar*H*), 5.72 (6H, s, CH_2-N iodotriazole), 4.64 (6H, s, CH_2-C iodotriazole), 3.84 (6H, s, CH_2-N tertiary amine), 3.53–3.68 (36H, m, TEG alkyl-CH_3), 3.37 (9H, s, TEG-alkyl CH_3); **^{13}C NMR** (125 MHz, $CDCl_3$) δ (ppm): 159.4, 153.4, 148.8, 137.6, 122.4, 119.7, 81.5, 71.9, 70.6, 70.5, 70.4, 69.7, 64.3, 59.6, 59.0, 55.5, one peak missing, presumed overlapped; **HRMS** (ESI +ve) *m/z*: 1440.2665 ($[M + H]^+$, $C_{51}H_{73}N_{13}O_{12}I_3$ calc. 1440.2635).

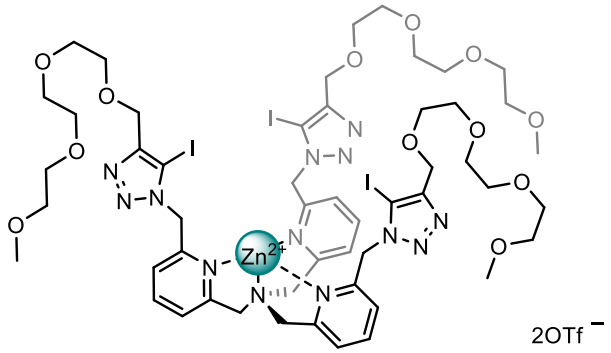
Tris(TEG)-appended XB Zn(II)-tripod (2.25I·2ClO$_4$)



To tripodal ligand **2.24I** (338 mg, 0.235 mmol) in a 1:1 mixture of CH_2Cl_2/MeOH (10 mL) was added zinc(II) perchlorate hexahydrate (87.5 mg, 0.235 mmol) and the solution stirred at room temperature under a N_2 atmosphere for 3 hours. Removal of the solvent *in vacuo* afforded metallo-tripodal receptor **2.25I**·2ClO$_4$ as a deep orange oil, which solidified to a dark orange crystalline residue upon drying under high vacuum (396 mg, quantitative).

^{1}H NMR (500 MHz, CD_3OD) δ (ppm): 8.16 (3H, t, ^3J = 7.8 Hz, pyridine Ar*H*), 7.76 (3H, d, ^3J = 7.6 Hz, pyridine Ar*H*), 7.58 (3H, d, ^3J = 7.9 Hz, pyridine Ar*H*), 5.81 (6H, s, C*H*$_2$-N iodotriazole), 4.46 (6H, s, C*H*$_2$-C iodotriazole), 4.27 (6H, s, C*H*$_2$-N tertiary amine), 3.50–3.61 (36H, m, TEG alkyl-*CH*$_2$), 3.33 (9H, s, TEG-alkyl *CH*$_3$); **^{13}C NMR** (125 MHz, CD_3OD) δ (ppm): 157.0, 153.8, 150.9, 143.2, 126.9, 126.6, 88.7, 73.1, 71.7, 71.7, 71.5, 71.5, 71.1, 65.1, 59.3, 57.3, 55.5; **HRMS** (ESI +ve) *m/z*: 1602.1326 ([M – ClO$_4$]$^+$, $C_{51}H_{72}N_{13}O_{16}ClI_3{}^{64}Zn$ calc. 1602.1328).

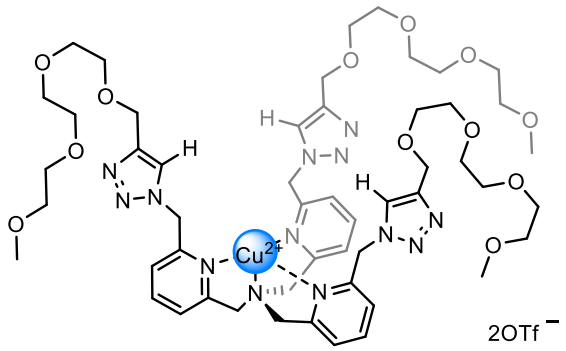
Tris(TEG)-appended XB Zn(II)-tripod (2.25I·2OTf)



To tripodal ligand **2.24I** (85 mg, 0.06 mmol) in a 1:1 mixture of CH_2Cl_2/MeOH (10 mL) was added zinc(II) trifluoromethansulfonate (21.8 mg, 0.06 mmol) and the solution stirred at room temperature under a N_2 atmosphere for 3 hours. Removal of the solvent *in vacuo* afforded metallo-tripodal receptor **2.25I**·2OTf as a deep orange oil, which solidified to a dark orange crystalline residue upon drying under high vacuum (105 mg, quantitative).

^{1}H NMR (500 MHz, $CDCl_3$) δ (ppm): 7.95 (3H, t, ^3J = 7.8 Hz, pyridine Ar*H*), 7.70–7.45 (6H, m, pyridine Ar*H*), 5.91 (6H, s, C*H*$_2$-N iodotriazole), 4.53 (6H, s, C*H*$_2$-C iodotriazole), 4.32 (6H, s, C*H*$_2$-N tertiary amine), 3.50–3.64 (36H, m, TEG alkyl-*CH*$_2$), 3.35 (9H, s, TEG alkyl-*CH*$_3$); **^{13}C NMR** (125 MHz, $CDCl_3$) δ (ppm): 155.1, 152.3, 149.3, 141.3, 125.2, 124.4, 121.7, 118.5, 71.8, 70.4, 70.4, 70.3, 70.2, 69.9, 64.1, 58.9, 56.2, 54.2; **HRMS** (ESI +ve) *m/z*: 1652.1359 ([M – OTf]$^+$, $C_{52}H_{72}N_{13}O_{15}SF_3I_3{}^{64}Zn$ calc. 1652.1367).

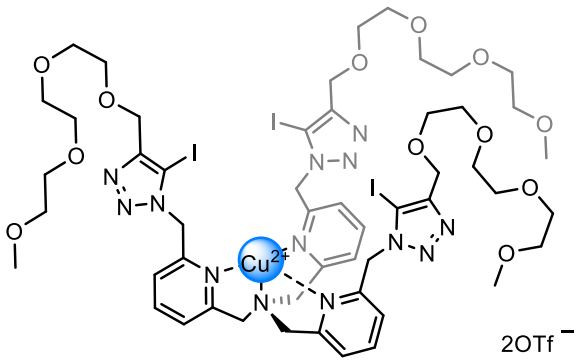
Tris(TEG)-appended HB Cu(II)-tripod (2.26H·2OTf)



To tripodal ligand **2.24H** (205 mg, 0.2 mmol) in a 1:1 mixture of CH_2Cl_2/MeOH (6 mL) was added copper(II) trifluoromethansulfonate (72.3 mg, 0.2 mmol) and the solution stirred at room temperature under a N_2 atmosphere for 3 hours. Removal of the solvent *in vacuo* afforded metallo-tripodal receptor **2.26H**·2OTf as a deep blue oil, which solidified to a dark blue crystalline residue upon drying under high vacuum (274 mg, quantitative).

UV-Vis (CH_3CN/ H_2O 6:4 *v/v*, 10 mM HEPES, λ_{max}/ nm, (ε/ M^{-1} cm^{-1})): 639 (125), 760 (98); **EPR** (CH_3CN, 95 K): $g\parallel$ = 2.225, $g\perp$ = 2.065, $A\parallel$ = 182.0 x 10^{-4} cm^{-1}; **HRMS** (ESI +ve) *m/z:* 562.2471 ($[M - 2OTf]^{2+}$, $C_{51}H_{75}N_{13}O_{12}{}^{63}Cu$ calc. 562.2472).

Tris(TEG)-appended XB Cu(II)-tripod (2.26I·2OTf)

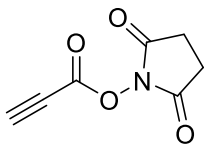


To tripodal ligand **2.24I** (199 mg, 0.139 mmol) in a 1:1 mixture of CH_2Cl_2/MeOH (6 mL) was added copper(II) trifluoromethansulfonate (50.3 mg, 0.139 mmol) and the solution stirred at room temperature under a N_2 atmosphere for 3 hours. Removal of the solvent *in vacuo* afforded metallo-

tripodal receptor **2.26I**·2OTf as a deep blue oil, which solidified to a dark blue crystalline residue upon drying under high vacuum (248 mg, quantitative).

UV-Vis (CH_3CN/ H_2O 6:4 *v/v*, 10 mM HEPES, λ_{max}/ nm, (ε/ M^{-1} cm^{-1})): 647 (117), 775 (91); **EPR** (CH_3CN, 95 K): $g\parallel$ = 2.225, $g\perp$ = 2.065, $A\parallel$ = 183.0 x 10^{-4} cm^{-1}; **HRMS** (ESI +ve) *m/z:* 751.0916 ($[M - 2OTf]^{2+}$, $C_{51}H_{72}N_{13}O_{12}I_3{}^{63}Cu$ calc. 751.0921).

Succinimidyl-3-propiolate (2.31)[15]



This literature compound was prepared according to modified procedures. To a stirring solution of propiolic acid (0.5 mL, 8 mmol) in dry acetonitrile (50 mL) at 0 °C was added *N*-hydroxysuccinimide (0.92 g, 8 mmol). Separately, dicyclohexylcarbodiimide (DCC) (1.65 g, 8 mmol) was added portion wise to the reaction mixture, which was kept stirring for 8 hours at 4 °C under N_2. After filtration of the white precipitate under gravity, removal of the solvent *in vacuo* gave the activated ester **2.31** in excellent purity as a pale yellow oil, which solidified to a crystalline solid upon standing for 1 – 2 hours at room temperature (909 mg, 68%). *(NB. due to the unstable nature of the compound, the obtained solid was stored in a vial at -20 °C until further used).*

^{1}H NMR (500 MHz, $CDCl_3$) δ (ppm): 3.34 (1H, s, C≡C*H*), 2.86 (4H, s, COCH_2); **^{13}C NMR** (125 MHz, $CDCl_3$) δ (ppm): 168.2, 147.7, 82.1, 70.1, 25.5; **LRMS** (ESI +ve) *m/z*: not observed.

N.B. For all of the *β*-cyclodextrin precursor compounds **2.27** – **2.30** leading up to the synthesis of the key permethylated-*β*-cyclodextrin (pm*β*CD) alkyne **2.32** in Chapter Two (see Scheme 2.13), all mono-functionalisation procedures were carried out at the 6- position on the narrow rim of the truncated cone as shown in Figure 6.1. Therefore, this numbering system is also used for the assignment of the relevant ^{1}H NMR signals in the following characterisation data of the novel pm*β*CD compounds **2.32** – **2.35I**.

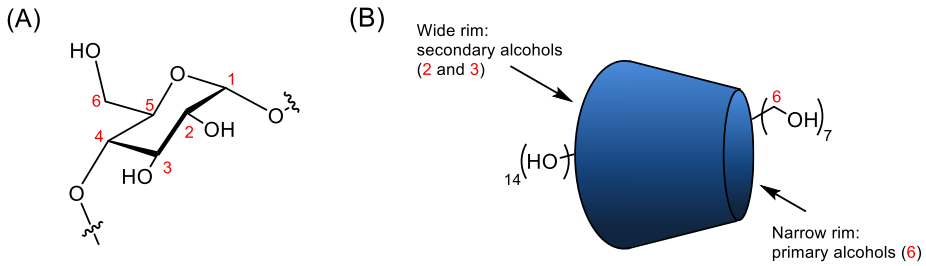
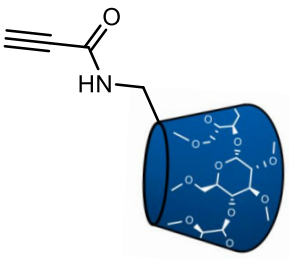


Figure 6.1: *(A) Numbering scheme for the glucopyranose units of the β-CD cone and (B) distribution of the primary and secondary alcohol moieties on its narrow and wide rims, respectively.*

(It should be further noted that by convention, in a mono-substituted *β*-CD derivative, the functionalised glucopyranose unit is denoted A, with the remaining units labelled B-G. 6^{A}-substituted therefore means that Carbon 6 of glucopyranose unit A is functionalised).

6^{A}-amido-pm*β*CD alkyne (2.32)

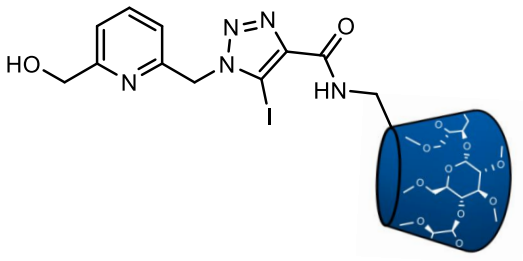


To a solution of succinimidyl-3-propiolate **2.31** (82.3 mg, 0.494 mmol) and permethylated *β*-cyclodextrin amine **2.30**[16] (500 mg, 0.353 mmol) in dry CH_2Cl_2 was added 4-dimethylaminopyridine (DMAP) (10 mg, 0.08 mmol). The mixture was left to stir at room

temperature under a N_2 atmosphere overnight, after which no evidence of the permethylated *β*-cyclodextrin amine was observed by TLC or ESI-MS. After removal of the solvent *in vacuo*, purification by silica gel column chromatography (4% MeOH in EtOAc) afforded **2.33I** as a crystalline white solid (362 mg, 70%).

^{1}H NMR (500 MHz, $CDCl_3$) δ (ppm): 6.74 (1H, t, ^3J = 5.9 Hz, amide N*H*), 5.08–5.18 (7H, m, *β*-CD H_1), 3.17–4.08 (102H, m, *β*-CD $H_{2\text{-}6}$ + CH_3O), 2.84 (1H, s, C≡C*H*); **^{13}C NMR** (125 MHz, $CDCl_3$) δ (ppm): 152.2, *β*-CD signals consistent with loss of C7 symmetry: (99.2–98.6; *β*-CD C_1), 82.1–81.3, 80.6–79.8, 77.7, 73.0, 71.5–70.1, 61.6–61.2, 59.5–58.3; **HRMS** (ESI +ve) *m/z*: 1488.6785 ($[M + Na]^+$, $C_{65}H_{111}NO_{35}Na$ calc. 1488.6828).

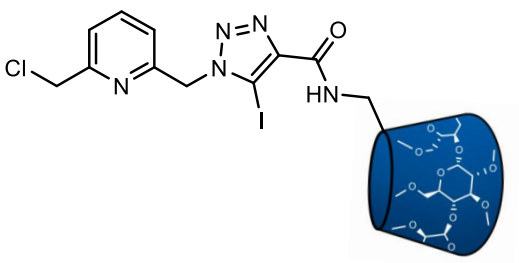
6^A-amido-pm*β*CD-appended XB 'arm' precursor (2.33I)



(6-(azidomethyl)pyridine-2-yl)methanol **2.9** (41 mg, 0.25 mmol) was dissolved in a 1:1 mixture of dry, degassed THF/CH_3CN (2 mL) and the reaction vessel covered in foil. Sodium iodide (149 mg, 1.00 mmol) and copper(II) perchlorate hexahydrate (185 mg, 0.5 mmol) were added and the solution stirred for 5 minutes. Further added were DBU (37.3 μL, 0.25 mmol) and pm*β*CD alkyne **2.32** (366 mg, 0.25 mmol) and the mixture stirred at room temperature under a N_2 atmosphere overnight. The reaction mixture was diluted with $CHCl_3$ (25 mL) and washed with $NH_4OH_{(aq)}$ (3 x 20 mL), brine (2 x 20 mL) and dried over $MgSO_4$. After removal of the solvent *in vacuo*, purification by silica gel column chromatography (gradient from pure $CHCl_3$ to 3% MeOH in $CHCl_3$) afforded the arm precursor **2.33I** as a crystalline off-white solid (232 mg, 53%).

^{1}H NMR (500 MHz, $CDCl_3$) δ (ppm): 7.70 (1H, t, ^{3}J = 7.8 Hz, pyridine Ar*H*), 7.47 (1H, t, ^{3}J = 5.8 Hz, amide N*H*), 7.23 (1H, d, ^{3}J = 7.8 Hz, pyridine Ar*H*), 6.93 (1H, d, ^{3}J = 7.6 Hz, pyridine Ar*H*), 5.79 (2H, ABquart., $\Delta\delta_{AB}$ = 0.04, $^{2}J_{AB}$ = 15.5 Hz, CH_2-N iodotriazole), 5.12–5.23 (7H, m, β-CD H_1), 4.74 (2H, d, ^{3}J = 4.9 Hz, CH_2OH), 3.18–3.99 (103H, m, β-CD $H_{2\text{-}6}$ + CH_3O + O*H*); **^{13}C NMR** (125 MHz, $CDCl_3$) δ (ppm): 159.6, 159.4, 152.4, 143.3, 137.9, 120.2, β-CD signals consistent with loss of C7 symmetry: (99.2–98.5; β-CD C_1), 82.1–81.4, 80.4–79.9, 71.5–70.9, 70.1, 63.8, 61.6–61.3, 59.2–58.3, 55.1, 39.9; **HRMS** (ESI +ve) *m/z*: 1778.6452 ($[M + Na]^+$, $C_{72}H_{118}O_{36}N_5INa$ calc. 1778.6493).

6^{A}-amido-pmβCD-appended XB 'chloro-arm' (2.34I)

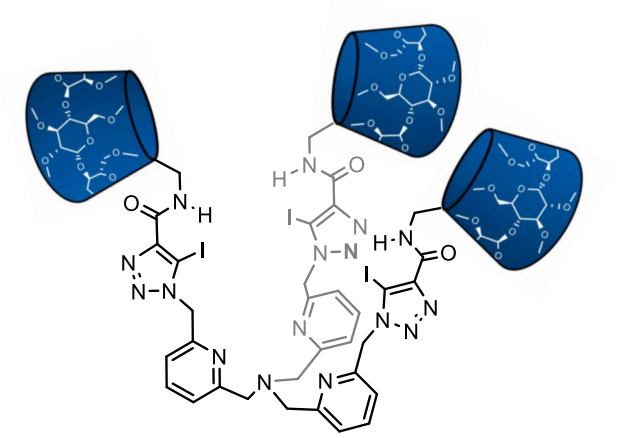


To a solution of **2.23I** (1.04 g, 0.59 mmol) in dry CH_2Cl_2 (25 ml) at 0 °C, was slowly added $SOCl_2$ (0.13 ml, 1.77 mmol) and the reaction stirred at rt under a N_2 atmosphere for 6 hrs. The stirring mixture was carefully quenched and neutralised by the slow addition of a saturated $Na_2CO_{3(aq)}$ solution at 0 °C resulting in vigorous gas evolution. Thereafter, the biphasic mixture was further diluted with $CHCl_3$ (25 ml) and washed with H_2O (2 x 25 ml). The organic layer was dried over $MgSO_4$ and solvent removal *in vacuo* gave the chloro-arm **2.34I** as a cream coloured powder in good purity which was used without further purification (809 mg , 77%).

^{1}H NMR (500 MHz, $CDCl_3$) δ (ppm): 7.72 (1H, t, ^{3}J = 7.8 Hz, pyridine Ar*H*), 7.45–7.49 (2H, m, pyridine Ar*H* + amide N*H*), 6.87 (1H, d, ^{3}J = 7.8 Hz, pyridine Ar*H*), 5.78 (2H, ABquart., $\Delta\delta_{AB}$ = 0.05, $^{2}J_{AB}$ = 16.0 Hz, CH_2-N iodotriazole), 5.12–5.23 (7H, m, β-CD H_1), 4.64 (2H, s, CH_2Cl), 3.18–4.01 (102H, m, β-CD $H_{2\text{-}6}$ + CH_3O); **^{13}C NMR** (125 MHz, $CDCl_3$) δ (ppm): 159.4, 157.0, 153.3,

143.3, 138.2, 122.3, 120.5, *β*-CD signals consistent with loss of C7 symmetry: (99.2–98.6; *β*-CD C_1), 82.2–81.7, 81.4, 80.4–80.0, 71.5 – 70.9, 70.1, 61.6 – 61.3, 59.2 – 58.3, 55.2, 46.2, 39.9; **HRMS** (ESI +ve) *m/z*: 1796.6112 ([M + Na]$^+$, $C_{72}H_{117}O_{35}N_5ClINa$ calc. 1796.6154).

Tris(pm*β*CD)-appended XB tripodal ligand (2.35I)

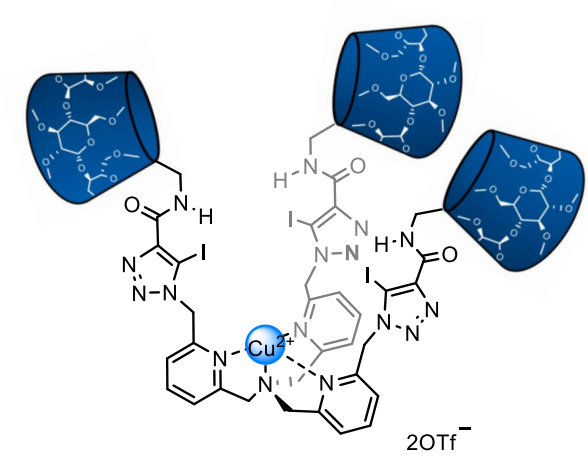


To a solution of **2.34I** (423 mg, 0.238 mmol) fully dissolved in dry CH_3CN (20 mL) was added NH_4OAc (550 mg, 7.14 mmol), Na_2CO_3 (757 mg, 7.14 mmol) and KI (39.5 mg, 0.238 mmol) as solid portions. The reaction flask was completely sealed, and the mixture vigorously stirred for two days at room temperature after which no evidence of **2.34I** was observed by TLC or ESI-MS analyses.. Thereafter, the creamy white suspension was directly transferred to a separating funnel and *ca.* 5-10 ml H_2O very gently pipetted into the vessel. The cloudy, lower aqueous layer was separated, and the remaining clear pale yellow organic layer concentrated *in vacuo*. The resultant crude residue was redissolved in $CHCl_3$ (25 mL) and washed with brine (2 x 10 mL) and the organics dried over $MgSO_4$. Solvent removal and purification by preparative thin layer chromatography (6% MeOH in CH_2Cl_2) afforded the tripodal ligand **2.35I** as a crystalline off-white solid upon drying *in vacuo* (216 mg, 52% yield).

^{1}H NMR (500 MHz, $CDCl_3$) *δ* (ppm): 7.66 (3H, t, ^3J = 7.7 Hz, pyridine Ar*H*), 7.46–7.49 (6H, m, pyridine Ar*H* + amide N*H*), 6.73 (3H, d, ^3J = 7.8 Hz, pyridine Ar*H*), 5.77 (6H, ABquart., $\Delta\delta_{AB}$ = 0.05, $^2J_{AB}$ = 16.1 Hz, CH_2-N iodotriazole), 5.13–5.23 (21H, m, *β*-CD H_1), 3.17–3.97 (312H, m, *β*-CD $H_{2\text{-}6}$ + CH_3O + CH_2-N tertiary amine); **^{13}C NMR** (125 MHz, $CDCl_3$) *δ* (ppm): 159.5, 153.1,

143.3, 137.7, 122.3, 119.5, *β*-CD signals consistent with loss of C7 symmetry: (99.0–98.6; *β*-CD C_1), 82.3–81.2, 80.4–79.9, 71.5–70.0, 61.5–61.4, 59.7–58.4, 55.5, 39.8; **HRMS** (ESI +ve) *m/z*: 2626.9897 ($[M + H + Na]^+$, $C_{216}H_{352}O_{105}N_{16}I_3Na$ calc. 2626.9858).

Tris(pm*β*CD)-appended XB Cu(II)-tripod (2.36I·2OTf)



To tripodal ligand **2.35I** (100 mg, 0.02 mmol) in a 1:1 mixture of CH_2Cl_2/MeOH (6 mL) was added copper(II) trifluoromethansulfonate (7.23 mg, 0.02 mmol) and the solution stirred at room temperature under a N_2 atmosphere for 3 hours. After removal of the solvent *in vacuo*, the resultant deep blue residue was triturated with ice cold Et_2O (*ca*. 5 mL). The ethereal layer was carefully decanted with a pipette and the contents of the flask dried under high vacuum to afford metallo-tripodal receptor **2.36I**·2OTf as a fine, pale blue crystalline powder (106 mg, quantitative).

UV-Vis (CH_3CN/ H_2O 6:4 *v/v*, 10 mM HEPES, λ_{max}/ nm, (ε/ M^{-1} cm^{-1})): 645 (182), 770 (119); **EPR** (CH_3CN/ H_2O 6:4 *v/v*, 10 mM HEPES, 105 K): $g\parallel = 2.225$, $g\perp = 2.065$, $A\parallel_1 = 185.0 \times 10^{-4}$ cm^{-1}, $A\parallel_2 = 220.0 \times 10^{-4}$ cm^{-1}; **HRMS** (ESI +ve) *m/z*: 2647.9654 ($[M - 2OTf]^{2+}$, $C_{216}H_{351}N_{16}O_{105}I_3{}^{63}Cu$ calc. 2647.4551).

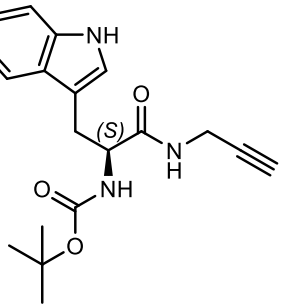
Tetrabutylammonium salt of pinacolyl methylphosphonic acid (TBAPMP)

To a chilled solution of 1.0 eqv of a methanolic solution of tetrabutylammonium (TBA) hydroxide at 0 °C directly was added 1.0 eqv of neutral pinacolyl methylphoshonic acid over 5 minutes. The resulting reaction mixture was allowed to warm to room temperature and stirred for 3 hours. The

appropriate TBA pinacolyl methyl phosphonate salt was obtained by removal of the solvent *in vacuo* and leaving the salt to dry under high vacuum for at least 5 days. The resultant salt was obtained a white powder and stored in a vacuum desiccator with P_2O_5 desiccant at room temperature.

6.2.2 Synthesis of novel compounds from Chapter Three

_N_Boc-(S)-tryptophan alkyne (3.1)

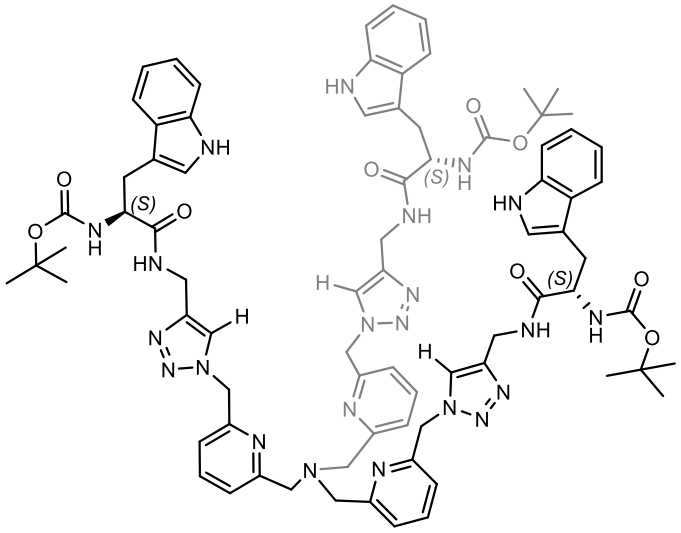


To a solution of N_α-(*tert*-Butoxycarbonyl)-L-tryptophan (1 g, 3.29 mmol) in dry DMF (40 mL) was added ethylcarbodiimide hydrochloride (EDC·HCl) (693 mg, 3.61 mmol) and hydroxybenzotriazole (HOBt) (488 mg, 3.61 mmol) and the cloudy suspension stirred at room temperature under a N_2 atmosphere for 30 minutes until all the reagents were fully dissolved. Further added were propargylamine (0.21 mL, 3.29 mmol) and DIPEA (2 mL, 11.5 mmol) and the reaction mixture left stirring overnight whereupon a clear, pale yellow solution was observed. After azeotropic removal of DMF on a rotary with toluene, the crude product was partitioned between H_2O (25 mL) and $CHCl_3$ (50 mL). The separated organic layer was washed with 1M HCl (25 mL) followed by brine (2 x 25 mL) and dried with $MgSO_4$. After removal of the solvent *in vacuo*, purification by silica gel column chromatography (gradient from pure CH_2Cl_2 to 3% MeOH in CH_2Cl_2) afforded alkyne **3.1** as a pastel yellow powder (897 mg, 80%).

^{1}H NMR (500 MHz, $CDCl_3$) δ (ppm): 8.23 (1H, br. s., indole N*H*), 7.65 (1H, d, ^3J = 7.6 Hz, indole Ar*H*), 7.37 (1H, d, ^3J = 8.1 Hz, indole Ar*H*), 7.21 (t, ^3J = 7.2 Hz, indole Ar*H*), 7.14 (t, 1H, ^3J = 7.2 Hz, indole Ar*H*), 7.06 (1H, s, indole Ar*H*), 6.08 (1H, m, CON*H*CH_2), 5.15 (1H, br. s., Boc N*H*),

4.45 (1H, br. s., C*H*-N Boc), 3.92 (2H, br. s., CH_2C≡C), 3.31 (1H, br. m, C$H_{2(1)}$-C indole), 3.21 (1H, br. m., C$H_{2(2)}$-C indole), 2.15 (1H, s, C≡C*H*), 1.43 (9H, s, Boc CH_3); **^{13}C NMR** (125 MHz, $CDCl_3$) δ (ppm): 171.5, 155.5, 136.2, 127.4, 123.3, 122.3, 119.8, 118.8, 111.2, 110.4, 80.2, 79.1, 71.5, 55.0, 29.0, 28.3, one peak missing, presumed overlapped; **HRMS** (ESI +ve) *m/z*: 342.1811 ([M + H]$^+$, $C_{19}H_{24}N_3O_3$ calc. 342.1812); $[\alpha]_D^{25}$ – 9.3 (c 1.00, $CHCl_3$).

Tris(*N*Boc-(S)-tryptophan)-appended HB tripodal ligand (3.2H)

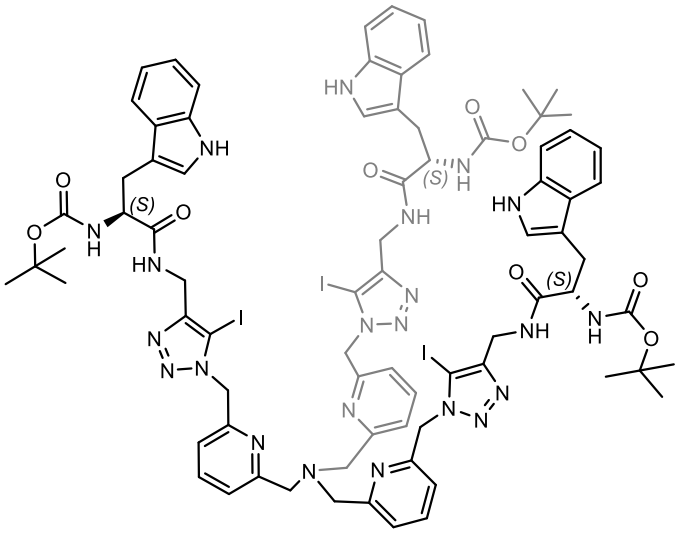


To a solution of Zn(II)-tripodal azide subunit **2.13**·2ClO_4 (100 mg, 0.139 mmol) and chiral alkyne **3.1** (171 mg, 0.5 mmol) in a 3:1 mixture of dry, degassed CH_2Cl_2/THF (4 mL) was added $[Cu(MeCN)_4][PF_6]$ (78 mg, 0.209 mmol) and DIPEA (18.2 μL, 0.104 mmol) and the reaction stirred at room temperature under a N_2 atmosphere for 2 days. The reaction mixture was diluted with CH_2Cl_2 (20 mL) and washed with $NH_4OH_{(aq)}$ (3 x 10 mL), brine (2 x 10 mL) and dried over $MgSO_4$. After removal of the solvent *in vacuo*, purification by preparative silica gel thin-layer chromatography (5% MeOH in CH_2Cl_2) afforded the chiral tripodal framework **3.2H** as a pale yellow solid (43 mg, 21%).

^{1}H NMR (500 MHz, Acetone-d_6) δ (ppm): 10.10 (3H, s, indole N*H*), 7.74 (3H, br. m., CON*H*CH_2), 7.68 (3H, t, ^3J = 7.7 Hz, pyridine Ar*H*), 7.60 (6H, m, indole Ar*H* + triazole C*H*), 7.43 (3H, d, ^3J = 7.6 Hz, pyridine Ar*H*), 7.34 (3H, d, ^3J = 8.1, indole Ar*H*), 7.10 (3H, s, indole Ar*H*), 7.05 (6H, m,

pyridine Ar*H* + indole Ar*H*), 6.97 (3H, t, ^{3}J = 6.9 Hz, indole Ar*H*), 6.01 (3H, br. d., ^{3}J = 5.5 Hz, Boc N*H*), 5.56 (6H, s, CH_2-N triazole), 4.35– 4.47 (9H, m, CH_2-C triazole + C*H*-N Boc), 3.78 (6H, s, CH_2-N tertiary amine), 3.24 (3H, dd, *J* = 14.7, 6.1 Hz, C$H_{2(1)}$-C indole), 3.12 (3H, dd, *J* = 14.0, 6.7 Hz, C$H_{2(2)}$-C indole), 1.32 (27H, s, Boc CH_3); **^{13}C NMR** (125 MHz, Acetone-d_6) δ (ppm): 172.8, 160.5, 156.3, 155.4, 146.3, 138.6, 137.6, 128.9, 124.7, 124.1, 123.4, 122.2, 121.3, 119.6, 112.3, 111.4, 111.3, 79.4, 60.5, 56.4, 55.7, 35.8, 28.7, one peak missing, presumed overlapped; **HRMS** (ESI +ve) *m/z*: 1479.7357 ([M + H]$^+$, $C_{78}H_{91}N_{22}O_9$ calc. 1479.7339); $[\alpha]_D^{25}$ – 9.9 (c 1.00, $CHCl_3$).

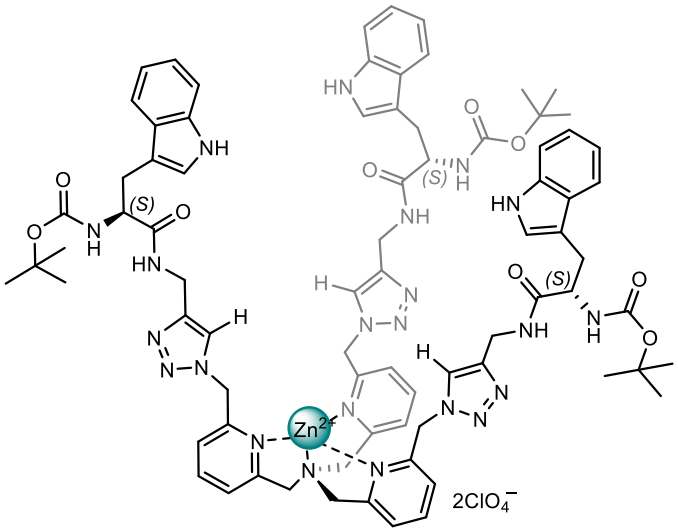
Tris(*N*Boc-(S)-tryptophan)-appended XB tripodal ligand (3.2I)



Zn(II)-tripodal azide subunit **2.13**·2ClO_4 (100 mg, 0.139 mmol) was dissolved in a 1:1 mixture of dry, degassed THF/CH_3CN (4 mL) and the reaction vessel covered in foil. Sodium iodide (250 mg, 1.67 mmol) and copper(II) perchlorate hexahydrate (309 mg, 0.834 mmol) were added and the solution stirred for 5 minutes. Further added were DBU (70.5 μL, 0.5 mmol) and chiral alkyne **3.1** (171 mg, 0.5 mmol) and the mixture stirred at room temperature under a N_2 atmosphere overnight. The reaction mixture was diluted with $CHCl_3$ (20 mL) and washed with $NH_4OH_{(aq)}$ (3 x 10 mL), brine (2 x 10 mL) and dried over $MgSO_4$. After removal of the solvent *in vacuo*, purification by preparative silica gel thin-layer chromatography (6% MeOH in CH_2Cl_2) afforded the chiral tripodal framework **3.2I** as a pale yellow solid (72.4 mg, 28%).

^{1}H NMR (500 MHz, Acetone-d_6) δ (ppm): 10.05 (3H, s., indole N*H*), 7.70 (3H, t, ^{3}J = 7.7 Hz, pyridine Ar*H*), 7.63 (3H, m, CON*H*CH$_2$), 7.60 (3H, d, ^{3}J = 7.8 Hz, indole Ar*H*), 7.40 (3H, d, ^{3}J = 7.6 Hz, pyridine Ar*H*), 7.34 (3H, d, ^{3}J = 7.9 Hz, indole Ar*H*), 7.16 (3H, s, indole Ar*H*), 7.06 (3H, t, ^{3}J = 7.6 Hz, indole Ar*H*), 6.98 (6H, m, pyridine Ar*H* + indole Ar*H*), 5.95 (3H, br. d., ^{3}J = 7.5 Hz, Boc N*H*), 5.72 (6H, s, C*H*$_2$-N iodotriazole), 4.39 – 4.5 (9H, m, C*H*$_2$-C iodotriazole + C*H*-N Boc), 3.70 (6H, s, C*H*$_2$-N tertiary amine), 3.28 (3H, dd, J = 14.6, 5.5 Hz, C*H*$_{2(1)}$-C indole), 3.14 (3H, dd, J = 14.0, 7.2 Hz, C*H*$_{2(2)}$-C indole), 1.33 (27H, s, Boc C*H*$_3$); **^{13}C NMR** (125 MHz, Acetone-d_6) δ (ppm): 172.6, 160.5, 156.3, 154.8, 149.5, 138.5, 137.6, 128.9, 124.6, 123.4, 122.1, 121.0, 119.6, 112.2, 111.4, 111.3, 82.0, 79.4, 60.1, 56.2, 56.0, 36.1, 28.7, one peak missing, presumed overlapped; **HRMS** (ESI +ve) *m/z*: 1857.4215 ([M + H]$^+$, $C_{78}H_{88}N_{22}O_9I_3$ calc. 1857.4239); $[\alpha]_D^{25}$ – 12.4 (c 1.00, $CHCl_3$).

Tris(*N*Boc-(S)-tryptophan)-appended Zn(II)-HB tripod (3.3H·2ClO$_4$)

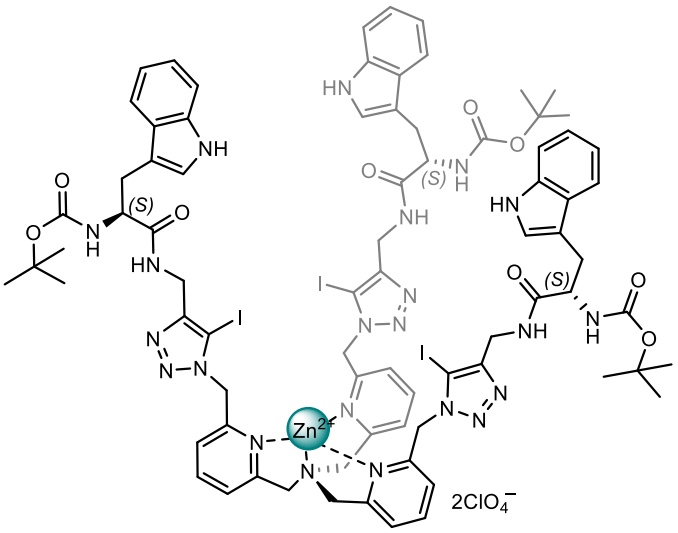


To tripodal ligand **3.2H** (100 mg, 0.068 mmol) in a 1:1 mixture of CH_2Cl_2/MeOH (10 mL) was added zinc(II) perchlorate hexahydrate (25.3 mg, 0.068 mmol) and the solution stirred at room temperature under a N_2 atmosphere for 3 hours. After removal of the solvent *in vacuo*, the resultant light yellow residue was triturated with ice cold Et_2O (*ca*. 5 mL). The ethereal layer was carefully

decanted with a pipette and the contents of the flask dried under high vacuum to afford metallo-tripodal receptor **3.3H**·2ClO_4 as a fine, light yellow crystalline powder (117 mg, quantitative).

^{1}H NMR (500 MHz, Acetone-d_6) δ (ppm): 10.03 (3H, s, indole N*H*), 8.18 (3H, br. t., pyridine Ar*H*), 8.06 (3H, br. s., CON*H*CH_2), 7.76 (3H, br. m., pyridine Ar*H*), 7.68 (6H, br. m., pyridine Ar*H* + triazole C*H*), 7.60 (3H, br. d., indole Ar*H*), 7.17 (3H, s, indole Ar*H*), 7.08 (3H, t, ^3J = 7.5 Hz, indole Ar*H*), 6.99 (3H, t, ^3J = 7.1 Hz, indole Ar*H*), 6.27 (3H, br. s., Boc N*H*), 5.69 (6H, s, CH_2-N triazole), 4.43–4.57 (9H, m, CH_2-N tertiary amine + C*H*-N Boc), 4.22 (6H, br. s., CH_2-C triazole), 3.30 (3H, m, C$H_{2(1)}$-C indole), 3.16 (3H, m, C$H_{2(2)}$-C indole), 1.33 (27H, s, Boc CH_3); **^{13}C NMR** (125 MHz, Acetone-d_6) δ (ppm): 183.2, 156.7, 153.8, 147.1, 142.8, 137.6, 128.7, 126.0, 124.8, 122.3, 119.7, 119.5, 112.4, 111.2, 80.0, 70.9, 60.4, 56.9, 49.3, 35.8, 28.7, three peaks missing, presumed overlapped; **HRMS** (ESI +ve) *m/z*: 771.3250 ([M – 2ClO_4]$^{2+}$, $C_{78}H_{90}N_{22}O_9{}^{64}Zn$ calc. 771.3270); $[\alpha]_D^{25}$ + 16.5 (c 1.00, CH_3CN).

Tris(*N*Boc-(S)-tryptophan)-appended Zn(II)-XB tripod (3.3I·2ClO_4**)**

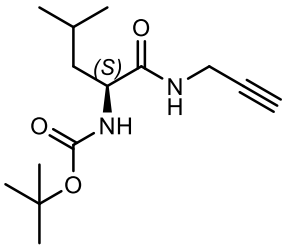


To tripodal ligand **3.2I** (94.4 mg, 0.051 mmol) in a 1:1 mixture of CH_2Cl_2/MeOH (10 mL) was added zinc(II) perchlorate hexahydrate (19 mg, 0.051 mmol) and the solution stirred at room temperature under a N_2 atmosphere for 3 hours. After removal of the solvent *in vacuo*, the resultant pale orange residue was triturated with ice cold Et_2O (*ca*. 5 mL). The ethereal layer was carefully

decanted with a pipette and the contents of the flask dried under high vacuum to afford metallo-tripodal receptor **3.3I**·2ClO_4 as a fine, pale yellow crystalline powder (106 mg, quantitative).

^{1}H NMR (500 MHz, Acetone-d_6) δ (ppm): 10.07 (3H, s, indole N*H*), 8.18 (3H, t, ^3J = 7.6 Hz, pyridine Ar*H*), 7.94 (3H, br. s., pyridine Ar*H*), 7.80 (3H, br. s., CON*H*CH_2), 7.65 (3H, d, ^3J = 7.2 Hz, pyridine Ar*H*), 7.60 (3H, d, ^3J = 8.1 Hz, indole Ar*H*), 7.36 (3H, d, ^3J = 8.1 Hz, indole Ar*H*), 7.18 (3H, s, indole Ar*H*), 7.07 (3H, t, ^3J = 7.4 Hz, indole Ar*H*), 6.99 (3H, t, ^3J = 7.5 Hz, indole Ar*H*), 6.15 (3H, br. s., Boc N*H*), 5.84 (6H, s, CH_2-N iodotriazole), 4.55 (3H, br. s., C*H*-N Boc), 4.47 (3H, d, ^3J = 16.4 Hz, C$H_{2(1)}$-N tertiary amine), 4.35 (3H, d, ^3J = 16.9 Hz, C$H_{2(1)}$-N tertiary amine), 4.24 (6H, s, CH_2-C iodotriazole), 3.27 (3H, m, C$H_{2(1)}$-C indole), 3.08 (3H, m, C$H_{2(2)}$-C indole), 1.34 (27H, s, Boc CH_3); **^{13}C NMR** (125 MHz, Acetone-d_6) δ (ppm): 173.3, 156.6, 156.6, 153.4, 150.3, 142.8, 137.6, 128.8, 127.1, 126.0, 124.7, 119.6, 112.3, 111.3, 86.0, 79.6, 56.7, 56.2, 55.0, 36.0, 28.7, three peaks missing, presumed overlapped; **HRMS** (ESI +ve) *m/z*: 2019.2883 ([M – ClO_4]$^+$, $C_{78}H_{87}N_{22}O_{13}ClI_3{}^{64}Zn$ calc. 2019.2931); $[\alpha]_D^{25}$ + 37.2 (c 1.00, CH_3CN).

***N*Boc-(S)-leucine alkyne (3.4)**

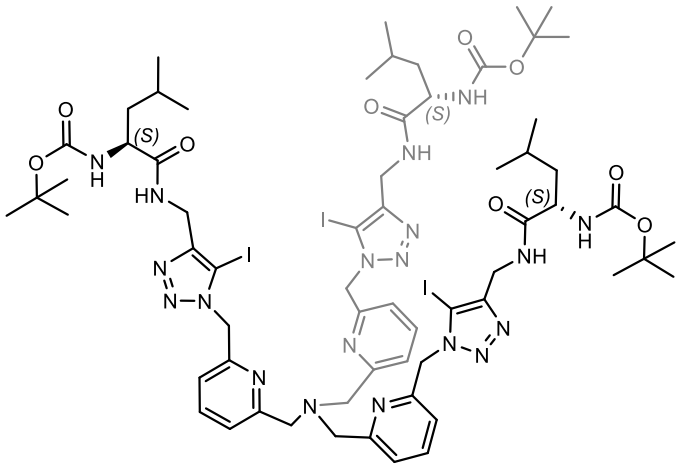


To a solution of N_α-(*tert*-Butoxycarbonyl)-L-leucine (1 g, 4.32 mmol) in dry DMF (40 mL) was added EDC·HCl (912 mg, 4.76 mmol) and HOBt (643 mg, 4.76 mmol) and the cloudy suspension stirred at room temperature under a N_2 atmosphere for 30 minutes until all the reagents were fully dissolved. Further added were propargylamine (0.28 mL, 4.32 mmol) and DIPEA (2.63 mL, 15.1 mmol) and the reaction mixture left stirring overnight whereupon a clear, pale yellow solution was observed. After azeotropic removal of DMF on a rotary with toluene, the crude product was partitioned between H_2O (25 mL) and $CHCl_3$ (50 mL). The separated organic layer was washed

with 1M HCl (25 mL) followed by brine (2 x 25 mL) and dried with $MgSO_4$. After removal of the solvent *in vacuo*, purification by silica gel column chromatography (gradient from pure CH_2Cl_2 to 1% MeOH in CH_2Cl_2) afforded alkyne **3.4** as an off-white powder (1.02 g, 88%).

^{1}H NMR (500 MHz, $CDCl_3$) δ (ppm): 6.61 (1H, br. s., CON*H*CH_2), 4.93 (1H, br. d, ^3J = 7.9 Hz, Boc N*H*), 4.13 (1H, br. s., C*H*-N Boc), 4.04 (2H, m, CH_2C≡C), 2.22 (1H, t, ^4J = 2.4 Hz, C≡C*H*), 1.64–1.68 (2H, m, C$H_{2(1)}$-C isopropyl + isopropyl C*H*), 1.49 (1H, m, C$H_{2(2)}$-C isopropyl), 1.45 (s, 9H, Boc CH_3), 0.94 (6H, t, ^3J = 6.6 Hz, isopropyl CH_3); **^{13}C NMR** (125 MHz, $CDCl_3$) δ (ppm): 172.3, 155.8, 80.2, 79.3, 71.6, 52.8, 41.0, 29.1, 28.3, 24.7, 22.9, 21.9; **HRMS** (ESI +ve) *m/z*: 269.1860 ([M + H]$^+$, $C_{14}H_{25}N_2O_3$ calc. 269.1859); $[\alpha]_D^{25}$ – 42.2 (c 1.00, $CHCl_3$).

Tris(*N*Boc-(S)-leucine)-appended XB tripodal ligand (3.5I)

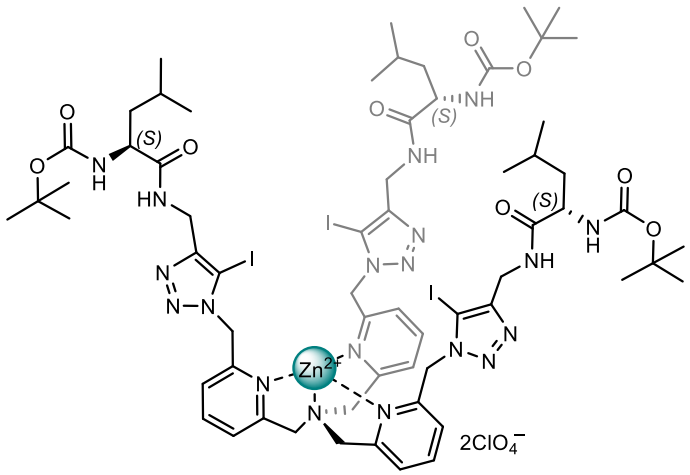


Zn(II)-tripodal azide subunit **2.13**·$2ClO_4$ (100 mg, 0.139 mmol) was dissolved in a 1:1 mixture of dry, degassed THF/CH_3CN (4 mL) and the reaction vessel covered in foil. Sodium iodide (250 mg, 1.67 mmol) and copper(II) perchlorate hexahydrate (309 mg, 0.834 mmol) were added and the solution stirred for 5 minutes. Further added were DBU (70.5 μL, 0.5 mmol) and chiral alkyne **3.4** (134 mg, 0.5 mmol) and the mixture stirred at room temperature under a N_2 atmosphere overnight. The reaction mixture was diluted with $CHCl_3$ (20 mL) and washed with $NH_4OH_{(aq)}$ (3 x 10 mL), brine (2 x 10 mL) and dried over $MgSO_4$. After removal of the solvent *in vacuo*, purification by

preparative silica gel thin-layer chromatography (5% MeOH in CH_2Cl_2) afforded the chiral tripodal framework **3.5I** as a pale yellow powder (125 mg, 55%).

^{1}H NMR (500 MHz, Acetone-d_6) δ (ppm): 7.75 (3H, t, ^3J = 7.7 Hz, pyridine Ar*H*), 7.62 (3H, br. s., CON*H*CH_2), 7.46 (3H, d, ^3J = 7.6 Hz, pyridine Ar*H*), 6.99 (3H, d, ^3J = 7.6 Hz, pyridine Ar*H*), 6.07 (3H, br. d, ^3J = 7.9 Hz, Boc N*H*), 5.76 (6H, s, CH_2-N iodotriazole), 4.39–4.49 (m, 6H, CH_2-C iodotriazole), 4.20 (3H, br. s., C*H*-N Boc), 3.76 (6H, s, CH_2-N tertiary amine), 1.71 (3H, m, isopropyl C*H*), 1.51–1.62 (6H, m, CH_2-C isopropyl), 1.38 (27H, s, Boc CH_3), 0.89 (18H, t, ^3J = 7 Hz, isopropyl CH_3); **^{13}C NMR** (125 MHz, Acetone-d_6) δ (ppm): 173.3, 160.5, 156.5, 154.9, 149.6, 138.5, 123.4, 120.8, 81.8, 60.2, 56.0, 54.0, 42.6, 36.1, 28.7, 25.5, 23.6, 22.1; **HRMS** (ESI +ve) *m/z*: 1638.4354 ([M + H]$^+$, $C_{63}H_{91}N_{19}O_9I_3$ calc. 1638.4381); $[\alpha]_D^{25}$ – 16.9 (c 1.00, $CHCl_3$).

Tris(*N*Boc-(S)-leucine)-appended Zn(II)-XB tripod (3.6I·2ClO$_4$)



To tripodal ligand **3.5I** (95 mg, 0.058 mmol) in a 1:1 mixture of CH_2Cl_2/MeOH (10 mL) was added zinc(II) perchlorate hexahydrate (21.6 mg, 0.058 mmol) and the solution stirred at room temperature under a N_2 atmosphere for 3 hours. After removal of the solvent *in vacuo*, the resultant light orange residue was triturated with ice cold Et_2O (*ca*. 5 mL). The ethereal layer was carefully decanted with a pipette and the contents of flask dried under high vacuum to afford metallo-tripodal receptor **3.6I**·2ClO_4 as a fine, pale yellow crystalline powder (110 mg, quantitative).

^{1}H NMR (500 MHz, Acetone-d_6) δ (ppm): 8.24 (3H, t, ^{3}J = 7.7 Hz, pyridine Ar*H*), 8.07 (3H, br. d., ^{3}J = 5.8 Hz, pyridine Ar*H*), 7.87 (3H, br. s., CON*H*CH$_2$),7.70 (3H, d, ^{3}J = 7.8 Hz, pyridine Ar*H*), 6.33 (3H, br. s., Boc N*H*), 5.91 (6H, br. s., C*H*$_2$-N iodotriazole), 4.54 (3H, d, ^{3}J = 16.5 Hz, C*H*$_{2(1)}$-N tertiary amine), 4.33–4.40 (6H, m, C*H*$_{2(2)}$-N tertiary amine + C*H*-N Boc), 4.24 (6H, br. s., C*H*$_2$-C iodotriazole), 1.75 (3H, m, isopropyl C*H*), 1.54–1.65 (6H, m, C*H*$_2$-C isopropyl), 1.43 (27H, s, Boc C*H*$_3$), 0.92 (18H, d, ^{3}J = 6.4 Hz, isopropyl C*H*$_3$); **^{13}C NMR** (125 MHz, Acetone-d_6) δ (ppm): 174.1, 156.9, 156.6, 153.5, 150.3, 142.7, 127.5, 126.0, 79.5, 56.7, 54.9, 53.8, 42.9, 35.7, 28.8, 25.6, 23.7, 21.9; **HRMS** (ESI +ve) *m/z*: 1800.3026 ([M – ClO$_4$]$^+$, $C_{63}H_{90}N_{19}O_{13}ClI_3{}^{64}Zn$ calc. 1800.3074); $[\alpha]_D^{25}$ + 59.6 (c 1.00, CHCl$_3$).

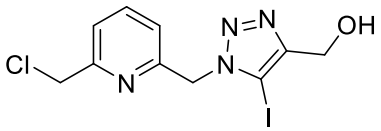
Tetrabutylammonium (TBA) salt of chiral anions

An analogous procedure as adopted as that reported by Dong et. al.[17]

To a chilled solution of the neutral monobasic acid (anion precursor) (1.0 eqv) in water/THF 10:1 *v/v* at 0 °C was added a 1.0 eqv of a methanolic solution of tetrabutylammonium (TBA) hydroxide over 5 minutes. The resulting reaction was allowed to warm up to room temperature and stirred for 3 hours following which, the reaction was extracted with dichloromethane (5 x 10 mL). The chiral TBA salt was obtained by removal of solvent *in vacuo* and leaving the salt to dry under high vacuum for at least 3 days. The salts were stored in a vacuum desiccator with P_2O_5 desiccant at -20 °C to minimise racemisation.

6.2.3 Synthesis of novel compounds from Chapter Four

Methanol-appended XB 'chloro-arm' (4.1I)



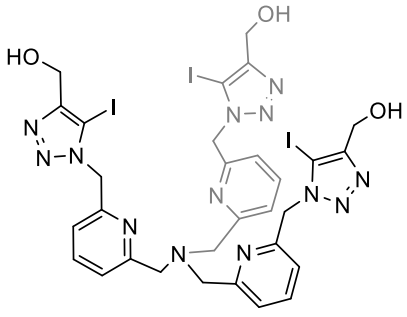
2-(azidomethyl)-6-(chloromethyl)pyridine **2.11** (350 mg, 1.92 mmol) was dissolved in a 1:1 mixture of dry, degassed THF/CH$_3$CN (6 mL) and the reaction vessel covered in foil. Sodium iodide

(1.15 g, 7.68 mmol) and copper(II) perchlorate hexahydrate (1.42 g, 3.84 mmol) were added and the solution stirred for 5 minutes. Further added were TBTA (21.2 mg, 0.04 mmol), 1,8-Diazabicyclo[5.4.0]undec-7-ene (DBU) (292 mg, 1.92 mmol, in 0.5 mL 1:1 THF/CH_3CN) and propargyl alcohol (0.11 mL, 1.92 mmol) and the mixture stirred at room temperature under a N_2 atmosphere overnight. The reaction mixture was diluted with CH_2Cl_2 (25 mL) and washed with $NH_4OH_{(aq)}$ (3 x 20 mL), brine (2 x 20 mL) and dried over $MgSO_4$. After removal of the solvent *in vacuo*, purification by silica gel column chromatography (gradient from 1% MeOH in CH_2Cl_2 to 4% MeOH in CH_2Cl_2) afforded **4.1I** as a pale yellow solid (384 mg, 55%).

^{1}H NMR (500 MHz, $CDCl_3$) δ (ppm): 7.70 (1H, t, ^3J = 7.8 Hz, pyridine Ar*H*), 7.45 (1H, d, ^3J = 7.8 Hz, pyridine Ar*H*), 6.86 (1H, d, ^3J = 7.8 Hz, pyridine Ar*H*), 5.75 (2H, s, C*H*$_2$-N iodotriazole), 4.77 (2H, d, ^3J = 4.9 Hz, C*H*$_2$OH), 4.66 (2H, s, C*H*$_2$Cl), 2.34 (1H, t, ^3J = 5.2 Hz, O*H*); **^{13}C NMR** (125 MHz, $CDCl_3$) δ (ppm): 156.8, 153.8, 151.3, 138.3, 122.2, 120.7, 79.6, 56.7, 55.4, 46.3; **HRMS** (ESI +ve) *m/z*: 364.9664 ($[M + H]^+$, $C_{10}H_{11}N_4OClI$ calc. 364.9661).

(*N.B.* During the purification process, a second compound was found to partially co-elute with **4.1I**. This was identified by ESI-MS analysis (peak at *m/z* = 456.9 $[M + H]^+$) as the corresponding '6-(iodomethyl)pyridine-*arm*' and also used in subsequent tripodal ligand formation procedures).

Tris(methanol)-appended XB tripodal ligand (4.2I)

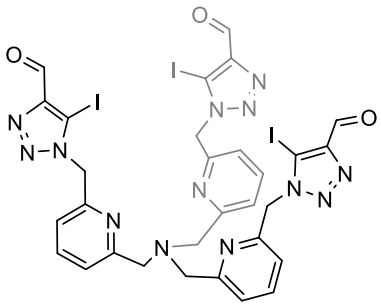


To a solution of **4.1I** (1 g, 2.74 mmol) fully dissolved in dry CH_3CN (30 mL) was added NH_4OAc (4.22 g, 54.8 mmol), Na_2CO_3 (5.8 g, 54.8 mmol) and KI (455 mg, 2.74 mmol) as solid portions. The reaction flask was completely sealed, and the mixture vigorously stirred for two days at room

temperature after which no evidence of **4.1I** was observed by TLC or ESI-MS analyses. Thereafter, the creamy white suspension was directly transferred to a separating funnel and *ca.* 40 ml H_2O very gently pipetted into the vessel. The cloudy, lower aqueous layer was separated, and to the remaining clear organic layer was added $CHCl_3$ (50 mL). The organic phase was washed with water (3 x 50 mL) and the organics dried over $MgSO_4$. After removal of the solvent *in vacuo*, purification of the residue by recrystallisation from a hot MeOH solution afforded tripodal ligand **4.2I** a fine white crystalline powder (385 mg, 42% yield)

^{1}H NMR (500 MHz, DMSO-d_6) δ (ppm): 7.74 (3H, t, ^3J = 7.8 Hz, pyridine Ar*H*), 7.38 (3H, d, ^3J = 7.8 Hz, pyridine Ar*H*), 6.90 (3H, d, ^3J = 7.6 Hz, pyridine Ar*H*), 5.69 (6H, s, CH_2-N iodotriazole), 5.24 (3H, t, ^3J = 5.5 Hz, O*H*), 4.43 (6H, d, ^3J = 5.5 Hz, CH_2OH), 3.64 (6H, s, CH_2-N tertiary amine); **^{13}C NMR** (125 MHz, DMSO-d_6) δ (ppm): 159.0, 154.0, 151.2, 137.9, 122.3, 120.0, 84.5, 59.0, 55.0, 54.8; **HRMS** (ESI +ve) *m/z*: 1001.9791 ([M + H]$^+$, $C_{30}H_{31}N_{13}O_3I_3$ calc. 1001.9801).

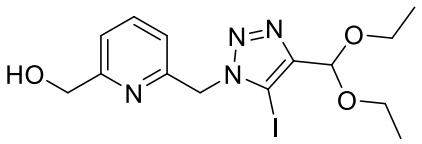
Tris(aldehyde)-appended XB tripodal ligand (4.3I)



To a solution of **4.6I** (1.25 g, 1.03 mmol) fully dissolved in a 3:1 mixture of CH_2Cl_2/H_2O (20 mL) was added TFA (1.5 mL) and the reaction mixture stirred at room temperature under a N_2 atmosphere overnight. Further added was CH_2Cl_2 (10 mL) and the organic phase washed with sat. $NaHCO_{3(aq)}$ (2 x 20 mL), brine (2 x 25 mL) and dried over $MgSO_4$. After removal of the *solvent in vacuo*, the residue was triturated with a cold Et_2O solution (2 x 10 mL) and dried under high vacuum to afford tris(aldehyde) **4.3I** as a fine yellow powder (918 mg, 90% yield).

^{1}H NMR (500 MHz, CD_3CN) δ (ppm): 10.0 (3H, s, CO*H*), 7.68 (3H, t, ^{3}J = 7.7 Hz, pyridine Ar*H*), 7.25 (6H, d, ^{3}J = 7.8 Hz, pyridine Ar*H*), 7.11 (6H, d, ^{3}J = 7.8 Hz, pyridine Ar*H*), 5.76 (6H, s, CH_2-N iodotriazole), 3.56 (6H, s, CH_2-N tertiary amine); **^{13}C NMR** (125 MHz, CD_3CN) δ (ppm): 185.4, 153.9, 148.8, 138.7, 123.8, 121.5, 87.3, 60.0, 55.8, one peak missing, presumed overlapped; **HRMS** (ESI +ve) *m/z*: 995.9321 ($[M + H]^+$, $C_{30}H_{25}N_{13}O_3I_3$ calc. 995.9331).

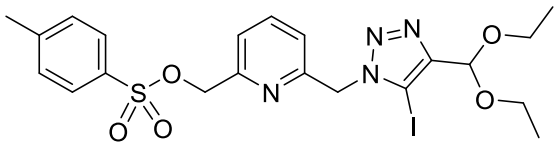
Diethoxyethane-appended XB 'arm' precursor (4.4I)



(6-(azidomethyl)pyridine-2-yl)methanol **2.9** (200 mg, 1.22 mmol) was dissolved in a 1:1 mixture of dry, degassed THF/CH_3CN (3 mL) and the reaction vessel covered in foil. Sodium iodide (731 mg, 4.88 mmol) and copper(II) perchlorate hexahydrate (904 mg, 2.44 mmol) were added and the solution stirred for 5 minutes. Further added were TBTA (13 mg, 0.024 mmol), DBU (186 mg, 1.22 mmol, in 0.5 mL 1:1 THF/CH_3CN) and 3,3-diethoxy-1-propyne (156 mg, 1.22 mmol, in 0.5 ml 1:1 THF/CH_3CN) and the mixture stirred at room temperature under a N_2 atmosphere overnight. The reaction mixture was diluted with CH_2Cl_2 (25 mL) and washed with $NH_4OH_{(aq)}$ (3 x 20 mL), brine (2 x 20 mL) and dried over $MgSO_4$. After removal of the solvent *in vacuo*, purification by silica gel column chromatography (in neat EtOAc) afforded **4.4I** as a white solid (276 mg, 55%).

^{1}H NMR (500 MHz, $CDCl_3$) δ (ppm): 7.67 (1H, t, ^{3}J = 7.7 Hz, pyridine Ar*H*), 7.19 (1H, d, ^{3}J = 7.8 Hz, pyridine Ar*H*), 6.91 (1H, d, ^{3}J = 7.6 Hz, pyridine Ar*H*), 5.77 (2H, s, CH_2-N iodotriazole), 5.70 (1H, s, C*H*-C iodotriazole), 4.75 (2H, d, ^{3}J = 4.9 Hz, CH_2OH), 3.62–3.76 (5H, m, OCH_2CH$_3$ + O*H*), 1.27 (6H, t, ^{3}J = 7.1 Hz, CH_3); **^{13}C NMR** (125 MHz, $CDCl_3$) δ (ppm): 159.2, 152.9, 148.9, 137.8, 120.1, 119.9, 96.5, 78.5, 63.8, 61.8, 54.9, 15.0; **HRMS** (ESI +ve) *m/z*: 441.0388 ($[M + Na]^+$, $C_{14}H_{19}N_4O_3INa$ calc. 441.0394).

Diethoxyethane-appended XB 'tosylate-arm' (4.5I)

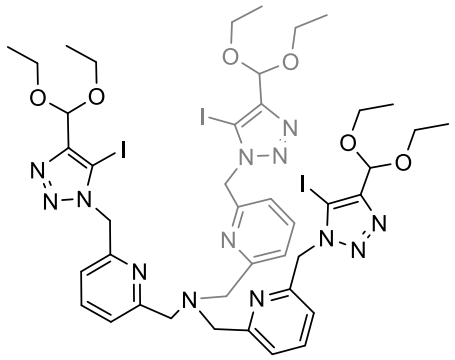


To a fully dissolved solution of **4.4I** (1.6 g, 3.82 mmol) in dry CH_2Cl_2 (50 mL) was added *p*-toluenesulfonic anhydride (1.37 g, 4.2 mmol), triethylamine (0.59 mL, 4.2 mmol) and DMAP (24.4 mg, 0.2 mmol). After stirring the reaction at room temperature under a N_2 atmosphere overnight, the mixture washed with sat. $NaHCO_{3(aq)}$ (2 x 25 mL), brine (2 x 25 mL) and dried over $MgSO_4$. After removal of the solvent *in vacuo*, purification by silica gel column chromatography (using 30% EtOAc in hexane to separate the first band, followed by 50% EtOAc in hexane to obtain the second product band) afforded **4.5I** as a cream solid (1.05 g, 48%).

^{1}H NMR (500 MHz, $CDCl_3$) δ (ppm): 7.82 (2H, d, ^3J = 8.3 Hz, tosyl Ar*H*), 7.66 (1H, t, ^3J = 7.8 Hz, pyridine Ar*H*), 7.36 (3H, m, tosyl Ar*H* + pyridine Ar*H*), 6.84 (1H, d, ^3J = 7.8 Hz, pyridine Ar*H*), 5.69 (1H, s, C*H*-C iodotriazole), 5.68 (2H, s, CH_2-N iodotriazole), 5.11 (2H, s, CH_2-O tosyl), 3.60–3.76 (4H, m, OCH_2CH$_3$), 2.45 (3H, s, tosyl CH_3), 1.26 (6H, t, ^3J = 7.1 Hz, OCH$_2$CH_3); **^{13}C NMR**: Due to the unstable nature of the compound, a ^{13}C NMR spectrum could not be obtained. **HRMS** (ESI +ve) *m/z*: 595.0479 ([M + Na]$^+$, $C_{21}H_{25}N_4O_5INaS$ calc. 595.0482).

(*N.B.* During the chromatographic purification process, the first band (535 mg) was identified by ESI-MS analysis (peak at *m/z* = 437.0 [M + H]$^+$) as the corresponding '6-(chloromethyl)pyridine-*arm*' and also used in subsequent tripodal ligand formation procedures).

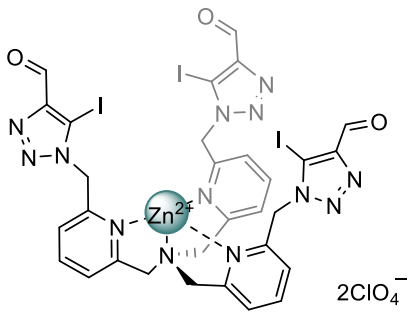
Tris(diethoxyethane)-appended XB tripodal ligand (4.6I)



To a solution of **4.5I** (2.4 g, 4.19 mmol) fully dissolved in dry CH_3CN (40 mL) was added NH_4OAc (6.46 g, 83.8 mmol), Na_2CO_3 (8.88 g, 83.8 mmol) and KI (696 mg, 4.19 mmol) as solid portions. The reaction flask was completely sealed, and the mixture vigorously stirred for two days at room temperature after which no evidence of **4.5I** was observed by TLC or ESI-MS analyses. Thereafter, the creamy off-white suspension was directly transferred to a separating funnel and *ca.* 40 ml H_2O very gently pipetted into the vessel. The cloudy, lower aqueous layer was separated, and the remaining clear organic layer concentrated *in vacuo*. The resultant crude pale yellow residue was redissolved in $CHCl_3$ (50 mL) and thoroughly washed with water (3 x 50 mL) and the organics dried over $MgSO_4$. Solvent removal and purification of the residue by successive trituration with a cold Et_2O solution (3 x 25 mL), followed by vacuum filtration of the resultant white solid afforded the tripodal ligand **4.6I** (1.39 g, 82% yield) which was deemed completely pure by ^{1}H NMR analysis.

^{1}H NMR (500 MHz, $CDCl_3$) δ (ppm): 7.63 (3H, t, ^3J = 7.7 Hz, pyridine Ar*H*), 7.42 (3H, d, ^3J = 7.8 Hz, pyridine Ar*H*), 6.77 (3H, d, ^3J = 7.6 Hz, pyridine Ar*H*), 5.73 (6H, s, CH_2-N iodotriazole), 5.68 (3H, s, C*H*-C iodotriazole), 3.83 (6H, s, CH_2-N tertiary amine), 3.60–3.76 (12H, m, OCH_2CH$_3$), 1.24 (18H, t, ^3J = 7.1 Hz, CH_3); **^{13}C NMR** (125 MHz, $CDCl_3$) δ (ppm): 159.3, 153.4, 148.8, 137.6, 122.5, 119.6, 96.6, 78.5, 61.8, 59.6, 55.3, 15.1; **HRMS** (ESI +ve) *m/z*: 1218.1500 ([M + H]$^+$, $C_{42}H_{55}N_{13}O_6I_3$ calc. 1218.1526).

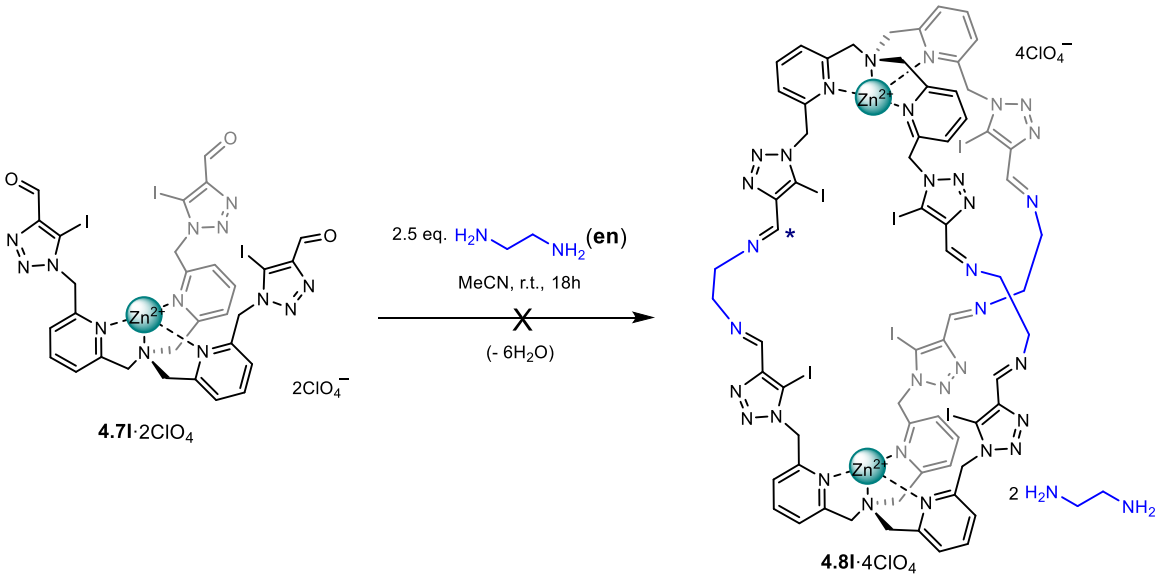
Tris(aldehyde)-appended XB Zn(II)-tripod (4.7I·2ClO$_4$)



To tripodal ligand **4.3I** (100 mg, 0.101 mmol) in a 1:1 mixture of CH_2Cl_2/MeOH (10 mL) was added zinc(II) perchlorate hexahydrate (37.6 mg, 0.101 mmol) and the solution stirred at room temperature under a N_2 atmosphere for 3 hours. After removal of the solvent *in vacuo*, the resultant residue was triturated with ice cold Et_2O (*ca*. 5 mL). The ethereal layer was carefully decanted with a pipette and the contents of the flask dried under high vacuum to afford the metallo-tripodal subunit **4.7I**·2ClO$_4$ as a fine, pale peach crystalline powder (126 mg, quantitative).

^{1}H NMR (500 MHz, CD_3CN) δ (ppm): 9.75 (3H, s, CO*H*), 8.13 (3H, t, ^3J = 7.8 Hz, pyridine Ar*H*), 7.69 (3H, d, ^3J = 7.6 Hz, pyridine Ar*H*), 7.54 (3H, s, ^3J = 7.8 Hz, pyridine Ar*H*), 5.70 (6H, s, C*H*$_2$-N iodotriazole), 4.25 (3H, s, C*H*$_2$-N tertiary amine); **^{13}C NMR** (125 MHz, CD_3CN) δ (ppm): 184.8, 157.0, 152.9, 148.7, 143.3, 126.9, 126.4, 89.6, 56.7, 54.7; **HRMS** (ESI +ve) *m/z*: 1157.8035 ([M – ClO$_4$]$^+$, $C_{30}H_{24}N_{13}O_7ClI_3{}^{64}Zn$ calc. 1157.8030).

Synthetic attempt towards diZn(II) XB polyimine cryptate (4.8I·4ClO$_4$) following Zonta's protocol[18]



To 2 mL (4.0 μmol) of a 2 mM solution of **4.7I**·2ClO$_4$ in MeCN, 0.5 mL (10 μmol) of a 20 mM solution of ethylenediamine in MeCN was added in 6 portions over a period of 6 hours. The mixture was left to further stir for 12 hours at room temperature. A white precipitate was formed and filtered under gravity. *Via* ^{1}H-NMR analysis (in d_6-DMSO) and ESI-MS analysis (peak at *m/z* = 1284.1), the crude precipitate was identified as the intermediate '1+3' polyimine condensation product.

6.3 References

1 B.-Y. Lee, S. R. Park, H. B. Jeon and K. S. Kim, *Tetrahedron Lett.*, 2006, **47**, 5105–5109.
2 A. Hassner and M. Stern, *Angew. Chem. Int. Ed. Engl.*, 1986, **25**, 478–479.
3 A. Hassner, M. Stern, H. E. Gottlieb and F. Frolow, *J. Org. Chem.*, 1990, **55**, 2304–2306.
4 A. Dalmia, R. F. Savinell and C. C. Liu, *J. Electrochem. Soc.*, 1996, **143**, 1827–1833.
5 M. J. Hynes, *J. Chem. Soc. Dalton Trans.*, 1993, **0**, 311–312.
6 R. Oliveira, S. Groni, C. Fave, M. Branca, F. Mavré, D. Lorcy, M. Fourmigué and B. Schöllhorn, *Phys. Chem. Chem. Phys.*, 2016, **18**, 15867–15873.
7 P. Thordarson, *Chem. Soc. Rev.*, 2011, **40**, 1305–1323.
8 BindFit v0.5 | Supramolecular, http://app.supramolecular.org/bindfit/, (accessed 7 October 2019).
9 S. L. Tobey and E. V. Anslyn, *J. Am. Chem. Soc.*, 2003, **125**, 14807–14815.
10 Y. Mikata, Y. Nodomi, R. Ohnishi, A. Kizu and H. Konno, *Dalton Trans.*, 2015, **44**, 8021–8030.
11 R. Ziessel and C. Stroh, *Synthesis*, 2003, **14**, 2145–2154.
12 T. Zhang and E. V. Anslyn, *Tetrahedron*, 2004, **60**, 11117–11124.
13 T. Cheisson and A. Auffrant, *Dalton Trans.*, 2016, **45**, 2069–2078.
14 T. Shiraki, A. Dawn, Y. Tsuchiya and S. Shinkai, *J. Am. Chem. Soc.*, 2010, **132**, 13928–13935.
15 J. Chao, W.-Y. Huang, J. Wang, S.-J. Xiao, Y.-C. Tang and J.-N. Liu, *Biomacromolecules*, 2009, **10**, 877–883.
16 S. W. Robinson, PhD thesis, The University of Oxford, 2016.
17 E. Zhou, J. Zhang, Y. Lu and C. Dong, *ARKIVOC*, 2014, **v**, 351–364.
18 C. Bravin, E. Badetti, F. A. Scaramuzzo, G. Licini and C. Zonta, *J. Am. Chem. Soc.*, 2017, **139**, 6456–6460.

Appendices

Appendices

Appendix A: Crystallographic data

Ferrocene-appended tripodal receptors **2.20I**·$2ClO_4$ and **2.20H**·$2ClO_4$

Crystals suitable for single crystal X-ray diffraction were obtained for **2.20I**·$2ClO_4$ and **2.20H**·$2ClO_4$ by slow evaporation of saturated solutions of each of the compounds in CD_3CN, and the corresponding structures solved by Dr Christopher Durr. Samples were isolated under a pool of fluorinated oil and mounted on MiTeGen MicroMounts. The crystal was then cooled to 150 K with an Oxford Cryosystems Cryostream nitrogen cooling device. Data collection was carried out with an Oxford Diffraction Supernova diffractometer using Cu Kα (λ = 1.5417 Å) radiation. The resulting raw data was processed using CrysAlisPro.[1] Structures were solved by SHELXT and Full-matrix least-squares refinements based on F^2 were performed in SHELXL-14[2], as incorporated in the WinGX package.[3] For each methyl group, the hydrogen atoms were added at calculated positions using a riding model with U(H) = 1.5Ueq (bonded carbon atom). The rest of the hydrogen atoms were included in the model at calculated positions using a riding model with U(H) = 1.2Ueq (bonded atom). Neutral atom scattering factors were used and include terms for anomalous dispersion.[4]

One cyclopentadienyl ring on the XB ligand of **2.20I**.$2ClO_4$ was found to be disordered over two positions. Both positions were found in the difference map and allowed to refine on a free variable. In order to allow for stable refinement, thermal restraints were applied to the disorder.

Table A1. Crystal structure data and refinement details for Ferrocene-appended tripods **2.20I**·2ClO_4 and **2.20H**·2ClO_4

Compound	**2.20H**.2ClO_4	**2.20I**.2ClO_4
Chemical formula	$C_{63}H_{60}Cl_2Fe_3N_{16}O_8Zn$	$C_{59}H_{51}Cl_2Fe_3I_3N_{14}O_8Zn$
Formula weight	1473.09	1768.66
Temp (K)	150(2)	150(2)
Space group	Monoclinic, P $2_1/c$	Monoclinic, P $2_1/c$
a (Å)	24.0554(2)	22.9444(3)
b (Å)	10.5065(1)	11.6083(2)
c (Å)	26.2168(3)	23.9102(4)
α (°)		
β (°)	108.855(1)	96.195(1)
γ (°)		
V (Å^3)	6270.43(11)	6331.19(17)
Z	4	4
D_{calcd} (Mg/m^3)	1.560	1.856
Crystal size (mm)	0.30 X 0.20 X 0.15	0.25 X 0.20 X 0.10
Theta range for data collection (°)	3.563 to 76.548	3.719 to 76.303
μ (mm^{-1})	(Cu, Kα) 7.251	(Cu, Kα) 18.642
Reflections collected	78092	85543
Unique reflections	13074 [R_{int} = 0.0679]	13203 [R_{int} = 0.0530]
Data Completeness to [θ]	100.0% [67.684]	100.0% [67.684]
Data/restraints/parameters	13074 / 0 / 841	13203 / 90 / 858
R1 (all data)	0.0424 (0.0515)	0.0900 (0.0921)
wR2 (all data)	0.1048 (0.1120)	0.1974 (0.2019)
Goodness-of-fit on F^2	1.037	1.160
Largest diff. peak and hole (e Å^{-3})	0.615 and -0.666	4.599 and -0.708

Appendix B: Electrochemical reversibility studies

B1. Criteria for electrochemical reversibility

For a reversible electrochemical system displaying fast electron transfer kinetics, the following criteria needs to be met (terms defined in Figure B1.1):

- E_{pa} and E_{pc} independent of scan rate
- $I_{pa}/ I_{pc} = 1$
- $\Delta E_p = (E_{pa} - E_{pc}) = (59/n)$ mV, where n is the number of electrons transferred during the redox process. Therefore for a one-electron transfer process, the difference = 59 mV.
- I_{pa} and I_{pc} varies proportionally to the square root of the scan rate.

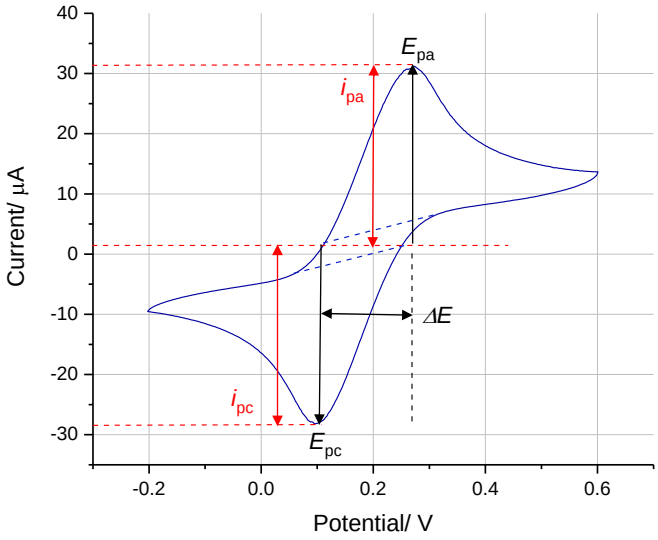


***Figure B1.1**: A labelled cyclic voltammogram (CV) for definition of the terms E_{pa}, E_{pc}, I_{pa} and I_{pc}.*

For all of the following receptors described herein, E_{pa} and E_{pc} were almost independent of scan rate at lower rates. With a few exceptions, I_{pa} / I_{pc} are typically in the range of 0.90 – 1.10 and ΔE_p show notable variations from 60 mV to 260 mV. In all cases, I_{pa} and I_{pc} vary almost proportionally with the square root of the scan rate (Pearsons's $R^2 > 0.94$). Thus the redox-active hosts generally showed 'quasi-reversible' electrochemical behaviour.

B2. Electrochemical Reversibility Studies on Redox-active Hosts

XB Zn(II)-Tripod **2.20I**·2ClO_4

Studies performed in 0.1 M $TBAClO_4$ in CH_3CN/ H_2O 9:1 *v/v*

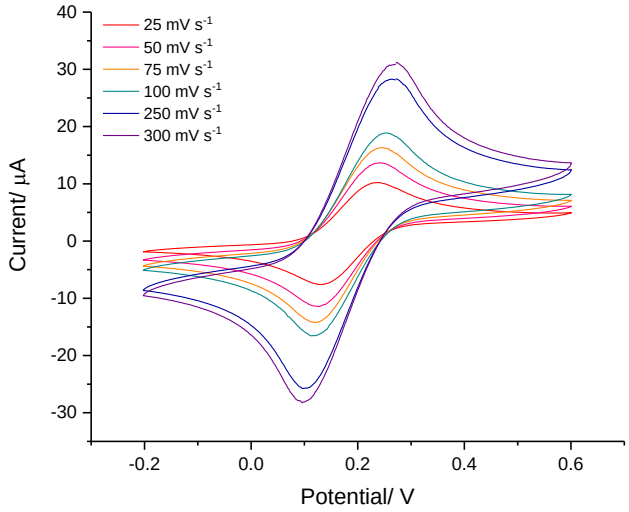


***Figure B2.1**: CVs of **2.20I**·2ClO_4 at different scan rates ([metallo-host] = 0.5 mM, T = 293 K).*

Table B1. Values of E_{pa}, E_{pc}, I_{pa}, I_{pc}, ΔE, and I_{pa}/I_{pc} for **2.20I**·2ClO_4 at different scan rates.

Scan rate (mV s^{-1})	E_{pa} (V)	E_{pc} (V)	I_{pa} (µA)	I_{pc} (µA)	ΔE_p (V)	I_{pa}/I_{pc}
25	0.235	0.137	8.497	9.306	0.098	0.913
50	0.237	0.127	12.392	12.814	0.110	0.967
75	0.244	0.120	13.921	16.721	0.124	0.833
100	0.259	0.132	16.798	18.88	0.127	0.889
250	0.259	0.105	27.926	26.703	0.154	1.071
300	0.259	0.103	28.427	31.017	0.156	0.916

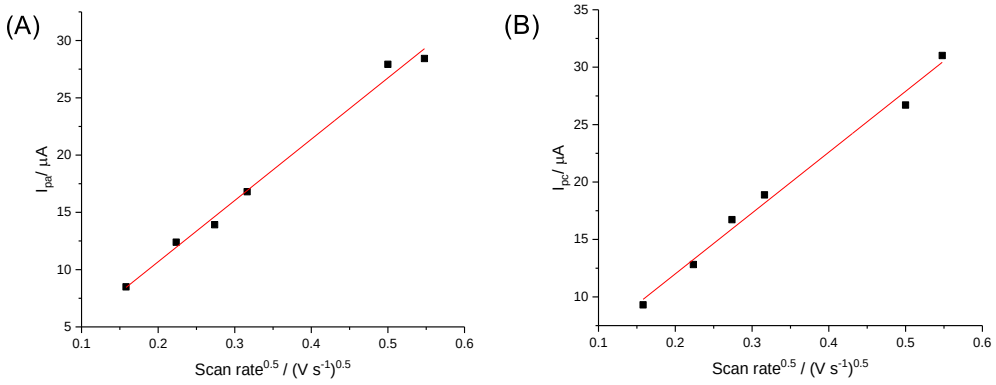


***Figure B2.2**: Plots of (A) I_{pa} and (B) I_{pc} against (Scan rate)$^{1/2}$ for **2.20I**·2ClO_4.*

HB Zn(II)-Tripod **2.20H**·2ClO_4

Studies performed in 0.1 M $TBAClO_4$ in CH_3CN/ H_2O 9:1 *v/v*

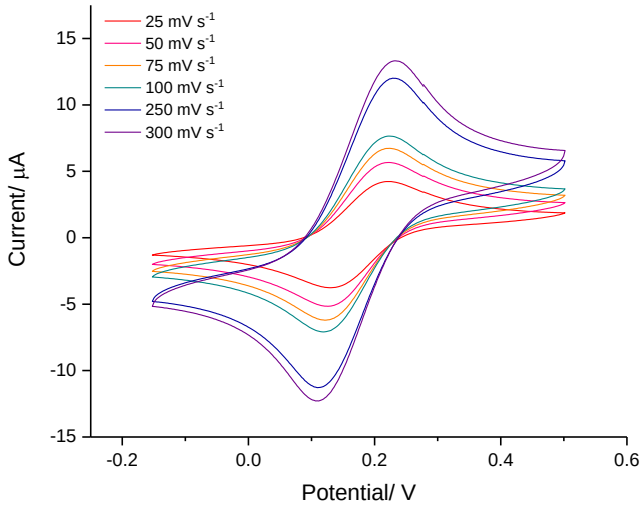


***Figure B2.3**: CVs of **2.20H**·2ClO_4 at different scan rates ([metallo-host] = 0.5 mM, T = 293 K).*

Table B2. Values of E_{pa}, E_{pc}, I_{pa}, I_{pc}, ΔE, and I_{pa}/I_{pc} for **2.20H**·2ClO_4 at different scan rates.

Scan rate (mV s^{-1})	E_{pa} (V)	E_{pc} (V)	I_{pa} (µA)	I_{pc} (µA)	ΔE_p (V)	I_{pa}/I_{pc}
25	0.216	0.133	3.971	4.073	0.083	0.975
50	0.216	0.131	5.339	5.539	0.085	0.964
75	0.216	0.126	6.129	6.852	0.09	0.894
100	0.216	0.124	6.937	7.867	0.092	0.881
250	0.224	0.119	11.056	12.332	0.105	0.896
300	0.226	0.116	12.498	13.083	0.11	0.955

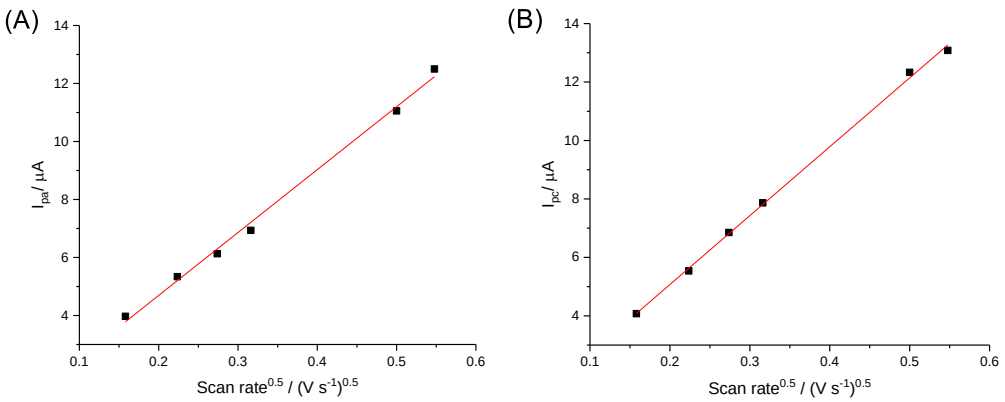


***Figure B2.4**: Plots of (A) I_{pa} and (B) I_{pc} against (Scan rate)$^{1/2}$ for **2.20H**·2ClO_4.*

XB Cu(II)-Tripod **2.26I**·2OTf

Studies performed in 0.1 M $TBAClO_4$ in anhydrous **CH_3CN**

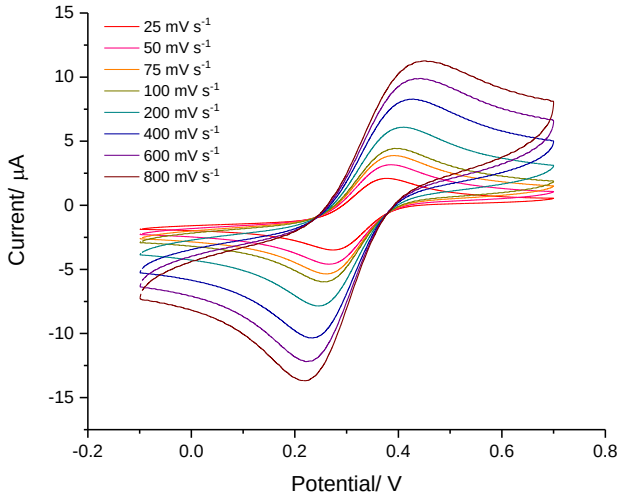


***Figure B2.5**: CVs of **2.26I**·2OTf at different scan rates ([metallo-host] = 0.5 mM, T = 293 K).*

Table B3. Values of E_{pa}, E_{pc}, I_{pa}, I_{pc}, ΔE, and I_{pa}/I_{pc} for **2.26I**·2OTf at different scan rates.

Scan rate (mV s^{-1})	E_{pa} (V)	E_{pc} (V)	I_{pa} (µA)	I_{pc} (µA)	ΔE_p (V)	I_{pa}/I_{pc}
25	0.381	0.268	3.119	3.284	0.113	0.949
50	0.391	0.266	4.143	4.372	0.125	0.948
75	0.393	0.261	4.764	5.173	0.132	0.921
100	0.395	0.256	5.219	5.683	0.139	0.918
200	0.403	0.246	6.839	7.441	0.157	0.919
400	0.422	0.232	8.808	9.957	0.19	0.885
600	0.439	0.222	9.947	11.297	0.217	0.880
800	0.481	0.219	10.084	12.149	0.262	0.830

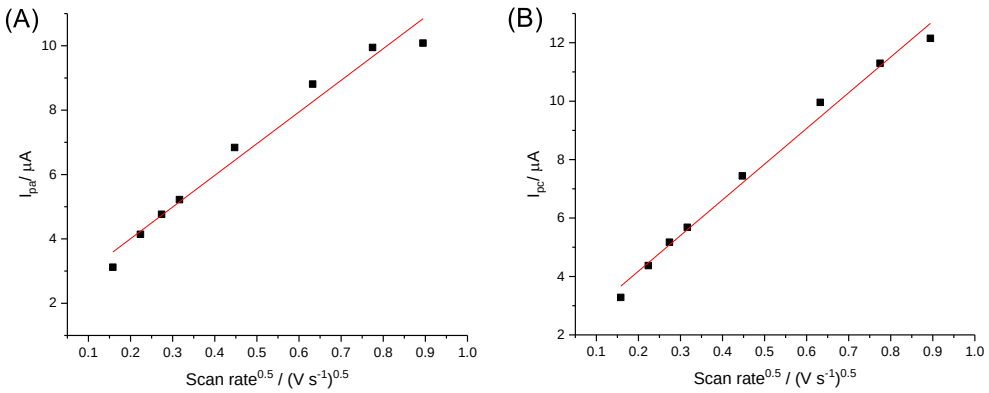


***Figure B2.6**: Plots of (A) I_{pa} and (B) I_{pc} against (Scan rate)$^{1/2}$ for **2.26I**·OTf.*

HB Cu(II)-Tripod **2.26H**·2OTf

Studies performed in 0.1 M $TBAClO_4$ in anhydrous **CH_3CN**

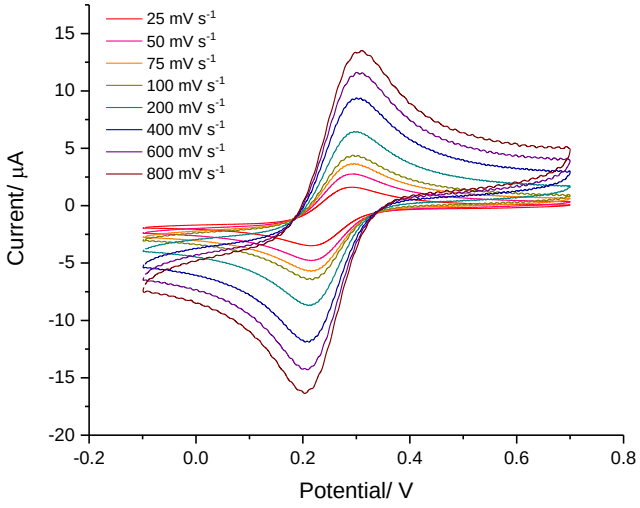


***Figure B2.7**: CVs of **2.26H**·2OTf at different scan rates ([metallo-host] = 0.25 mM, T = 293 K).*

Table B4. Values of E_{pa}, E_{pc}, I_{pa}, I_{pc}, ΔE, and I_{pa}/I_{pc} for **2.26H**·2OTf at different scan rates.

Scan rate (mV s^{-1})	E_{pa} (V)	E_{pc} (V)	I_{pa} (µA)	I_{pc} (µA)	ΔE_p (V)	I_{pa}/I_{pc}
25	0.288	0.219	2.951	2.883	0.069	1.024
50	0.290	0.215	4.191	4.192	0.075	0.999
75	0.295	0.210	5.051	5.074	0.085	0.995
100	0.293	0.210	5.744	5.839	0.083	0.984
200	0.295	0.210	8.029	8.384	0.085	0.958
400	0.300	0.205	10.981	11.442	0.095	0.959
600	0.302	0.205	13.161	13.821	0.097	0.952
800	0.310	0.202	14.892	15.642	0.108	0.952

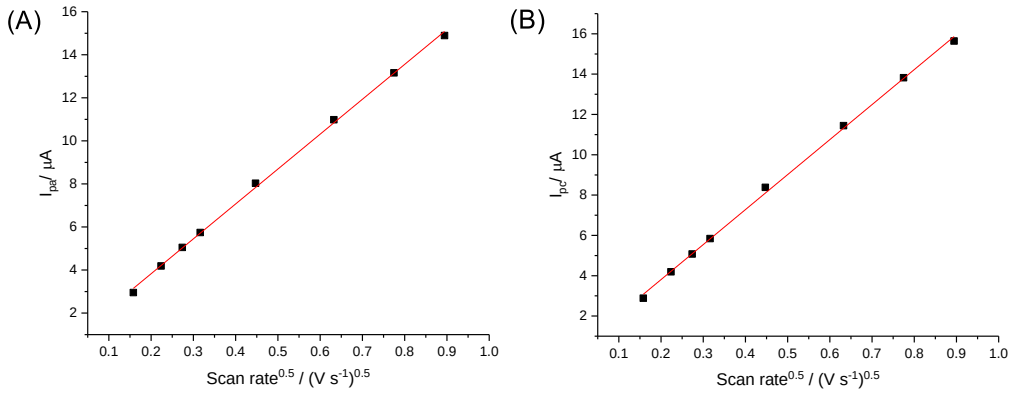


***Figure B2.8**: Plots of (A) I_{pa} and (B) I_{pc} against (Scan rate)$^{1/2}$ for **2.26H**·OTf.*

XB Cu(II)-Tripod **2.26I**·2OTf

Studies performed in 0.1 M $TBAClO_4$ in **H_2O**

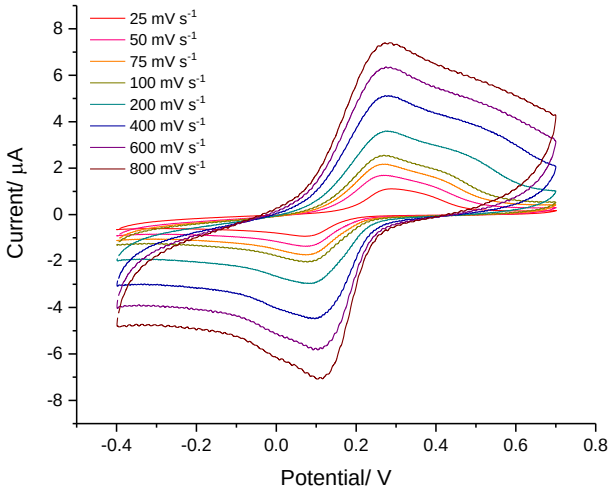


***Figure B2.9**: CVs of **2.26I**·2OTf at different scan rates ([metallo-host] = 0.25 mM, T = 293 K).*

Table B5. Values of E_{pa}, E_{pc}, I_{pa}, I_{pc}, ΔE, and I_{pa}/I_{pc} for **2.26I**·2OTf at different scan rates.

Scan rate (mV s^{-1})	E_{pa} (V)	E_{pc} (V)	I_{pa} (µA)	I_{pc} (µA)	ΔE_p (V)	I_{pa}/I_{pc}
25	0.291	0.071	1.021	1.016	0.22	1.005
50	0.269	0.079	1.515	1.553	0.19	0.976
75	0.269	0.078	2.046	1.844	0.191	1.109
100	0.271	0.081	2.259	2.521	0.19	0.896
200	0.279	0.083	3.286	3.225	0.196	1.019
400	0.279	0.096	4.842	4.771	0.183	1.015
600	0.276	0.105	6.159	5.913	0.171	1.042
800	0.276	0.115	6.968	7.493	0.161	0.929

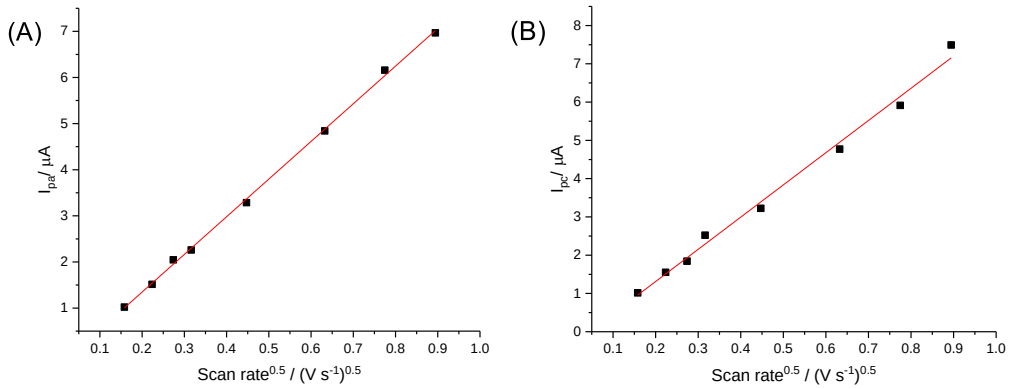


***Figure B2.10**: Plots of (A) I_{pa} and (B) I_{pc} against (Scan rate)$^{1/2}$ for **2.26I**·OTf.*

HB Cu(II)-Tripod **2.26I**·2OTf

Studies performed in 0.1 M $TBAClO_4$ in **H_2O**

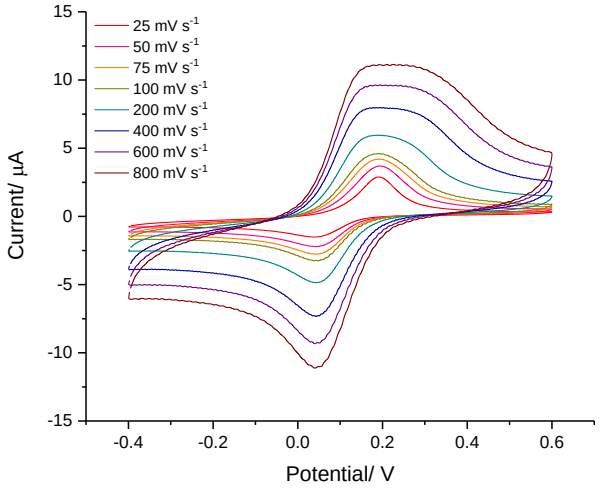


***Figure B2.11**: CVs of **2.26I**·2OTf at different scan rates ([metallo-host] = 0.25 mM, T = 293 K).*

Table B6. Values of E_{pa}, E_{pc}, I_{pa}, I_{pc}, ΔE, and I_{pa}/I_{pc} for **2.26H**·2OTf at different scan rates.

Scan rate (mV s^{-1})	E_{pa} (V)	E_{pc} (V)	I_{pa} (µA)	I_{pc} (µA)	ΔE_p (V)	I_{pa}/I_{pc}
25	0.191	0.039	2.726	1.667	0.152	1.635
50	0.19	0.037	3.507	2.395	0.153	1.464
75	0.191	0.044	3.918	3.304	0.147	1.186
100	0.191	0.042	4.244	3.640	0.149	1.166
200	0.193	0.044	5.476	5.355	0.149	1.023
400	0.196	0.044	7.406	7.919	0.152	0.935
600	0.205	0.044	9.198	9.781	0.161	0.940
800	0.203	0.041	10.728	11.501	0.162	0.933

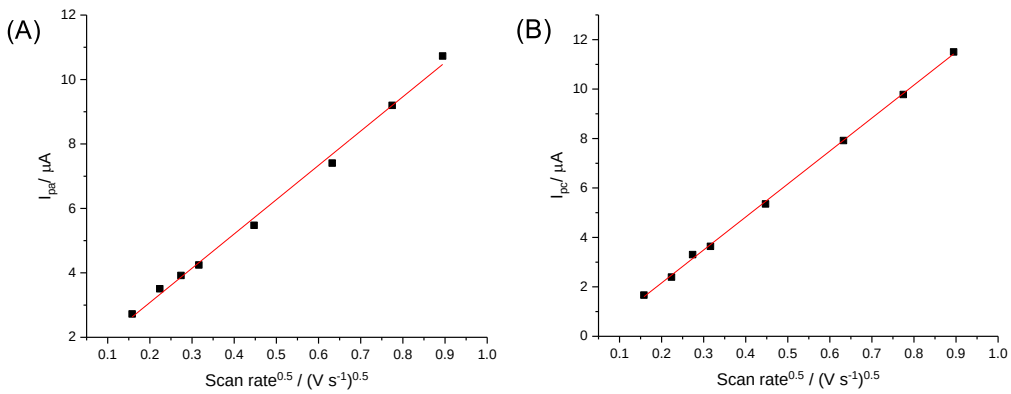
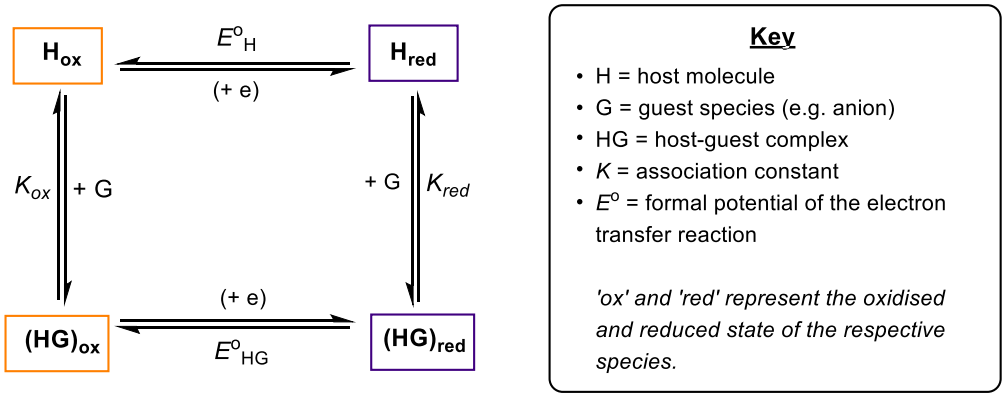


***Figure B2.12**: Plots of (A) I_{pa} and (B) I_{pc} against (Scan rate)$^{1/2}$ for **2.26H**·OTf.*

Appendix C: Theory of electrochemical anion sensing

Electrochemical anion sensing occurs by a detectable change in the redox-potential (ΔE) of a reporter group (e.g. ferrocene) in the presence of an added anion, which can be measured using techniques such as cyclic voltammetry (CV), square-wave voltammetry (SWV) or differential-pulse voltammetry (DPV). Generally, the sensing process can be represented by the one-square scheme shown in Scheme C1, where the four reactions constitute a thermodynamically closed loop and therefore the total Gibbs free energy change in the cycle is zero.



Scheme C1: *The one-square scheme showing the electron transfer processes and anion binding.*[5]

Considering the equilibrium to be approached *via* a clock-wise route starting from H_{ox}, the prior statement can then be mathematically expressed as in eqn. (1):

$$\Sigma\Delta G = \Delta G_H + \Delta G_{red} + \Delta G_{HG} + \Delta G_{ox} = 0$$

$$nF(E - E^o_H) - RT\ln(K_{red}) + nF(E^o_{HG} - E) + RT\ln(K_{ox}) = 0 \quad \text{Eqn. 1}$$

Further re-arrangement leads to eqn. (2):

$$nF(E^o_{HG} - E^o_H) = RT\ln(K_{red}/K_{ox}) \quad \text{Eqn. 2}$$

which conveniently relates the experimentally measurable perturbation of the host's redox potential ($\Delta E = E^o_{HG} - E^o_H$) in the presence of the guest to the quotient: K_{red}/K_{ox}, also known as the binding enhancement factor (BEF) or reaction coupling efficiency (RCE).[5,6] In the case of ferrocene-based receptors, the oxidation process leads to the formation of the cationic ferrocenium species, which

has an enhanced binding affinity towards anionic guests (K_{ox}) compared to the original (reduced) ferrocene host (K_{red}). Accordingly, this gives a detectable *cathodic* (negative) potential shift, the magnitude of which depends on the degree of enhancement in values of K_{ox} over K_{red} and notably, does not necessarily require strong host-guest binding. The redox-active reporter group is often covalently linked in close proximity to the anion binding site to facilitate efficient communication *via* through-space or through-bond pathways.[5]

References

1 *CrysAlis CCD, CrysAlis RED and associated programs: Oxford Diffraction*, Oxford Diffraction Ltd, Abingdon, UK, 2006.
2 G. M. Sheldrick, *Acta Crystallogr. A*, 2008, **64**, 112–122.
3 L. J. Farrugia, *J. Appl. Crystallogr.*, 2012, **45**, 849–854.
4 A. J. C. Wilson, *International Tables for Crystallography.*, Kluwer Academic Publishers, Dordrecht, 1st edn., 1992, vol. C: Mathematical, Physical and Chemical Tables.
5 P. D. Beer, P. A. Gale and G. Z. Chen, *J. Chem. Soc. Dalton Trans.*, 1999, 1897–1910.
6 P. D. Beer, P. A. Gale and G. Z. Chen, *Coord. Chem. Rev.*, 1999, **185**–**186**, 3–36.